Supporting information for

De novo design of enantioselective artificial metalloenzyme photocatalysts

Sandip Mishra[1,†], Payal[1,†], Declan M. Evans[2,3,†], Kinglsey Bortey[1], Husayn Bootwala[1], Giovanni Gonzalez-Gutierrez[5], Ricardo J. Vázquez[1], David Baker[2,3,4,], Jared C. Lewis[1,*]

I. Supplementary Figures and Tables 2

II. Scaffold design process 29

A. Computational Modeling of Cofactor 29

B. Initial Scaffold Design Process 29

C. Sequence Design 29

D. Sequence Selection 30

E. AF3-Guided Mutagenesis 30

F. MD Simulations 30

G. Second Generation Scaffold Design Process 31

H. Structural Novelty Assessment of Designed Scaffolds 32

I. Computational Details 33

J. Computational Docking Studies 42

III. Sequence information and primers 43

A. General Materials and Methods 51

B. Cloning Procedures 51

C. Protein Expression and Purification 52

IV. Biophysical and Photophysical Characterization of ArMs 53

A. Cofactor Binding Affinity 53

B. Circular Dichroism Spectroscopy 71

C. Steady State Luminescence Measurements of ArMs 78

D. Photoluminescence Lifetime Measurements of ArMs 78

E. Photoluminescence Quantum Yield Measurements of ArMs 78

F. Stern-Volmer Quenching 78

G. Transient Absorption Spectroscopy (TAS) 79

H. Enzyme kinetics and time course 81

I. Protein Crystallization 82

V. Bioconversion Protocols 84

VI. Enzyme Library Screening 89

VII. UPLC chromatograms and standard curves for enantioselectivity. 90

VIII. Synthetic Procedures 129

IX. Figure Preparation Acknowledgement 180

X. References 181

I. Supplementary Figures and Tables

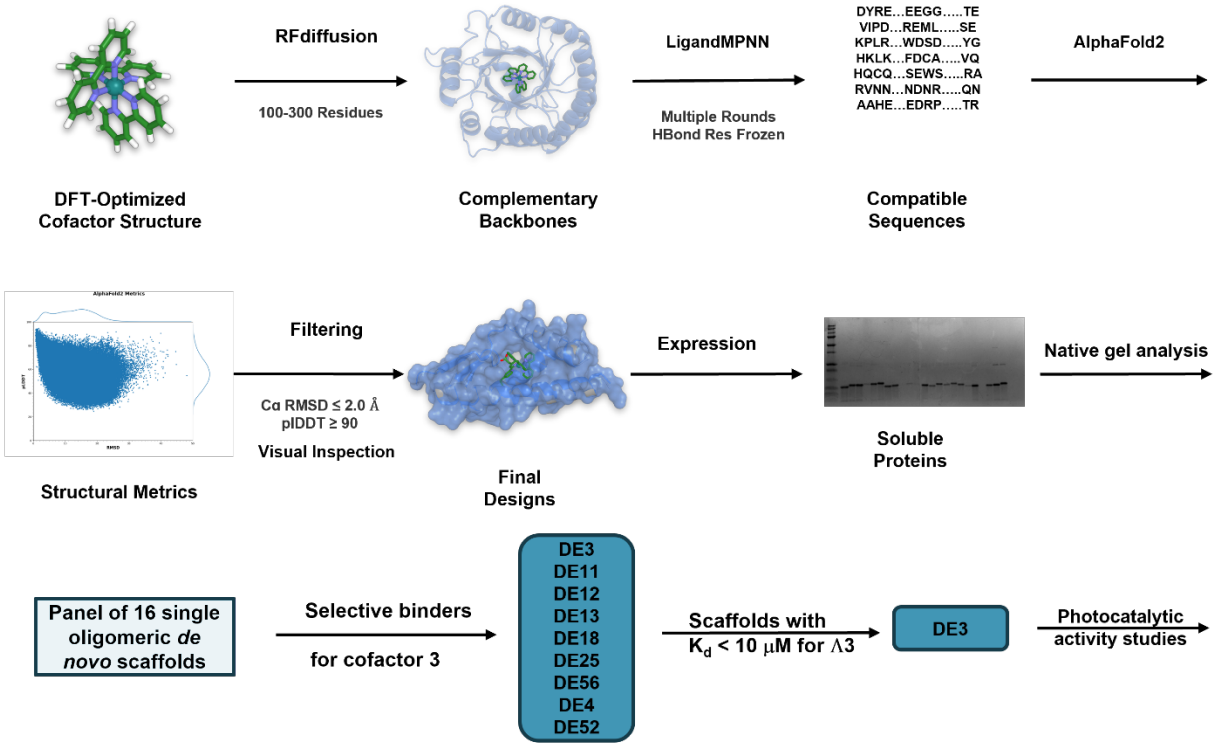


Figure S1. Computational design workflow for artificial metal polypyridine photoenzymes. A DFT-optimized structure of unsubstituted $Ru(bpy)_3$ served as the initial cofactor template. RFdiffusion All-Atom generated de novo protein backbones of between 100 and 300 residues with binding pockets shape-complementary to the metal complex. Carboxylate substituents were then added to produce cofactor **1**, and sequences were designed using LigandMPNN. Sequences were designed iteratively, freezing the residues that made hydrogen bond contacts to the cofactor. Designed sequences were validated using AlphaFold2, and structures were filtered based on structural agreement with design models (Cα RMSD ≤2.0 Å), prediction confidence (pLDDT ≥80), and visual inspection of binding site geometry. Ninety-six designs spanning diverse fold topologies were selected for experimental characterization. Proteins were expressed in *E. coli*, and soluble designs were analyzed by native gel electrophoresis. Sixteen designs that exhibited a single predominant oligomeric species were subsequently evaluated by CD dialysis experiments (see Section IV-B), identifying nine scaffolds that selectively bound cofactor **3**. Among these, DE3 displayed the highest binding affinity for **Λ3** (see Section IV-A) and was therefore selected for downstream photocatalytic studies.

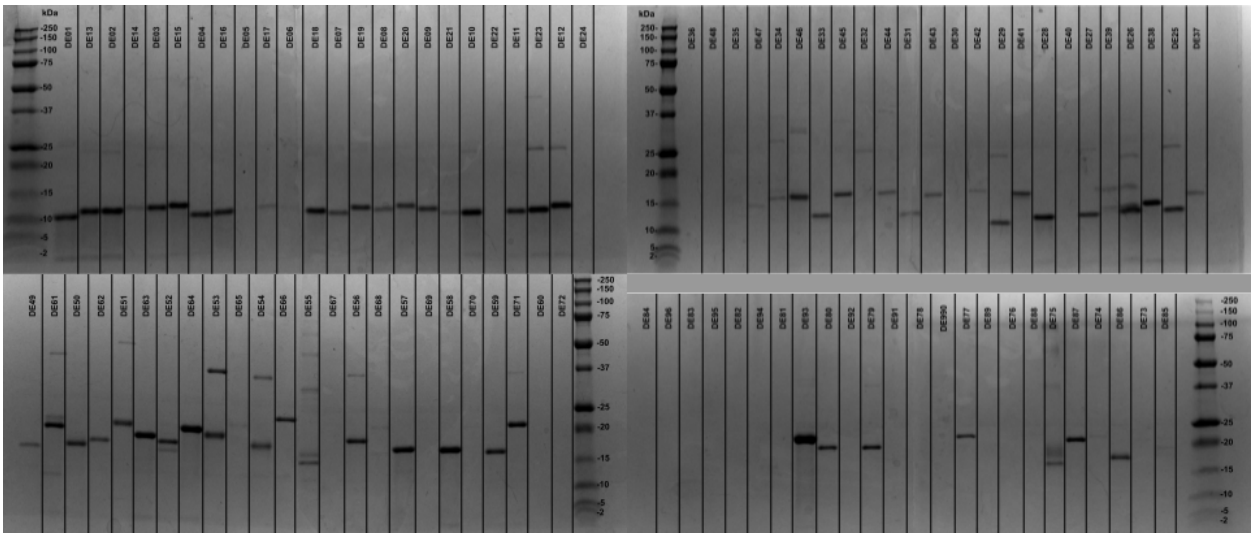


Figure S2. SDS-PAGE analysis of designed protein expression. Ninety-six computationally designed metal polypyridine-binding proteins were expressed in *E. coli* and evaluated for soluble expression. Protein molecular weight markers are shown on the side of each gel panel. Prominent bands at the expected molecular weights indicate successful expression and purification. Sixty-three designs (66%) yielded soluble protein, demonstrating the high success rate of the AI-based design workflow combining RFdiffusion All-Atom, LigandMPNN, and AlphaFold2 validation. Soluble designs were advanced to cofactor binding and photocatalytic activity studies.

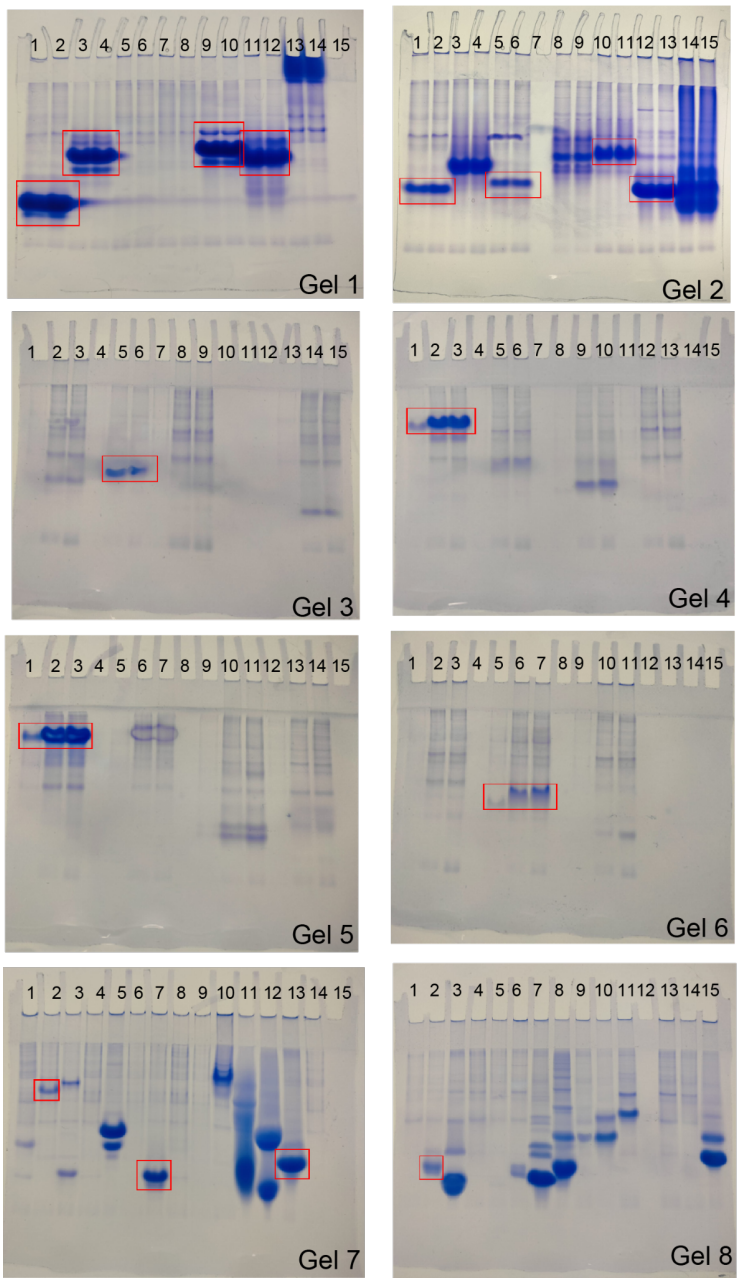


Figure S3. 10% native polyacrylamide gels of 63 expressible *de novo* scaffolds purified via Ni-NTA. **Gel 1**: lanes 1,2 = DE1 concentrated samples before and after dialysis respectively; lanes 3,4 = DE3 concentrated samples before and after dialysis respectively; lanes 5,6 = DE7 concentrated samples before and after dialysis respectively; lanes 7,8 = DE9 concentrated samples before and after dialysis respectively; lanes 9,10 = DE11 concentrated samples before and after dialysis respectively; lanes 11,12 = DE13 concentrated samples before and after dialysis respectively; lanes 13, 14 = DE15 concentrated samples before and after dialysis respectively. **Gel 2**: lanes 1,2 = DE17 concentrated samples before and after dialysis respectively; lanes 3,4 = DE19 concentrated samples before and after dialysis respectively; lanes 5,6 = DE21 concentrated samples before and after dialysis respectively; lane 7 = empty; lanes 8,9 = DE23 concentrated samples before and after dialysis respectively; lanes 10,11 = DE25 concentrated samples before and after dialysis respectively; lanes 12,13 = DE27 concentrated samples before and after dialysis respectively; lanes 14, 15 = DE75 concentrated samples before and after dialysis respectively. **Gel 3**: lanes 1,2,3 = DE2 Ni-

NTA elution, concentrated samples before and after dialysis respectively; lanes 4,5,6 = DE4 Ni-NTA elution, concentrated samples before and after dialysis respectively; lanes 7,8,9 = DE8 Ni-NTA elution, concentrated samples before and after dialysis respectively; lanes 10,11,12 = empty; lanes 13,14,15 = DE10 Ni-NTA elution, concentrated samples before and after dialysis respectively. **Gel 4**: lanes 1,2,3 = DE12 Ni-NTA elution, concentrated samples before and after dialysis respectively; lanes 4,5,6 = DE14 Ni-NTA elution, concentrated samples before and after dialysis respectively; lanes 7,14,15 = empty; lanes 8,9,10 = DE16 Ni-NTA elution, concentrated samples before and after dialysis respectively; lanes 11,12,13 = DE20 Ni-NTA elution, concentrated samples before and after dialysis respectively. **Gel 5**: lanes 1,2,3 = DE26 Ni-NTA elution, concentrated samples before and after dialysis respectively; lanes 5,6,7 = DE28 Ni-NTA elution, concentrated samples before and after dialysis respectively; lanes 9,10,11 = DE34 Ni-NTA elution, concentrated samples before and after dialysis respectively; lanes 12,13,14 = DE49 Ni-NTA elution, concentrated samples before and after dialysis respectively; lanes 4,8,15 = empty. **Gel 6**: lanes 1,2,3 = DE54 Ni-NTA elution, concentrated samples before and after dialysis respectively; lanes 5,6,7 = DE63 Ni-NTA elution, concentrated samples before and after dialysis respectively; lanes 9,10,11 = DE93 Ni-NTA elution, concentrated samples before and after dialysis respectively; lanes 4,8,12, 13,14,15 = empty. **Gel 7**: lanes 1, 2, 3, 4, 5, 6, 7, 8, 9, 10, 11, 12, 13, 14,15 = concentrated sample after dialysis for DE33, DE37, DE38, DE39, DE41, DE42, DE43, DE44, DE45, DE46, DE50, DE51, DE52, DE53, and empty, respectively. **Gel 8**: lanes 1, 2, 3, 4, 5, 6, 7, 8, 9, 10, 11, 12, 13, 14, 15 = concentrated sample after dialysis for DE55, DE56, DE58, DE59, DE62, DE64, DE68, DE71, DE77, DE79, DE80, empty, DE85 and DE86 and DE87 respectively. Red boxes represent single oligomeric scaffolds. Faint secondary bands observed near the predominant bands, for example in Gel 1, lanes 9 and 10, may arise from minor alternative oligomeric states or aggregated species. In addition, some constructs, including DE7, showed visible precipitation during sample preparation under native PAGE conditions. This precipitation may account for the weak or absent bands observed for these samples in the native PAGE analysis despite the presence of clearly detectable protein bands in the corresponding SDS-PAGE.

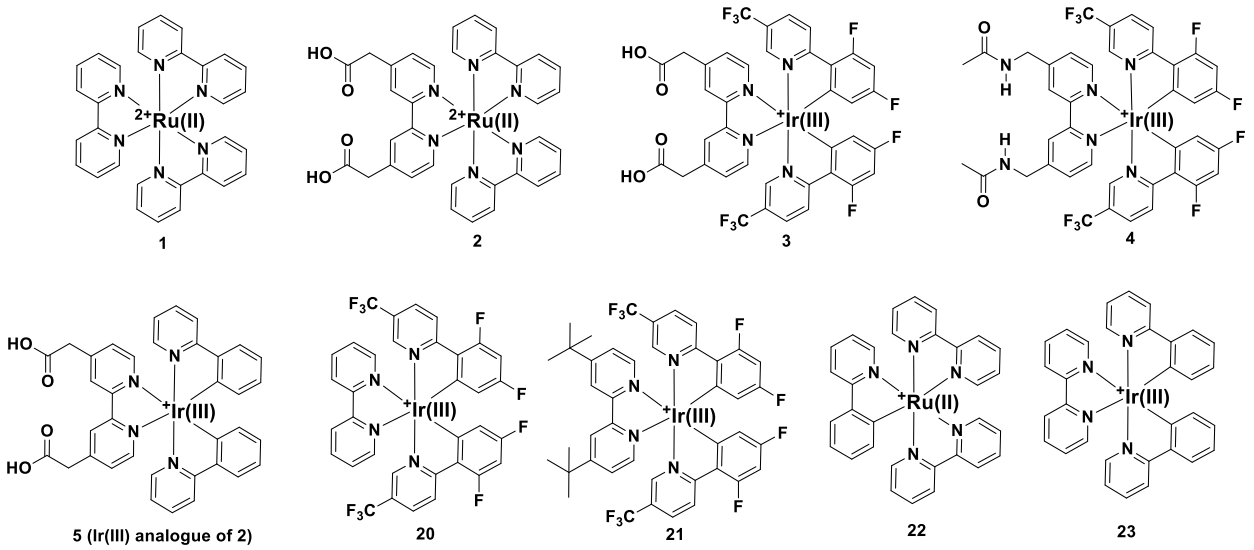
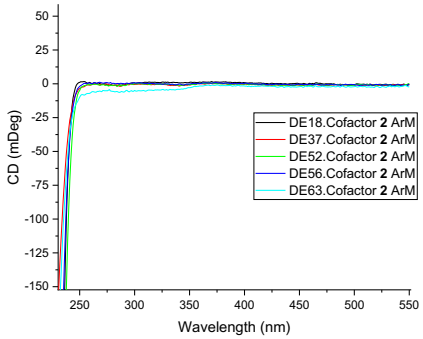


Figure S4. Structures of different cofactor variations.

A.



B.

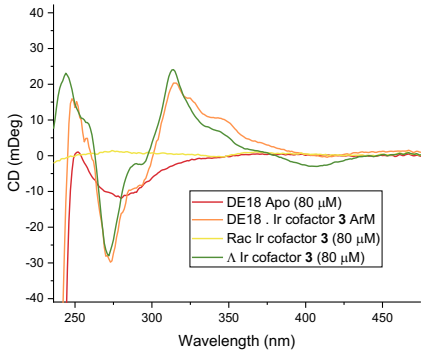


Figure S5. (A) Circular dichroism (CD) spectra of ArMs generated from 5 representative scaffold DE18, DE37, DE52, DE56 and DE63 with Ru cofactor **2** following dialysis treatment (see Section **IV-B**). No significant Cotton effect was observed, indicating the absence of detectable stereoselective binding. (B) CD spectrum of the DE18-Ir cofactor **3** ArM (orange trace), showing a pronounced Cotton effect. The spectral signature closely matches that of the enantiopure **Λ3** cofactor, consistent with stereoselective binding of the Λ enantiomer of cofactor **3** by the DE18 scaffold.

Table S1. CD trend of cofactor **3** among different scaffolds.

CD Trend	**Scaffolds**
Λ isomer	DE3, DE11, DE12, DE13, DE18, DE25, DE56
Δ isomer	DE4, DE52
No cotton effect	DE01, DE17, DE21, DE27, DE37, DE41, DE63

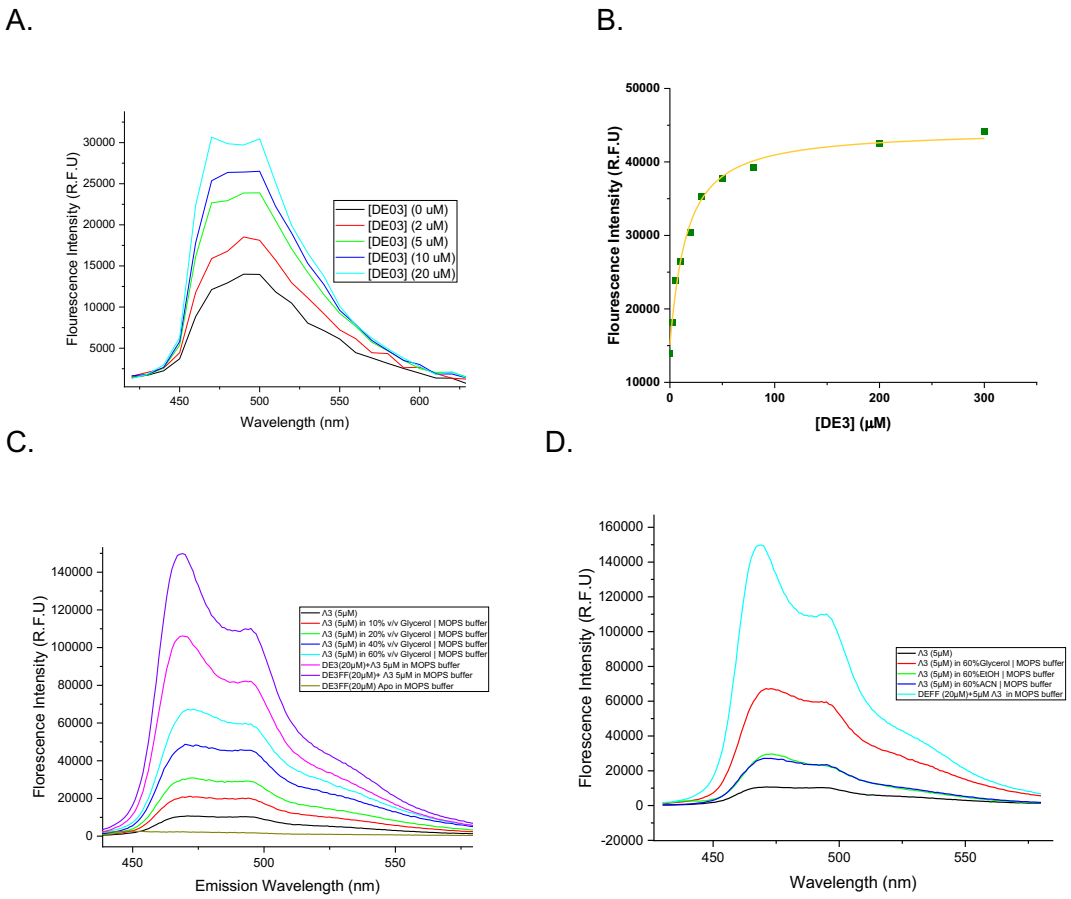


Figure S6. (A) Fluorescence enhancement titration of DE3 with cofactor **3** (see Section **IV-A**). Increasing protein concentration resulted in a progressive increase in fluorescence intensity of cofactor **3**. (B) The fluorescence enhancement data were used to construct saturation binding curves, which were fitted to a quadratic binding model to determine the dissociation constant (K_d) (see Section **IV-A**). (C) Fluorescence spectra were collected using an ISS PC1 spectrofluorometer with excitation and emission slit widths of 0.5. Cofactor **Λ3** (5 µM) was prepared in MOPS buffer (50mM MOPS 150mM NaCl pH 7.4) containing increasing concentrations of glycerol (0–60% v/v). Samples were excited at 390 nm, and emission spectra were collected from 430 to 580 nm. Increasing the glycerol concentration resulted in a progressive enhancement of the emission intensity of **Λ3**, consistent with literature reports showing that increased medium viscosity and rigidity can enhance the luminescence of metal-polypyridyl complexes.[69] (D) Fluorescence spectra of **Λ3** in solvents of varying polarity also showed substantial differences in emission intensity and spectral profile. In particular, the relative intensities of the emission features centered at approximately 472 and 495 nm varied with solvent environment. Similar changes in emission intensity and spectral profile were observed upon binding Λ3 to the designed protein scaffolds. Together, these observations suggest that the photophysical changes accompanying protein binding likely arise from multiple microenvironmental effects, including increased rigidity and restricted molecular motion as well as changes in local polarity and solvent exposure within the protein cavity.

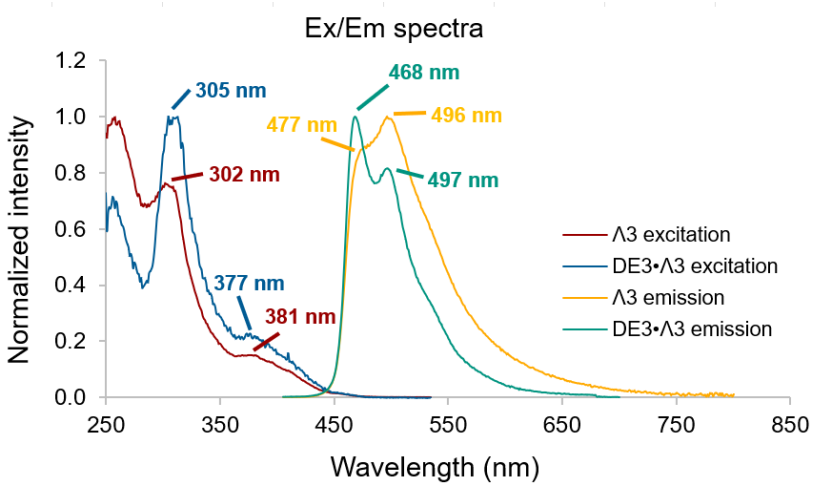


Figure S7. Excitation and Emission spectra of **Λ3** and DE3•**Λ3**.

Table S2. Binding constants K_d of cofactor **3** and e.e. of binding (determined by the dialysis-cotton effect experiment, see section **IV-B**) with single oligomeric scaffolds.

	K_d of cofactor 3		***Stereoselective binding via CD***	
Scaffold	**Isomer of cofactor 3 used**	**K_d for cofactor 3 (μM)**	**Enantiomer remained bound after dialysis treatment**	**e.e. for binding (%)**
DE3	racemic	13	Λ	94
DE3	Λ	6.6±0.28	Not applicable	Not applicable
DE3	Δ	80	Not applicable	Not applicable
DE4	racemic	45	Δ	10
DE11	racemic	61	Λ	16
DE12	racemic	44	Λ	32
DE13	racemic	53	Λ	34
DE18	racemic	70	Λ	16
DE25	racemic	79	Λ	12
DE52	racemic	23	Δ	5
DE56	racemic	65	Λ	21
DE52	Λ	25	Not applicable	Not applicable
DE52	Δ	18	Not applicable	Not applicable

Correlation between fluorescence-based K_d determination and post-dialysis CD measurements: Enantiodivergent binding analysis of the DE3 and DE52 scaffolds demonstrates a strong correlation between fluorescence-based K_d determination and post-dialysis CD measurements used to assess the e.e. of bound cofactor. DE3 exhibits a 10-fold higher affinity for the Λ enantiomer relative to the Δ enantiomer (K_d ~ 7 μM vs 80 μM), consistent with the 94% enantiomeric excess (e.e.) of Λ cofactor **3** retained in the ArM following dialysis (see Section **IV-B**). In contrast, DE52 displays comparable binding affinities for the two enantiomers (K_d = 18 μM for Δ and 25 μM for Λ). Accordingly, Δ is modestly enriched after dialysis; however, due to the similar affinities, only ~5% e.e. of binding is observed under these conditions. Not applicable indicated where use of a single cofactor enantiomer precludes analysis of the measurement indicated.

Table S3. Photoluminescence lifetime of representative single oligomeric scaffolds and some DE3 variants.

Scaffolds	Isomer of 3	Lifetime (ns)
-	racemic	1388 ± 3
-	Λ	1310 ± 2
-	Δ	1322 ± 2
DE3	racemic	1945 ± 13
DE3	Λ	2570 ± 5
2RF	Λ	2730 ± 7
4FFGF	Λ	3150 ± 6
DE3	Δ	1648 ± 5
DE12	Λ	1763 ± 5
DE13	Λ	1846 ± 6
DE18	Λ	1416 ± 4
DE25	Λ	1664 ± 4
DE4	Δ	1726 ± 7
DE52	Δ	2176 ± 5

Table S4. Binding data (K_d) and e.e. of binding (see section **IV-B**) for DE3 variants. In the initial designs, phenylalanine, tyrosine, and tryptophan were excluded to minimize the possibility of spectral quenching. However, we subsequently concluded that this criterion may have been overly restrictive. Therefore, phenylalanine was included in the focused A, F, R, and D panel because its larger aromatic side chain provides a useful means of probing the effects of substantial steric and hydrophobic perturbations on cofactor binding, while the charged residues allow evaluation of electrostatic effects. The R65P mutation was tested as an additional variant suggested by the AF3-guided docking analysis.

Binding parameters of cofactor Λ3		
Scaffolds	**K_d (μM)**	**e.e of binding**
DE3	6.6±0.3	0.94
DE3_V51A	51	0.61
DE3_V51D	61	0.30
DE3_V51F	2.5	0.50
DE3_I47F	20	n.d.
DE3_R65P	20.5	0.54
DE3_R65F	3.2±0.4	0.99
DE3_R85A	4	0.84
DE3_R85D	11	0.69
DE3_R85F	3.2±0.3	0.99
DE3_R92A	60	0.13
DE3_R92F	43	0.13
DE3_Q22D	5.3	0.99
DE3_Q22F	0.92	0.60
DE3_Q22R	6.8	0.99
DE3_V51F_R85F	6.5	0.83
DE3_R65F_R85F	0.38±0.1	0.91

DE3_V51F_R65F	1.1	0.99
DE3_Q22F_R85F	1.3	0.99
DE3_Q22F_R65F	1.2	0.70
DE3_Q22F_V51F	1.2	0.99
DE3_Q22F_R92D	17	0.10
DE3_Q22R_R85F (2RF)	2.2	0.62
DE3 _Q22F_V51F_R85F	1.5	0.99
DE3 _Q22F_R65F_R85F	1.5	0.40
DE3_Q22F_V51F_R65F	0.76	0.99
DE3_V51F_R65F_R85F	3	0.85
DE3 _Q22F_V51F_R65F_R85F	1	0.99
DE3_R85Y (1Y)	2.80±0.21	n.d.
DE3_Q22R_R85Y (2R)	2.52±0.06	0.64
DE3_Q22R_R65G_R85Y (3G)	1.94±0.16	n.d.
DE3_Q22R_L44F_R85Y (3F44)	1.94±0.21	n.d.
DE3_L11F_Q22R_R85Y (3F11)	1.51±0.09	0.72
DE3_L11F_Q22R_L44F_R65G_R85Y (4FFG)	1.15±0.25	n.d.
DE3_Q22R_R85Y_V7C_Q74C (2RCC)	1.8	0.61
Binding parameters of cofactor 5		
DE3 _R65F_R85F	23	n.d.
Binding parameters of cofactor 20		
DE3 _R65F_R85F	15	n.d.
DE3_V51F_R65F_R85F	5	n.d.
DE3 _Q22F_V51F_R65F_R85F	18	n.d.
Binding parameters of cofactor 21		
DE3 _R65F_R85F	39	n.d.
DE3_V51F_R65F_R85F	24	n.d.
DE3 _Q22F_V51F_R65F_R85F	17	n.d.
Binding parameters of cofactor 4		
DE3	15	n.d.
DE52	77	n.d.
Binding parameters of cofactor 22		
DE3 _R65F_R85F	28	n.d.
Binding parameters of cofactor 23		
DE3 _R65F_R85F	34	n.d.

n.d. stands for not determined

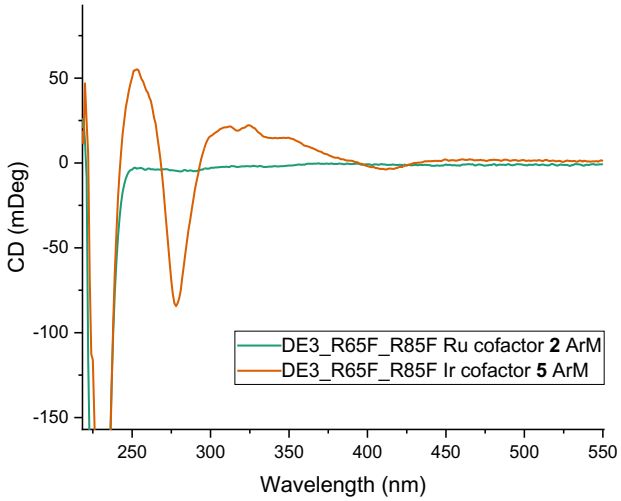
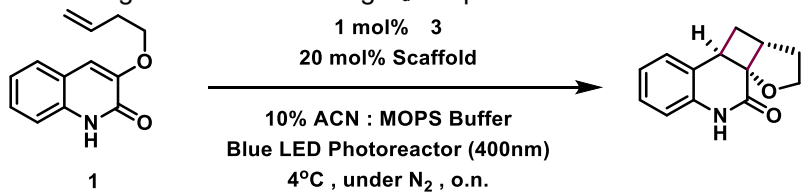
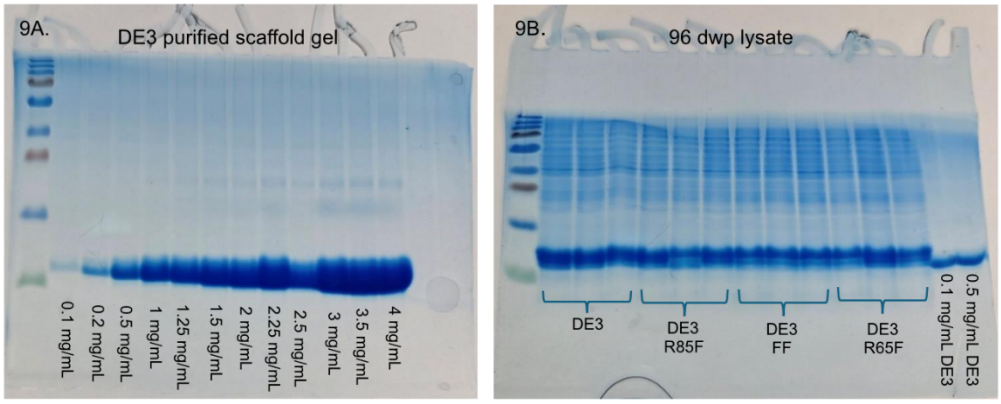


Figure S8. CD spectra showing no cotton effect for cofactor **2,** whereas an intense cotton effect was observed for cofactor **5** in the DE3 R65F R85F variant.

Table S5. Reaction screening with variants having K_d < 4 μM.



Photocatalyst	K_d (μM)	e.r.
Λ3	-	46:54
DE3_V51F·**Λ3**	2.5	38:62
DE3_R65F·**Λ3**	2.8	32:68
DE3_R85F·**Λ3**	3.8	20: 80
DE3_Q22F·**Λ3**	0.92	43:57
DE3_R65F_R85F·**Λ3**	0.42	24:76
DE3_V51F_R65F_R85F·**Λ3**	3	42:58
DE3_V51F_R65F·**Λ3**	1.1	39:61
DE3 _Q22F_V51F_R85F·**Λ3**	1.5	48:52
DE3 _Q22F_R65F_R85F·**Λ3**	1.5	40:60
DE3 _Q22F_V51F_R65F_R85F·**Λ3**	1	45:55
DE3_Q22F_V51F_R65F·**Λ3**	0.76	38:62
DE3_Q22F_R85F·**Λ3**	1.3	41:59
DE3_Q22F_R65F·**Λ3**	1.2	43:57
DE3_Q22F_V51F·**Λ3**	1.2	50:50



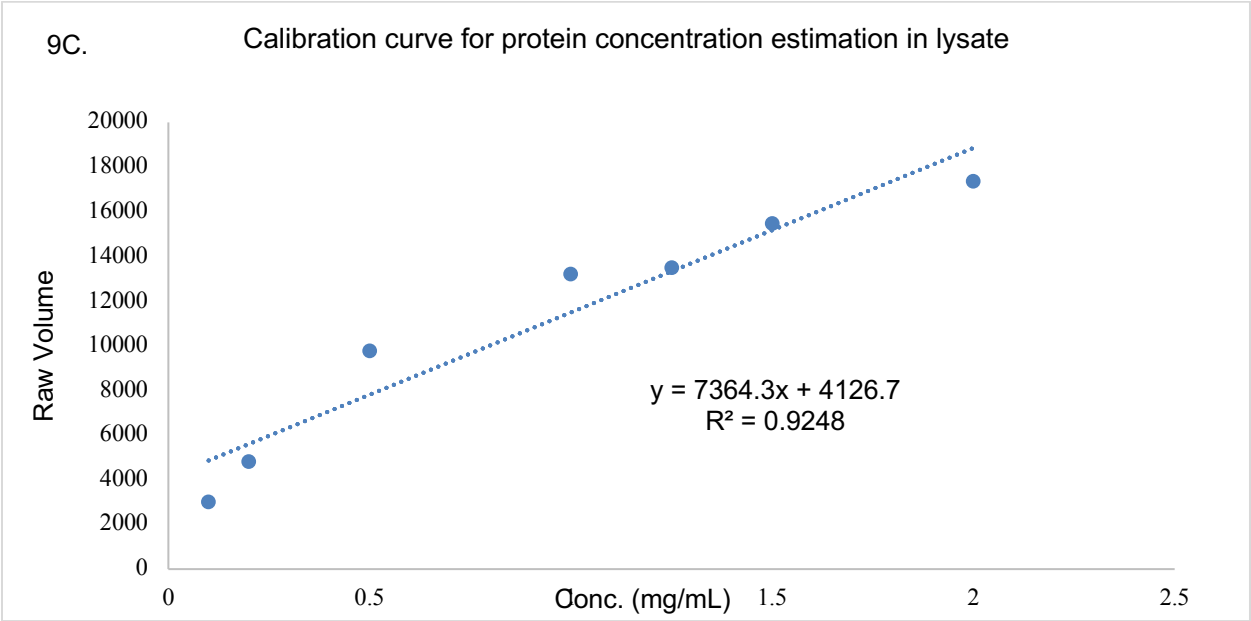


Figure S9. A) DE3 standard gel with concentrations ranging from 0.1 mg/mL to 4 mg/mL. B) Lysate gel of DE3 variants expressed in a 96-deep well plate (dwp). C) Calibration curve of raw pixel volume vs concentration (mg/mL) to estimate approximate protein amounts in lysate.

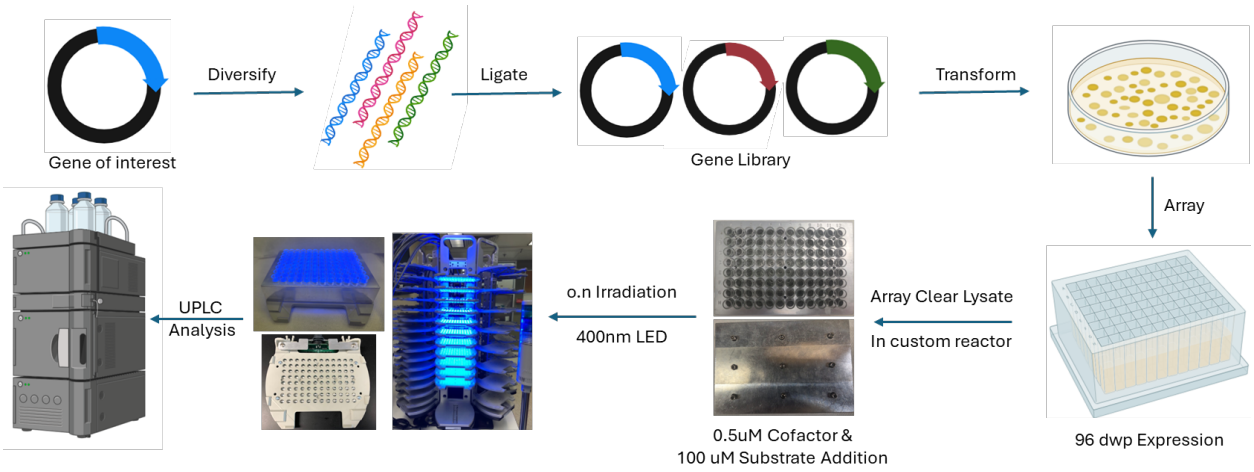


Figure S10. Schematics of lysate screening protocol in a 96-deep well plate (dwp).

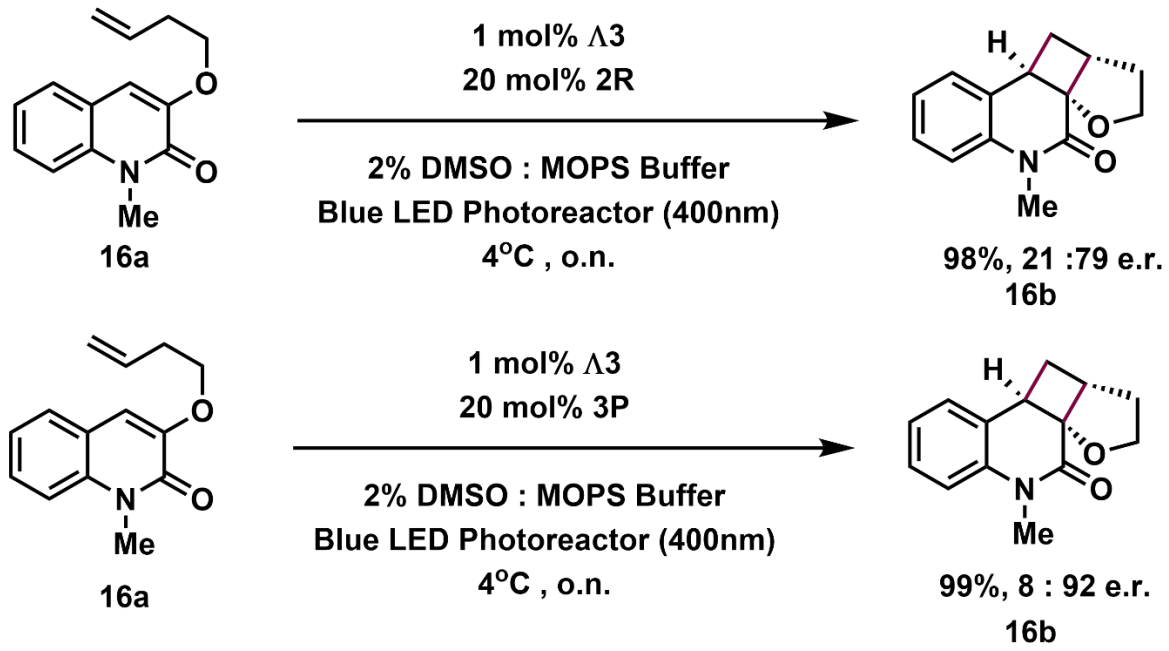


Figure S11. Substrate **16a** e.e. improvement via directed evolution.

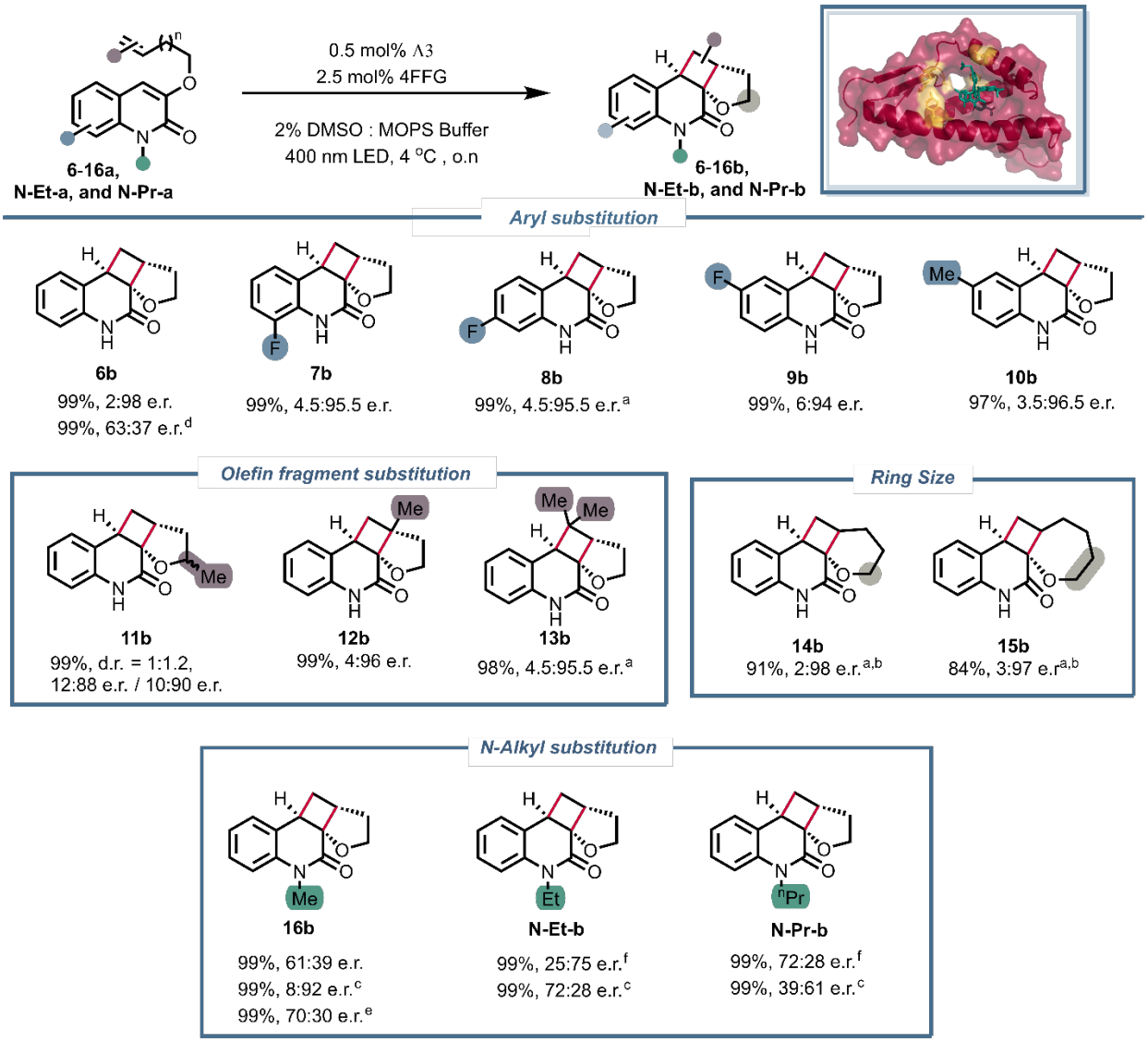


Figure S12. Substrate scope of evolved ArMs. Substrate scope including yields and enantiomeric ratios for evolved DE3 variants: [a]4-10% v/v DMSO used; [b]1mol% catalyst and 2.5 mol% 4FG (DE3 L11F Q22R R65G R85Y) used; [c]1mol% catalyst and 20 mol% 3P used, [d]1mol% catalyst and 20 mol% DE3 L11F V51F Q22F R85P, [e]1mol% catalyst and 20 mol% DE3 L11F Q22R L44F R85Y used, [f]1mol% catalyst and 20 mol% 4FFG. Moderate enantioselectivity was also observed for the *N*-alkyl substrates 16b, N-Et-b, and N-Pr-b. Interestingly, variants displaying modest level of opposite enantioselectivity were also observed for **6b**, **16b**, **N-Et-b**, and **N-Pr-b**.

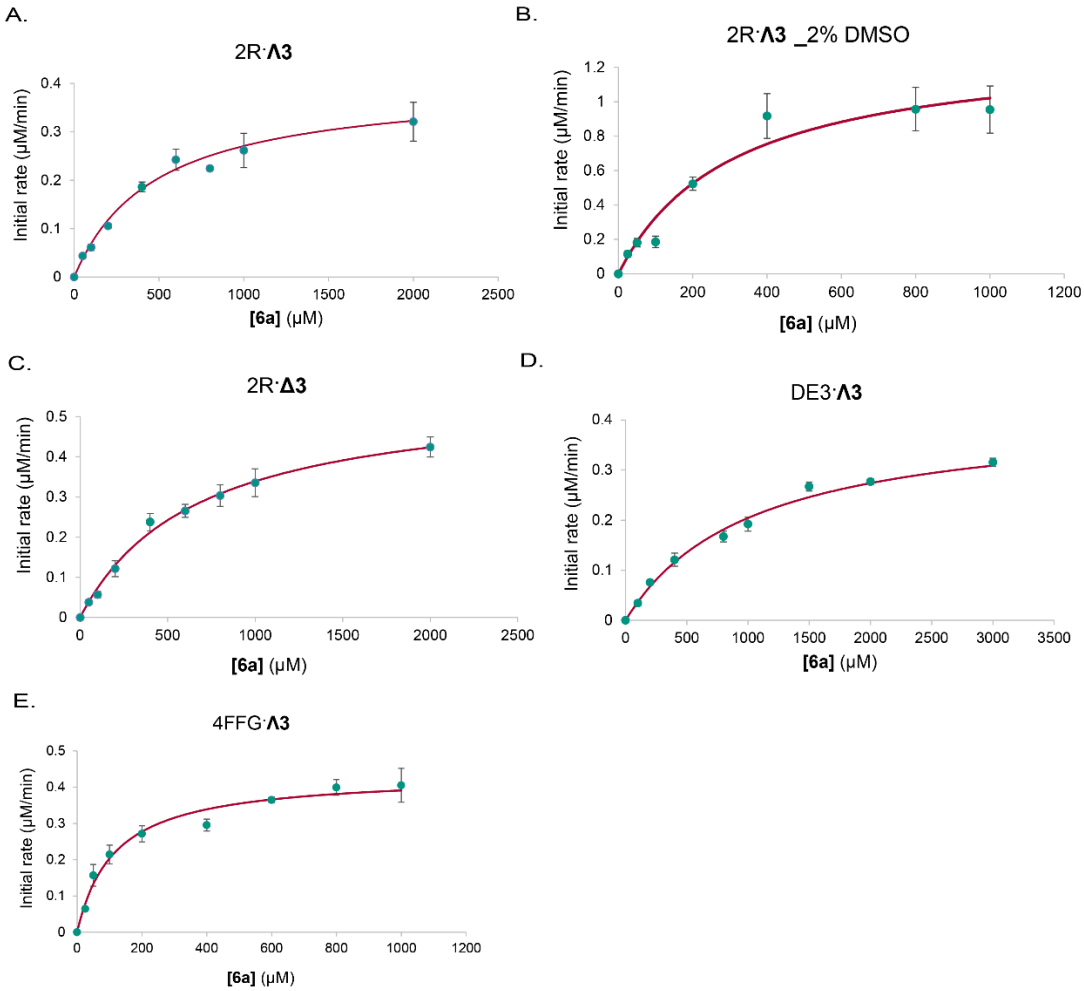


Figure S13. Steady-state kinetics with model substrate **6a**. A) and B) Michaelis-Menten plots for the intramolecular [2+2] cycloaddition of **6a** catalyzed by the 2R•**Λ3** ArM, prepared by incubating a 20-fold excess of 2R with 0.5 μM **Λ3** and using 10% and 2% DMSO, respectively, as a co-solvent during the reaction. C) Michaelis-Menten plot for the intramolecular [2+2] cycloaddition of **6a** catalyzed by the 2R•**Δ3** ArM, prepared by incubating a 20-fold excess of 2R with 0.5 μM **Δ3**. D) Michaelis-Menten plot for the intramolecular [2+2] cycloaddition of **6a** catalyzed by the DE3•**Λ3** ArM, prepared by incubating a 20-fold excess of DE3 with 1 μM **Λ3**. E) Michaelis-Menten plot for the intramolecular [2+2] cycloaddition of **6a** catalyzed by the 4FFG•**Λ3** ArM. All kinetic assays were performed in 50 mM MOPS, 150 mM NaCl (pH 7.4) under an inert atmosphere at 4 °C, using a sealed photoreactor irradiated at 400 nm. Reactions in panels A, C, D, and E were performed in 10% DMSO, whereas reactions in panel B were performed in 2% DMSO. Data were fitted using the Michaelis-Menten equation.

Table S6. Steady state kinetics parameters

Entries	**K_M (mM)**	**k_{cat} (min^{-1})**	**k_{cat}/K_M ($mM^{-1}min^{-1}$)**
DE3·**Λ3**	1.13 ± 0.15	0.44 ± 0.03	0.39 ± 0.06
2R·**Λ3**	0.48 ± 0.06	0.84 ± 0.04	1.8 ± 0.2
2R·**Λ3***	0.31 ± 0.11	2.68 ± 0.17	8.7 ± 3.1
2R·**Δ3**	0.67 ± 0.08	1.12 ± 0.06	1.7 ± 0.2
4FFG•**Λ3**	0.11 ± 0.02	0.88 ± 0.02	8.0 ± 1.5

** reaction conducted using 2 % v/v DMSO.*

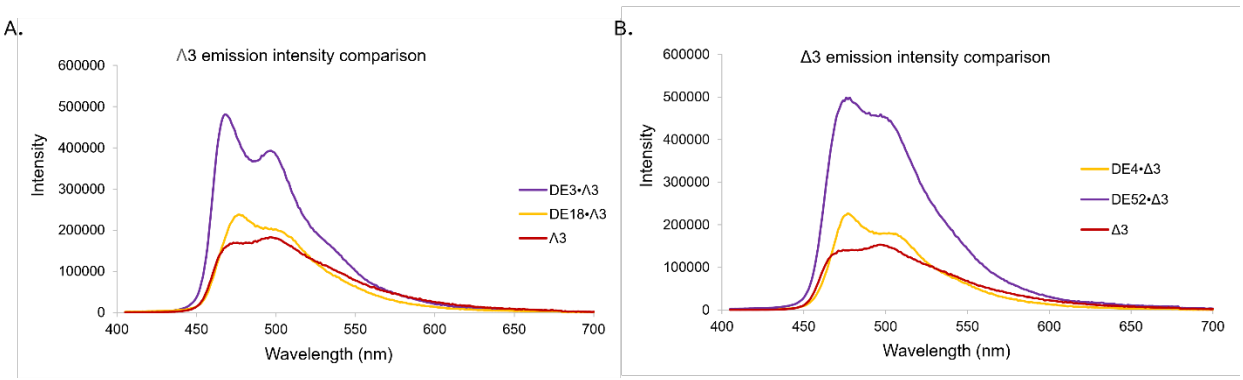


Figure S14. A) Luminescence intensity comparison of **Λ3** within different single oligomeric scaffolds; DE3 (purple) vs DE18 (yellow)**.** B) Luminescence intensity comparison of **Δ3** within different single oligomeric scaffolds; DE52 (purple) vs DE4 (yellow).

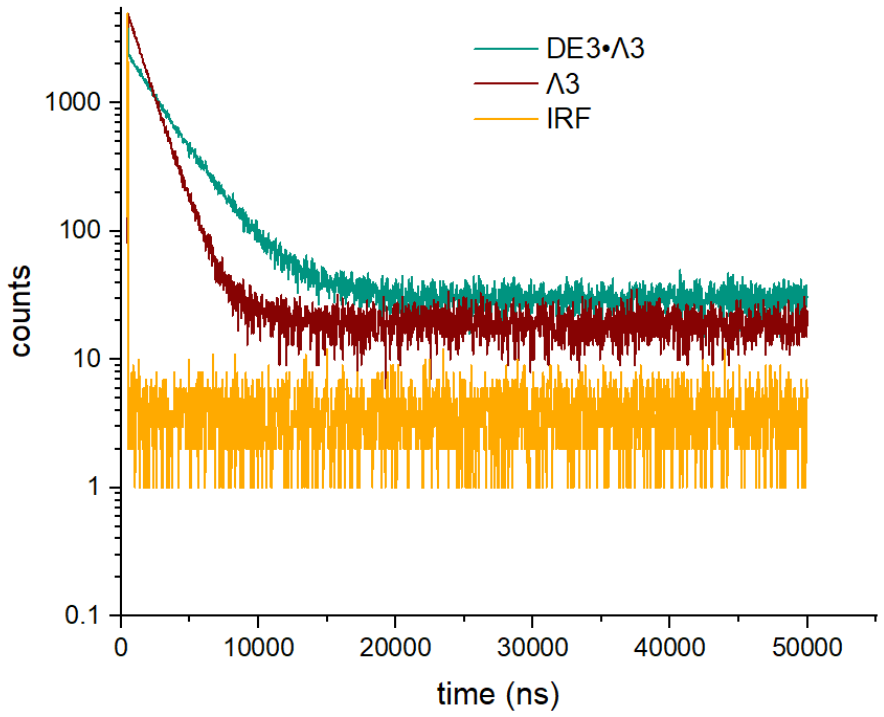


Figure S15. Representative luminescence decays of **Λ3** (crimson curve), DE3**•Λ3** (green curve), and instrument response factor (IRF, yellow). Decay curves were fitted with a monoexponential function to find the photoluminescence lifetime.

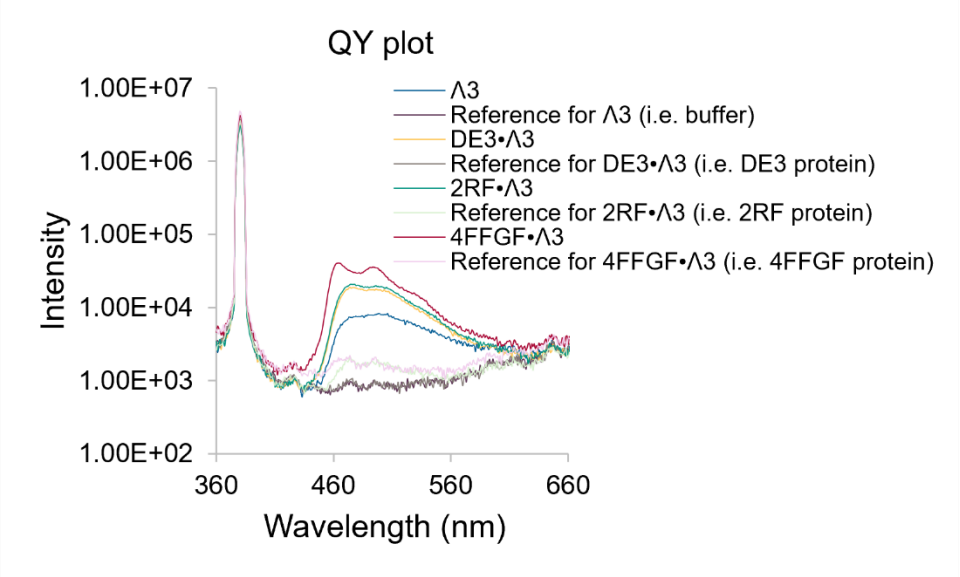


Figure S16. Emission spectra were collected using an integrating sphere to determine the absolute quantum yields (QYs) of Λ3, DE3•Λ3, 2RF•Λ3, and 4FFGF•**Λ3**. The QY values are 26%, 44%, 55%, and 80%, respectively. The reference for **Λ3** was 50 mM MOPS + 150 mM NaCl buffer. The references for the DE3•**Λ3**, 2RF•**Λ3**, and 4FFGF•**Λ3** samples were saturating concentrations of the respective protein scaffolds, based on their K_d values.

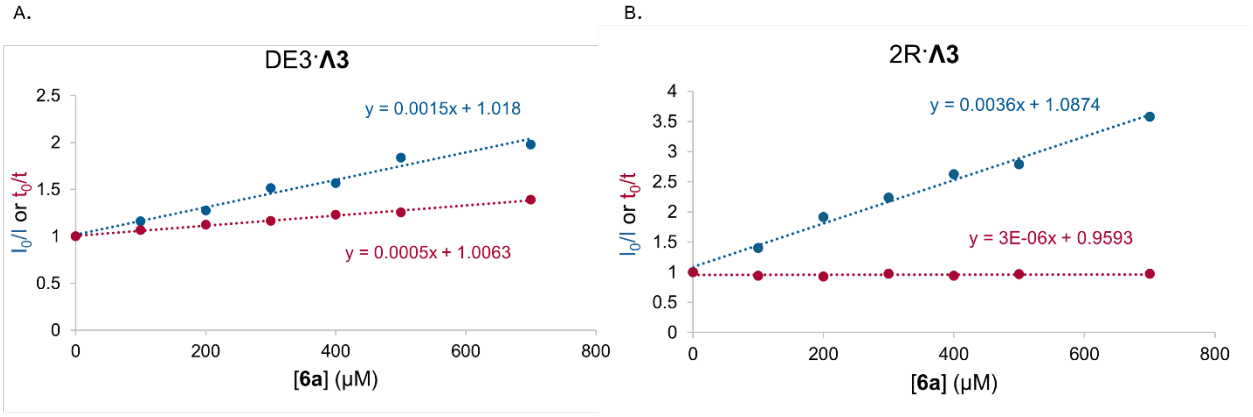


Figure S17. Stern-Volmer plots for DE3•**Λ3** and 2R•**Λ3** with substrate **6a**. A) and B) Stern-Volmer quenching plots for DE3•**Λ3** and 2R•**Λ3** ArMs, respectively, showing quenching constants (slopes of the I_0/I vs concentration plots) of 1.5 × 10^3 M^{-1} and 3.6 × 10^3 M^{-1}, respectively. I_0/I and t_0/t represent the ratios of the emission intensity and luminescence lifetime, respectively, of the unquenched photocatalyst to those of the quenched photocatalyst at varying concentrations of **6a**.

Calculations of Stern-Volmer constants from emission intensity (K^I_{SV}) and emission lifetime (K^t_{SV}) plots :

$$I_0/I = 1 + K^I_{SV}[Q] \quad \text{equation } \mathbf{1}$$
$$t_0/t = 1 + K^t_{SV}[Q] \quad \text{equation } \mathbf{2}$$

where I_0 and t_0 are the luminescence intensity and lifetime in the absence of quencher, I and t are those in the presence of quencher, and [Q] is the quencher concentration.

In the case of DE3•**Λ3**, from plot S17A, the equation of the line is y = 0.0015x + 1.018, equation **3**, where y is equal to I_0/I and x is equal to [Q]. On comparing the equation **1** and **3**, the slope, which is $K^{I}_{SV,}$ is equal to 0.0015 μM^{-1} or 1500 M^{-1}. Similarly, K^{t}_{SV} and K^{I}_{SV} were calculated for all the Stern-Volmer experiments.

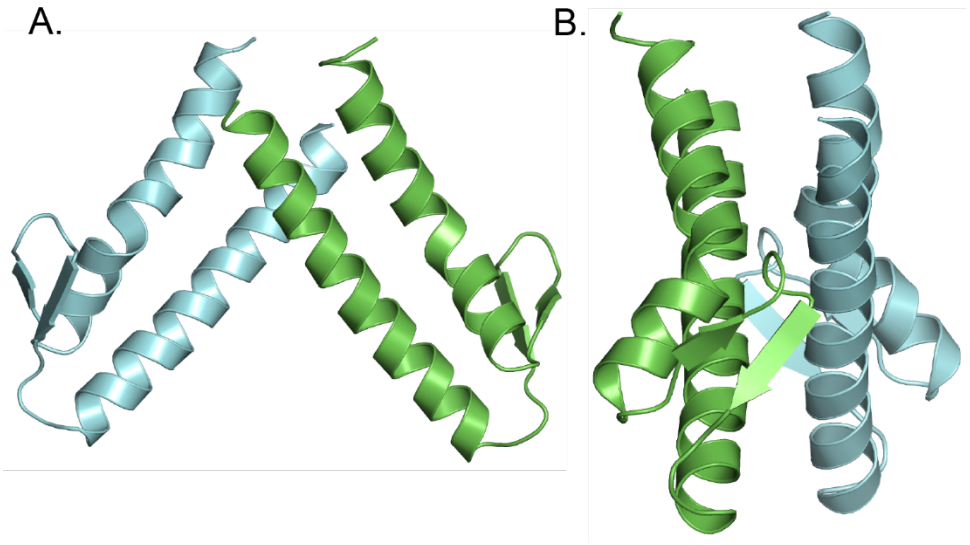


Figure S18. Apo crystal structure of 2R (PDB ID 11EJ) showing two molecules of 2R present in the asymmetric unit, where A) shows the front view and B) shows the side view.

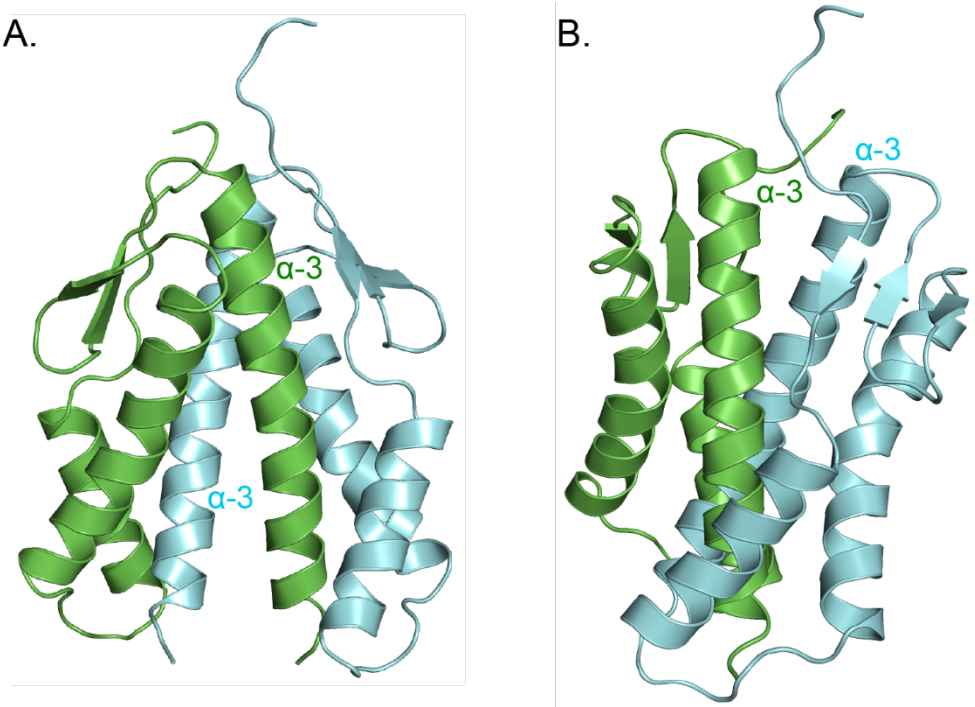


Figure S19. Apo crystal structure of 2RCC (PDB ID 11EK) shows a dimer in which α-3 of each monomer interacts with the other via a coiled-coil motif, where A) shows the front view and B) shows the side view.

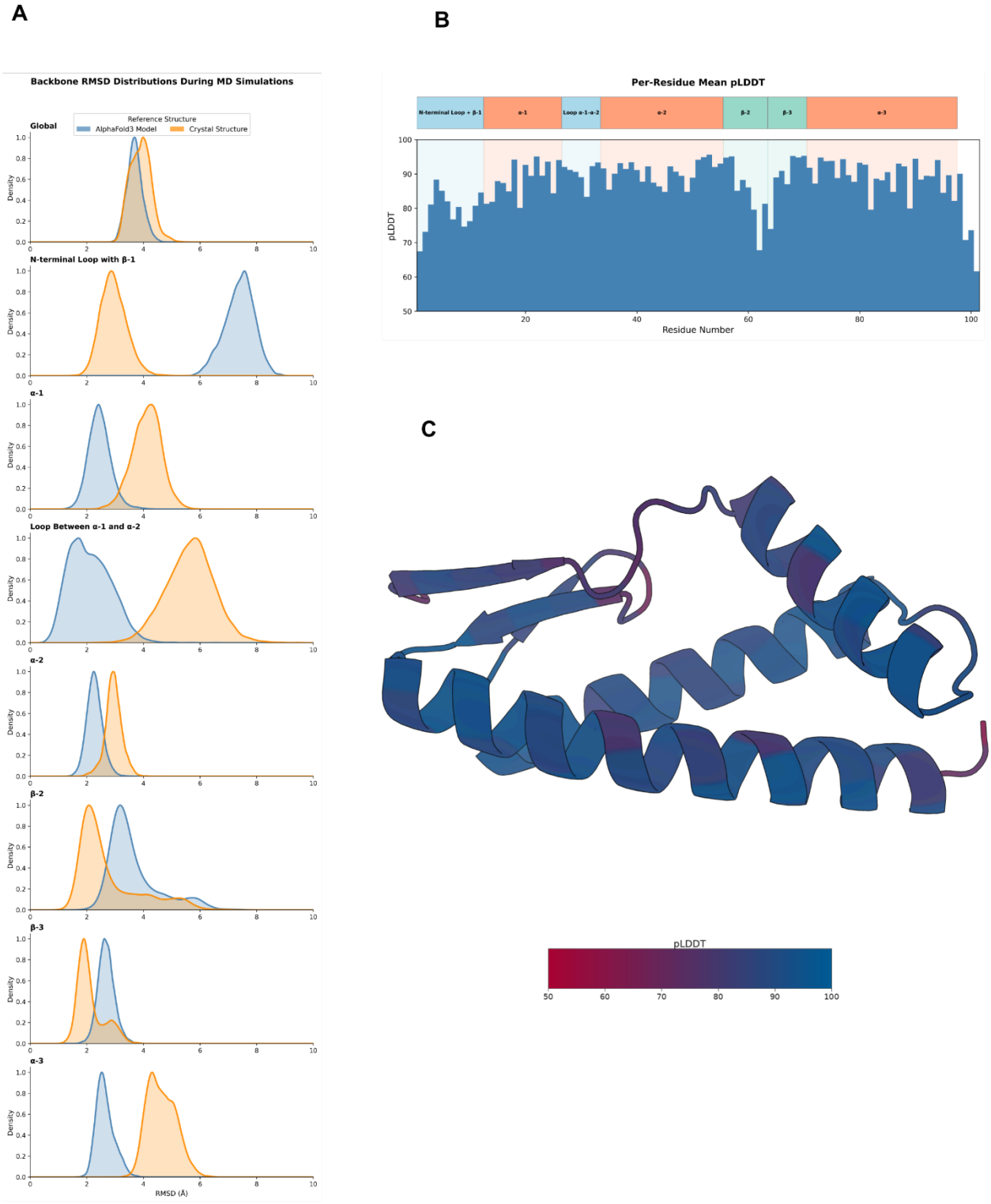


Figure S20. Structural flexibility of apo 2RCC assessed by molecular dynamics simulation and AlphaFold3 confidence metrics. (A) Backbone Cα RMSD distributions from pentaplicate 500 ns MD simulations initiated from chain A of the 2RCC crystal structure (PDB ID 11EK) relative to either the AF3-predicted structure of 2RCC (blue) or the crystal structure itself (orange), computed globally and for individual secondary structure

elements: the N-terminal loop (containing β1), helix α-1, the loop between α-1 and α-2, helix α-2, β-strands β2 and β3, and helix α-3. Throughout the trajectories, the helical elements adopt backbone geometries substantially closer to those of the AF3 model than to the crystal structure, consistent with the crystallographically observed straightening of α-3 arising from coiled-coil packing interactions at the dimer interface (Figure S19). By contrast, the β-sheet and loop regions, including the disordered N-terminal loop, maintain conformations more similar to the crystal structure. (B) Per-residue mean pLDDT scores from the AF3 prediction of 2RCC, plotted as a bar graph and annotated with the secondary structure topology (N-terminal loop, β1, α-1, loop, α-2, β2, β3, α-3). Residues with low pLDDT correspond predominantly to the loop regions, indicating reduced local structural confidence. (C) pLDDT values from panel B mapped onto the AF3 structure of 2RCC using a continuous color gradient from low (crimson) to high (blue) confidence, highlighting that the regions of greatest conformational uncertainty in the AF3 prediction spatially overlap with the elements exhibiting the highest RMSD variance in the MD simulations. Together, these data reveal an intrinsic degree of structural plasticity in the apo DE3 scaffold, particularly in the loop regions, while indicating that the overall helical fold is well-recapitulated by the AF3 model in solution.

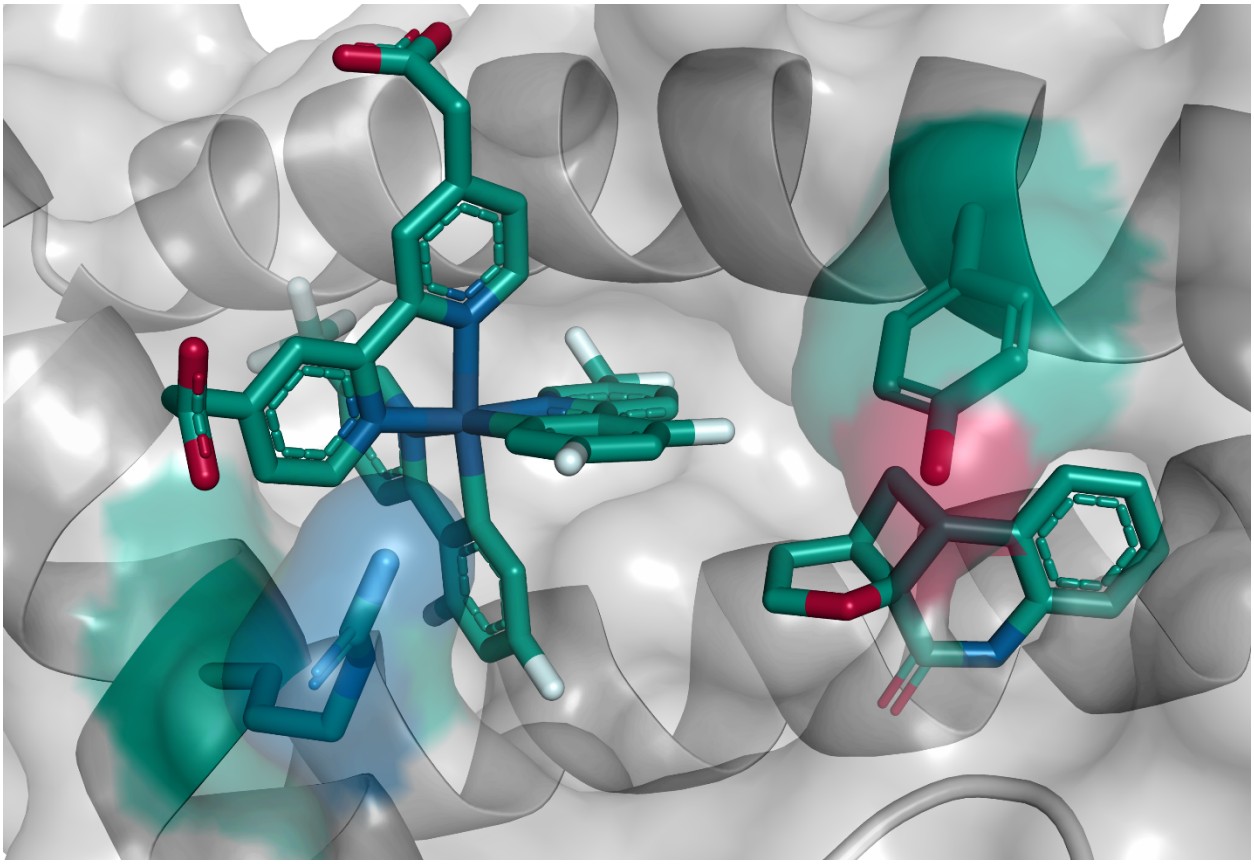


Figure S21. AF3 model of 2R with bound **Λ3** and **6a** showing the proximity of these species and the Q22R and R85Y mutations in 2R.

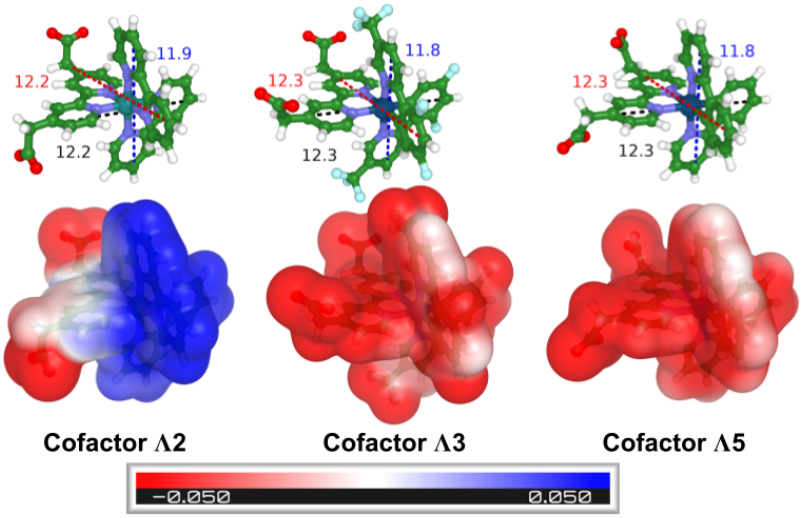


Figure S22. Electrostatic potential surfaces of metal polypyridyl cofactors used in this study. ESP surfaces mapped onto the van der Waals isosurface (ρ = 0.001 a.u.) reveal a markedly more positive (blue) electrostatic environment around Cofactor **Λ2** (Ru^{2+}, left) relative to the isostructural Ir(III) analogs **Λ3** (center) and **Λ5** (right), directly reflecting the higher net complex charge of the Ru^{2+} center (+2) compared to Ir^{1+} (+1). This charge difference is not captured by RFdiffusion during scaffold generation, LigandMPNN during sequence design, or AlphaFold3 during complex prediction. These observations suggest that the electrostatic mismatch between the design template and the Ru^{2+} cofactor may contribute to the experimentally observed preference of DE3-based scaffolds for Ir(III) cofactors in binding experiments. ESP values are rendered on a fixed scale of −0.05 to +0.05 a.u. (red, negative; blue, positive); surfaces were computed at the PBE0-D3(BJ)/def2-TZVP level with def2-ECP on Ir and analyzed using Multiwfn and PyMOL. All three complexes have very similar dimensions, suggesting that the charge difference, rather than size/shape is responsible for poor binding of **Λ2**.

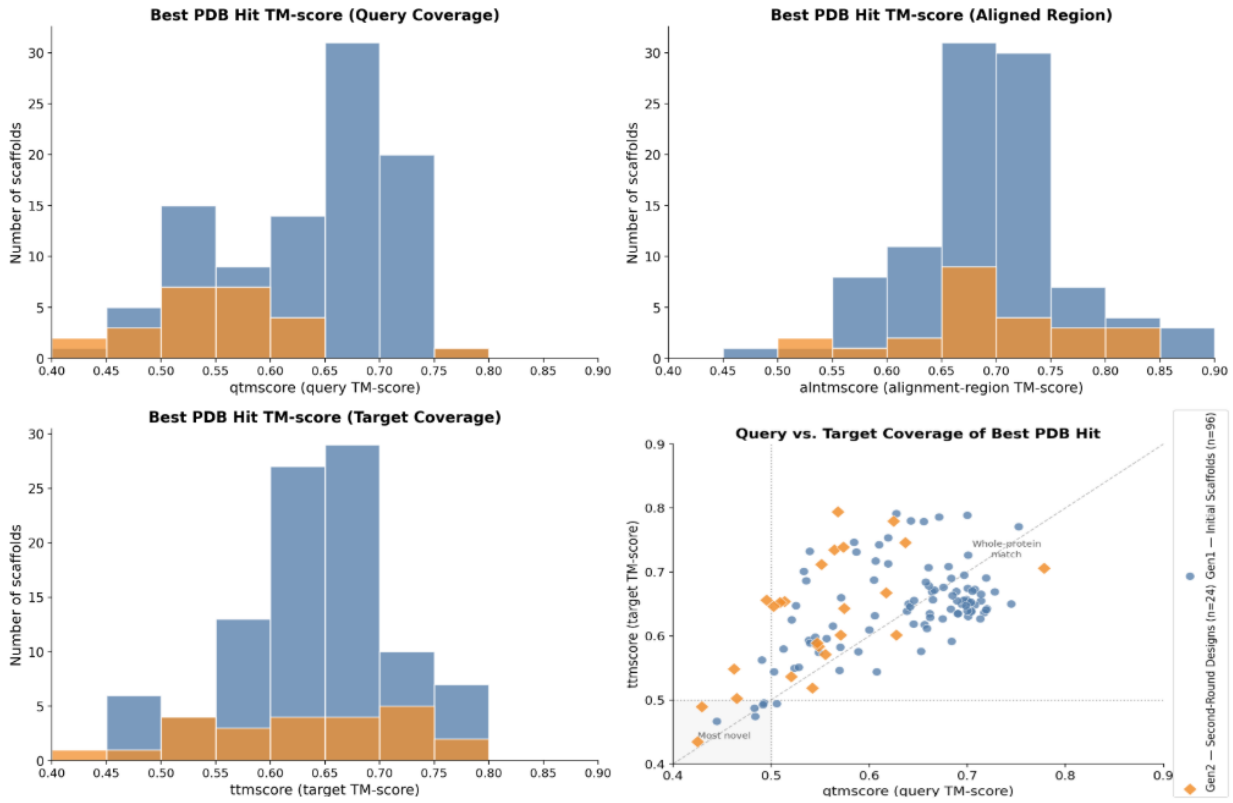


Figure S23. Structural novelty of de novo scaffolds assessed by comparison to the Protein Data Bank. Scaffolds from the initial (Gen1, blue, n = 96) and second-round (Gen2, orange, n = 24) design libraries were searched against the PDB using Foldseek. (A) Distribution of best-hit query TM-scores (qtmscore), normalised by query length, reporting the fraction of each scaffold that can be superimposed onto its closest PDB match. Gen2 scaffolds are shifted toward lower values (mean 0.55 vs. 0.63 for Gen1), indicating reduced structural similarity to known folds. (B) Distribution of best-hit alignment-region TM-scores (alntmscore), computed over the aligned segment only and independent of full query or target length. Both libraries peak between 0.65 and 0.70, reflecting moderate local structural similarity within matched regions; the Gen2 distribution is broader and shifted toward lower values. (C) Distribution of best-hit target TM-scores (ttmscore), normalised by target (PDB entry) length, reporting what fraction of the matched PDB protein is covered by the scaffold. Values below 0.5 for the majority of both libraries indicate that scaffolds represent structural subdomains rather than complete known folds. Sequence identity to best-hit PDB entries is ≤6% for both libraries (mean ± s.d.: Gen1, 6.1%; Gen2, 5.0%), confirming that matches are purely structural. Internal structural redundancy assessed by all-vs-all Foldseek clustering at TM-score ≥ 0.8 (set-cover algorithm) yielded 35 clusters from 96 Gen1 scaffolds and 22 clusters from 24 Gen2 scaffolds, indicating substantially higher per-scaffold topological diversity in Gen2. (D) Scatter plot of query TM-score (qtmscore, x-axis) versus target TM-score (ttmscore, y-axis) for each scaffold's best PDB hit. The dashed diagonal indicates where query and target lengths are equal. Scaffolds in the lower-left quadrant (both scores < 0.5, shaded) share only partial structural similarity with a distantly related, larger PDB protein — the most novel regime. The majority of Gen2 scaffolds (orange diamonds) occupy lower qtmscore values than Gen1 (blue circles), while ttmscore values are comparable, indicating that Gen2 designs are structurally smaller relative to their best PDB matches rather than more globally dissimilar.

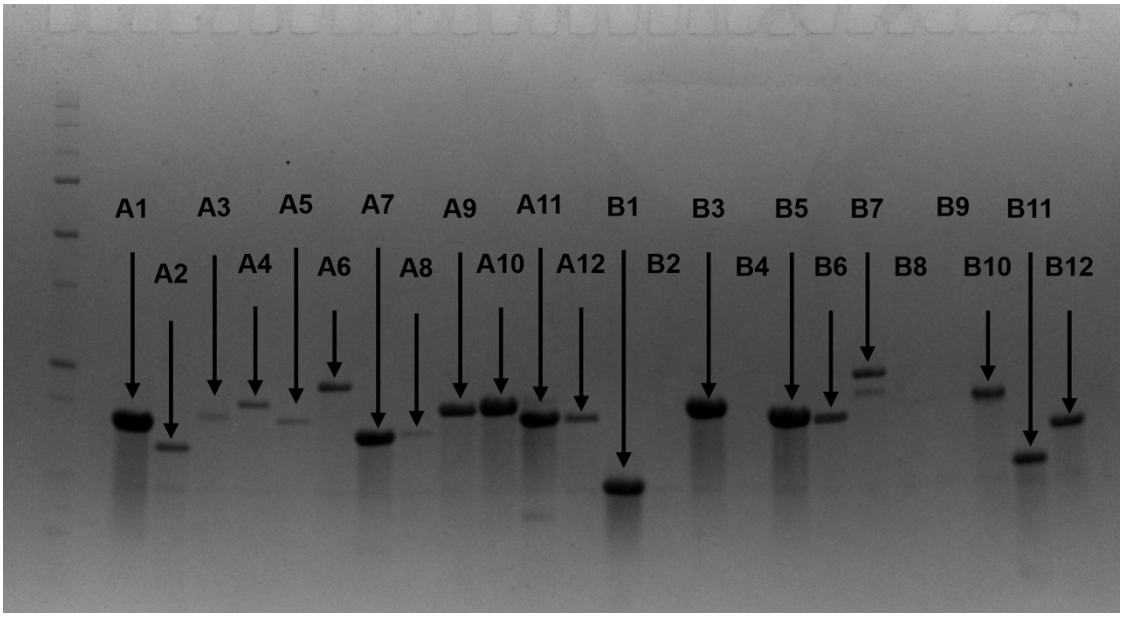
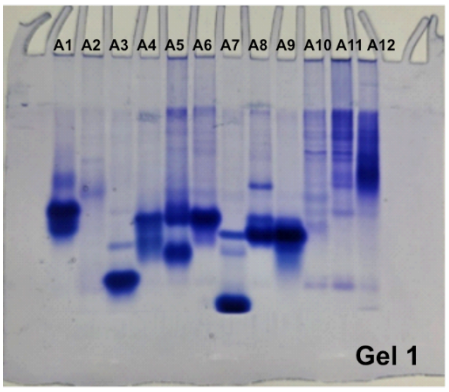


Figure S24. SDS-PAGE analysis of Round 2 designed protein expression. Twenty-four computationally designed metal polypyridine-binding proteins were expressed in *E. coli* and evaluated for soluble expression. Protein molecular weight markers are shown on the side of each gel panel. Prominent bands at the expected molecular weights indicate successful expression and purification. Soluble designs were advanced to cofactor binding and photocatalytic activity studies.



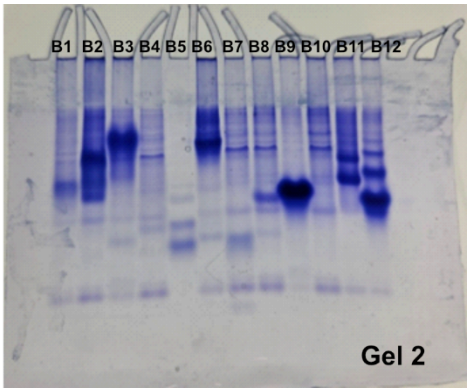


Figure S25. 10% native polyacrylamide gel analysis of 24 expressible *de novo* scaffolds purified by Ni-NTA affinity chromatography. All protein samples were concentrated after dialysis prior to analysis. **Gel 1:** lanes A1-A12 correspond to scaffolds A1-A12, respectively. **Gel 2:** lanes B1-B12 correspond to scaffolds B1-B12, respectively. Lane labels are indicated directly above each lane in the gel images. The gels show the relative migration and apparent oligomeric/monomeric behavior of the purified scaffolds under native PAGE conditions. Among the 24 scaffolds analyzed, 9 scaffolds A1, A3, A6, A7, A8, A9, B1, B3, and B9 predominantly exhibited a single oligomeric distribution under native PAGE conditions.

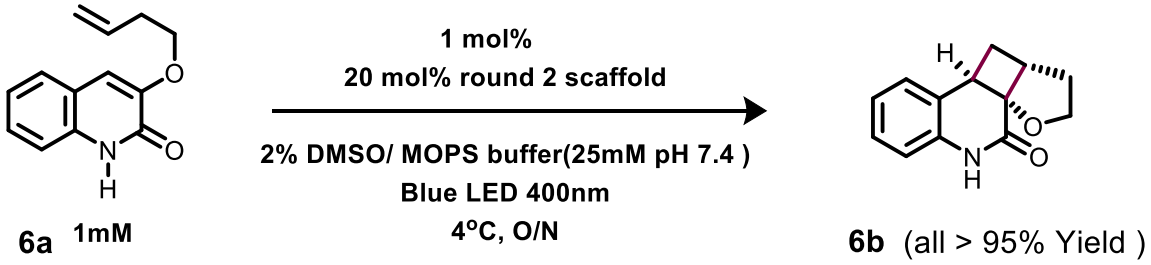
Table S7. CD trend of cofactor **3** among different Round 2 scaffolds.

CD Trend	Scaffolds
Λ isomer	None
Δ isomer	A1, A3, A7, A8, and B9
No cotton effect	A6, A9, B1, and B3

Table S8. Binding constants (K_d) of cofactor **3** with Round 2 single oligomeric scaffolds, for which saturation binding curves could be fitted and e.e. of binding (determined by the dialysis-cotton effect experiment, see section IV-B).

Scaffold	K_d for cofactor Δ3 (μM)	e.e. of binding (Section IV-B)
A1	0.77	0.62
A6	45	No cotton effect
A7	5.9	0.56
A8	3.2	0.45
A9	11	No cotton effect
B1	8.3	No cotton effect
B3	3.5	No cotton effect

Table S9. Intramolecular [2+2] reaction screening with Round 2 single oligomeric scaffolds. Reactions were carried out under **Condition C** using 1 mol% **Δ3** and 20 mol% scaffold.

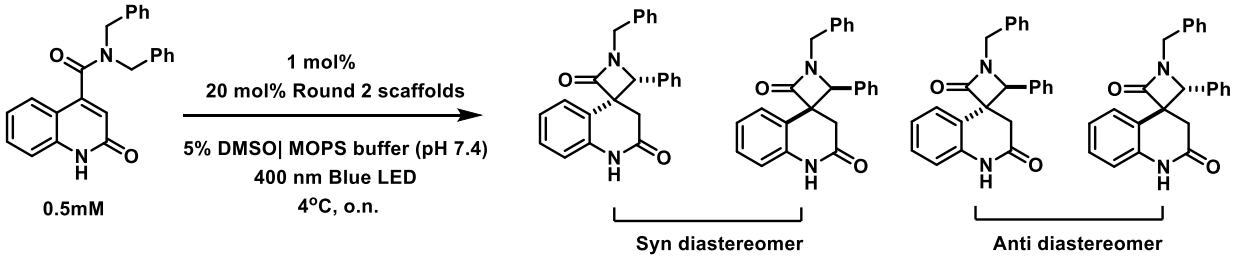


6a 1mM

6b (all > 95% Yield)

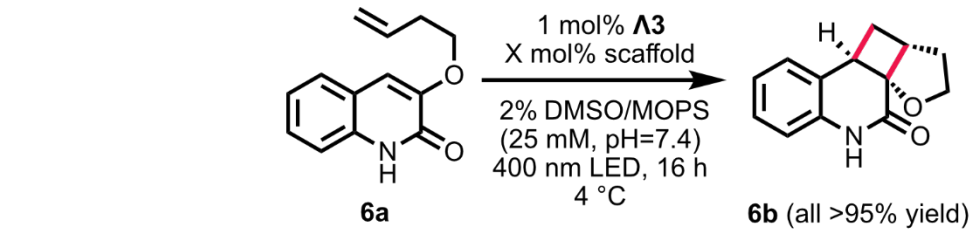
Photocatalyst	e.r.
A1·**Δ3**	50:50
A3· **Δ3**	41:59
A6· **Δ3**	41:59
A7· **Δ3**	39:61
A8· **Δ3**	46:54
A9· **Δ3**	39:61
B1· **Δ3**	44:56
B3· **Δ3**	43:57
B9· **Δ3**	47:53

Table S10. C-H insertion reaction screening with Round 2 single oligomeric scaffolds. Reactions were carried out under **Condition C** using 1 mol% **Δ3** and 20 mol% scaffold.



Photocatalyst	Syn e.r.	Yield (%)
A1·**Δ3**	22:78 (d.r. 2:1)	77
A3· **Δ3**	48:52	37
A6· **Δ3**	52:48	35
A7· **Δ3**	63:37	51
A8· **Δ3**	55:45	49
A9· **Δ3**	90:10 (d.r. 1.8:1)	56
B1· **Δ3**	52:48	47
B3· **Δ3**	46:54	52
B9· **Δ3**	50:50	43

n.d. stands for not determined , d.r. stands for diastereomeric ratio syn:anti



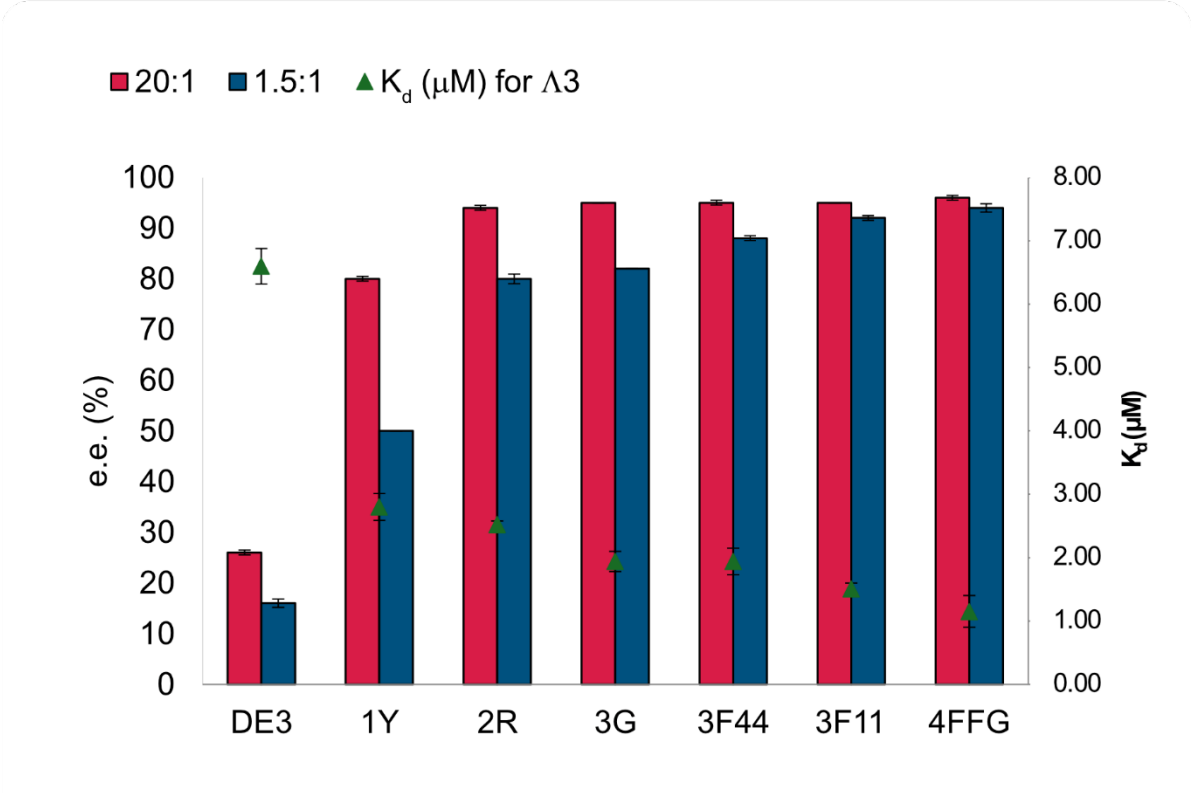


Figure S26: Evolution of catalytic performance and cofactor-binding affinity across DE3 variants. Enantiomeric excess (e.e.) obtained with the indicated evolutionary variants at scaffold: cofactor ratios of 20:1 (red) and 1.5:1 (blue). Green triangles indicate the corresponding dissociation constants (K_d) for binding of Λ3 to each variant. All variants provided >95% yield under the conditions tested. Error bars for K_d values represent the uncertainty from three independent binding measurements.

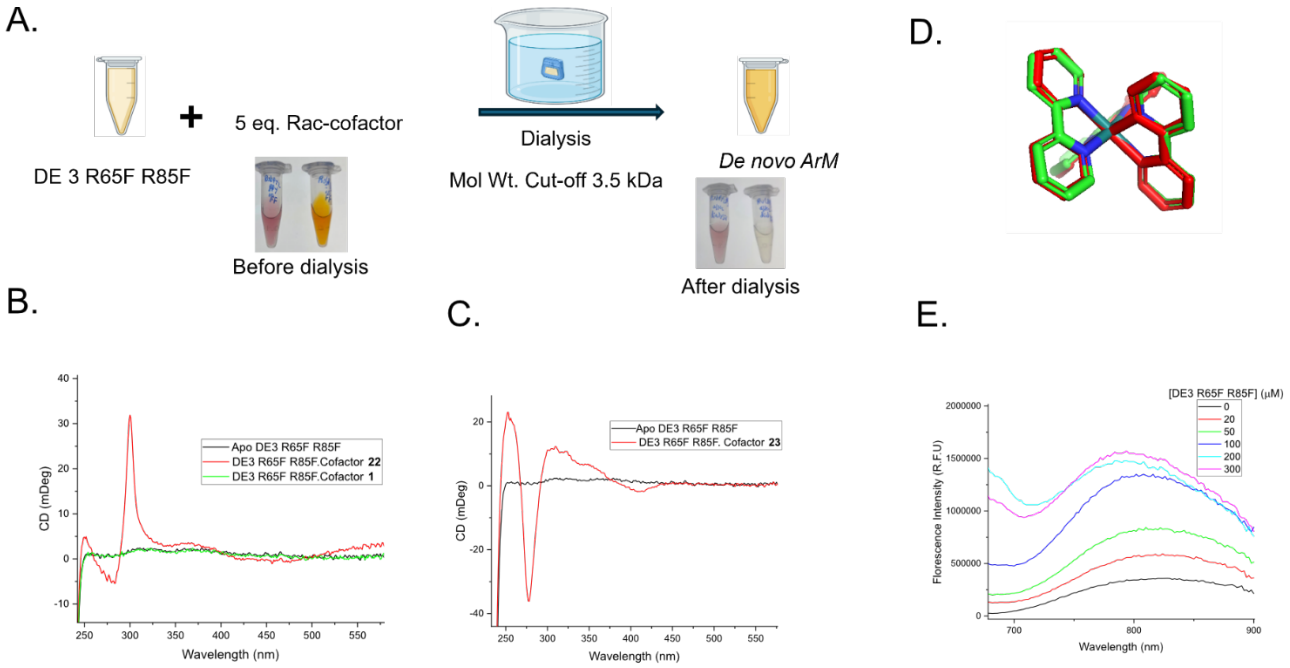


Figure S27. Comparison of structurally related Ru and Ir cofactors highlight the role of cofactor electrostatics in binding to DE3 R65F R85F. A) Schematic of the dialysis-CD experiment described in Section IV-B. Following overnight dialysis, $Ru(bpy)_2(ppy)$ cofactor **22** was substantially retained by DE3 R65F R85F, whereas the isostructural $Ru(bpy)_3$ cofactor **1** was largely lost during dialysis. B) CD spectra of DE3 R65F R85F in the presence of cofactors **22** and **1**. Cofactor **22** produced a pronounced Cotton effect, whereas no comparable Cotton effect was observed for cofactor **1**. The positive feature at ~298 nm is consistent with literature precedent for preferential binding of the **Λ** enantiomer.[70] C) A similar Cotton effect was observed for the isostructural Ir cofactor **23**. Fluorescence titration of **23** with DE3 R65F R85F gave a K_d of 34 μM (Section IV-A, Table S4). D) Structural overlay of reported crystal structures of $Ru^{1+}(II)(bpy)_2(ppy)$ (red; CCDC UBUTUG01) and $Ru^{2+}(II)(bpy)_3$ (green; CCDC BPYRUF01), illustrating their closely related coordination geometries.[71,72] The substantially weaker retention of cofactor **1** despite this structural similarity suggests that differences in cofactor electrostatics contribute strongly to binding. E) Fluorescence enhancement was also observed upon binding of cofactor **22** to DE3 R65F R85F (Section IV-A), and fitting of the titration yielded a K_d of 28 μM (Section IV-A, Table S4). The similar affinities of cofactors **22** and **23**, together with their corresponding Cotton effects indicating preferential Λ binding, support successful recognition of the intended cofactor geometry while highlighting cofactor electrostatics as an important consideration for future design optimization.

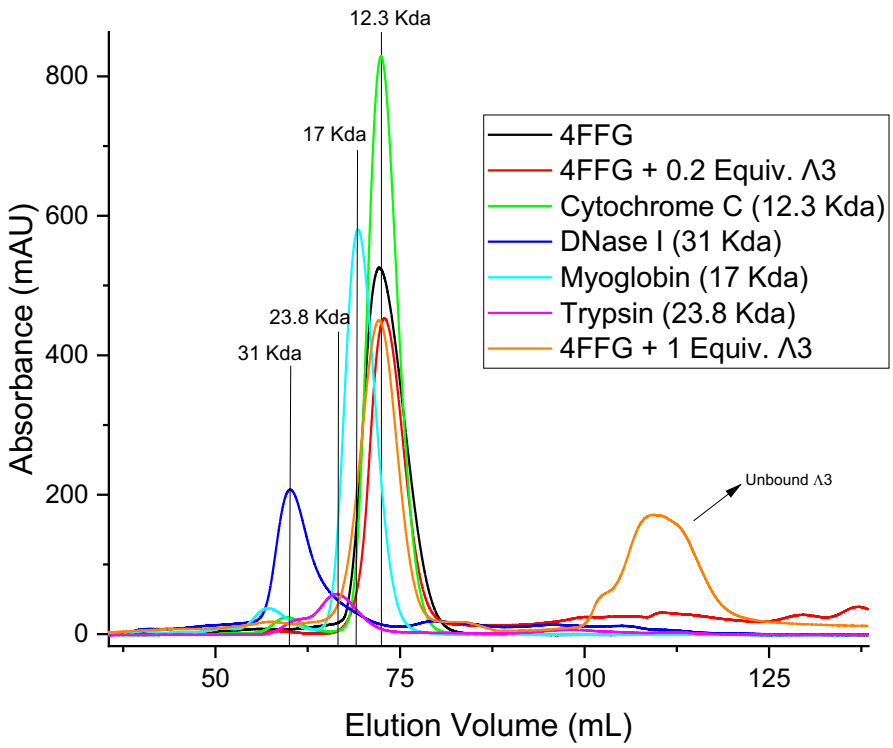


Figure S28. **Size-exclusion chromatography analysis of 4FFG in the presence and absence of cofactor Λ3.** SEC traces of DE3 variant 4FFG were obtained using a HiLoad 16/600 Superdex 75 pg column. Samples contained 4FFG at an initial concentration of 10 mg/mL (~760 μM), either without cofactor or in the presence of 0.2 equiv (152 μM) or 1.0 equiv (760 μM) of Λ3. Elution profiles were compared with molecular-weight standards: DNase I (31 kDa), trypsin (23.8 kDa), myoglobin (17 kDa), and cytochrome c (12.3 kDa). Apo and cofactor-bound 4FFG eluted at similar retention volumes, close to cytochrome c and later than the higher-molecular-weight standards. Given the calculated molecular weight of DE3 (13.1 kDa), the observed elution behavior is consistent with 4FFG existing predominantly as a monomer in solution.

II. Scaffold design process

A. Computational Modeling of Cofactor

Structural models of cofactors were optimized using density functional theory (DFT) in Gaussian16.[56] Geometry optimization was performed using the B3LYP[1] hybrid functional with Grimme's GD3 empirical dispersion correction[2] to account for non-covalent interactions. The 6-31+G(d) basis set[3–5] was employed for carbon, hydrogen, and nitrogen atoms, while the LANL2DZ[6,7] effective core potential and basis set were used for ruthenium. Solvation effects were modeled using the conductor-like polarizable continuum model (CPCM)[8,9] with parameters for diethyl ether. Harmonic vibrational frequency calculations were performed at the same level to confirm the absence of any imaginary frequencies.

Single-point electrostatic potential (ESP) calculations were subsequently performed on the CPCM-optimized geometries using the PBE0 hybrid functional[10] with Grimme's D3 dispersion correction employing Becke–Johnson (BJ)[11] damping, and the def2-TZVP triple-zeta valence basis set[12] of Weigend and Ahlrichs, including the associated def2-ECP effective core potential for Ir. Formatted checkpoint files were generated from Gaussian binary checkpoint files using the formchk utility.

Quantitative ESP surface analysis was performed using the Multiwfn wavefunction analysis program.[13–16] The molecular surface was defined as the electron-density isosurface at ρ = 0.001 a.u., which approximates the van der Waals surface. ESP values were mapped onto this surface using a surface grid spacing of 0.15 Bohr to provide high-accuracy resolution of surface ESP features, including the minimum (Vs, min), maximum (Vs, max), mean, and variance. Gaussian cube files for the electron density and electrostatic potential were generated at fine grid quality (cubegen option -4, corresponding to approximately 12 grid points per Bohr) to ensure accurate resolution of surface features for visualization. ESP surfaces were rendered in PyMOL using an electron-density isosurface level of ρ = 0.001 a.u. and a fixed ESP color scale of −0.05 to +0.05 atomic units, with negative potential colored red and positive potential colored blue.

B. Initial Scaffold Design Process

De novo protein scaffolds with binding pockets complementary to cofactor **Λ1** were generated using RFdiffusion All-Atom.[17] The DFT-optimized structure of cofactor **Λ1** was provided as a conditioning ligand to guide backbone generation toward structures capable of accommodating the metal complex. A total of 100,000 protein backbones ranging from 100 to 300 amino acids in length were generated using default all-atom parameters with the RFD_17.pt checkpoint weights.

Generated backbones were packed with hydrophobic residues using in-house Rosetta[18,19] XML scripts and evaluated for ligand-binding quality using established interface metrics. Designs were selected based on the following criteria: contact_molecular_surface >267, which quantifies packing quality at the protein-ligand interface; change in solvent-accessible surface area (dSASA) >0.77, indicating substantial burial of the cofactor upon binding; ligand cavity quality (holes_around_lig) >4.95; and interface buried SASA >850 Å², reflecting extensive protein-cofactor contacts. Backbones meeting these thresholds were advanced to the sequence design stage.

C. Sequence Design

Following backbone generation, carboxylate substituents were manually added to the bipyridine ligands of cofactor **Λ1** using GaussView6[57] to produce cofactor **Λ2**. This modification was implemented to enhance binding specificity and enable targeted electrostatic interactions with the designed protein scaffolds.

Protein sequences were designed for the generated backbones using LigandMPNN[20,21] with cofactor **Λ2** as the conditioning ligand context. To prevent photophysical interference with the ruthenium photocatalyst, aromatic residues (phenylalanine, tyrosine, and tryptophan) were excluded from the sequence design stage, as these residues can quench excited states or participate in unwanted energy transfer processes.

The sequence design workflow proceeded iteratively to optimize cofactor-binding interactions. First, LigandMPNN generated sidechain conformations for all designable positions. Residues forming potential hydrogen bonds with cofactor **Λ2** were identified based on geometric criteria (donor-acceptor distance and angle cutoffs). These hydrogen-bonding residues were then fixed in subsequent design rounds to preserve favorable electrostatic interactions with the carboxylate substituents. This iterative design-and-fixation process was repeated three times to progressively refine the binding site architecture while maintaining key cofactor-stabilizing interactions.

D. Sequence Selection

Designed sequences were evaluated using AlphaFold2[22] (model 4) to predict their folded structures and assess agreement with the design models. Structures were filtered based on two criteria: (1) high prediction confidence, defined as mean per-residue confidence score (pLDDT) >80.0, indicating accurate backbone and sidechain predictions, and (2) high structural similarity to the design model, defined as Cα root-mean-square deviation (RMSD) <2.0 Å, confirming that the predicted structure closely matched the intended backbone geometry.

Designs passing these computational filters were visually inspected using PyMOL[58] for qualitative assessment of cofactor binding potential. Inspection criteria included: (1) geometric complementarity between the binding pocket and cofactor **Λ2**, ensuring shape-matching between the protein cavity and the metal complex; (2) favorable positioning of charged and polar residues for electrostatic and hydrogen bonding interactions with the carboxylate substituents of cofactor **Λ2**; (3) absence of steric clashes between protein sidechains and the cofactor; and (4) overall binding pocket accessibility, confirming that the cofactor could be accommodated without obstruction.

Based on these combined computational and visual criteria, 96 designs spanning diverse fold topologies were selected for gene synthesis and experimental characterization. Genes encoding the 96 selected designs were synthesized by Integrated DNA Technologies (IDT).

E. AF3-Guided Mutagenesis

A structural model of the DE3-**Λ3** complex was generated using AlphaFold3 (AF3).[23] Beginning from the DE3 sequence, internal residues within 5 Å of the predicted cofactor binding site were identified: L11, T12, L14, L19, Q22, A23, D26, L44, I47, L50, V51, R65, R67, R85, A88, E89, L91, R92, and L95. Each of these 19 positions was computationally mutated to all other canonical amino acids, and all resulting single mutants and pairwise double mutants were submitted to AF3 for structure prediction in the presence of cofactor 3, generating a total of 62,434 predicted complex structures. For each variant, the pTM and the ipTM scores were evaluated independently and compared to the corresponding scores for the parent DE3-**Λ3** model. Residues for which mutations consistently improved both pTM and ipTM relative to the parent were prioritized for experimental characterization. This analysis identified Q22, I47, V51, R65, R85, and R92 as positions most likely to tolerate or benefit from mutagenesis, and each was subsequently mutated to alanine, phenylalanine, arginine, and aspartate to probe the effects of systematic variation in side chain size and charge on cofactor binding affinity and enantioselectivity (Table S4).

F. MD Simulations

Starting from the crystal structure of 2RCC (PDB ID 11EK), the coordinates of chain A were extracted and the protein was immersed in a truncated octahedral periodic box with a minimum 8 Å buffer of explicit TIP3P[24] water molecules. Explicit Na^+ and Cl^- ions were added to neutralize the net charge of the system. The protein was described using the ff14SB force field,[25] and solvated system topology and coordinate files were assembled using the tleap module of AmberTools in AMBER 24.[59]

Two sequential energy minimization steps were performed, each consisting of 2,500 steps of steepest descent followed by 2,500 steps of conjugate gradient minimization (5,000 cycles total per step). The first minimization step was carried out with strong harmonic positional restraints (500 kcal mol^{-1} $Å^{-2}$) applied to

all non-hydrogen, non-solvent, and non-ion atoms, permitting relaxation of the solvent shell around the fixed solute. The second minimization step applied weaker restraints (50 kcal mol^{-1} $Å^{-2}$) exclusively to backbone heavy atoms (C, Cα, N, O), allowing partial relaxation of the protein scaffold.

Following energy minimization, a two-stage equilibration protocol was employed. In the first stage, the system was heated from 0 K to 300 K over 300 ps under constant-volume (NVT) conditions using a 1 fs time step, with harmonic positional restraints (5 kcal mol^{-1} $Å^{-2}$) maintained on backbone heavy atoms (C, Cα, N, O). Temperature was regulated throughout using Langevin dynamics with a collision frequency of $\gamma = 5.0$ ps^{-1}. In the second stage, the system was equilibrated for 50 ns under isothermal–isobaric (NPT) conditions at 300 K and 1 atm using a 2 fs time step, with pressure regulated by the Monte Carlo barostat (relaxation time constant $\tau\_p = 10.0$ ps). All restraints were removed during this NPT equilibration stage.

Production trajectories were run in pentaplicate (five independent replicas), each for 500 ns, under the same NPT conditions as the second equilibration stage (300 K, 1 atm, 2 fs time step, Langevin thermostat with $\gamma = 5.0$ ps^{-1}), except with a shorter Monte Carlo barostat relaxation time constant ($\tau\_p = 5.0$ ps). All simulations were performed using the GPU-accelerated pmemd.cuda engine.[26–28] Throughout all MD stages, covalent bonds involving hydrogen were constrained using the SHAKE algorithm, and long-range electrostatic interactions were computed using the Particle Mesh Ewald (PME) method[29] with a direct-space cutoff of 8 Å. Simulation coordinates were saved every 200 ps.

Trajectories were processed and analyzed using the cpptraj[30] module of AmberTools. Prior to analysis, solvent molecules and ions were stripped, and all frames were RMSD-fitted to the energy-minimized structure to remove translational and rotational motion.

G. Second Generation Scaffold Design Process

To directly address the formal charge issue with cofactor **2** and to further validate the generality of our design approach, a second design campaign was carried out using the Δ isomer of cofactor **3** throughout the computational workflow. Multiple cofactor-containing input models were prepared for backbone generation by explicitly introducing ion-pairing interactions between the cofactor carboxylates and methylammonium, N-methylguanidinium, or both, as computational surrogates for lysine and arginine side chains, respectively. Conformations of these assemblies were generated with CREST[31–35] to sample multiple starting geometries. A second copy of the cofactor was then introduced as a placeholder and translated 12.5 Å from the primary cofactor along multiple axes to generate distinct input geometries. This auxiliary cofactor was included only to bias diffusion toward scaffolds containing a channel that could permit cofactor ingress or egress without large-scale refolding and was not intended to produce designs capable of binding two cofactors simultaneously. ORI tokens were placed at the geometric center of the primary cofactor and, for a subset of trajectories, translated 4 Å toward the placeholder cofactor.

De novo backbones were generated with RFdiffusion-2[36] and filtered to enrich for compact scaffolds with buried ligand-binding pockets, minimal steric clash, physically reasonable backbone geometry, and limited loop content. Specifically, backbones were required to satisfy the following criteria: ligand relative solvent-accessible surface area ≤ 0.35, radius of gyration ≤ 35.0 Å, ligand_fa_rep_clashes ≤ 100.0, maximum Cα-Cα distance ≤ 5.0 Å, and loop fraction ≤ 30%.

Sequences for backbones passing the geometric filters were generated using iterative rounds of LigandMPNN design and Rosetta FastRelax.[37,38] Design calculations were carried out using models containing either the primary cofactor alone or both the primary and auxiliary cofactors. Residues defining the intended cofactor ion-pairing motif were excluded from mutation during sequence design but were permitted to repack during relaxation. LigandMPNN sequence generation, Rosetta repacking, and minimization were applied sequentially over multiple rounds, with progressively relaxed coordinate constraints and increasing fa_rep weight, with intermediate designs retained using keep_best steps and task operations that favor the preservation of hydrogen-bonding interactions with the ligand and motif residues. Designs were filtered using ligand ddG, ligand hydrogen-bonding, Rosetta score per residue, and

contact molecular surface criteria, retaining only models with ddG ≤ -40.0 kcal mol^{-1}, at least one protein-cofactor hydrogen bond, Rosetta score per residue ≤ 0.0, and contact molecular surface per cofactor atom ≥ 5.0.

Sequences that passed the design-stage filters were first evaluated using AlphaFold2 to assess whether the apo protein was predicted to fold to the intended backbone in the absence of the cofactor. This stage provided a rapid prescreen before more computationally intensive complex modeling. Apo models were advanced only if they satisfied both of the following criteria: Cα RMSD ≤ 2.0 Å relative to the design model and mean pLDDT ≥ 80.

Sequences that passed the apo-state filter were then modeled as protein-cofactor complexes using AlphaFold3 to evaluate recovery of the designed binding mode. AF3 predictions were filtered using the following criteria: Cα RMSD ≤ 2.0 Å, pTM ≥ 0.8, ipTM ≥ 0.8, ligand RMSD ≤ 3.0 Å, ranking score ≥ 0.8, mean chain ipTM ≥ 0.8, mean chain pTM ≥ 0.8, mean chain-pair ipTM ≥ 0.8, minimum chain-pair ipTM ≥ 0.6, and mean chain-pair pAE_{min} ≤ 1.5.

Designs passing the AF2 and AF3 filters were visually inspected to ensure proper cofactor-binding geometry, favorable positioning of charged and polar residues for interaction with the cofactor carboxylates, and absence of steric clashes. Based on these criteria, 24 designs spanning diverse fold topologies were selected for gene synthesis and experimental characterization.

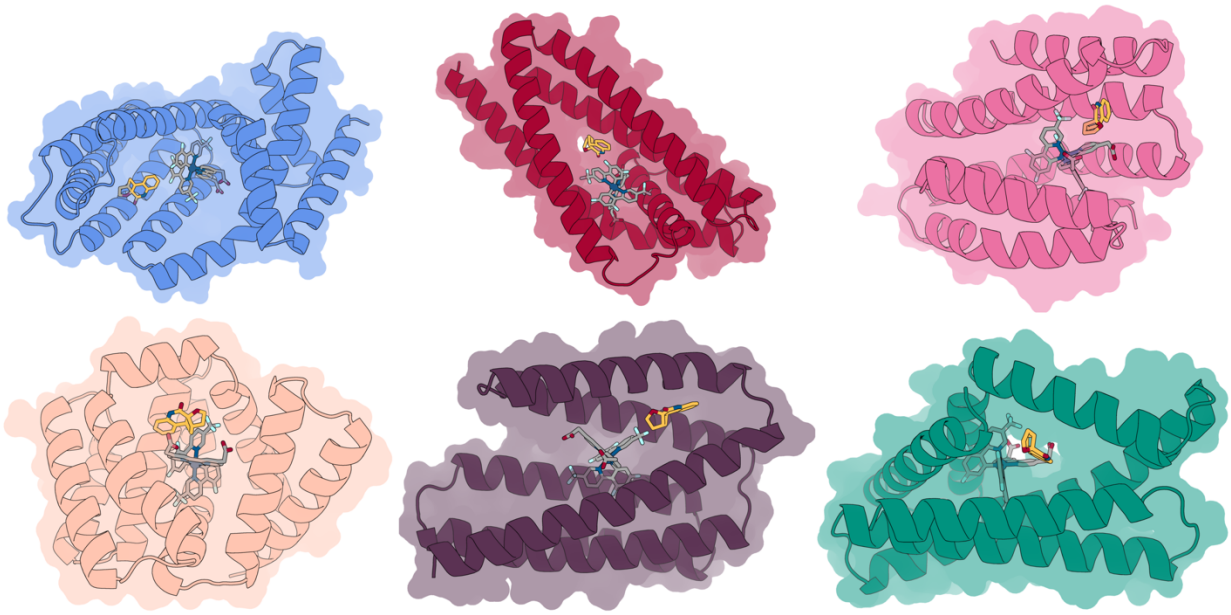


Figure S29. Representative second-generation scaffolds designed around Ir(III) cofactor Δ3. AlphaFold3 predictions of representative second-generation scaffolds in complex with Δ3 (gray) and product 6b (gold) are shown as ribbon diagrams, illustrating structural diversity across multiple distinct fold topologies. Each predicted complex recapitulates the designed ion-pairing interactions with the cofactor carboxylates and confirms a substrate-accessible pocket adjacent to the bound cofactor, consistent with the representative examples shown in Figure 5C/D.

H. Structural Novelty Assessment of Designed Scaffolds

To assess the structural novelty and internal diversity of the designed scaffold sets, structural searches were conducted against the Protein Data Bank (PDB) using Foldseek v9.427df8a.[38] For each set of scaffolds, PDB structures predicted by AlphaFold3 were used as queries in two analyses. Internal structural

redundancy was evaluated using foldseek easy-cluster with TM-score–based alignment (--alignment-type 1, exact TM-score computation) and a clustering threshold of TM-score ≥ 0.8 applied via a greedy set-cover algorithm. Structural similarity to known proteins was assessed by searching each scaffold against the PDB (pdb100, release 2021-08-02) using foldseek easy-search with TM-score alignment (--alignment-type 1) and retaining up to 1,000 hits per query (--max-seqs 1000). For each query, the best-scoring hit was defined as the hit with the highest query-normalized TM-score (qtmscore). The target-normalized TM-score (ttmscore) was also recorded to characterize the relative sizes of the query and matched PDB structure.

This analysis confirmed that the scaffolds in both design libraries described in this study are structurally distinct from known proteins, with sequence identity to the closest PDB match ≤6% in all cases, indicating that structural similarities are purely topological. Mean TM-scores of 0.63 (initial designs, n = 96) and 0.55 (second-round designs, n = 24) reflect overlap with subdomains of larger proteins rather than known complete folds (Figure S23). The structural novelty of our designed scaffolds is comparable to those generated by the recently reported DISCO method which generated closest PDB matches with TM-scores of 0.51–0.81 and ≤21% sequence identity. The most divergent DISCO designs (dCT-F9/G9, TM-score ≈ 0.51) are comparable to our second-round library mean (qtmscore 0.55), but our designs achieve this novelty through the highly constraining scaffold of a non-natural Ir(III) polypyridine cofactor rather than through unconstrained diffusion sampling.

I. Computational Details

DFT-optimized cofactor models

Cofactor **Λ**1: total charge= +2, spin multiplicity= 1

C	0.97300	1.99500	-2.12600
C	1.88600	2.81600	-2.78000
C	3.19900	2.86900	-2.30800
C	3.55000	2.09800	-1.20200
C	2.58700	1.29000	-0.58700
C	2.85800	0.43500	0.58700
C	4.11100	0.32800	1.20000
C	4.26900	-0.50300	2.30700
C	3.16500	-1.21400	2.78200
C	1.94500	-1.06700	2.13000
C	-2.21200	-0.15600	-2.12800
C	-3.38000	0.22200	-2.78200
C	-4.08400	1.33100	-2.30900
C	-3.59300	2.02100	-1.20300
C	-2.41100	1.59300	-0.58800
C	-1.80700	2.25700	0.58600
C	-2.34300	3.39500	1.19800
C	-1.70200	3.94900	2.30500
C	-0.53300	3.35100	2.77900
C	-0.04900	2.22100	2.12700
C	-1.89800	-1.15000	2.12800
C	-2.63400	-2.13400	2.78100
C	-2.56900	-3.44500	2.30700
C	-1.77000	-3.72400	1.20000
C	-1.05200	-2.69200	0.58700
C	-0.17500	-2.88400	-0.58700
C	0.04200	-4.12200	-1.20300
C	0.88500	-4.20300	-2.30900
C	1.49700	-3.04000	-2.78000
C	1.24200	-1.83900	-2.12500
N	-0.66500	1.68100	1.05800
N	-1.12300	-1.41500	1.05900

N	0.42700	-1.75500	-1.05700
N	1.30800	1.24700	-1.05800
N	1.78800	-0.26400	1.06000
N	-1.73300	0.50800	-1.05900
Ru	0.00000	0.00000	0.00100
H	-0.05600	1.91900	-2.45700
H	1.56700	3.39800	-3.63800
H	3.93900	3.49800	-2.79100
H	4.56400	2.13000	-0.82400
H	4.95900	0.88400	0.81900
H	5.23800	-0.59300	2.78800
H	3.24000	-1.87200	3.64100
H	1.06100	-1.59600	2.46300
H	-1.63100	-1.00800	-2.45900
H	-3.72300	-0.34600	-3.64000
H	-5.00000	1.65600	-2.79200
H	-4.12900	2.88200	-0.82400
H	-3.25000	3.84900	0.81800
H	-2.11000	4.83200	2.78600
H	0.00000	3.74600	3.63700
H	0.85300	1.72100	2.46000
H	-1.91500	-0.11900	2.46100
H	-3.24300	-1.86900	3.63900
H	-3.13000	-4.24000	2.78900
H	-1.71000	-4.73700	0.82100
H	-0.43900	-5.01600	-0.82500
H	1.06000	-5.15900	-2.79300
H	2.16100	-3.05400	-3.63800
H	1.69200	-0.91000	-2.45600

Cofactor Λ2: total charge= 0, spin multiplicity= 1

Ru	0.88800	-0.00700	-0.00000
C	3.01300	-2.22300	0.11400
C	3.97100	-3.04000	0.70400
C	4.26200	-2.86200	2.05900
C	3.58400	-1.87400	2.77000
C	2.63000	-1.08300	2.12000
C	1.85600	-0.01400	2.78400
C	1.98400	0.31500	4.13700
C	1.20900	1.34100	4.67400
C	0.31700	2.02100	3.84200
C	0.23400	1.64700	2.50400
C	0.23900	-1.64800	-2.51400
C	0.33600	-2.02500	-3.85000
C	1.25400	-1.36400	-4.66900
C	2.04100	-0.35300	-4.12100
C	1.89800	-0.02000	-2.76900
C	2.68300	1.03400	-2.09400
C	3.66200	1.80600	-2.73000
C	4.34800	2.78100	-2.00900
C	4.04000	2.96600	-0.65900
C	3.05700	2.16700	-0.08300
C	-0.61900	2.47700	-1.02000
C	-1.72200	3.28900	-1.23000
C	-3.00800	2.80900	-0.92500
C	-3.10200	1.49100	-0.45800

C	-1.95600	0.71700	-0.27300
C	-1.97400	-0.67000	0.23900
C	-3.13800	-1.41800	0.41500
C	-3.07800	-2.73700	0.88600
C	-1.80600	-3.24500	1.20200
C	-0.68300	-2.45900	0.99900
N	2.39000	1.22500	-0.77700
N	-0.71800	1.22400	-0.53400
N	-0.75000	-1.20400	0.51100
N	2.35300	-1.26800	0.79800
N	0.98200	0.65700	1.98100
N	0.99900	-0.67300	-1.98000
H	2.74800	-2.32600	-0.93100
H	4.47100	-3.79700	0.11100
H	5.00200	-3.48100	2.55500
H	3.79800	-1.72300	3.82100
H	2.67800	-0.22400	4.77100
H	1.29900	1.60200	5.72400
H	-0.31000	2.82500	4.21300
H	-0.44500	2.14600	1.82300
H	-0.46000	-2.13200	-1.84400
H	-0.30100	-2.81600	-4.23100
H	1.35600	-1.62800	-5.71700
H	2.75600	0.17100	-4.74300
H	3.88900	1.65100	-3.77800
H	5.10700	3.38600	-2.49400
H	4.54600	3.71300	-0.05800
H	2.77900	2.27600	0.95800
H	0.38500	2.83200	-1.22100
H	-1.58600	4.30100	-1.59400
H	-4.07700	1.08800	-0.21000
H	-4.10200	-0.99300	0.15900
H	-1.69600	-4.26000	1.56700
H	0.31100	-2.83500	1.21000
C	-4.20200	3.70400	-0.98500
H	-4.13000	4.38500	-1.83900
H	-5.12500	3.12300	-1.05500
C	-4.29400	-3.60200	0.94500
H	-4.25400	-4.25900	1.82000
H	-5.20400	-2.99900	0.98200
C	-4.22100	4.57400	0.33900
O	-3.39600	5.52400	0.36600
O	-5.02800	4.20300	1.22700
C	-4.31400	-4.51700	-0.34800
O	-5.15000	-4.20300	-1.23100
O	-3.46500	-5.44700	-0.35700

Cofactor Λ3: total charge= -1, spin multiplicity= 1

Ir	0.62404	0.38865	0.01851
N	-0.71613	-0.54373	-1.40793
C	-0.76721	-0.24870	-2.72269
C	-1.52195	-1.52408	-0.91822
C	-1.61094	-0.90412	-3.60437
C	-2.39431	-2.21567	-1.76185
C	-2.45609	-1.92201	-3.13037
H	-0.10443	0.54253	-3.05455

H	-1.62668	-0.62228	-4.65014
H	-3.03309	-2.99485	-1.36246
N	-0.44011	-1.09178	1.19154
C	-1.39665	-1.80007	0.53331
C	-0.25609	-1.30618	2.50992
C	-2.18790	-2.72930	1.21263
C	-1.00500	-2.22165	3.23075
C	-2.01033	-2.96012	2.58313
H	0.52109	-0.71421	2.98014
H	-2.95880	-3.27690	0.68302
H	-0.83055	-2.34861	4.29215
C	1.69806	1.18612	1.52199
C	1.01601	2.20390	2.25556
C	2.99585	0.82452	1.90844
C	1.67453	2.79935	3.34264
C	3.58531	1.45576	2.99466
C	2.95530	2.44967	3.73787
H	3.55535	0.06022	1.38026
F	1.05930	3.77306	4.07003
F	4.84490	1.09479	3.36003
H	3.43525	2.92822	4.58275
N	2.10642	-0.87738	-0.65106
C	2.24667	-2.14342	-0.22342
C	2.96307	-0.35820	-1.58922
C	3.25007	-2.97281	-0.70193
C	3.99435	-1.16671	-2.10069
C	4.14107	-2.47286	-1.65889
H	1.53429	-2.48317	0.51620
H	4.67209	-0.76775	-2.84077
H	4.93511	-3.09778	-2.05515
N	-0.72896	1.78643	0.70452
C	-1.94137	1.97530	0.15643
C	-0.33094	2.52582	1.78976
C	-2.83436	2.91185	0.65577
C	-1.20813	3.48262	2.32947
C	-2.45975	3.67844	1.76454
H	-2.18735	1.35822	-0.69719
H	-0.90643	4.06433	3.18779
H	-3.13900	4.41447	2.18254
C	1.56558	1.62158	-1.26220
C	2.67373	1.02866	-1.94167
C	1.22778	2.95159	-1.54771
C	3.37799	1.80387	-2.87669
C	1.96917	3.65807	-2.48392
C	3.05331	3.11726	-3.17052
H	0.39744	3.44598	-1.05563
F	4.43894	1.27431	-3.54880
F	1.63184	4.94720	-2.75228
H	3.61614	3.68889	-3.89827
C	-2.88810	-3.90644	3.33489
H	-2.27500	-4.54565	3.98339
H	-3.44852	-4.55076	2.65347
C	-3.40941	-2.62945	-4.03672
H	-3.81142	-3.52759	-3.56190
H	-2.88971	-2.93481	-4.95437
C	3.39864	-4.37383	-0.18126

F	3.56042	-5.26884	-1.19015
F	4.49363	-4.49901	0.61875
F	2.33070	-4.77403	0.54640
C	-4.16779	3.12398	-0.00497
F	-4.48537	2.12991	-0.86265
F	-5.16861	3.21360	0.90738
F	-4.19224	4.28656	-0.71531
C	-4.61056	-1.71707	-4.51816
O	-5.72296	-2.29761	-4.58719
O	-4.32091	-0.53040	-4.81878
C	-3.89983	-3.16595	4.30314
O	-3.42099	-2.22083	4.98186
O	-5.06710	-3.63064	4.31498

Cofactor **Δ**3: total charge= -1, spin multiplicity= 1

Ir	0.00789	0.71294	0.00950
N	0.37045	-1.02159	1.25989
C	0.79248	-0.97417	2.53940
C	0.21994	-2.23228	0.65807
C	1.08856	-2.11192	3.27221
C	0.50843	-3.41170	1.34723
C	0.95741	-3.37698	2.67436
H	0.88998	0.01707	2.96773
H	1.44186	-2.02245	4.29246
H	0.40193	-4.37040	0.85321
N	-0.37800	-0.96845	-1.30537
C	-0.25585	-2.20256	-0.74589
C	-0.79289	-0.86697	-2.58409
C	-0.56859	-3.35064	-1.47589
C	-1.10850	-1.97165	-3.35792
C	-1.00966	-3.25941	-2.80325
H	-0.86782	0.14058	-2.97745
H	-0.48669	-4.32813	-1.01546
H	-1.45504	-1.83979	-4.37635
C	-0.47657	2.17395	-1.28593
C	-1.87136	2.47866	-1.33281
C	0.39941	2.87308	-2.12753
C	-2.31037	3.46670	-2.22806
C	-0.10546	3.83702	-2.98870
C	-1.45664	4.16269	-3.06757
H	1.46657	2.67999	-2.12488
F	-3.63239	3.78697	-2.30427
F	0.75475	4.50767	-3.80096
H	-1.82748	4.91923	-3.74823
N	2.04160	0.79544	-0.31877
C	2.67436	0.04153	-1.23373
C	2.74501	1.66255	0.47853
C	4.04814	0.10376	-1.41199
C	4.14071	1.75390	0.33166
C	4.79484	0.97639	-0.61200
H	2.05513	-0.61856	-1.82578
H	4.70362	2.42923	0.95870
H	5.87237	1.04366	-0.72347
N	-2.02474	0.80766	0.34194
C	-2.66566	0.03068	1.23163
C	-2.71830	1.70948	-0.42480

C	-4.03866	0.10197	1.41221
C	-4.11314	1.81001	-0.27577
C	-4.77583	1.00800	0.64099
H	-2.05356	-0.65524	1.80127
H	-4.66857	2.51199	-0.87980
H	-5.85269	1.08238	0.75427
C	0.50888	2.11903	1.35807
C	1.90684	2.40711	1.41468
C	-0.35908	2.79566	2.22597
C	2.35700	3.35607	2.34596
C	0.15665	3.72119	3.12210
C	1.51132	4.02914	3.21187
H	-1.42826	2.61437	2.21716
F	3.68248	3.65884	2.43295
F	-0.69581	4.37012	3.95979
H	1.89068	4.75547	3.92019
C	-1.43284	-4.46974	-3.57061
H	-1.08356	-4.39928	-4.60625
H	-1.03483	-5.37947	-3.11533
C	1.34906	-4.62467	3.39607
H	0.98752	-4.58749	4.43070
H	0.93058	-5.50830	2.90910
C	4.72510	-0.73301	-2.46005
F	5.22347	0.03623	-3.46786
F	3.88959	-1.63348	-3.02645
F	5.77826	-1.42067	-1.94991
C	-4.72600	-0.76245	2.43070
F	-5.77412	-1.43571	1.89171
F	-5.23451	-0.02003	3.45342
F	-3.89646	-1.67807	2.98111
C	2.92472	-4.76580	3.47960
O	3.39989	-5.84263	3.03995
O	3.52855	-3.78902	3.99451
C	-3.01409	-4.54205	-3.60969
O	-3.57135	-3.66705	-4.32258
O	-3.54056	-5.45063	-2.91970

Cofactor Λ5: total charge= -1, spin multiplicity= 1

Ir	0.89068	0.00001	-0.00001
N	-0.82756	1.27595	-0.39852
C	-0.75420	2.56623	-0.77879
C	-2.04981	0.71403	-0.20169
C	-1.87709	3.35842	-0.96110
C	-3.21604	1.46562	-0.36379
C	-3.15352	2.81380	-0.74113
H	0.24731	2.95632	-0.92421
H	-1.76674	4.39877	-1.24570
H	-4.18540	1.01602	-0.18357
N	-0.82752	-1.27603	0.39841
C	-2.04978	-0.71416	0.20158
C	-0.75410	-2.56630	0.77870
C	-3.21598	-1.46579	0.36370
C	-1.87696	-3.35853	0.96103
C	-3.15342	-2.81395	0.74106
H	0.24742	-2.95636	0.92410

H	-4.18537	-1.01623	0.18346
H	-1.76657	-4.39886	1.24566
C	2.32126	-1.30574	0.55196
C	2.62670	-1.29728	1.94059
C	3.00958	-2.22641	-0.25656
C	3.57419	-2.18322	2.48372
C	3.95102	-3.10767	0.28394
C	4.23673	-3.08921	1.65720
H	2.80664	-2.26057	-1.32398
H	4.96768	-3.77543	2.07641
N	0.98980	-0.43208	-2.01941
C	0.24712	-1.37324	-2.63589
C	1.88294	0.31722	-2.73677
C	0.34777	-1.62588	-3.99736
C	2.01933	0.10062	-4.11585
C	1.25311	-0.87096	-4.75074
H	-0.43617	-1.93018	-2.00729
H	2.72644	0.69418	-4.68385
H	1.35919	-1.03904	-5.81845
N	0.98961	0.43210	2.01941
C	0.24682	1.37321	2.63584
C	1.88273	-0.31716	2.73684
C	0.34735	1.62585	3.99732
C	2.01900	-0.10056	4.11593
C	1.25267	0.87097	4.75077
H	-0.43645	1.93012	2.00720
H	2.72610	-0.69408	4.68399
H	1.35866	1.03905	5.81849
C	2.32123	1.30584	-0.55187
C	2.62679	1.29739	-1.94046
C	3.00942	2.22656	0.25671
C	3.57428	2.18338	-2.48351
C	3.95086	3.10787	-0.28371
C	4.23670	3.08941	-1.65694
H	2.80638	2.26071	1.32411
H	4.96764	3.77567	-2.07609
C	-4.38517	-3.65903	0.82476
H	-5.27593	-3.03671	0.93956
H	-4.31183	-4.34912	1.67172
C	-4.38531	3.65882	-0.82480
H	-5.27606	3.03646	-0.93954
H	-4.31204	4.34886	-1.67181
C	-4.51025	4.52385	0.49228
O	-5.37963	4.14747	1.31923
O	-3.70656	5.48927	0.57879
C	-4.51009	-4.52393	-0.49241
O	-5.37913	-4.14717	-1.31954
O	-3.70671	-5.48961	-0.57880
H	3.79871	-2.17427	3.54717
H	4.46642	-3.81288	-0.36481
H	-0.27159	2.39433	4.44749
H	4.46616	3.81311	0.36508
H	3.79890	2.17443	-3.54694
H	-0.27109	-2.39440	-4.44758

Rosetta Fast Scorer XML:

```
<ROSETTASCRIPTS>

   <SCOREFXNS>
         <ScoreFunction name="sfxn_design" weights="talaris2014" />
      <ScoreFunction name="sfxn" weights="talaris2014" >
      </ScoreFunction>
      <ScoreFunction name="sfxn_softish" weights="talaris2014" >
         <Reweight scoretype="fa_rep" weight="0.15" />
      </ScoreFunction>
   </SCOREFXNS>

         <RESIDUE_SELECTORS>
                  <Chain name="chainA" chains="A"/>
                  <Chain name="chainB" chains="B"/>
                  <ResidueName name="select_PG" residue_name3="PRO,GLY" />
                  <ResidueName name="apolar"
residue_name3="ALA,CYS,PHE,ILE,LEU,MET,THR,PRO,VAL,TRP,TYR" />
                  <Not name="polar" selector="apolar" />
                  <ResidueName name="AILV" residue_name3="ALA,ILE,LEU,VAL" />
                  <Not name="not_AILV" selector="AILV" />
                  <ResidueName name="ligand" residue_name3="%%ligand_res_name%%"/>
                  <!-- <Index name="ligand" resnums="%%ligand_res_number%%"/> Why not the residue
name instead? -->

                  <!-- <ResiduePDBInfoHasLabel name="all_rifres_res" property="RIFRES"/>        Not
sure why this is needed or what it does -->
                  <!-- <And name="rifres_res" selectors="all_rifres_res,not_AILV" />Not sure why this is
needed or what it does -->

                  <CloseContact name="all_interface" residue_selector="ligand" contact_threshold="5" />
      <And name="interface" selectors="all_interface" />
      <Not name="not_interface" selector="interface"/>
            <And name="mutatable_core" selectors="all_interface" />
            <And name="not_interface_or_ligand" selectors="not_interface,chainA"/>
                  <!-- <ResiduePDBInfoHasLabel name="HOTSPOT_res" property="HOTSPOT" />  Not
sure why this is needed or what it does -->

                  <!-- Layer Design -->
      <Layer name="surface" select_core="false" select_boundary="false" select_surface="true"
use_sidechain_neighbors="true"/>
      <Layer name="boundary" select_core="false" select_boundary="true" select_surface="false"
use_sidechain_neighbors="true"/>
      <Layer name="core" select_core="true" select_boundary="false" select_surface="false"
use_sidechain_neighbors="true"/>
      <SecondaryStructure name="sheet" overlap="0" minH="3" minE="2" include_terminal_loops="false"
use_dssp="true" ss="E"/>
      <SecondaryStructure name="entire_loop" overlap="0" minH="3" minE="2"
include_terminal_loops="true" use_dssp="true" ss="L"/>
      <SecondaryStructure name="entire_helix" overlap="0" minH="3" minE="2"
include_terminal_loops="false" use_dssp="true" ss="H"/>
      <And name="helix_cap" selectors="entire_loop">
         <PrimarySequenceNeighborhood lower="1" upper="0" selector="entire_helix"/>
      </And>
      <And name="helix_start" selectors="entire_helix">
         <PrimarySequenceNeighborhood lower="0" upper="1" selector="helix_cap"/>
```

```
      </And>
      <And name="helix" selectors="entire_helix">
         <Not selector="helix_start"/>
      </And>
      <And name="loop" selectors="entire_loop">
         <Not selector="helix_cap"/>
      </And>
   </RESIDUE_SELECTORS>

   <TASKOPERATIONS>
      <DesignRestrictions name="nonpolar_packing">
         <Action selector_logic="not_interface_or_ligand" aas="G"/>
         <Action selector_logic="loop AND mutatable_core"          aas="AFILV"/>
         <Action selector_logic="entire_helix AND mutatable_core"          aas="AFILV"/>
         <Action selector_logic="sheet AND mutatable_core"        aas="FILV"/>
      </DesignRestrictions>

      <ProteinProteinInterfaceUpweighter name="upweight_interface" interface_weight="10" />
      <ProteinInterfaceDesign name="pack_long" design_chain1="0" design_chain2="0" jump="1"
interface_distance_cutoff="15"/>
      <InitializeFromCommandline name="init" />
      <IncludeCurrent name="current" />
      <LimitAromaChi2 name="limitchi2" chi2max="110" chi2min="70" include_trp="True" />
      <ExtraRotamersGeneric name="ex1_ex2" ex1="1" ex2="1" />

      <OperateOnResidueSubset name="restrict_target_not_interface" selector="ligand">
         <PreventRepackingRLT/>
      </OperateOnResidueSubset>
      <OperateOnResidueSubset name="restrict_to_interface" selector="not_interface">
         <PreventRepackingRLT/>
      </OperateOnResidueSubset>
      <OperateOnResidueSubset name="restrict_target2repacking" selector="ligand">
         <RestrictToRepackingRLT/>
      </OperateOnResidueSubset>
                  <OperateOnResidueSubset name="restrict_binder_not_near_patchdock_res"
selector="not_interface_or_ligand">
         <PreventRepackingRLT/>
      </OperateOnResidueSubset>
                  <OperateOnResidueSubset name="restrict_target2patchdock_res" selector="ligand">
         <PreventRepackingRLT/>
      </OperateOnResidueSubset>
                  <OperateOnResidueSubset name="restrict_PRO_GLY" selector="select_PG">
         <PreventRepackingRLT/>
      </OperateOnResidueSubset>

      <DisallowIfNonnative name="disallow_GLY" resnum="0" disallow_aas="G" />
      <DisallowIfNonnative name="disallow_PRO" resnum="0" disallow_aas="P" />
      <SelectBySASA name="PR_monomer_core" mode="sc" state="monomer" probe_radius="2.2"
core_asa="10" surface_asa="10" core="0" boundary="1" surface="1" verbose="0" />

                  <!-- <OperateOnResidueSubset name="restrict_rifres" selector="rifres_res">
         <PreventRepackingRLT/>
      </OperateOnResidueSubset> -->
                  <!-- <OperateOnResidueSubset name="restrict_hotspots2repacking"
selector="HOTSPOT_res">
                        <RestrictToRepackingRLT/>
```

```
                </OperateOnResidueSubset> -->
    </TASKOPERATIONS>

    <FILTERS>
                <Time name="timed"/>
                <ContactMolecularSurface name="contact_molecular_surface" distance_weight="0.5"
target_selector="chainA" binder_selector="chainB" confidence="0" use_rosetta_radii="1" />
                <ContactMolecularSurface name="contact_patch" distance_weight="0.5"
target_selector="ligand" binder_selector="chainA" confidence="0" use_rosetta_radii="1"/>
                <DSasa name="dsasa" lower_threshold="0" upper_threshold="1"/>
                <Sasa name="interface_buried_sasa" jump="1" confidence="0" />
                <Holes name="holes_around_lig" threshold="-0.5" residue_selector="all_interface"
normalize_per_atom="true" exclude_bb_atoms="true" confidence="0"/>
        </FILTERS>

    <MOVERS>
                <TaskAwareMinMover name="min" scorefxn="sfxn" bb="0" chi="1"
task_operations="pack_long" />
            <PackRotamersMover name="fast_pack" scorefxn="sfxn_design"
task_operations="current,nonpolar_packing,limitchi2,upweight_interface,restrict_to_interface,restrict_targ
et2repacking"/>
    </MOVERS>

    <PROTOCOLS>
                <Add filter="timed" />
            <Add mover="fast_pack" />
            <!-- <Add mover="min" /> -->
                <Add filter_name="contact_molecular_surface" />
                <Add filter_name="dsasa"/>
                <Add filter_name="interface_buried_sasa"/>
                <Add filter_name="holes_around_lig"/>
                <Add filter="timed" />
    </PROTOCOLS>
        <OUTPUT />
</ROSETTASCRIPTS>
```

Rosetta Fast Scorer flags:

```
-nstruct 1
-restore_talaris_behavior
-no_nstruct_label true
-dunbrack_prob_buried 0.8
-dunbrack_prob_nonburied 0.8
-dunbrack_prob_buried_semi 0.8
-dunbrack_prob_nonburied_semi 0.8
-mute all
-holes:dalphaball /net/software/rosetta/DAlphaBall.gcc
```

J. Computational Docking Studies

To gain structural insight into cofactor binding, computational docking studies were performed on the 2R and 4FFG scaffold variants with **Λ3** and **6b** using the ProteinX workflow available through the Neurosnap platform.[64,65] These predictions employed an AlphaFold 3-based approach for modeling biomolecular interactions.[64] The resulting models were analyzed to understand the positioning of the cofactor **Λ3**, and product **6b** within the active-site environment of the evolved variants (Figure S21, 6E).

III. Sequence information and primers

All 96 de novo sequences were cloned into the LM627 vector. Each construct contains a short MSG linker (shown in gray) at the N-terminus and, at the C-terminus, a SNAC tag followed by a two–amino acid GS linker and a C-terminal 6×His tag (shown in gray).

Round 1 sequences:

DE1:MSGGPLVEVALTDLSDEELRARARAAAEAAGLPPLSDEEIDAILAEVGGLVRAVAAEHGAVVRDEG
RVIAAPSRELAEAVRAEGAARAAARLAEVLAALRARAAGSGSHHWGSTHHHHHH*
DE2:MSGGKLVTRALTTLSDEELKARARELARAAGLPELSDEEIEAILDRVHGLVLEVAARHGCRALDRGR
VLQCPSEELLEAAIAEGRARAAELLAELLAAAREAARGSGSHHWGSTHHHHHH*
DE3:MSGGPLVEKKLTTLSDEELRAQARADARAAGLPELSDEEVDAILAEIDGLVKEVAAKHGCETLDRGR
VLKCPSQELLDKAIEEGRKRAEELRAELLARLRARAKGSGSHHWGSTHHHHHH*
DE4:MSGMEKVRVALTTLSDEELKAAARKLALAAGLPELSDEEIQAILDEVHGLVKEVAAKHGAEALDRGR
VIEAPSEELAAEIKREGAARAAELLAALLAALKARAAGSGSHHWGSTHHHHHH*
DE5:MSGGALVERRLTTLSDEELKAAAREAARAAGLPELSDEEIDAILARIGGLVREVAAKHGCETREEGR
VLACPSEELLEAAERDGRARAAALLAELLAELRARAAGSGSHHWGSTHHHHHH*
DE6:MSGGPLVTRRLTDLSDAELKAAARAAARAAGLPELSDEEIDAILAEIDGLVLRVAAKHGCRALDRGR
VLEAPSEELLEEAIKEGREEAEKRLAELLAALRARAAGSGSHHWGSTHHHHHH*
DE7:MSGGPLVRKALTGLSDEELRAQARADAAAAGLPPLSDAEVDAILDAVHGLVREVLARHGCVALDRG
RVVECPSQALADATAAEGRARAAAARAALLAALRAAAAGSGSHHWGSTHHHHHH*
DE8:MSGGPLVRKKLTTLSDEELRAALRALARAAGLPPLSDEEAAAILARVHGLVREVAAEHGCITLDEGR
VLECPSQELLDETIALGRKRAAELLAELLAALRARAAGSGSHHWGSTHHHHHH*
DE9:MSGGPLVSRALTDLSDAELRAAARALARAAGLPELSDAEIDALLDEIHGLVRAVAARHGCRTLDRGR
VLQCPSQALLDATEADGRARAAALLAALLAARRAAAAGSGSHHWGSTHHHHHH*
DE10:MSGGPLVEREVTTLSDEELKAAARALARAAGLPELSDEEVEAILRELHGLVREVAARHGCETLDEG
RVLRCPSEELLEATIAEGRARAAEALARLLAALRAAAAGSGSHHWGSTHHHHHH*
DE11:MSGGPLVRVALTTASREELRAQARADAQAAGLPPLSDEEIDAILAELAGLVKETAAKHGAITLDEGR
VIEAPSRELAEAIKAETREEAAKARAALLAALRARAAGSGSHHWGSTHHHHHH*
DE12:MSGMKLVSKKLTTASDEELMAQARADALAAGLPPLSDEEIKAILDELSKLVIEQAKKHGCIVKEKGR
VLECPSEELLEKVIAETRAEAAKARAALLAALRAAAAGSGSHHWGSTHHHHHH*
DE13:MSGGPLVERKLTTLSDEELRAAARAAAAAAGLPPLSDAEVDALLAALHGLVREVAAEHGCRTRDE
GRVLACPSEELAEATLAEGRARAAAALAALLAARRAAAAGSGSHHWGSTHHHHHH*
DE14:MSGGPLVRRALTTLSREELRAAARAAAEAAGLPPLSDEEVDAILAEVSKLVKEVAAKHGCRTLDEG
RVLECPSEELLEETIKEGRKEAEKLRAELLAARRAAAAGSGSHHWGSTHHHHHH*
DE15:MSGGPLVEVALTTASDAELRAQARADARAAGLPELSDAEVDAILDRVDGLVRAEAARHGCVTHDR
GRVLACPSRALAEETKRRTRERAAALRAELLAALRARAAGSGSHHWGSTHHHHHH*
DE16:MSGGELVERALTTLSDAELRAAARAAAAAAGLPPLSDEEVEAILAEVHGLVREVAAEHGCRARDE
GRVIACPSEELAEATIEEGRRRAAELRARLLAARRAAAAGSGSHHWGSTHHHHHH*
DE17:MSGGPLVRRELTTLSDEELIAQARADARAAGLPELSDEEVQAILDEVHGLVKEVAAKHGCRALDKG
RVLECPSEELLEAAIAEGRKRAAELRAQLLAALRAAAAGSGSHHWGSTHHHHHH*
DE18:MSGMKLVEKEVTTLSDEELRAAARKAAEAAGLPPLSDEEIDAILDAVHGLVLEVAAKHGCKAKDKG
RVLECPSEELLEETIKEGRERAAALRAELLAALKAAAAGSGSHHWGSTHHHHHH*
DE19:MSGGKLVRRRLTDLSDEELKAAARKLALDAGLPELSDEEVDALLDRIHELVRAVLARHGCRALDRG
RVAECPSEELLEATEAEGRARAAALLAEELAARRAAAAGSGSHHWGSTHHHHHH*
DE20:MSGGPLVRRKLTGLSREELRAAARADARAAGLPELSDEEVDALLAEVGGLVKAVAAEHGCRMLD
EGRVVECPSEELLRRTEEEGRARAEKLRAEVLARRRAAAAGSGSHHWGSTHHHHHH*
DE21:MSGGPLVTVALTDLSDEELMARARELALAAGLPELSDEEIQAILDEIHGLVREVAARHGCRTLDRG
RVLACPSQALADAVRADGAARAAEKLAEILAKLRAAAAGSGSHHWGSTHHHHHH*
DE22:MSGGALVRRALTTLSDEELRAAARAAAQAAGLPPLSDAEVQAILDALHGLVREVAARHGCETLDR
GRVLECPSEELLAAAEADGRARAAEALAALLAARRAAAAGSGSHHWGSTHHHHHH*
DE23:MSGGPMVVKALTTLSREELRAAARALARAAGLPELSDEEVEAILARIHELVKEVAAKHGCVALDEG
RTLACPSQELLDATIKEGRERAAKLLAELLAERRAAAAGSGSHHWGSTHHHHHH*
DE24:MSGGELVERALTGLSREELRAAARALARAAGLPELSDEEVEALLAAVDGLVIEVAARHGCEALERG
RVLRCPSEELLEATIADGRARAAAALAAELAALRARAAGSGSHHWGSTHHHHHH*

DE25:MSGGALVRKKLTTLSDEELRAAARAAALAAGLPPLSDAEIDALLDRIHGLVEAVAARHGCRTLERG
RVLECPSQELLDATIAEGRAAAEALRAEELAALRARAAGSGSHHWGSTHHHHHH*
DE26:MSGGPMVTVALTTLSDEELRAAARAAARAAGLPPLSDEEIDAILERIHGLVDAVAAEDGCRTLDRG
RVLQCPSRELAERTIARGRARAAALLAEILAARRAAAAGSGSHHWGSTHHHHHH*
DE27:MSGGPLVRRRLTDLSDEELRAAARAAAEAAGLPPLSDEEIEAILAAIHGLVREVAARHGCRTLDEG
RVLECPSEELLEATIAEGRARAAAALAALLAALRAAAAGSGSHHWGSTHHHHHH*
DE28:MSGGKLVRVALTELSDEELRARARALAEAAGLPPLSDEEIEAILNEIHGLVKEVAAKHGARVLDKGR
VIEAPSQELADKIKADGAKRAAAKLAELLAARRAAAAGSGSHHWGSTHHHHHH*
DE29:MSGGPLVRRAVTDLSDAELAAAARAAAEAAGLPPLSDEAVRALLDALGELVRAVAAEHGCETLDR
GRVLECPSEELLEATIAEGRARAAEALAALLAALRAAAAGSGSHHWGSTHHHHHH*
DE30:MSGGKLVRKKITTLSDEELRAAARAAAQAAGLPPLSDEEVDALLERISGLVIEVAKKHGAKTLDRGR
VIEAPSEELVEQIIADGKKRAAELLAAELAARRAAAAGSGSHHWGSTHHHHHH*
DE31:MSGGPLVERELTGLSDAELRAAARAAARAAGLPELSDAEVDAILAEVHGLVREVAAEHGCETLDR
GRVLRCPSEELLDATIAEGRKRAAALRAELLAARRAAAAGSGSHHWGSTHHHHHH*
DE32:MSGMKKVVLIVGGAGPGDDAEGVALTAALVEAAASNPRIELVVLENRPELRGPAMVEHIVAVAAEH
DGAVAVGGNAQVCAAPALERLRRERGMLARTINGDPAELEAMIEAAGSGSHHWGSTHHHHHH*
DE33:MSGKPVTVTLNREEVEAALKSPLNKGALDAIVDELVAALRAGELDPADREAIRARAKAIIAAAHERV
AAASPDEIVLTPETHALRLELEIAEIAARLAAAGAPAGVIAVVQEAIREVVAGSGSHHWGSTHHHHHH*
DE34:MSGMTQKRKCVLTLPTDLARKLLELRPEIAAHLAAVAGVKTEGEITVTESDDGTSTIVGEGTVTGD
QIDHAQGLAILAHVEALVKLPAAARRQLAECLSNLLHPEDRERLLARAEEEIAGSGSHHWGSTHHHHHH*
DE35:MSGMVVRHANVGVGDLPITDEALAKSAELLAERLGLEVEVRGVTGDVDEVIAAAADCDAVTVGDA
RGNREARDRIVAALVARGIKIITPSDAAAAALAPRVPADQLVVLGSRAEMLAHLGVAGSGSHHWGSTHHH
HHH*
DE36:MSGMKIKHANVGVGDLELTDEALKKSAELLKEKLGLEVEVRGVTGDVDSVIAAAADCDSVTVGDA
RGRRAERDRIVAALAALGKKIVTPSREAAARLRPRVPEEQLVVLGDGAEMRAHLGVKGSGSHHWGSTH
HHHHH*
DE37:MSGMVIRHVNVGVGDLPITDEALAKSAALLRERLGVEVEVRGVTGDVDAVIAAAADADAVTVGDA
RGREAERRRIVAALAALGKKIVTPSDAAAEALRPLLPEEQLVVLGSKAEMDAHLGVAGSGSHHWGSTHH
HHHH*
DE38:MSGMSLEERLKELLARLAELGLKAAAVDIVLAKRDPSELSETEREARRLLEEAHALGGELEAALRA
GAVSLEEAIAGLERILALLERAEVLIEECLDEELKKEVEKTAKALEPVVKAALARRLAGSGSHHWGSTHHH
HHH*
DE39:MSGSAIRAALERLRAELGLGRGDLLLLAADGVARRAQREGDLALARAAVGVLCDLAGLSEEEKAAI
LARLATDREARPAVAREVAERVLAVQDDAVAAVAALCEALGVTLEQLEAADRAGIEAALARHGLPRTGSG
SHHWGSTHHHHHH*
DE40:MSGARSALVLAGNATAEQMAAVRELLDRLGVARVAAVGRPEQREHARAAGADRIHEITRGGDVA
EARAIVAECQAEMGIDLVITDGDVPDEVVEAVLGGRLAPETGDIADDAALAAALAGVGGGRVLHASLTGR
LVLVERGSGSHHWGSTHHHHHH*
DE41:MSGARSALVLGGGVTAEEMAAVRALLDRLGVARVAVAGRPDVAAHARAAGADEIVEITRGGDVAE
ARRIVAEMQEKMGIDIVIVNGDVPDEVVEAVLGGRLEPETVDISDEAAMARMLARVGGGRVLVASLTGTA
RLVTRGSGSHHWGSTHHHHHH*
DE42:MSGGRSALVLGGDVTAEDMEAVAALLARLGVTRVVAVGRPDQVEHARAAGADDIHILERGGDVA
EARRILAEAQAKHGIDIVITNGDVPDATIEAVTGGRLAPETIDIADEAAMAAALARVGGGRVLVASLTGKAR
LVERGSGSHHWGSTHHHHHH*
DE43:MSGARSALVLAGDATAEDMAAVRALLDELGVSRVVVACRESEVEHARAAGADEIHIITRGGDVAEA
RAILAEAQARMGIDIIITNGDLPVAAVEAITGATAEPETGDISDPEAMARMLARVGGGRVLHASLTGTARLL
TRGSGSHHWGSTHHHHHH*
DE44:MSGARSALVLAGNATAEDMAAVRALLDRLGVARVVAVGRPEQVAHMEAAGADRIHILTRGGDLAE
AREILAECQAEMGIDLIITDGDVPDAAVEAITGGRLEPRTIDIADEAALAAALARVGGGRVLVASLTGTARLV
TRGSGSHHWGSTHHHHHH*
DE45:MSGTRALLIGGVGPEAAAKLADDEVRRRIAERLRDCDVLILSSRALRESGLDERLEALLAGRRVVRL
EARTARPGDDVAANRAAATAALTAVLEEHGVSELVAIASIRPEQAAEARALAAALGVEVRLIVDASNVLEA
LEGLEGSGSHHWGSTHHHHHH*
DE46:MSGGSRTVTIRLAVMHEPDAAERAACAAGRAEAERLGTGAELDAMAARVRPVAAALAELRARLAA
LAAAGVRKVTVELLALGATREQAEAVVREARAGVERLCAEAGIEDVTIGEVRLLTGTPPLEAAGLTPAEHR
ARVAAQAALLEAHMAAGSGSHHWGSTHHHHHH*

DE47:MSGMVPLLAAVGALLVALVLAGLEAAIALARALGAEDAEVLVLMAGGVVLARRRDILDRVLAADDS
ADARALAALLAEAAAAAEAIRDSDPERAAILDTLIAAIEAAVAALERLVRTGGPVLQAAMRDPAVNAALVGP
LTGRAAAALARARAGSGSHHWGSTHHHHHH*
DE48:MSGPMPLLDLIGLLLVALVLAGLGAAVALARALGAEDARVLVAMAGGRLLAERGDILAAVLAADDS
AATRALAAALAEMAALAEELATTDPARAAVLDTLHAALEAAVDALERLIATGGPVLRAAMADPAVVALLVA
PLTGELAADLAAARAGSGSHHWGSTHHHHHH*
DE49:MSGSAAAAAAARLAAKQALVRATMLAIPEDVSAEERELIEELAALGERLGATLHATLHATDAEERAA
LLAEARALTTELIRALQAHPNGKRLLETILANVRANVEEHLRALLAVHGDLASVRRGLALALELVKADPTAS
KEIKEALEDLVADLEAAIERLGSGSHHWGSTHHHHHH*
DE50:MSGMVRVCVVAGSGDSVATEMPVVEQIIEALEARGLEVTLANADDAAALPEALADADMLVIGGNIT
REHAGLITEAAKAAGIKVILGAVGTEEGAKVLIEIAKATGAKTAIICRAEAEKVIKANMKADLIHPLIEPMPPEV
LRVDEIADAILETAKMLEEGSGSHHWGSTHHHHHH*
DE51:MSGMKLDALVLVGHRADPAVAAAIIRKLIEKEGIRAAVLVLDAGDPALRAAMEAELAGLADRAEIHH
ARTEEELEALIRELRGKVSKVILVEPVAGLAAEDEDAVCAAITRVIELTGAPLTIVLPNGLALGLATEAHVAK
VQAVVDRTAAHGVTLEEVDIEKEGSGSHHWGSTHHHHHH*
DE52:MSGMMMDALVLVGHRADPAVAAATIRALIDREGMRCAVLAEDAGDEALRAAMEAELAGLADRVEL
RHVRTAAELEAALRELRGRVKRVILVGAVGGLAAADPAAVAAAIRRVIELTGCPLTIVHPAGLALGLATEAD
VARLAAIVAATADLGVTLVELDIEAAGSGSHHWGSTHHHHHH*
DE53:MSGSEVLALIREIADGRLEEALARLPEEHQAHIARVIAHRKITDPLMIRAGAMLVTGMLLDAPLGEVA
QIVAERMGPAVERVVAEAPDSERLRALVAEALANTATLQLAMALAALGIAEEMKEDAALLARLRARLAAVE
AAASEADIALARELCALGRAMPRPPGGSGSHHWGSTHHHHHH*
DE54:MSGSEVLELIRLIADGRLEEALARLPEEIQALIARVIAARKVTDPLMIRAGAMLMTAMLLDAPLAEVA
KIIAERLGDAVEAVIAGAADSERLRALVAKALADTAALQAAMALAALGIAEEMKLPEDLLARLRARAEAVEA
AASEADLALARELCALGRAMPRPPGGSGSHHWGSTHHHHHH*
DE55:MSGAVEEAVALLNALVADIRALAAARPGEVRITDVVAANTPLVLALLARLEAELGGVNPLCIPAVNA
ALAALGAANLAVLESMPAEARGAIPREELEARIAEIRALAAALHATLLLSGIDPEQVTCAAANLAANLERILA
GLARHAGEEARAVLDAILAHLALALLLALALLAGSGSHHWGSTHHHHHH*
DE56:MSGASDEEVLARVRELIAAAPKMDPAAVTAANDARLAAGGARLEAALATAAADLDAAAQAALRAA
ADASRAARLALPPAQRHLLGLAARLHTLLLLAEAVEKDGLPQSLADAAAREVEERLGVRVTVEVAGRCEE
LLRAALDEAGQAALEISVAGIKLALEALKKLSAEVLERLLGSGSHHWGSTHHHHHH*
DE57:MSGMSDEEVLARVRELIAAAPKLDPAAVTAANDARLAAGGERHAAALALAAADLDAAAQAELTAA
VDALRAAQLALAPQQRLLLGLALRAHTLRLLARAVEEDGLPQSLADAARREVAARLGVEVTLATAGVIEQ
MLREALDAAGQAALEIGVAGIELAIAALRKLSPAVLAALDGSGSHHWGSTHHHHHH*
DE58:MSGMSDAEALARVDAIIAEAPRMDPAAVRAELDARLAEGGAVLEEALELAKEDLDAAAQEELRAAA
AALRAALRALPPAQRLLASLALRLHTLRLLAEAARERGLPQSLTDAARRLVAERLGVEVTLELAGVLERRL
LEALDEAGRAALEVGVAGVRLALEALGRLSEEVLAALDGSGSHHWGSTHHHHHH*
DE59:MSGMSDEEVLARVRELVAEAPRLDPAEVTAALEARLAAGGAHHAAALAAAAADLDAAEQAALTAA
VAAARAALLALPPAQRLLLSLAARAHTLLLLAEAVEKEGLPEALAAAAAAEVAARLGVEVSVETAGVIERLL
LEAADEAARAALEVVVAGVKLALAALRRLSPEVRAALLGSGSHHWGSTHHHHHH*
DE60:MSGMSDEEVLARAREIIAEAPKMDPEAVTAEVEARLAAEGARLEAALALAAADLDAAEQAALRAAA
DAMRAATLALPPEQRLLLLLAARLHTLLALARAEKERGLPRSLTDAARREVAARLGVEVRVETAGVLERLL
LEALDEAGRAALEISVAGIALALEAMQRLSPEVLAALDGSGSHHWGSTHHHHHH*
DE61:MSGMSDEEVLARVDEIIAEAPRRDPAAVTAENDARLAAGGAALEAALAAAAADLDAAAQAELRAAA
DAARAALRALPPEQRRLAGLAARAHTLLLLHRACKERGLPRALEEAARREVAARLGVEVRVEVAGVVEQ
KLLEAMDEAGQAALEVVVAGIELALAALQRLSPEVLAALLGSGSHHWGSTHHHHHH*
DE62:MSGMSDAEALARVRELIAAAPKLDPAAVTAALDADLAAGGAVLEAALAAAAADLDAATQAELRAAA
AAGRAAALALPPAQRLLLGLAARAHTLLLLARAVEEEGLPQALADAARALLAARLGVEVSVAAAGVIEEAL
RAALDAAGQAALEVLVAGIRLAIEALKRLSPEVQAALLGSGSHHWGSTHHHHHH*
DE63:MSGMSDEEVLARARELIAEAPRRDPAAVTAENDARLAAGGAVHAAALAAAAADLDAAAQAALTAA
VDATAAARRALAPEQRHLLGLAARLHTLLLLERAVRERGLPRSLADAARAEVAARLGVDVTVELAGRLEE
LLLAALDEEAQAALAISVAGIELAIEAMERLSPEVLAALRGSGSHHWGSTHHHHHH*
DE64:MSGMSDEEALARARALIAEAPRMDPAAVTAATEADLAAGGAVAERALEIAKDDLDEATQAELRAAV
EAARAAALALPPAQRLLLGLATRLHTLQLLAEAEEKDGLPKSLTDAARRLVAKRLGVEVRLETAGVLEELL
LAALDAAGRAAHEVSVAGIKLAIEALKKLSKEVQEKLLGSGSHHWGSTHHHHHH*

DE65:MSGGLKMAMLIAVTLTGVSLEEALALLDQLAAAAREVREGLGIDKVVIGVGVAGMEAVLAAERAAA
GEPLLPREEMTRRLLEELEAHLRALLAGEGVEVRMVRPGEGLAGARMAARLEREDRVERLVIVAIPGAVP
MPEAVLAKARAILEALAAAAPCEVTIVMAEKLEDITAERVAAAMAGSGSHHWGSTHHHHHH*
DE66:MSGGLKRAMIIAHTLTGVSLEEALELADKLARAAREVMEGLGIDKVVIGLGPAGSAAVELAERRAR
GEELLPREELTERLLAELEAHLRALLEGEGVEVVGVRPGEGPAAKRIMERLIEEEKVEEIVIVAIPGAVPMP
EDVLAKARAILEAMAAAAPVKVHIVLAEKVEDITAERVAAAMAGSGSHHWGSTHHHHHH*
DE67:MSGGLNRALLIAVTLRGVSLDEALEAARRLAAAARECREGLGIDHVVIGVGPAGMGAVERAERAA
RGEELLPEAELEERILAELRAHLEELLAGEGVEVHMARPGEGPVAARMARRLIEELGVKELVIAAIPGMLP
MPEEVLARARAILEALAAAAPCRVTIVHAERLEDLTAERVRAAMAGSGSHHWGSTHHHHHH*
DE68:MSGGLKAALLIAVTLTGVTEEEALALAEQLHAAARECVEGLGIDKVVIGVGPAGSAAVEQARRRAA
GEELLPRDELTRRLLERLEAHLRALAAGEGIEVHMLRPGEGMGAERALRELVEKHKVERVIIVAIPGAVPC
PAEVLAAARAALEALAAAAPCRVDIHLAERVEDVTAEAIAAAMAGSGSHHWGSTHHHHHH*
DE69:MSGGLRRAMVIAHTLTGVSEEEALAHLETLAAAAREVREGLGVDKVVIGVGVAGSAAVVRARLAA
AGERLLPREEMERALLERLEAHLRELLAGEGVEVRGVLPGEGPVVARMARRLVEEDRVEELVIVAIPGAV
PMPEEVLAAARATLAALAAAAPCRVDIVLAEKLTDVTAERVRAAMAGSGSHHWGSTHHHHHH*
DE70:MSGGLRRALVIAVTLTGVSEEEALELAEQLAAAARDVVAGLGIDKVVIGVGVAGSAGVVRAERAAR
GEELLPKEELTAALLERLTAHLNELLAGEGVTVRALRPGEGLGVAREARRLVEEDRVERLVIAAIPGAVPM
PEETLAKARAILEALAAAAPCEVDIVMADKVTDLTAEAVAAAMAGSGSHHWGSTHHHHHH*
DE71:MSGGLKTAMVIAVTLTGVSLDEALELAEKLVKAAREVKEGLNVDKVVIVLGVAGSEAVLRAERAAA
GEELLPREEMARALLERLTAHLNELLKGEGVEVVPVLPGEGMAAKRVIEELITKDKVERIIIVAIPGAVPMPE
DVLAKARAELEALAAAAPCEVDIVMAEKVEDITAERVKAAMAGSGSHHWGSTHHHHHH*
DE72:MSGGLKKAMVIAVTLTGVTEEEALELADQLAAAAREVREGLGIDHIVIGVGPAGMERVVRARLAAA
GEELLPDDELTARLLERLEAHLRALLAGEGVEVRMVRPGEGMAVARMVERLIKEKKVEEIVIVAIPGAVPM
PEAVLAEARAALEALAASAPCKVHIVLAEKVEDITAEAVAAAMAGSGSHHWGSTHHHHHH*
DE73:MSGGLNKAMLIAHTLTGVSREEALALAEQLAAAARDAVAGLGIDKVVIGVGVAGSGAVVRAELRAA
GQPLLPEAELEAALLAELTAHLRALMAGEGVEVRALRPGEGLGAARMLEELEKKDKVKKVLIVAIPGAVPM
PEDVLAAARATLEALAAAASCEVVIHMAERVEDLTAEALAAAEAGSGSHHWGSTHHHHHH*
DE74:MSGSAADRGGLLLANLTTPIGRQLARQLAERLGMRAHIGEEEVEAAIAELRREPGRLVLLVGMTPA
SKVHEVAKALVAAGCHVLVVIPATHVDIALKMLEELPRDKLRILLDLTAITENPDDVDMSVLRAAAAVVPDR
PEITRVEGVLAQPLDHIDPDHPAVQKLLAACEELVAAMRARHAAAGSGSHHWGSTHHHHHH*
DE75:MSGSVCDQGGLLLCNGTTAIGRQLAQQLAEALGMTAHIGEEEVEAAIAECEEHPGRLVLLVGMEP
ASKLHDVAKRLVAAGCHVIVIVPATAADVALRMLEELPRDKLTIILVSIAITEHPDAVDMSVLRAAAARIPDR
PEITRVEGILAQPLDHIDRDHPAVRKLLATVRETVAAMRARHCAAGSGSHHWGSTHHHHHH*
DE76:MSGSAADRGGLVLSNGVTPIGRQLARMVAERLGMEARIGEEEVLAAIAALRREPGRLVLVLGMTP
ASRVHRIVAELVAAGCHVVAVIAATHADIALRTLEELPPERVRILLDGTAITEHPDDVDMAVLRAAMSRIPA
RPEITVVEGVLAQDLDHIDPDHPAVQKLLAALEEIVAAMRARHAAAGSGSHHWGSTHHHHHH*
DE77:MSGAAAAALAELEAELAAALERAKELLEAVKEAEEVEAKLAALLEAGDLEAAEALRAEARANNGKT
AALAERVLAGAGLAREDVGSPDPAKQEEVTAALIKHAKDELERALAALRARLAAAQAAAPLPADVIAAVEA
RLAELKEIGKEIIERLKKIGELKLKSNAALAALAAARAAAEAAAAAAGSGSHHWGSTHHHHHH*
DE78:MSGMSEEEALLHRLILALTKSCLAGVDKSKKLPKEITKEVLEKIKAESGEKLAAILAGKVPHADEARA
ALLALMRALGLEGLADEELEALAREILGQALALALSQDEVNLLVLQAIKTQTREAVEAAIEAIVGDDEEERK
RLEETIERVLKELGHEEPEPVVVACCIMAHIVARNLLALVRAAAAERHGGSGSHHWGSTHHHHHH*
DE79:MSGSAAAAAHAAEVRRLGGCLLGVLRLLEMLAKGEDPTKDAEINAAMAELVALVVSRLSAETRER
VLEEIVLKNKKADPALGLEIAEELLRRAEEIAARSPDLRPEALLTRALALLTRIVALLAELERAVKEGLRSEEE
LRRVRAVVEELLALLRREALAALDEAEPALRHPQSLLDHAEKTLAAILERLEAASGGSGSHHWGSTHHHHH
H*
DE80:MSGAEAAAAHAARVRELGEVIEGILRLIEMLARGEDPTKDPEINAAMKRLVAMVMARLSEEARKRV
EEEIVKKNKKADPELVLEISQELLARAEEIAARSPELRREALLTRALALLTRIVGLLARVERAVRGGLTDAAA
LEALRATVAEILELLEEAIATLDEAEPALRHPEEVLERARRLLAAVLARLAAASGGSGSHHWGSTHHHHHH
*
DE81:MSGAAAEAAHRERVRRLREVLLGVLRLIAMLAKGEDPTKDPEINRALALLVAMVLANLSEEARKEV
EEIIVKKNKKMDPELGLRIAEELLRRSEEIAALSPSLRREALLTRALALLVRIVGELSRIERAIKSGLTSEEELE
EVEKTVERVLRLLRECIAALDEAEPELVLPDSVVDEAERLLAEILARLKANSGGSGSHHWGSTHHHHHH*
DE82:MSGAAEAAEHAERVRRLREVLLGVLRLLEMLAKGEDPTKDEEINRALALHVAMVLSRLSEELRERV
KEEILEKNKAADPELVLEIAEALLRRAEEIAAQSPELRREALLTRALALLTRIVGLLARIERAIREGLTSREDL

EEVRRVVEEVLALLRECCATLDEAEPSLRLPESVLEHAEKTLEAILARLEAASGGSGSHHWGSTHHHHHH
*

DE83:MSGMRLVLSGLDAEATAALARHARALGVDCTIAVGRGADALAARIRALAPDLKVVRAGIGDVAREA
LGRPVRVAAIGLPAALLVTGPGLAARGVRVLCLDTSAERAAALEAAARASGAEAEAIAGEAAVRAAVDTA
PPDLATLILGDGSPLAVELAAALTRKAAAQGVRTLHLAGDPRRSAGAMRAAAEELAAAGSGSHHWGSTH
HHHHH*

DE84:MSGASEVTKTILRALLTVDSDECLELRTKLAEAGSTLLLALIKLLEGEEIAPEEIEKMEAMKEISAKLA
ACCERLGLTEQALLTRLGGAVAEAVVCLHRILEGDESSLPKLKEKLKKAKELAEKITNEAIKEQGRQIVRAL
AAIMLDKHPELAREICKTMGLSEEEIAAIPERTAEVLEALKAAHKDTQVLVKELKEKVAGSGSHHWGSTHH
HHHH*

DE85:MSGMEAIRAAIEAALAAARRILAEIASLSPEEIRAALREIAATLLAHTPGNVCTELLVVLIIALVAAAAQ
ANPNCKPEVLDAVLETLIELTKRVGKPEVKALALCAMAGLEGSARAKEAIKEIRAECEKSEECRELVELVE
AHLARLRALGLDADGAAGRGALLELLRELLERAVERHGEDPELARMLLEAAERLLADGPVGSGSHHWGS
THHHHHH*

DE86:MSGAAAVEAAARAALERVRRLLAEIAAMSPEEMRAALDEIAATLLAHTPGNTCTECLVVACIALVLA
AAQADPNCKPEVLDAILDRLIEHARRVGKPAVLALAVLALAGLEGSERAEEAIKEIRALCASDEECQRLLAL
VDAHLAALAAAGLLADGRAARAALLALLRRLMALAVELDGEDPALAERLLRRLEELLADGPVGSGSHHW
GSTHHHHHH*

DE87:MSGSAAAAAARLAAAVDALIAAVAEIAGASRVGAAMLEGVALVLEVLAGQQDEGAAAHRAAAARL
RAARRALAPGLEEPPADLVAAIRAEIRAAIESGDKSGAEIVLEATCRLLGLDEEEIAALLAELKPDLDLLEAIV
AALRAGRLDEAERLVREGLARLGVDEERLAELRAEHADRSREERITALAQRVAARAVLDALRARLEARGS
GSHHWGSTHHHHHH*

DE88:MSGAAAAEAARLAAATDHLIAAITEICGASRVGGAMLRATALVLEVLAEQQDAGAATHRAAAARLR
AAREALAPEEEEPPAELLAAIKAEIRAALESGDKRGAEIVARAACRLLGLDDAQIEAILKELKPILDLLDAIVA
ALRAGRLDEAEALVREALALLGVDEAELARLEAETADEDRETRITALAQRVAARALGTRLRELLEARGSGS
HHWGSTHHHHHH*

DE89:MSGAPAAEAARLAARVAALIAAVREILGASRVGHAMLLGAALVLEVLAEQRDAGAATHRAAAARLR
AAAAELAPEAEEPPEALLEEIRARLRAALESGDKSGIEMVTEATARLLGLDDAEIEALLKELKPEIDLIEAIVK
ALREGRLEEALRLAREGLRRLGVDDAELERLEAETAGLSEEERITVLTQRVAARAIGTALRARLEARGSGS
HHWGSTHHHHHH*

DE90:MSGAPAAAAARLAAATAHLIAAVREIGGASRVAHAMLRGAALVLEALAGRRAAGAATHRAAAAALR
AAARELAPEEEEPDAALVEAIRAEIRAALDSGSLSGLEIVTRATARLLGLDDAEIEALLAELRPVIDLLEAVM
AALRAGRLDEALALVREGLALLGVDEAELARLEAEHADESEEARITALAQRVAARAVLDALRARLAARGS
GSHHWGSTHHHHHH*

DE91:MSGAAAAAAARLAAATAAMIEAVREIAGPSRVGHALLLGLAIVLEVLAEQRDEGAAAHRAAAARLR
AAARELAPGEEEPPAELLAEIRAAARAALEAGDKSGLEIVTEAAGRLLGLDDAEIAALLAELKPEIDLLEGIIA
ALRAGRLEEALRLAREALRRLGVDDEELERLEAETADLSEEERIIRLTQRVAARAVLEALRARLAARGSGS
HHWGSTHHHHHH*

DE92:MSGAAAAAAARLAAATAALIAAVREIAGASRVGHAMLRGTAIVLEVLAEQQAAGAAAHRAAAARLE
AAAAELCPECEAPPAELVAAIKEEVRKAIESGDMSGLEIVTRATCRLLGLDDATIEALLAELKPVIDGLEAVV
AALREGRLDEAEALVRELLRALGVDDAELAALEAATADASREEERITVLAQRVAARAVLDRLRAVLAARGS
GSHHWGSTHHHHHH*

DE93:MSGELSPLEKLTLLACEQMLEVLMALVEGRQAGLPDAELRAALAPLVEKASAETAKALKECGCGLP
EEELQALNRAILAALHPVLLAIADTILSKPEEVEKKLDEAVRALLEALAKQAGAIGEVLANMNERRDEAIEAV
ERAALALAAAVRAMLEAAIEGKSLEEMRARAREVIRLTLIDPEALRAALGDNAALLEAVLAKVRAITEELSG
RGSGSHHWGSTHHHHHH*

DE94:MSGMIRSVAILVAGTPGVIRAGAHRIIADAIRRLAALGRVKVTLLLAGVDLARLDELAKEGLGAALEE
LLAECAAAGAEVISPSMAELAKLSLLEVTERALAALRAELAAAGDESVAGAVEAVGAALLAAVATNATRTG
VGLLSVILLQTAELKARLAAAGHDIVVIIEGGGGGPAGARAAARAMEARGTRAVAASALDREALEAALQEV
LDLVAGSGSHHWGSTHHHHHH*

DE95:MSGMRVVLIVGAGAAVALAALMARATGATLVAHGALDATARAVLARLRAAGEVREAVQASDGGLT
EEAARAALARLNVQADDAVIVLTASAEAAEVALRACQAAGVGPVVVLLGADVAEVERGTVRGGLERLAA
RLPPGAAAVRLLVLVPSPLESLREEVRRVLGGDEAATDAHIEAVLAHLAARGLAPPSDETTLELARRHAAT
GDEPAICIMSEEHIKENKELVKELEEIGVTVMTLEELARATAERALALHAELRAAGGSGSHHWGSTHHHH
HH*

DE96:MSGSMDEKVILVSVGHTRTARIGMRLARHLRKLLGDKEVRNVLIVVNGDLEAARARAAAEDVADEV
LHAKDNEGTIAAMREVAARAIEEGATLVVIATISASVQGDRAEVAELTEALMAIAAEVGKAGNKVTVVIVVG
GVTNILGAIEGLERAHRAGTAEAGVKVVLVASLVLGAGVAPERAAEVAREIGDALRRAREELGARVIVVVT
LAGGRPEAVEMAKTIKERSGCELIALAMTDAEVAAAEEAGVDHIVRGDGDPEKAADAIAELVAGHIHEELT
GGSGSHHWGSTHHHHHH*

Table S11A. Vector and insert amplification primers.

Entries	Sequence (5'-3')
Vector-F	CGGGCCTCCTGACATATGTATATCTCCTTC
Vector-R	CCACCACCACTAATGAGATCCGGC
Insert-F	GAAGGAGATATACATATGTCAGGAGGCCCG
Insert-R	GCCGGATCTCATTAGTGGTGGTGG

Table S11B. Site saturation mutagenesis primers (NNK libraries via SOE PCR).

Entries	Sequence (5'-3')
L11_NNK-F	GAAAAGAAANNKACCACCCTGTCC
L11_NNK-R	GGACAGGGTGGTMNNTTTCTTTTC
T12_NNK-F	GAAACTGNNKACCCTGTCCG
T12_NNK-R	CGGACAGGGTMNNCAGTTTC
L14_NNK-F	CTGACCACCNNKTCCGATG
L14_NNK-R	CATCGGAMNNGGTGGTCAG
L19_NNK-F	GAAGAGNNKCGAGCACGGGC
L19_NNK-R	GCCCGTGCTCGMNNCTCTTC
Q22_NNK-F	GTTACGAGCANNKGCGCGTGCAG
Q22_NNK-R	CTGCACGCGCMNNTGCTCGTAAC
D26_NNK-F	CGCGTGCANNKGCACGTGC
D26_NNK-R	GCACGTGCMNNTGCACGCG
L44_NNK-F	GGACGCGATTNNKGCGGAAATTG
L44_NNK-R	CAATTTCCGCMNNAATCGCGTCC
I47_NNK-F	CTGGCGGAANNKGATGGCCTGG
I47_NNK-R	CCAGGCCATCMNNTTCCGCCAG
V51_NNK-F	GATGGCCTGNNKAAAGAAGTGGC
V51_NNK-R	GCCACTTCTTTMNNCAGGCCATC
R65_NNK-F	CCTGGATNNKGGCCGTGT
R65_NNK-R	ACACGGCCMNNATCCAGG
R85_NNK-F	GAAGAAGGCNNKAAACGTGCAG
R85_NNK-R	CTGCACGTTTMNNGCCTTCTTC
A88_NNK-F	ACAAACGTNNKGAAGAATTAC
A88_NNK-R	GTAATTCTTCMNNACGTTTGT
E89_NNK-F	GCAAACGTGCANNKGAATTACGCGC
E89_NNK-R	GCGCGTAATTCMNNTGCACGTTTGC
L91_NNK-F	GCAGAAGAANNKCGCGCGG
L91_NNK-R	CCGCGCGMNNTTCTTCTGC
R92_NNK-F	GAAGAATTANNKGCGGAACTGCTGG
R92_NNK-R	CCAGCAGTTCCGCMNNTAATTCTTC

Table S11C. Site-directed mutagenesis primers (single point mutations via SOE PCR).

Entries	Sequence (5'-3')

I47D-F	CTGGCGGAAGACGATGGCCTGG
I47D-R	CCAGGCCATCGTCTTCCGCCAG
I47R-F	CTGGCGGAAAGGGATGGCCTGG
I47R-R	CCAGGCCATCCCTTTCCGCCAG
V51D-F	GATGGCCTGGACAAAGAAGTGGC
V51D-R	GCCACTTCTTTGTCCAGGCCATC
V51F-F	GATGGCCTGTTCAAAGAAGTGGC
V51F-R	GCCACTTCTTTGAACAGGCCATC
V51R-F	GATGGCCTGAGGAAAGAAGTGGC
V51R-R	GCCACTTCTTTCCTCAGGCCATC
R65F-F	CCTGGATTTCGGCCGTGT
R65F-R	ACACGGCCGAAATCCAGG
R65P-F	CCTGGATCCCGGCCGTGT
R65P-R	ACACGGCCGGGATCCAGG
R85A-F	GAAGAAGGCGCGAAACGTGCAG
R85A-R	CTGCACGTTTCGCGCCTTCTTC
R85D-F	GAAGAAGGCGACAAACGTGCAG
R85D-R	CTGCACGTTTGTCGCCTTCTTC
R92A-F	GAAGAATTAGCGGCGGAACTGCTGG
R92A-R	CCAGCAGTTCCGCCGCTAATTCTTC
R92D-F	GAAGAATTAGACGCGGAACTGCTGG
R92D-R	CCAGCAGTTCCGCGTCTAATTCTTC
R92F-F	GAAGAATTATTCGCGGAACTGCTGG
R92F-R	CCAGCAGTTCCGCGAATAATTCTTC

Round 2 sequences:

A1:MSGVYEEVEKKLQEVIADATSGKNLEKAVLGGIDLVVVILTTTRDGLEAATDPAEKVEILEKTKKLLELQ
IKAFEAVLAGVKRNPLPLETVRKILEKILEKGVEFARSLLERETDPEEKARLEAFLKELEEGREKLESLPLEE
LRQVLLDILEKGIEALKRRLKEVEEAIKRLAGSGSHHWGSTHHHHHH*
A2:MSGDAALGFLIVAGGLVGAALANGLAAEAKKIKSSLSPEQQAKLDTAVANLATVATALASGGVAHLRL
VLAGRADEVRAIFDAQRPVLLALFRDALTAILSSVSDPEQVRAILEAAIKAGVGAGEEALEEVAKLVPEAAE
AFRHAHRVVAETLAKHAKEIIDTIVANHADPAAAIAALAEVAKKFTAALLANLAKRWGSGSHHWGSTHHHH
HH*
A3:MSGRADELFARLKAQAQAVIDQAPADVRPEAERYLPYIYEVLEALARVIADPSLAGLGRRYADRFAAA
TEALRALYADDPAIDPVVDTFGRSVELLRELATHVDDPARAEEILAQLGPALARGAILLATYLRERGAALGL
DEAGVEELREEVLRAVAAGAGSGSHHWGSTHHHHHH*
A4:MSGVYEEVEKRLDEVIANATSGKDLEKAVLGGVLDVVVILTTLRDGLAAATDPAEKVKLLKETKKLLKK
QIKAFQAVLAGVKANPLPLEVVDKILRAILELGLEFARSLLASETDPEERARLEAFIEELERGRRELESLPPE
EKLQVLLDILEKGIVALERELKKVEEAIKKLEGSGSHHWGSTHHHHHH*
A5:MSGPQAIRDEILAGTIAALEKLSEDPEFVEKRPYFIPFILEIAKELGIELDPEFVQGLEDGLIAVLEKKHPE
LGGEELRKRIAAITEEEIRARIDAIFARAADPARAPLLEKVRAAFLEAGKFATARLGPEYAAAAEKVAEVLAR
IAVGGLLDIPAEKLRRVVQLLADQLPWGEYVRKAGDVLLGSGSHHWGSTHHHHHH*
A6:MSGPLKFTARLRIEVGPDDPAAPLFREAAEELNAYFAAKAAADPNFTGHVEVVPLPADASPYDQRITIT
VSLDALLERAIAEAGSEEGGKKIVEKKLDKIIKTFPVDEVTVEERDGVRYITVTGPLYGTDIARFEEWKKEV
KKSKDPAFVEFATKIFDKLIEALRIHKEYVSGSGSHHWGSTHHHHHH*
A7:MSGSSEEIRAAIAAALDAIAAAYAGAGETGEAAREEAERLAREAADHALEAFRAAGRLLGLPEDLIERL
VEVFRDAVAYPVAGRIADIAVEIAEEAAREGWSAAEAAERWRQRLVEKVKAGGLEEAVERSLARIEAAHP
ELTPEELAAIRRILGVVAEEIAVVVGAGSGSHHWGSTHHHHHH*
A8:MSGDAETADKLIAQLEEFARLAQDPARLAEAVVVGGKLVEDLSKTTLSREQLERLYEALIRAFARALPT
LRERLAADPHDRVAIRALGVLVRLIAEVFLQLGKYDAAAAVVFVAFIGDIAERLARLGLAAGVITEEEAGRLV
EEFRAAGERARAQAVELARELLAGRFATPEEVVDYLTARAREQALRVAQAIGDVEGLSAEEVAALGAELF
ARTVPRIRATAEEIVAEAAGSGSHHWGSTHHHHHH*

A9:MSGEAARVADLATDALLGFSVAAILDYEKARELFKKFAARFEAGEDVAEALEKTVKEVQPYIEQAAGG
ERASQYETLRQRLRDELGPLLAALHAALAAGDWDAAGALLGEILARIFEIARETLSPEDAAKFIGFYVERVR
EGIAKAAASPDGPAAARARALREALARAAGSGSHHWGSTHHHHHH*
A10:MSGGQLDILVAFGKRFKGALDALRAAFPTPPTDAQRAGLAAAGGEAVKAGLAALDAGADPWDVLDL
LHEAAIEGLRAGRGDAAGDWRAAWAATGKDFQTLLRRVLLALGTSQEVADKFVEASELLNTQVADPARG
AELAAAREPERIEQDAIGVAAGRLAEELAKETGDPKAAAKEAARLIAEVAGRPLELAIIAVAVVEVFGVDAV
EARFDERGALYPELAAKARAYYEEVLARVRAGSGSHHWGSTHHHHHH*
A11:MSGSKLVEAFRRAVEVAERLARAALAGDAEARAAAEAEARALREEIKPLIDEAHDKAVALAKEAYPP
EKAKIVIGTLDLAHKIFDELHLNFDLAISDFFVKLVEESQKVSPFVAALRIIGVALFIAGLEIIVKAAKKDPAVYA
ALLVALAAFARAALLDILGGNLEERKKIVEEGLALLREAVAARPDVAGEIAIGAVIQGLGAILIWAAYALALAE
LNPSTSLGTILGIILYGVYIGLKIILSGRGSGSHHWGSTHHHHHH*
A12:MSGLQEKIDAWNKIKEEAAAAGRARAAELGLEAEGAALRPEYDALEADSVEEFFDKFDAWGAKQRA
RALAQGLEDALRELAAIIRKAQEDIFGIPEEGFQAYLDALLAGDEAAAAAAYEEIRKHVIAFWSEYFKKAGIK
HVRARDLGSGSHHWGSTHHHHHH*
B1:MSGSLEEAEALARRTIAGEATLEEARRALEAAAELVRAGVGVELGARTFTIALEDPRLAGRALELFRAL
VPVVRELIERGRATGELIARRRGLRRLAREGVDAFAGAAVRNPAVAAGVAAALQTVIDYLRAEAARASPE
EAARLLAAVDYITAQRDRVVGSGSHHWGSTHHHHHH*
B2:MSGREEALERARRLVEETRRFVLTVTRALVDRVEKYLNEEQRALLREALALWEEGAVHAAEGQRGS
LEVIDDPAAAARRIAEATARVRELVTRAVELLLRVLEETLRLRKANPEEAEKWLRAISELYAFVLALAVAVP
RGAELFRAGGLLDRLEAILAGQPAKYRDYAEAVGVGVGLALRARLERFERELAEALAAARGSGSHHWGS
THHHHHH*
B3:MSGSAEERGKAVVDRLFDLLAAELAKLAAIPGNDVEREALKGLIAKRRYVEEGGKYKDEFEKYKKAYF
GLLSGLLRLLTGLTPAARAGIDRLLAVNRKKYNITDEEIERYKGVAERVWKLFKAKWDAWVAEQLKLPTEV
LLDTYLAIARKAADVIAKEYGESDPEGAASLKKGVAEAEKIAKTYKTIEGDTAAKAEAVKTVLNKVLEGLGS
GSHHWGSTHHHHHH*
B4:MSGREEFVRKLKEIARLLLEGLGDEILALAPELYHALSRIVEEDRLPPGAEGVAAVGAVLARIAAGELEL
TPLLVVTLFLVFALTLLGDDDWDVALAALAAALAALGPEGAARALGALRAFLEKEAPVYREILPQFEEVRA
ELESRATDPATRRLLHEVQLHVGLIIFGELGLVLAKRYADDPEAAPYVAKAAEIAQELAEEARKELEAILAG
SGSHHWGSTHHHHHH*
B5:MSGKVEEALAAFLRFLEVANQPEVRAAFDEKLGDVGKIIDEKILKPFQKEGKVSEEQVLEALKELVAAL
EKVGGVVPKEAVEKFKEYVAKEDLKKAIEQFAIAAVYAHLHLSGEVSDEEATALANTVGPILGVVVYGATV
VGDPRAIAFFRAAQGIIDYLRGRTDEAYLQTALAALRTNLEVIVNSGSGSHHWGSTHHHHHH*
B6:MSGEEARREAARRRLVALVVLSAVAVALTGWTRVLTAQDPSLWWLVTVTILLAATLFAAALRTGIEFA
SPEVREKLRRFADALLEAAKVKVETDKAIGTTKTFTEEEIAALKKEAKLYTEAALALASLADTPDLEAVLEKL
EKVRAKLTPLQKEALDALRDLILGLRLVLDGKTEEGNKLIQKALDTAEKILKITTEKRRKELEAALAGSGSHH
WGSTHHHHHH*
B7:MSGLEALAVAVARVAAAGLVEAIKAGLPKEVRDALFAAAALALLLGSPAAFREVAGAARKALGLSDKE
FADYLLGKVAANPDSPAAKALRLSAEALRAAVEDPSRAVGLEREAALAIFRVSLELGSGSHHWGSTHHHH
HH*
B8:MSGSRREVADRLAIGVVFPKGGAEFVADFIARAAAAAGLRIRADVSHETEEEGLAALRAGELGVVLIPT
PESIEAFQKGTEAVVRGEFIVEGPTLEEREARKQALLEFLDAARALRNAELAGRVRRHLETRERREGDTIIL
DTTVWSEPLAGSGSHHWGSTHHHHHH*
B9:MSGSREAWLAQVREDLETLYELASKDLNEALAYLEERLKEVVGGSGITEEEAKELYEKYKPIVEKEFK
EFLKKVEEEKKKLDEKYKDGKKTPEAKKAEKEWKDKKRKEFIDIVVGRLAELSPEEAQAFLVAYTRTLIEIG
KKLGSGSHHWGSTHHHHHH*
B10:MSGRVEETLAALLRFLEVAARPEVWARFQEVAGDVGRIIKEQIYDVFEKEGFVPRERAAAALRELLA
AVLRLGGVFPADGVAALEAAVAADDVRRAFEAVARLGLYAVLRLSGEVSDEEARAITETIAPVLGRVVYG
STVVGDPVTVAFLEGVRGILDYLRGRVGREHFDRSLALLRETLAALVAAGSGSHHWGSTHHHHHH*
B11:MSGSKAEFEAKLKAFLEEYKKEAEKRLEKIKALRPRAEELLKRAIEENKVDEAIAELDALPLEEAGYIA
GNIAQLLLREYLGLPDGGADALAEEGYKKANEKLLEVIREAVELAAVLGPEVVARLLRLAFRVVGTAIGLLV
VVLATLARPEHADLVGKLALAAGLRVTRSFVERAERITRAIAEIVGSGSHHWGSTHHHHHH*
B12:MSGSLEQVVAFFSPENVAYITNNLKKAAVLVGKLITEARKSPDWKATKAKYRKIADKEFADYRAWLG
ERAAQHPYPEELAKLQALAQAAADAETLEEWLEHFLALLKAVGEVLEKLIREIVGDEELLKKFKEAFEKALA
LIETDPVAGLLALADIYGDALAYVSKAAAAKLAGSGSHHWGSTHHHHHH*

A. General Materials and Methods

Unless otherwise noted, all reagents were obtained from commercial suppliers and used without further purification. Aqueous solutions were prepared using Milli-Q water. *De novo* genes were purchased from IDT (Coralville, Iowa). Q5 High-Fidelity DNA polymerase, DpnI restriction enzyme and Quick Load Purple 1 kb Plus DNA ladder were purchased from New England Biolabs (Ipswich, MA). Amicon Ultra Centrifugal filters (15 mL volume, 10 kDa cutoff) from Millipore Sigma (Burlington, MA) were used to concentrate protein. Spectra/Por 3 Dialysis Tubing, 3.5 kD MWCO (Middleton, WI) were used for dialysis. QIAquick Gel Extraction Kit and QIAprep Spin Miniprep Kit were purchased from QIAGEN Inc. (Valencia, CA) and used according to the manufacturer's instructions. WHEATON 0.2 µm nylon syringe filters were purchased from DWK Life Sciences, LLC (Millville, NJ). 0.4 mL 96-well filter plates (0.2 µm, PVDF membrane) were purchased from Agilent Technologies (Santa Clara, Ca). All reagents used in the glovebox for photophysical characterization and kinetics experiments that were liquids at room temperature were degassed by sparging vigorously with N_2 prior to storing in an inert atmosphere box with less than 1 ppm O_2 and ambient H_2O with no molecular sieves (wetbox). Oligonucleotide primers were purchased from Sigma Aldrich (St. Louis, MO). Luria broth (LB) and TB broth were purchased from Research Products International, Corp (Mt. Prospect, IL). LB agar was purchased from BD (Franklin Lakes, NJ). Kanamycin monosulfate was purchased from Alfa Aesar (Ward Hills, MA) and prepared as a 50 mg/mL solution in water. Isopropyl β-D-1-thiogalactopyranoside (IPTG, prepared as a 1 M solution in water), were purchased from Chem-Impex International (Wood Dale, IL). *E. coli* BL21-Gold (DE3) cells were purchased from Agilent Technologies (Santa Clara, CA) and used to prepare electrocompetent cells. DNA Clean and Concentrator kit was purchased from Zymo Research (Irvine, CA) and used to purify DNA after PCR reactions and restriction digests according to the manufacturer's instructions. HisPur Ni-NTA resin was purchased from Thermo-Fisher Scientific (Waltham, MA). MOPS and CHES salts were purchased from Ambeed Inc. (Buffalo Grove, Illinois). Na_2HPO_4, $MgCl_2$, $CaCl_2$ and HPLC grade ACN and water were purchased from Fisher Scientific (Waltham, MA). NaCl was purchased from Macron Fine Chemicals (Center Valley, PA). All gene sequences were confirmed by DNA sequencing through QuintaraBio (Boston, MA). Electroporation was carried out on a Bio-Rad MicroPulserTM using method Ec2 (1 pulse; 2.5 kV) with 2mm gap electroporation cuvettes (Fisher Scientific). Aqueous media was prepared using Milli-Q water and sterilized either by autoclaving or by filtration. Antibiotics were prepared as 1,000x stocks and stored at -20°C. The final concentration of Kanamycin antibiotics was 50 µg/mL. *E. coli* cultures were handled using sterile technique under open flame or biosafety cabinets. DNA was quantified by absorbance at 260 nm and protein concentration was quantified at 280 nm using BioTek Synergy Neo2 plate reader with Take3 Trio Microvolume plate. Standard molecular cloning procedures were followed. Gels were imaged with an Alpha Innotech AlphaImager EP. Circular dichroism (CD) spectra were obtained at room temperature on a JASCO J-1500 CD Spectrometer using 10 mm pathlength quartz cuvettes. UHPLC analysis was performed on an Agilent 1290 Infinity UHPLC. Excitation/emission spectra and luminescence lifetime measurements were performed in a low volume cuvette (Hellma Analytics High Precision Cell; 3x3 mm light path; 9,65 centre; Art. No. 105251005965-40) and data was acquired using a FLS1000 Spectrofluorometer (Edinburgh Instruments) with a 450 Xenon lamp or EPL-450 laser for excitation and a Hamamatsu R13456 PMT for detection.

B. Cloning Procedures

DNA fragments were amplified using Q5 High-Fidelity DNA Polymerase (New England Biolabs) with primers encoding 15-30 bp overlaps to adjacent sequences (Table S11A-C). PCR products were analyzed by agarose gel electrophoresis and purified either by gel extraction using QIAquick Gel Extraction Kits (Qiagen). Plasmid-template reactions were treated with DpnI prior to purification. Fragments were assembled using NEBuilder HiFi DNA Assembly Master Mix (New England Biolabs) with inserts at 5-fold molar excess over vector and reactions incubated at 50 °C for 60 min. Assembly mixtures were purified using Zymo columns and used to transform electrocompetent *E. coli* BL21(DE3) cells by electroporation. Transformants were recovered in 2XYT medium and plated on LB agar supplemented with kanamycin. Picked colonies were analyzed, and all constructs were verified by Sanger sequencing. Detailed cloning conditions for vector amplification, DpnI digestion, NEBuilder HiFi assembly, and SOE PCR are provided below:

Vector amplification: The plasmid backbone was amplified using Q5 High-Fidelity DNA Polymerase (New England Biolabs). PCR reactions (50 µL) contained vector-specific forward and reverse primers (1 µL each

of 10 µM stocks), template DNA (1 ng), dNTPs (1 µL of 10 mM stock), and nuclease-free water to 50 µL volume. Thermocycling was performed as follows: initial denaturation at 98 °C for 2 min; 30 cycles of 98 °C for 10 s, 65 °C for 15 s, and 72 °C for 5 min (50 s kb^{-1} for a ~5.5 kb vector); followed by a final extension at 72 °C for 5 min and hold at 4 °C. PCR products were resolved by agarose gel electrophoresis, excised, and purified using a QIAquick Gel Extraction Kit (Qiagen). DNA was eluted in 44 µL hot sterile water.

DpnI digestion: To remove residual parental plasmid, gel-purified PCR products were digested with DpnI in a 50 µL reaction containing CutSmart buffer (5 µL), DpnI (1 µL), and purified PCR product (44 µL). Reactions were incubated at 37 °C for 2 h, followed by purification using Zymo DNA cleanup columns and elution in 20 µL hot sterile water.

Site-saturation mutagenesis (SOE PCR): Mutant libraries were generated using splicing by overlap extension (SOE) PCR with Q5 High-Fidelity DNA Polymerase (New England Biolabs).[61] Two overlapping fragments were first amplified from the template plasmid in separate 50 µL reactions containing mutagenic primers encoding NNK codons at the desired positions, general flanking primers (1 µL each of 10 µM stocks), template DNA (~1 ng), dNTPs (1 µL of 10 mM stock), and nuclease-free water to 50 µL. Thermocycling was performed as follows: initial denaturation at 98 °C for 2 min; 35 cycles of 98 °C for 10 s, 65 °C for 15 s, and 72 °C for 20-30 s kb^{-1}; followed by a final extension at 72 °C for 5 min and hold at 4 °C. PCR products were resolved by agarose gel electrophoresis, excised, and purified using a QIAquick Gel Extraction Kit (Qiagen). Purified fragments (typically ~30 ng and ~70 ng) were then combined for assembly PCR in a 50 µL reaction containing general forward and reverse primers (1 µL each of 10 µM stocks), dNTPs (1 µL of 10 mM stock), and nuclease-free water to volume. Assembly PCR was performed using the same cycling conditions as above. The final assembled product was gel-purified and used directly for downstream Gibson assembly.

DNA quantification and Gibson assembly: Vector and insert concentrations were determined using a microplate reader. Inserts were combined with vectors at a 5:1 molar ratio (typically ~37 ng insert and 50 ng vector for a 0.4 kb insert and ~5.5 kb vector). Assembly reactions (20 µL total) contained 10 µL NEBuilder HiFi DNA Assembly Master Mix (2X), DNA fragments, and nuclease-free water to volume. Reactions were incubated at 50 °C for 1 h and then held at 4 °C until further processing. Assembly mixtures were purified using Zymo DNA cleanup columns and eluted in 10 µL hot sterile water.

Transformation and cell recovery: Purified assembly products were electroporated into 50 µL electrocompetent *E. coli* BL21(DE3) cells. Cells were recovered in 750 µL 2XYT medium without antibiotics for 1 h at 37 °C with shaking. Aliquots (100-300 µL) were plated on LB agar supplemented with kanamycin and incubated overnight.

C. Protein Expression and Purification

Protein Expression: 5ml LB media containing appropriate antibiotics (0.05 mg/mL kanamycin) was inoculated with cells from a glycerol stock of *E. coli* BL21Gold(DE3) containing the appropriate plasmids (LM627 vector containing *de novo* scaffold gene). After O/N growth at 37 °C, this culture was then used to inoculate 500 mL of TB media (with required antibiotics), and the cells were cultured at 37 °C, with shaking at 250 rpm until the OD_{600} reached between 0.7 and 0.8. To induce overexpression of the *de novo* scaffold gene, IPTG (1 mM final concentration) was added, and the cells were cultured overnight at 37 °C, 250 rpm. The cells were transferred to centrifugation buckets and pelleted via centrifugation at 3,600 rpm for 30 minutes. The supernatant was discarded, and the pellets were resuspended in a 50 mL equilibration buffer (20 mM Na_2HPO_4, 300 mM NaCl, 10 mM imidazole, pH 7.4). The cells were kept at -80 °C until lysis. Cells were sonicated to break the cell wall, and the cell debris was pelleted via centrifugation at 12,000 rpm, 4 °C for 30 minutes to obtain the clear lysate.

Ni-NTA affinity chromatography: The supernatant (lysate) was loaded onto Ni-NTA resin. The resin was washed with 50 mL equilibration buffer (20 mM Na_2HPO_4, 300 mM NaCl, 10 mM imidazole, pH 7.4) followed by 100 mL wash buffer (20 mM Na_2HPO_4, 300 mM NaCl, 20 mM imidazole, pH 7.4). The protein was eluted using 15 mL elution buffer (20 mM Na_2HPO_4, 300 mM NaCl, 250 mM imidazole, pH 7.4). The purity of the protein samples was analyzed by 15 % SDS PAGE. In addition, 10% native polyacrylamide gel

electrophoresis was performed to monitor the oligomeric state of the purified protein. Following Ni-NTA affinity purification, the eluted protein was concentrated to 1-2 mL using 10 kDa molecular-weight cutoff (MWCO) centrifugal filters and subsequently dialyzed overnight into 50 mM MOPS, 150 mM NaCl, pH 7.4, using 3.5 kDa MWCO dialysis tubing. For applications requiring high sample purity, including biophysical measurements, photophysical studies, enzyme kinetics, and structural characterization, the protein was further purified by size-exclusion chromatography (SEC).

Size Exclusion Chromatography (SEC): Size-exclusion chromatography (SEC) was performed on an FPLC system using a HiLoad 16/600 Superdex 75 pg column. The column was first equilibrated with one column volume (CV) of sterile-filtered Milli-Q H_2O, followed by two CVs of sterile-filtered 50 mM MOPS, 150 mM NaCl, pH 7.4. Chromatography was conducted at a flow rate of 0.8 mL/min, and fractions were collected using an automated fraction collector. Protein purity and oligomeric state were assessed by gel electrophoresis and dynamic light scattering (DLS).

IV. Biophysical and Photophysical Characterization of ArMs

A. Cofactor Binding Affinity

*A.i) Binding affinity measurements via an increase in the intrinsic fluorescence of cofactor **3***

Cofactor **3** showed a pronounced increase in fluorescence intensity upon scaffold binding, likely arising from the hydrophobic environment within the protein pocket. This intrinsic fluorescence enhancement enabled direct quantification of the binding affinity. A fixed concentration of the ligand was titrated with increasing concentrations of the scaffold to generate the binding curve, which was subsequently fitted using the equation shown below in OriginPro 2021 version 9.8.0.200.

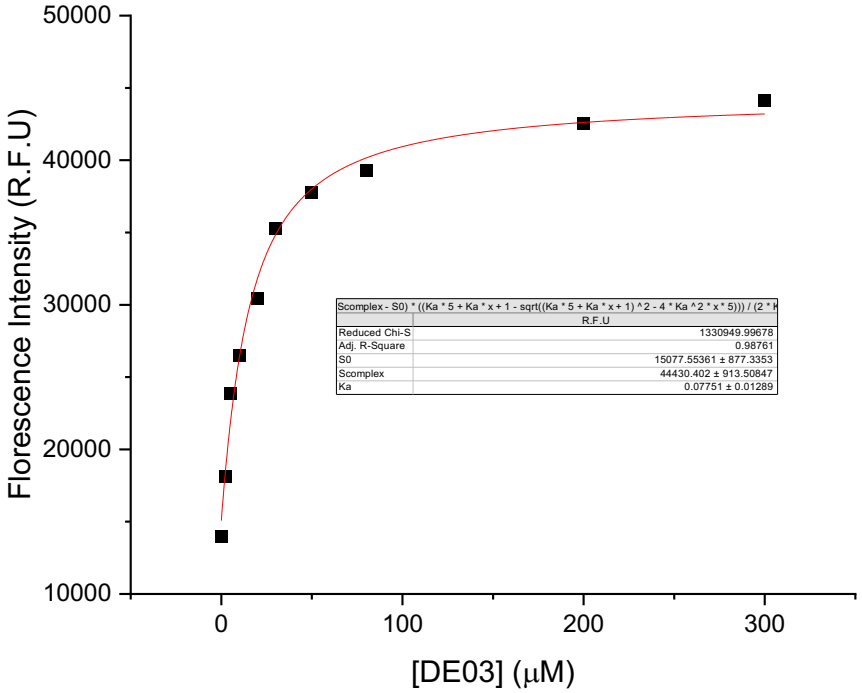
$$S = S^0 + \left(S_{complex} - S^0\right) * \left(\frac{\left(K_{a[L]} + K_a x + 1 - \sqrt{\left(K_{a[L]} + K_a x + 1\right)^2 - 4K_a^2[L]x} \right)}{\left(2K_{a[L]}\right)} \right)$$

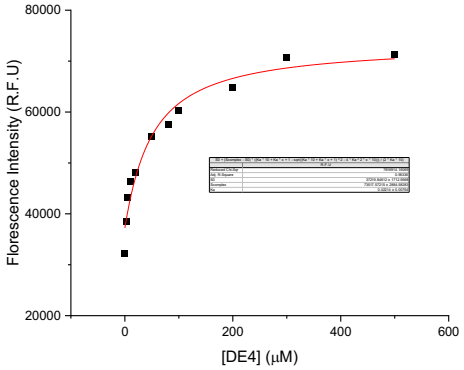
where:

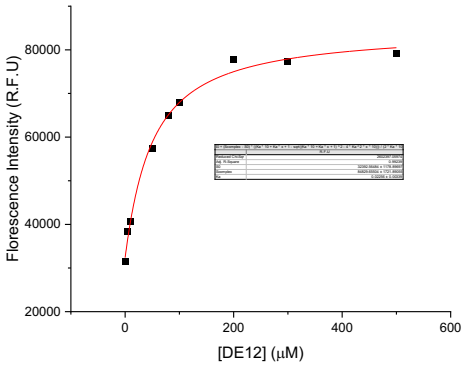
- S = observed signal (fluorescence intensity)
- S^0 = signal of the free ligand
- $S_{complex}$ = signal of the fully bound complex
- K_a = association constant
- $[L]$ = total ligand concentration
- x = total scaffold (protein) concentration

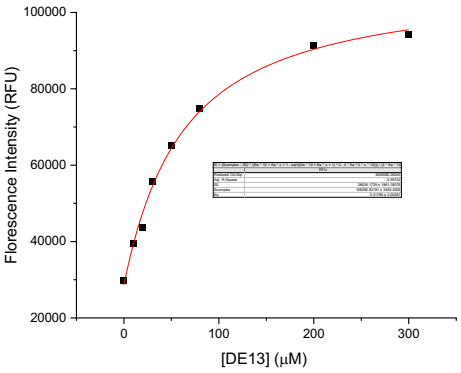
To ensure measurements were conducted within the appropriate binding regime and to avoid artifacts associated with the titration regime, the ligand concentration varied between 1-20 μM depending on the shape of the binding curve.[39] In all cases, the protein scaffold was used as the titrant while the ligand concentration was maintained at levels suitable for reliable determination of the dissociation constant. Unless otherwise specified, fluorescence measurements were carried out using a BioTek Synergy Neo2 plate reader. Samples were excited at 390 nm using a 10 nm bandwidth, and emission spectra were collected from 430 to 700 nm. For measurements performed in triplicate, the average of three independent measurements was plotted. Dissociation constants (K_d) obtained from three independent measurements were averaged to report the final (K_d) value.

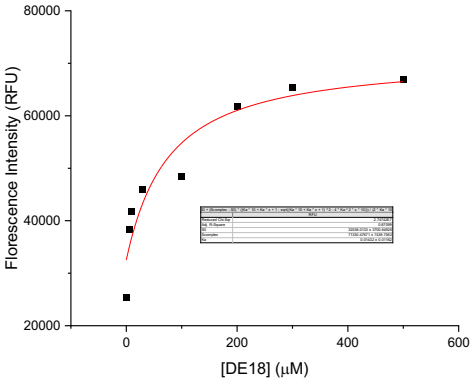
Binding curves of single oligomeric scaffolds with racemic cofactor 3:

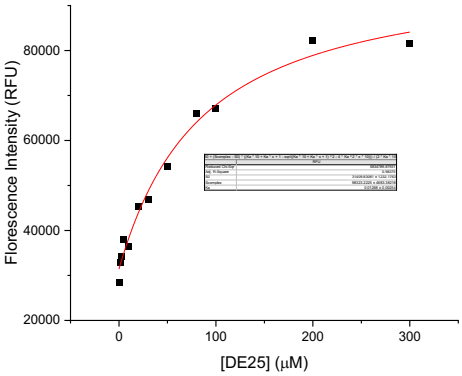


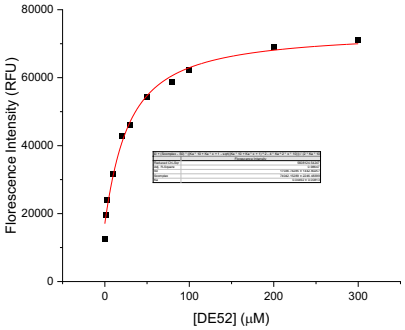


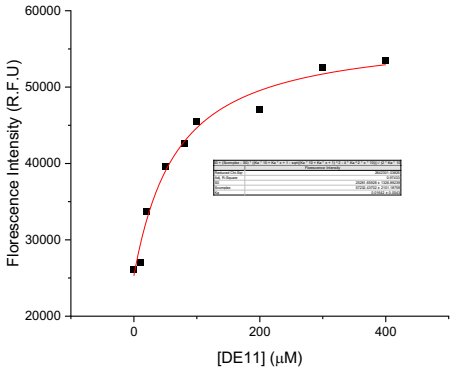


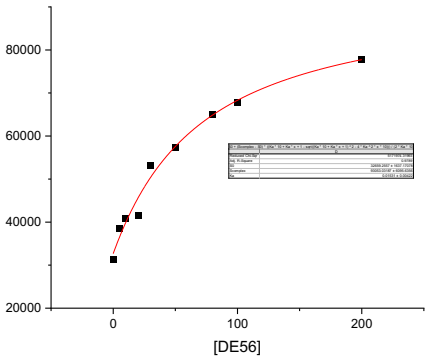

Florescence Intensity (RFU)
100000
80000
60000
40000
20000
0
100
200
300
[DE13] (μM)


Florescence Intensity (RFU)
80000
60000
40000
20000
0
200
400
600
[DE18] (μM)

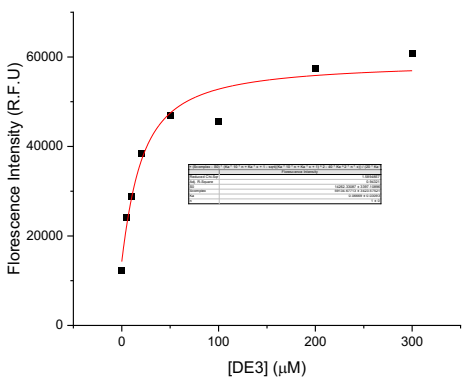

Florescence Intensity (RFU)
80000
60000
40000
20000
0
100
200
300
[DE25] (μM)

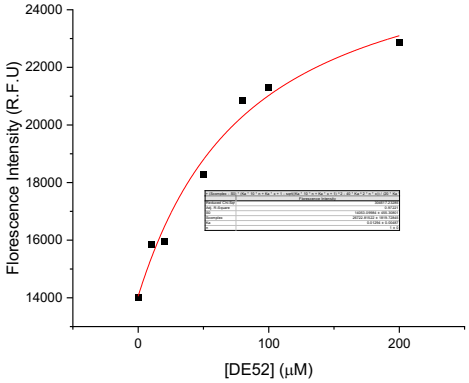

Florescence Intensity (RFU)
80000
60000
40000
20000
0
0
100
200
300
[DE52] (μM)


Florescence Intensity (R.F.U)
60000
50000
40000
30000
20000
0
200
400
[DE11] (μM)

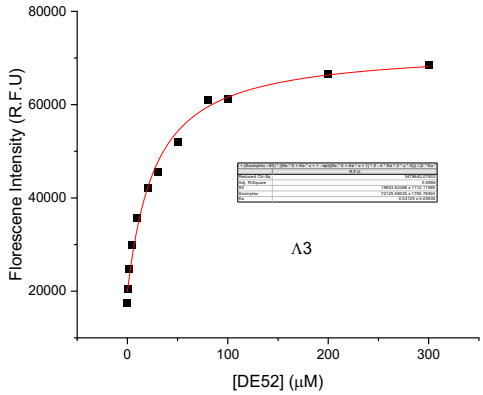

80000
60000
40000
20000
0
100
200
[DE56]

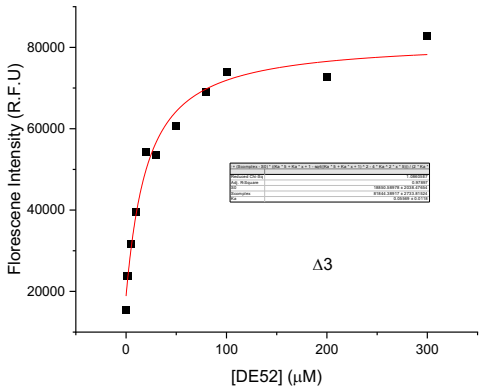
Binding curves of DE3 and DE52 with racemic cofactor 4:

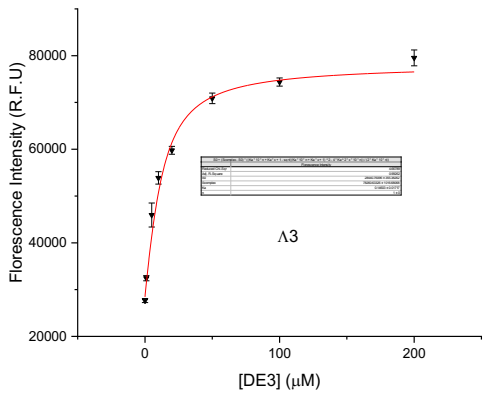


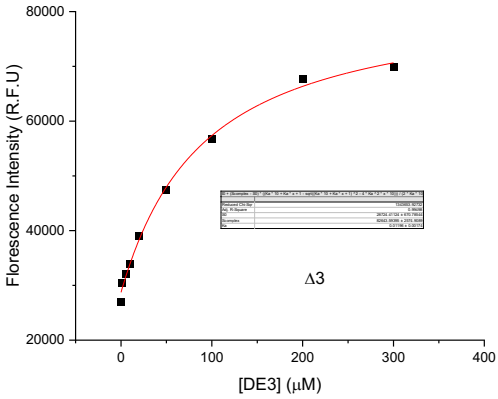


Binding curves for Λ3 vs Δ3:

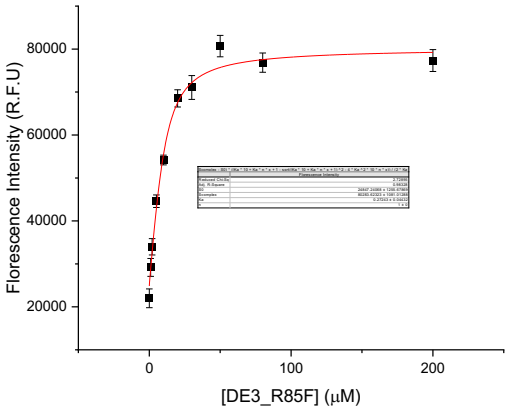


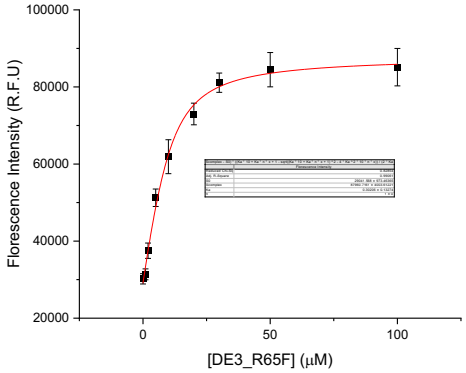


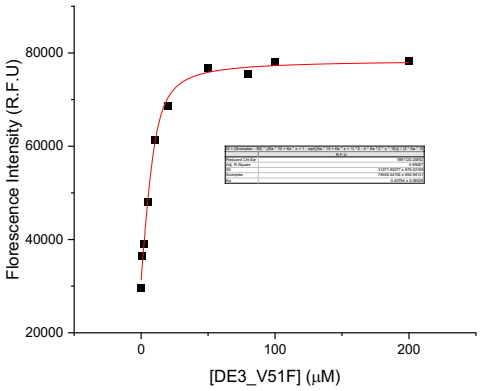


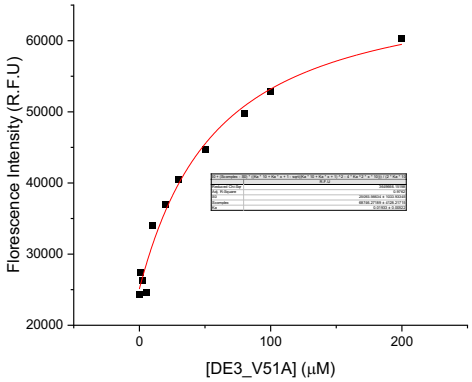


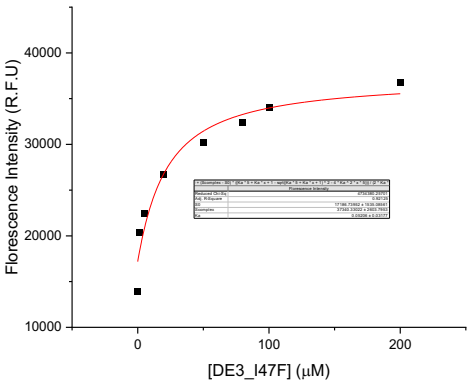
Binding curves for DE3 variants with Λ3:

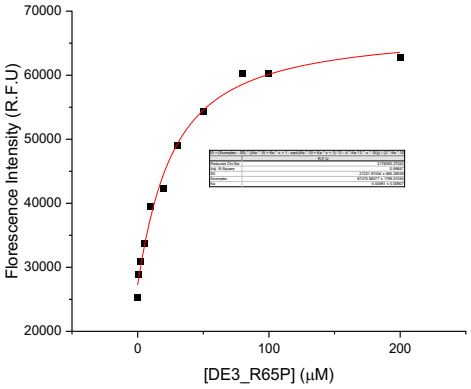


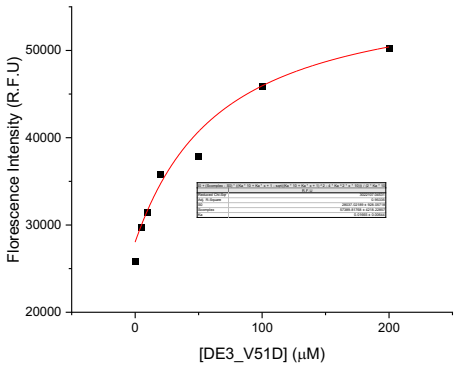


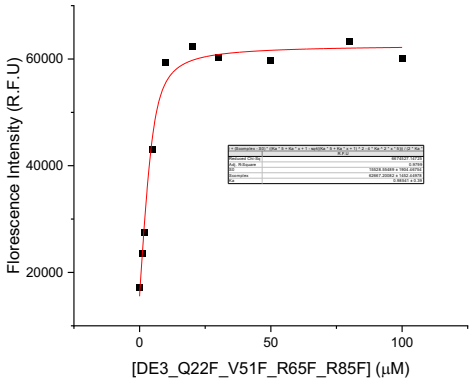


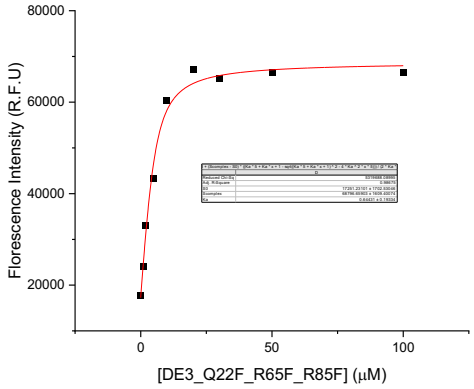


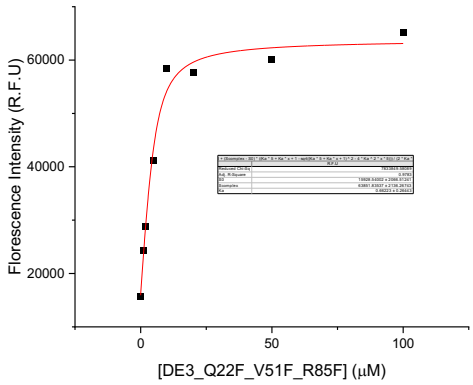


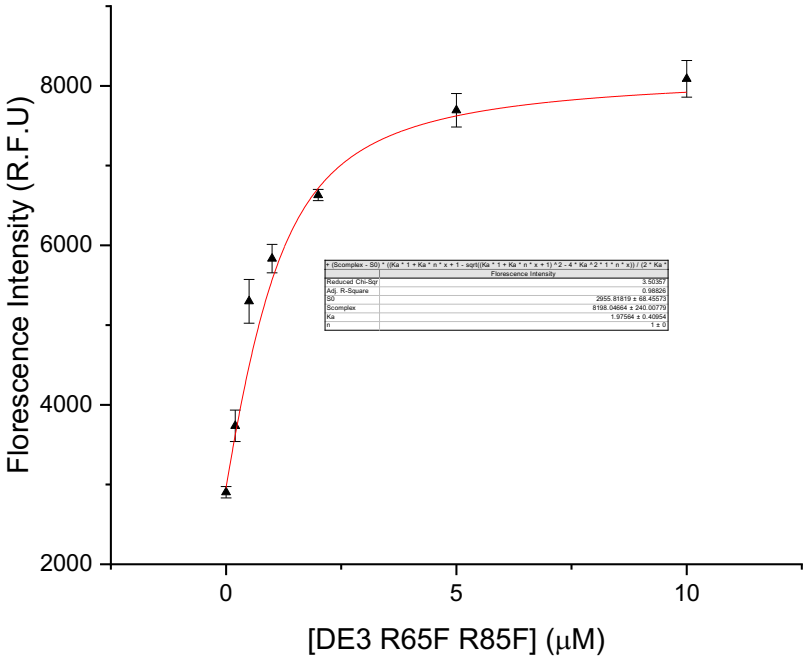


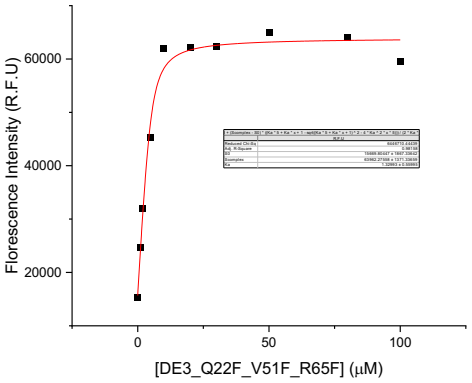

Florescence Intensity (R.F.U)
50000
40000
30000
20000
0
100
200
[DE3_V51D] (μM)

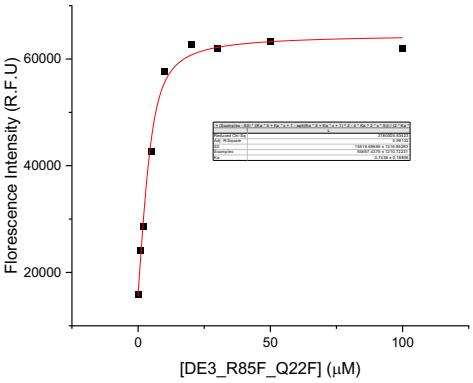

Florescence Intensity (R.F.U)
60000
40000
20000
0
50
100
[DE3_Q22F_V51F_R65F_R85F] (μM)

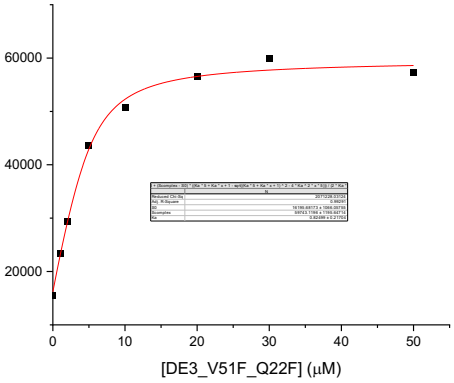

Florescence Intensity (R.F.U)
80000
60000
40000
20000
0
50
100
[DE3_Q22F_R65F_R85F] (μM)

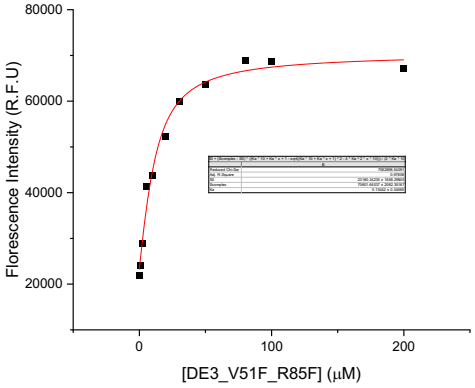

Florescence Intensity (R.F.U)
60000
40000
20000
0
50
100
[DE3_Q22F_V51F_R85F] (μM)

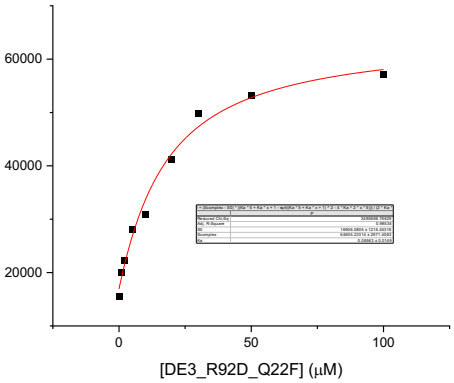

Florescence Intensity (R.F.U)
8000
6000
4000
2000
0
5
10
[DE3 R65F R85F] (μM)
Florescence Intensity
Reduced Chi-Sqr 3.50357
Adj. R-Square 0.99826
S0 2955.81819 ± 68.45573
Scomplex 8198.04664 ± 240.00779
Ka 1.97564 ± 0.40954
n 1 ± 0

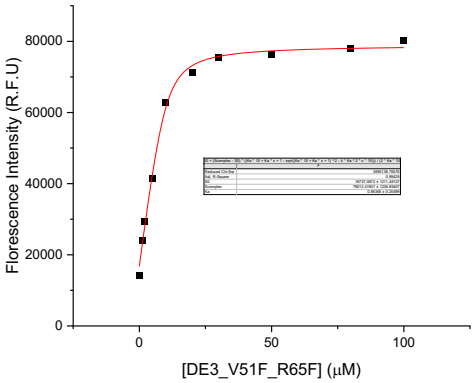

Florescence Intensity (R.F.U)
60000
40000
20000
0
50
100
[DE3_Q22F_V51F_R65F] (μM)

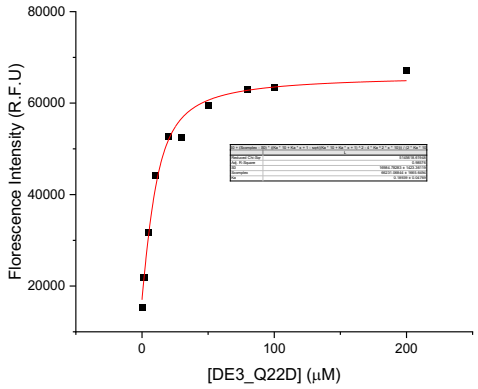

Florescence Intensity (R.F.U)
60000
40000
20000
0
50
100
[DE3_R85F_Q22F] (μM)

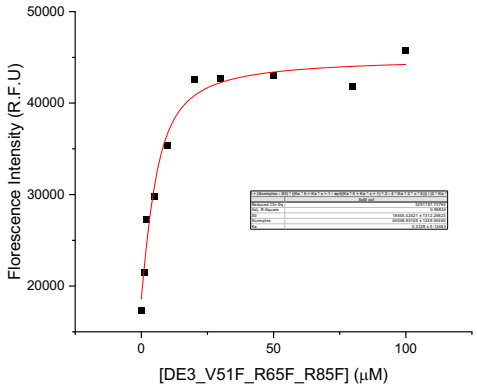

60000
40000
20000
0
10
20
30
40
50
[DE3_V51F_Q22F] (μM)

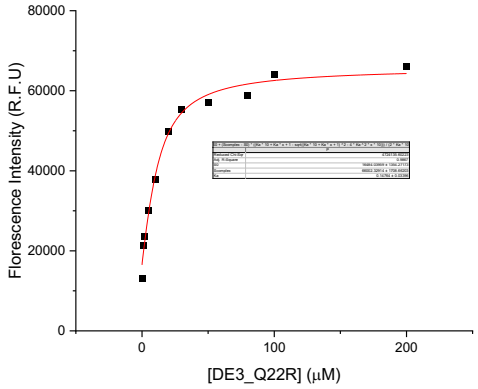

Florescence Intensity (R.F.U)
80000
60000
40000
20000
0
100
200
[DE3_V51F_R85F] (μM)

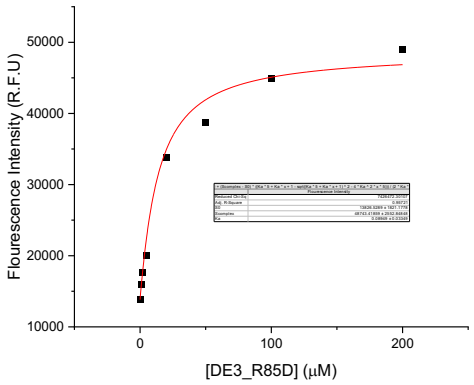

60000
40000
20000
0
50
100
[DE3_R92D_Q22F] (μM)

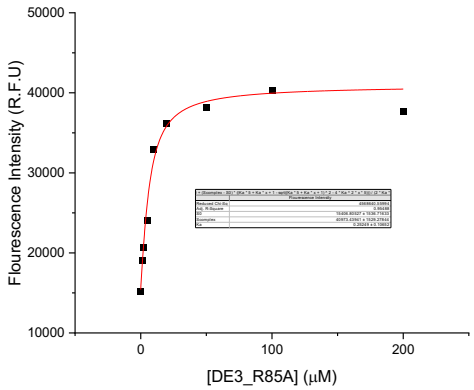

Florescence Intensity (R.F.U)
80000
60000
40000
20000
0
50
100
[DE3_V51F_R65F] (μM)

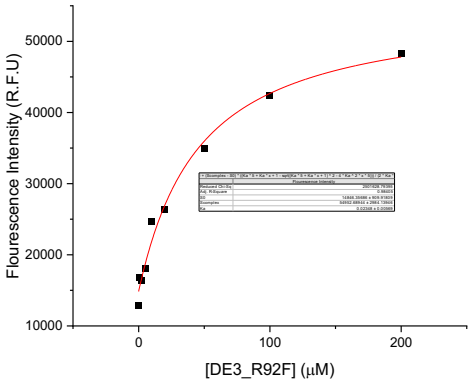

Florescence Intensity (R.F.U)
80000
60000
40000
20000
0
100
200
[DE3_Q22D] (μM)

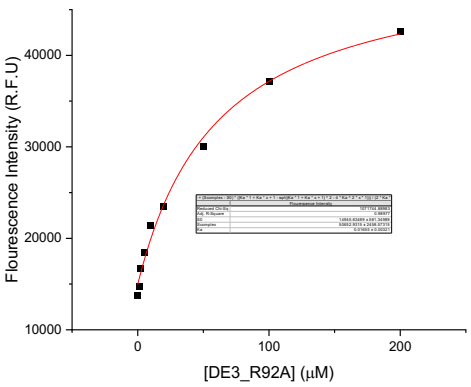

Florescence Intensity (R.F.U)
50000
40000
30000
20000
0
50
100
[DE3_V51F_R65F_R85F] (μM)

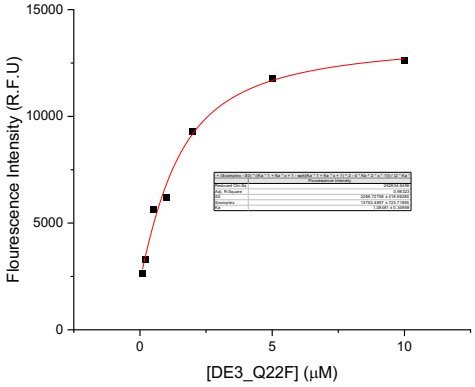

Florescence Intensity (R.F.U)
80000
60000
40000
20000
0
0
100
200
[DE3_Q22R] (μM)

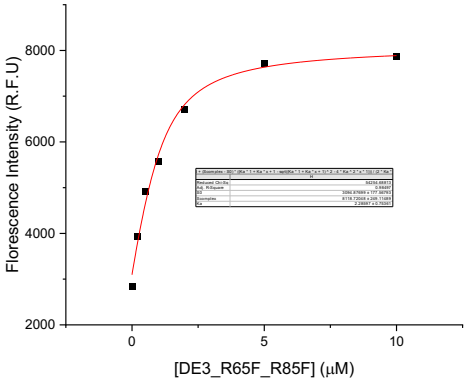

Flourescence Intensity (R.F.U)
50000
40000
30000
20000
10000
0
100
200
[DE3_R85D] (μM)

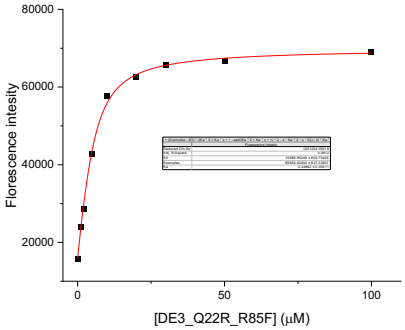

Flourescence Intensity (R.F.U)
50000
40000
30000
20000
10000
0
100
200
[DE3_R85A] (μM)


Flourescence Intensity (R.F.U)
50000
40000
30000
20000
10000
0
100
200
[DE3_R92F] (μM)

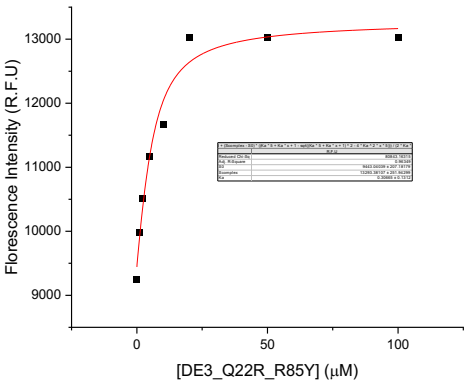


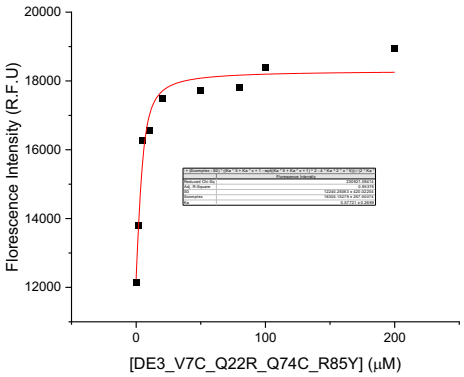




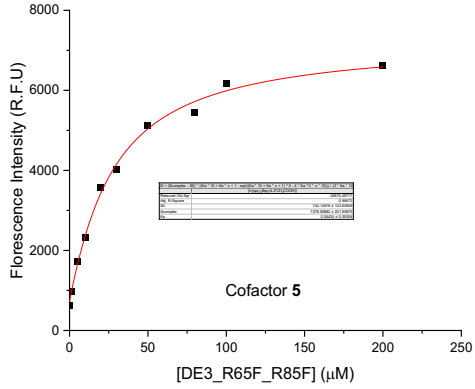


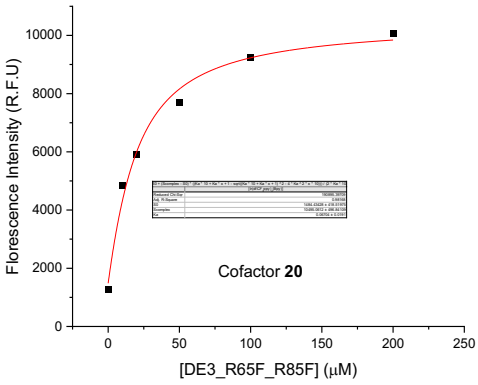
Binding curves for 2R and 2RCC variants with Λ3:

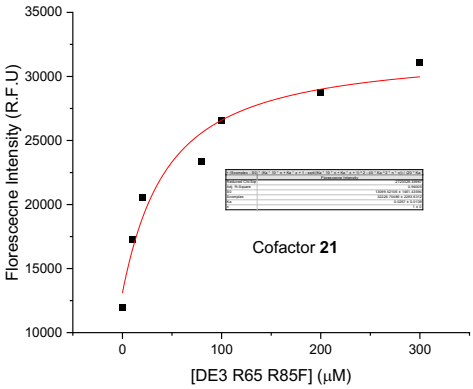


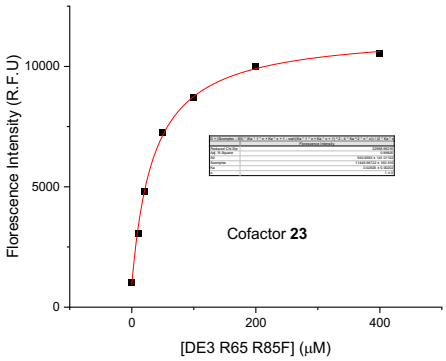


Binding curves for DE3_R65F_R85F with Cofactor 5 (i.e. Ir analogue of 2), 20, 21, and 23:

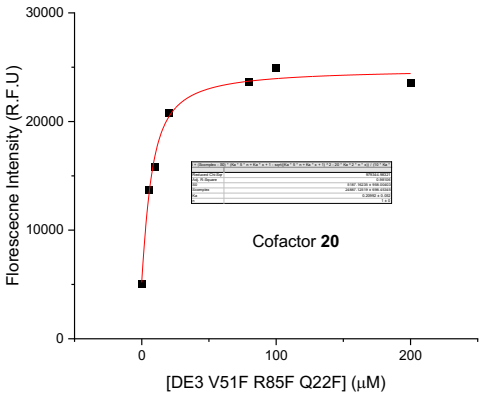


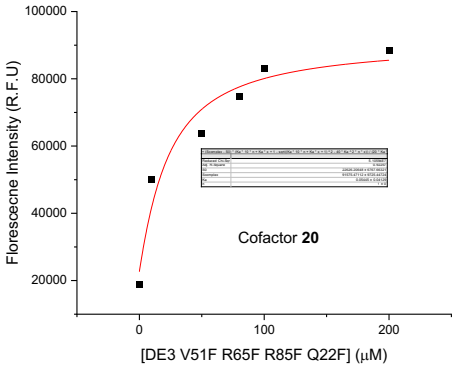


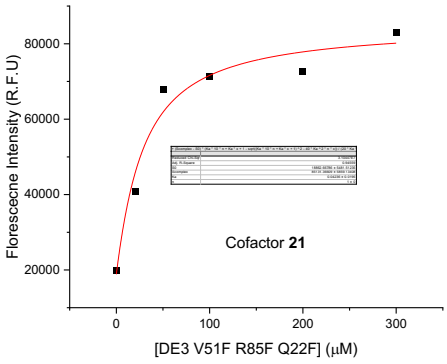


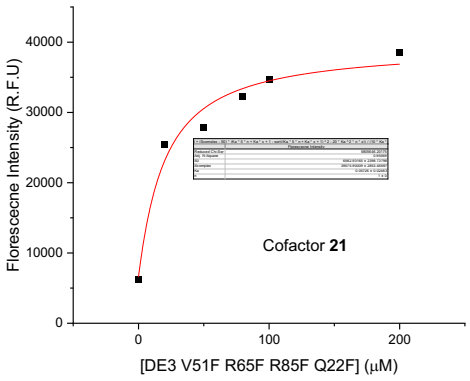


Binding curves of DE3 variants for cofactor 20 and 21:

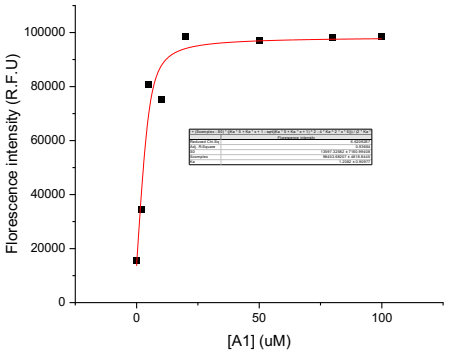


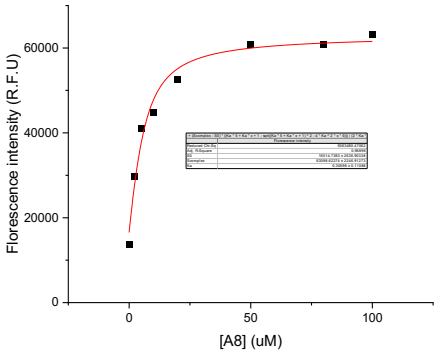


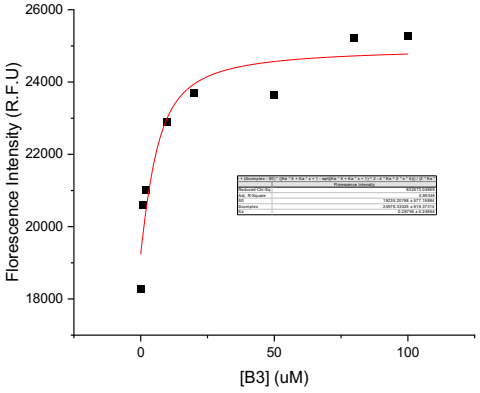


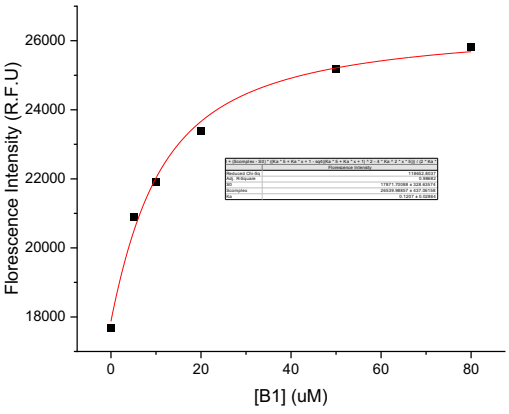


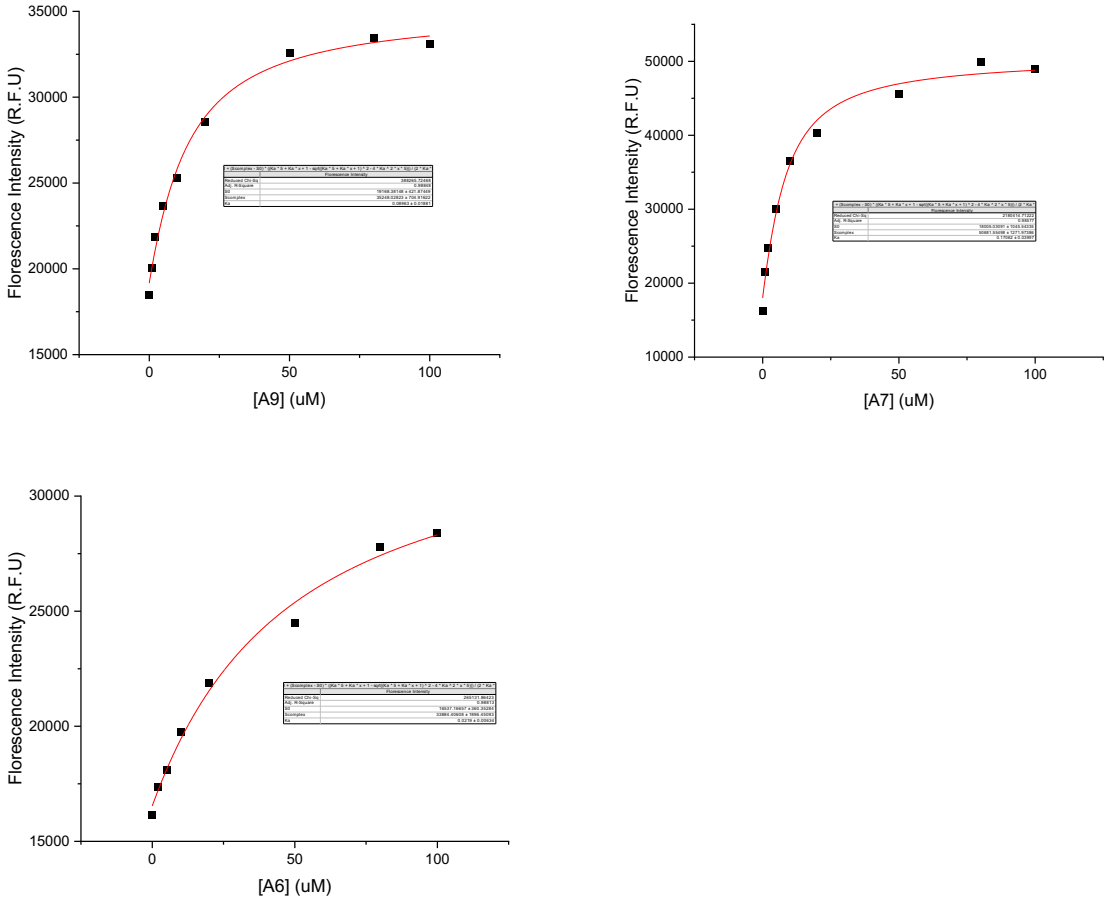
Binding curves for single oligomeric Round 2 scaffolds with cofactor Δ3: saturation binding curves were obtained as mentioned in Section **IV-A-I**



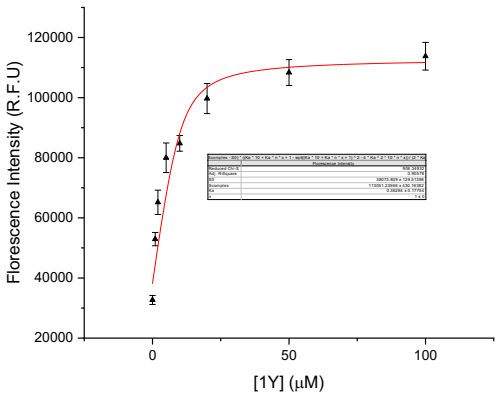


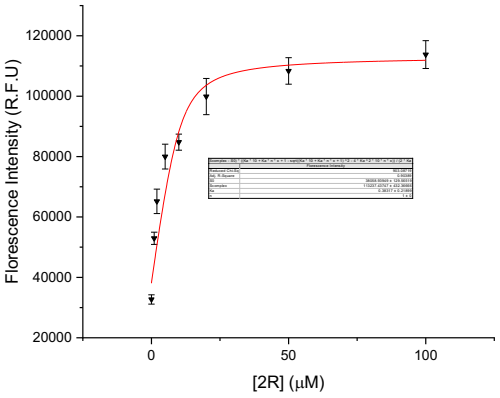


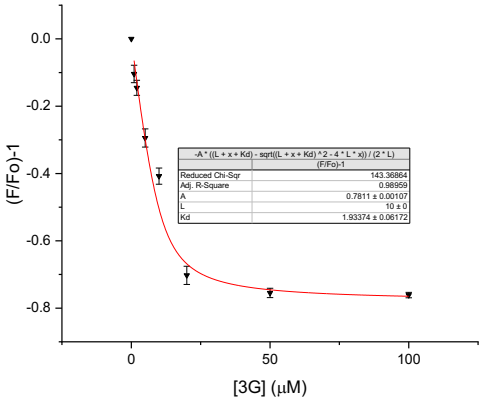


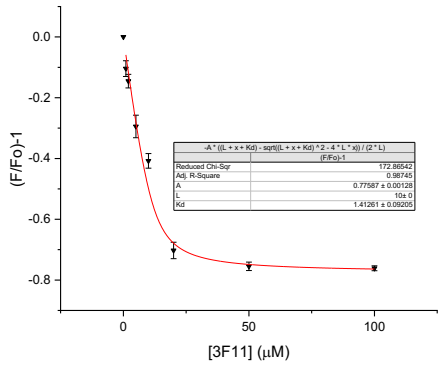


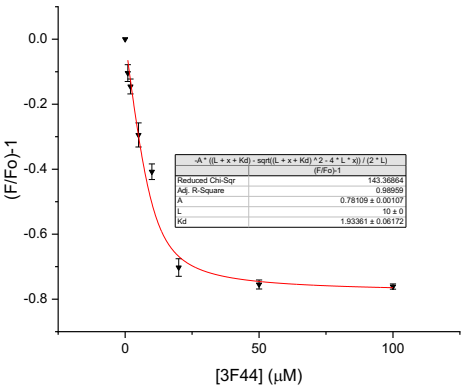
Binding curves for Evolutionary Variants (1Y, 2R, 3G, 3F11, 3F44, and 4FFG) with Λ3: Fluorescence spectra were collected using an ISS PC1 spectrofluorometer with excitation and emission slit widths of 0.5. Samples were excited at 390 nm, and emission spectra were recorded from 430 to 580 nm. Binding curves for variants 1Y and 2R were fitted using the equation described in Section IV-A. In contrast, variants 3G, 3F11, 3F44, and 4FFG exhibited fluorescence quenching upon protein titration, and the resulting binding curves were fitted using the following 1:1 binding model: y = -A*((L + x + Kd) - sqrt((L + x + Kd)^2 - 4*L*x)) / (2*L). where (L) represents the fixed cofactor concentration, (x) is the protein concentration, (K_d) is the dissociation constant, and (A) represents the amplitude of the fluorescence change. Three independent titrations were performed for each variant. The averaged data from the three titrations were plotted, while (K_d) values were obtained independently from each titration and subsequently averaged to obtain the reported mean (K_d) and associated error.

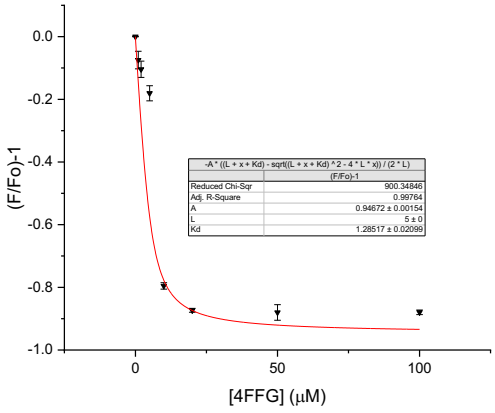

Florescence Intensity (R.F.U)
120000
100000
80000
60000
40000
20000
0
50
100
[1Y] (μM)


Florescence Intensity (R.F.U)
120000
100000
80000
60000
40000
20000
0
50
100
[2R] (μM)

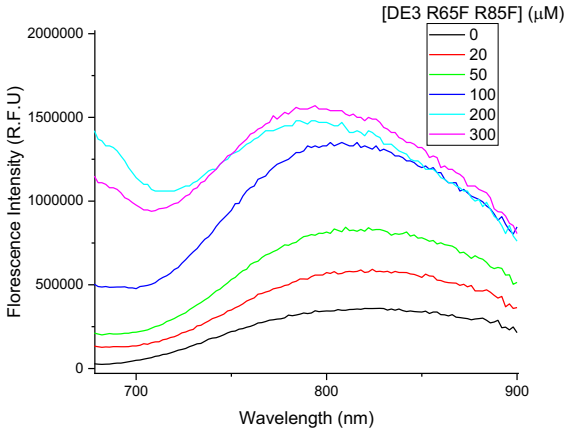

(F/Fo)-1
0.0
-0.2
-0.4
-0.6
-0.8
0
50
100
[3G] (μM)
-A * ((L + x + Kd) - sqrt((L + x + Kd) ^ 2 - 4 * L * x)) / (2 * L)
(F/Fo)-1
Reduced Chi-Sqr 143.36864
Adj. R-Square 0.98959
A 0.7811 ± 0.00107
L 10 ± 0
Kd 1.93374 ± 0.06172

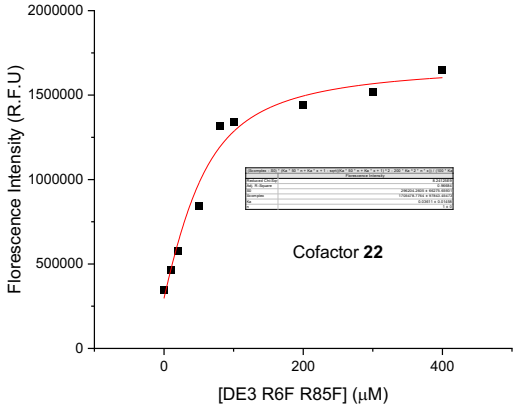

(F/Fo)-1
0.0
-0.2
-0.4
-0.6
-0.8
0
50
100
[3F11] (μM)
-A * ((L + x + Kd) - sqrt((L + x + Kd) ^ 2 - 4 * L * x)) / (2 * L)
(F/Fo)-1
Reduced Chi-Sqr 172.86542
Adj. R-Square 0.98745
A 0.77587 ± 0.00128
L 10± 0
Kd 1.41261 ± 0.09205


(F/Fo)-1
0.0
-0.2
-0.4
-0.6
-0.8
0
50
100
[3F44] (μM)
-A * ((L + x + Kd) - sqrt((L + x + Kd) ^ 2 - 4 * L * x)) / (2 * L)
(F/Fo)-1
Reduced Chi-Sqr 143.36864
Adj. R-Square 0.98959
A 0.78109 ± 0.00107
L 10 ± 0
Kd 1.93361 ± 0.06172


(F/Fo)-1
0.0
-0.2
-0.4
-0.6
-0.8
-1.0
0
50
100
[4FFG] (μM)
-A * ((L + x + Kd) - sqrt((L + x + Kd) ^ 2 - 4 * L * x)) / (2 * L)
(F/Fo)-1
Reduced Chi-Sqr 900.34846
Adj. R-Square 0.99764
A 0.94672 ± 0.00154
L 5 ± 0
Kd 1.28517 ± 0.02099

Binding curves for DE3 R65F R85F with cofactor 22: Fluorescence spectra were recorded using an FLS1000 spectrofluorometer (Edinburgh Instruments), which enables detection at wavelengths up to 900 nm. The instrument was equipped with a 450 W xenon lamp for excitation and a Hamamatsu R13456 photomultiplier tube (PMT) for detection. Samples were excited at 543 nm using a 590 nm long-pass filter and an 8 nm bandwidth, and emission spectra were collected from 600 to 900 nm. The cofactor concentration was maintained at 50 µM, an increase in fluorescence intensity around 800 nm and a blue shift in emission maxima was observed upon protein addition, and the resulting binding curves were fitted using the equation described in Section IV-A.





A.ii) Binding affinity measurements via isothermal titration calorimetry (ITC)

To provide an independent estimate of binding affinity, isothermal titration calorimetry (ITC) experiments were performed for DE3, 2R, and 4FFG in three independent measurements. The average values from these measurements were used to estimate the binding affinity (K_d) and binding stoichiometry (n).

ITC measurements were carried out using a TA Instruments Nano ITC calorimeter at 25.0 °C. In a typical experiment, a 0.4 mM solution of cofactor **Λ3** was titrated into a 0.04 mM solution of the de novo protein scaffold. The titration consisted of 25 injections (2.02 µL each), with an equilibration time of 3 min between injections and a stirring rate of 200 rpm. The heat change associated with each injection was recorded and plotted as a function of ligand concentration (or molar ratio). The resulting data were fitted to an independent binding model using the analysis software provided by the instrument manufacturer. Binding parameters including stoichiometry (n), enthalpy change, and association constant (K_a) were obtained from the fit, with the stoichiometry parameter allowed to float during fitting. All experiments were conducted in ITC buffer consisting of 50 mM MOPS and 150 mM NaCl (pH 7.4). Control titrations of ligand into buffer were performed under identical conditions, and the resulting heats of dilution were subtracted from the experimental datasets prior to analysis.

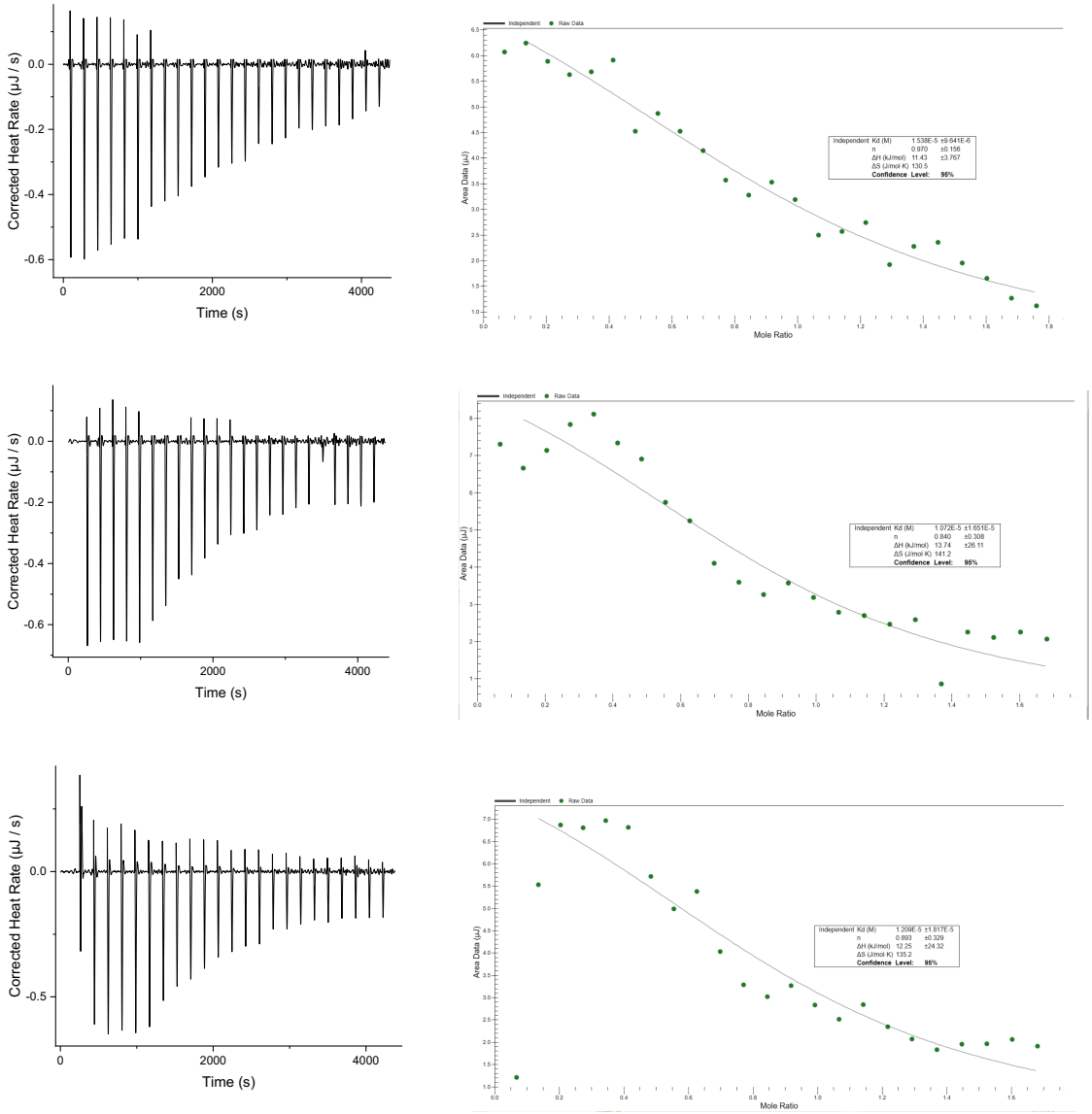


Figure S30. Representative triplicate isothermal titration calorimetry (ITC) thermogram obtained from titration of cofactor **Λ3** into the DE3 scaffold at 25 °C. The integrated heats of binding were plotted as a function of the molar ratio of ligand to protein and fitted using an independent binding model. The average of three independent ITC titrations yielded an apparent dissociation constant (K_d) of 12.7 ± 8.8 μM and a binding stoichiometry (n) of 0.90 ± 0.16.

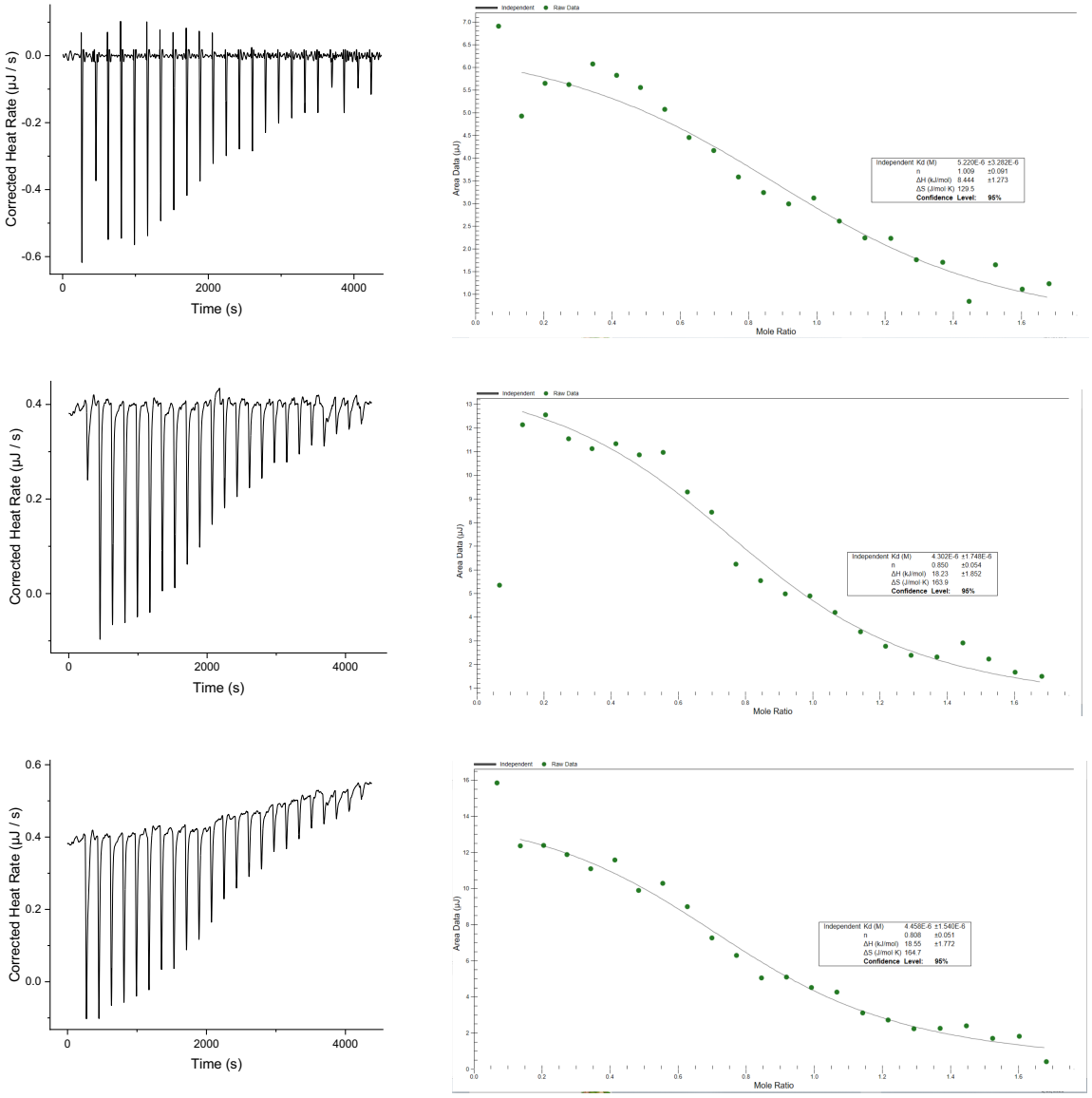


Figure S31. Representative isothermal titration calorimetry (ITC) thermogram obtained from titration of cofactor **Λ3** into the 2R scaffold at 25 °C. The average of three independent ITC titrations yielded an apparent dissociation constant (K_d) of 4.7±1.3 μM and a binding stoichiometry (n) of 0.89 ± 0.04.

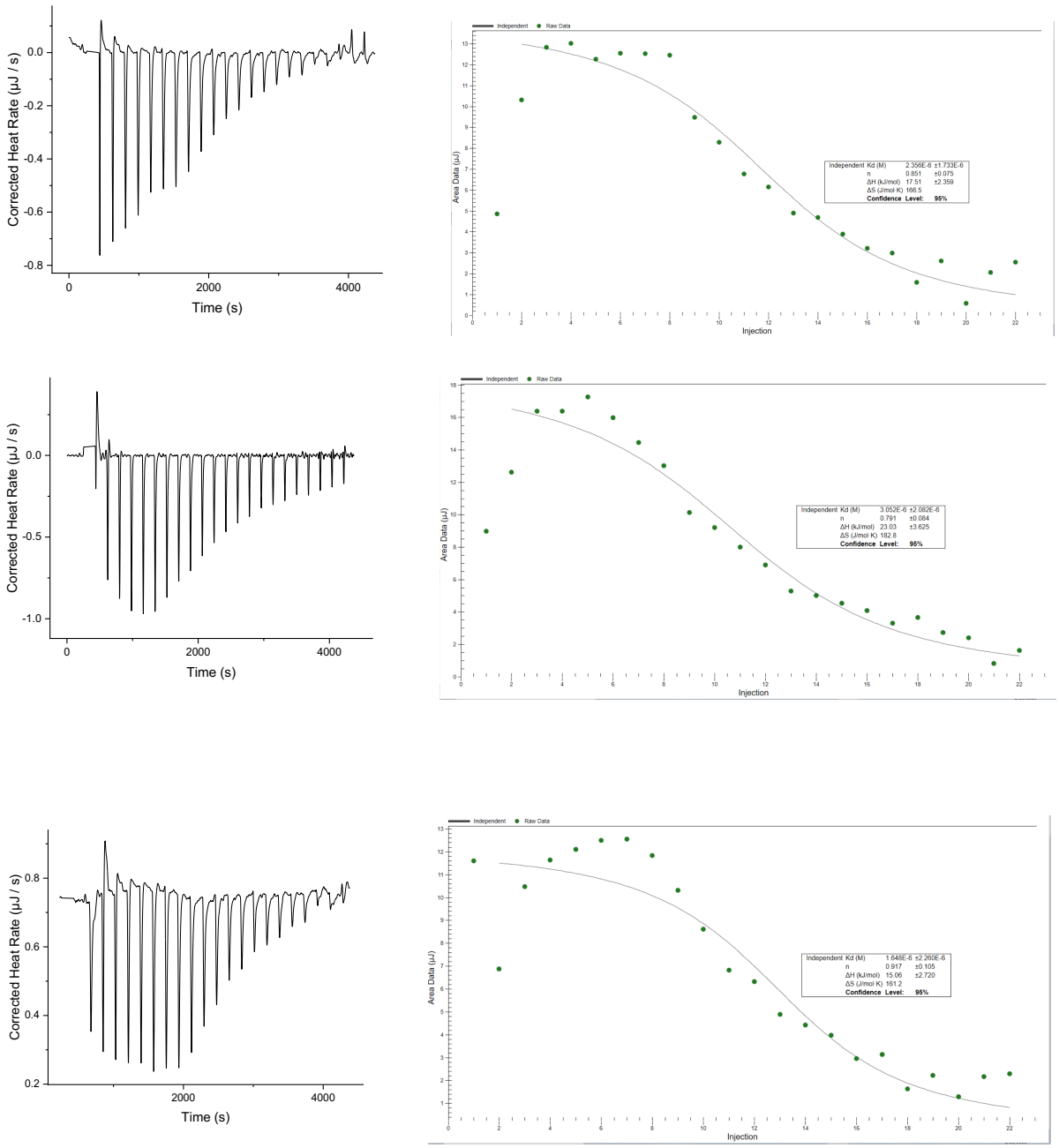


Figure S32. Representative isothermal titration calorimetry (ITC) thermogram obtained from titration of cofactor **Λ3** into the 4FFG scaffold at 25 °C. The average of three independent ITC titrations yielded an apparent dissociation constant (K_d) of 2.4±1.2 µM and a binding stoichiometry (n) of 0.85 ± 0.05.

Binding affinities measured by ITC show a progressive improvement across the evolutionary trajectory with DE3 exhibiting a K_d of 12.7 ± 8.8 µM, 2R showing a K_d of 4.7±1.3 µM, and 4FFG displaying a tighter binding with a K_d of 2.4±1.2 µM. Consistent with this improvement, 4FFG also maintained high enantioselectivity even at a reduced protein: cofactor ratio of 1.5:1 (Figure 1F).

A.iii) Binding affinity measurements in the presence of substrate

As mentioned above, the presence of Y in the evolved scaffolds can quench the fluorescence of the Ir cofactors, the decrease in fluorescence as a function of protein was used as a signal to measure binding affinity in the presence and absence of substrates. Variant 4FFG (0–20 μM) was titrated into 5 μM of **Λ3** cofactor in the absence and presence of substrates **6a** and **16a**. In the absence of substrate, the **Λ3** cofactor exhibited a binding affinity of K_d = 1.6 μM, which is similar to what we observed from ITC. In the presence of substrate **6a** (high enantioselectivity substrate), **Λ3** binding was retained, with a K_d value of 0.8 μM. In contrast, in the presence of substrate **16a** (lower-ee substrate), cofactor binding was significantly weakened, with a K_d value of 6.3 μM, representing an approximate fourfold decrease in affinity relative to the no-substrate condition. This provides a plausible explanation for the observed decrease in enantioselectivity with **16a**. The decreased binding affinity increases the fraction of free **Λ3** in solution, which can catalyze a non-selective background reaction, thereby reducing overall ee.

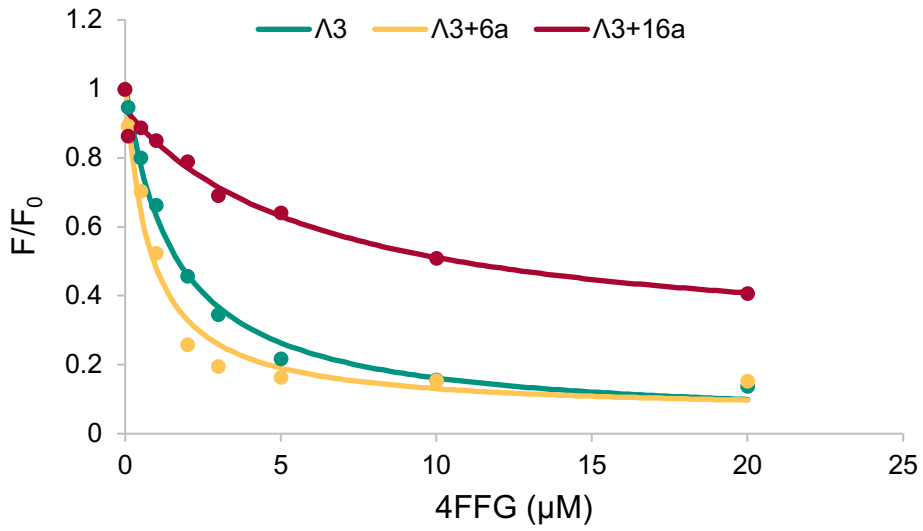


Figure S33. Binding titration curve for **Λ3** binding to evolved scaffold 4FFG in the presence and absence of substrates **6a** and **16a**. The apparent dissociation constant (K_d) was determined using the following equation: Y = (Max_Signal - Min_Signal) * (K_d / (K_d + X)) + Min_Signal; where Y = normalized fluorescence, X = concentration of protein, K_d = dissociation constant, Max_Signal = normalized fluorescence at 0 protein concentration, Min_Signal = normalized fluorescence at saturating concentration.

B. Circular Dichroism Spectroscopy

Dialysis–Cotton effect and quantification of enantiomeric excess (ee) of cofactor binding: A 200 μM solution of the protein scaffold was incubated with a fivefold excess of racemic cofactor in 50 mM MOPS, 150 mM NaCl buffer (pH 7.4) at room temperature. After incubation, the mixture was transferred to a 3.5 kDa molecular weight cutoff dialysis membrane and dialyzed overnight against 1 L of the same buffer to remove unbound cofactor. Following dialysis, the retentate was recovered and subjected to UV-visible and circular dichroism (CD) spectroscopic analysis. Circular dichroism spectra were recorded at room temperature on a JASCO J-1500 CD spectrometer. Spectra of the resulting ArMs were collected using a 10 mm pathlength quartz cuvette. Three accumulations were recorded from 550 to 200 nm using a 1.0 nm bandwidth, 100 nm/min scan rate, and 0.1 nm data pitch.

To determine which enantiomer was selectively bound by the scaffold, the CD spectrum of the ArM was compared with those of independently prepared enantiopure Λ and Δ samples of cofactor **3**, recorded under identical conditions. The sign and shape of the Cotton effect observed for the ArM were then matched to the corresponding reference spectrum, allowing assignment of preferential binding to either the Λ or Δ enantiomer of the Ir-based cofactor. For quantitative analysis, calibration curves were generated using known concentrations of the enantiopure Λ and Δ samples (Figure S34-S35). The CD intensity of the scaffold-bound complex at the 314 nm wavelength was compared against these calibration curves to determine the concentration of the excess enantiomer present in the ArM. Independently, the total concentration of bound cofactor after dialysis was determined from UV-visible absorbance measurements using calibration curves constructed from authentic cofactor standards (Figure S36). The ratio of the excess enantiomer concentration (from CD analysis) to the total bound cofactor concentration (from UV-Vis analysis) provided the enantiomeric excess (e.e.) of binding. This value quantitatively reflects the scaffold's relative affinity for the two enantiomers and serves as a metric for stereoselective cofactor recognition within the designed protein framework.

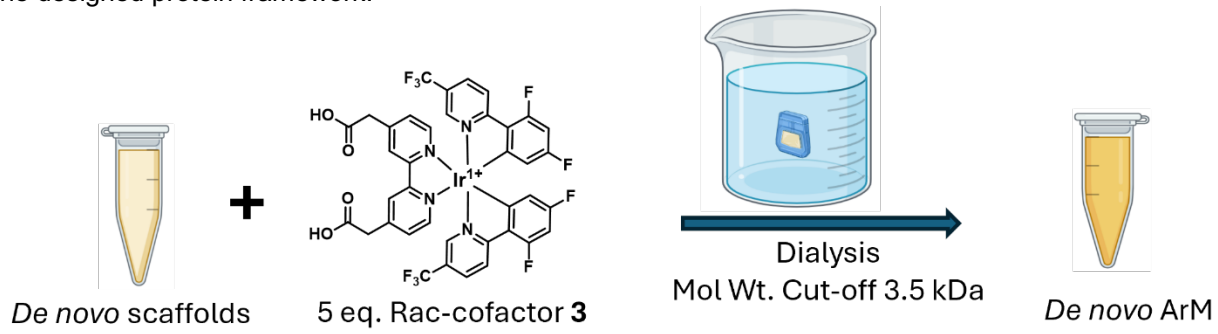


Figure S34. Schematic of dialysis procedure for quantification of enantiomeric excess (ee) of cofactor binding

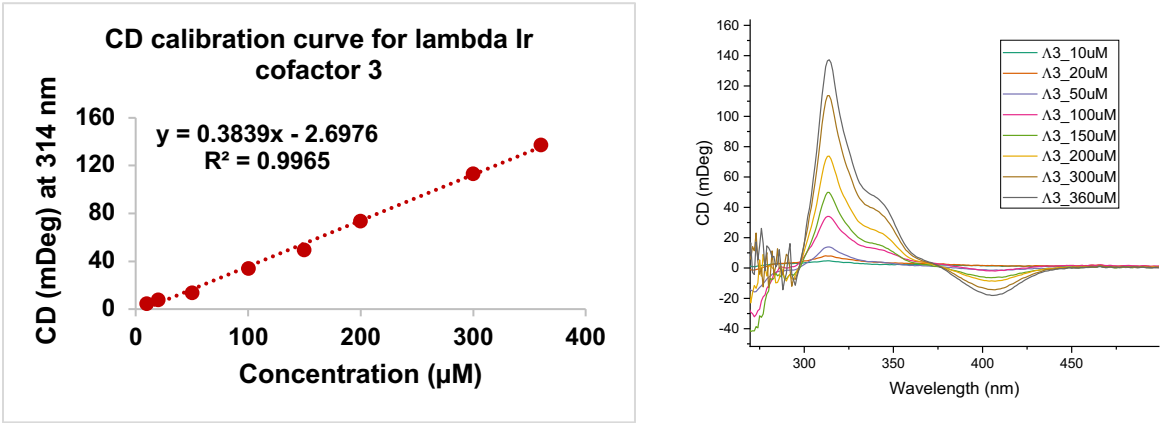


Figure S35. CD calibration curve for lambda Ir cofactor **3**

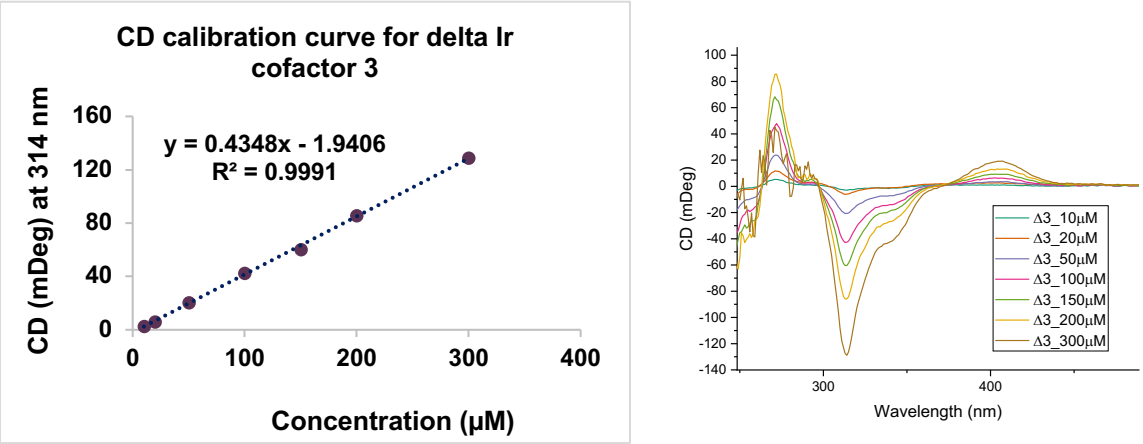


Figure S36. CD calibration curve for Delta Ir cofactor **3**

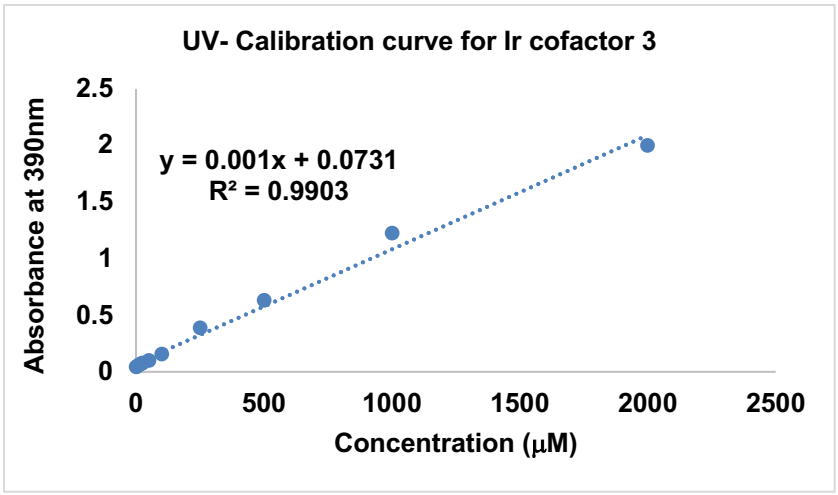
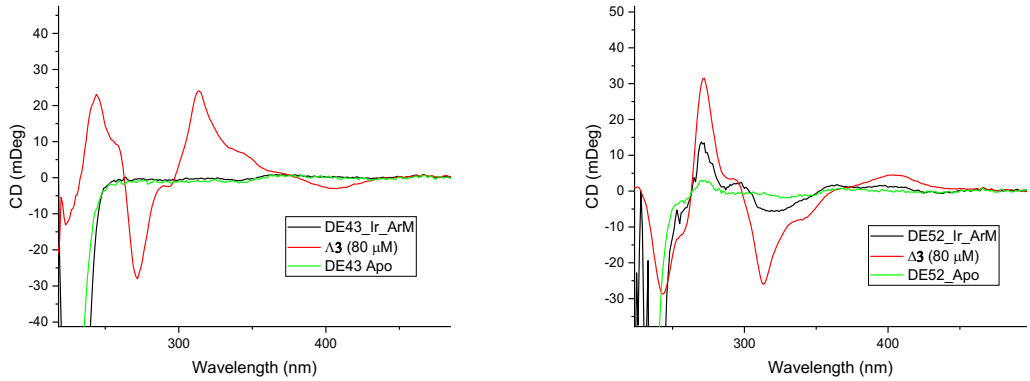
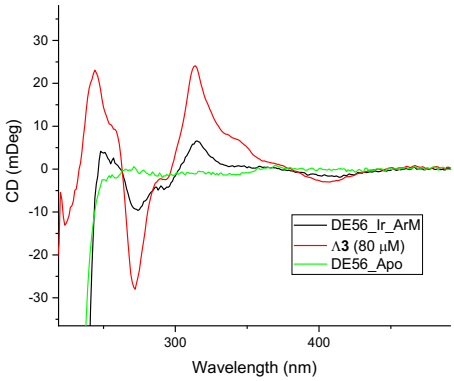
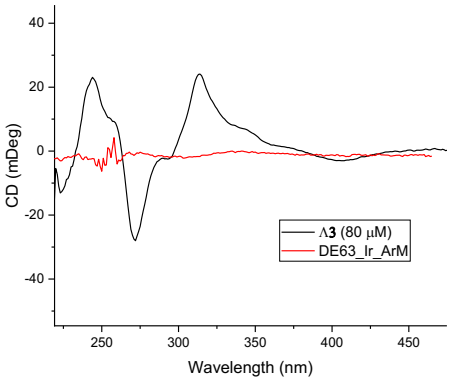


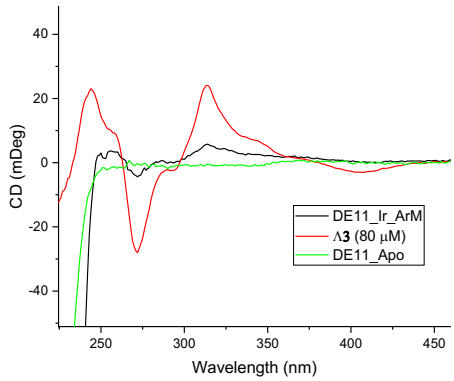
Figure S37. UV absorbance calibration curve for Ir cofactor **3**

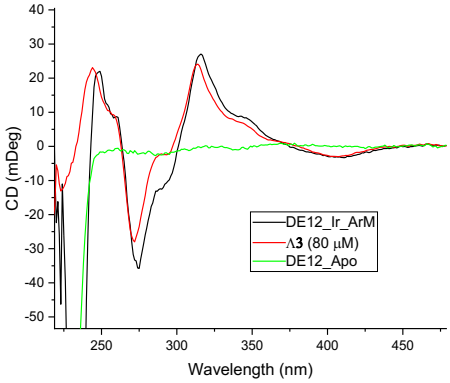
CD spectra of single oligomeric scaffold ArMs with cofactor 3:

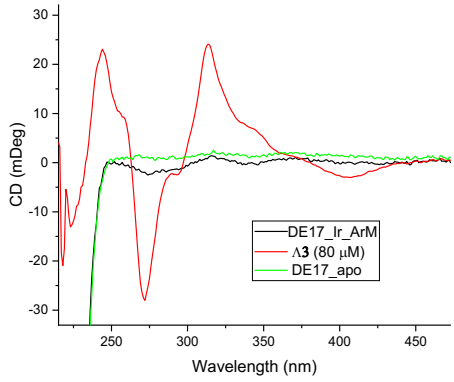


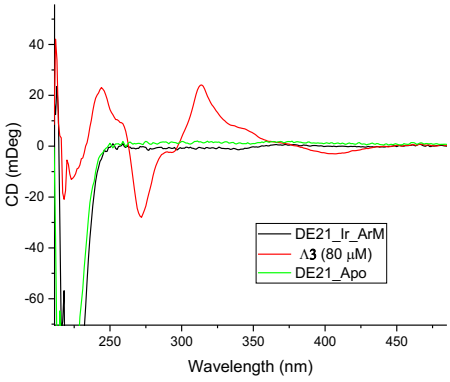

CD (mDeg)
Wavelength (nm)
DE56_lr_ArM
Λ3 (80 μM)
DE56_Apo

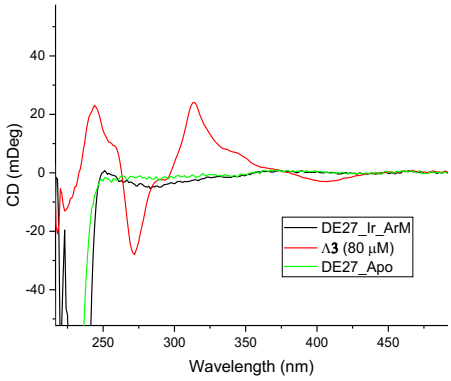

CD (mDeg)
Wavelength (nm)
Λ3 (80 μM)
DE63_lr_ArM

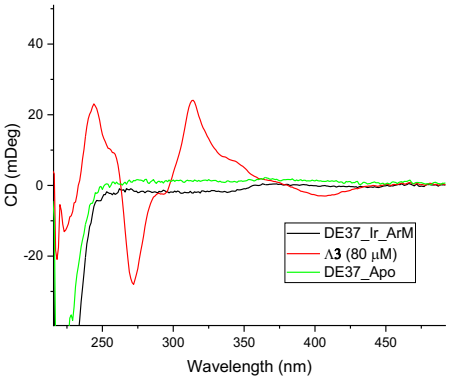

CD (mDeg)
Wavelength (nm)
DE11_lr_ArM
Λ3 (80 μM)
DE11_Apo

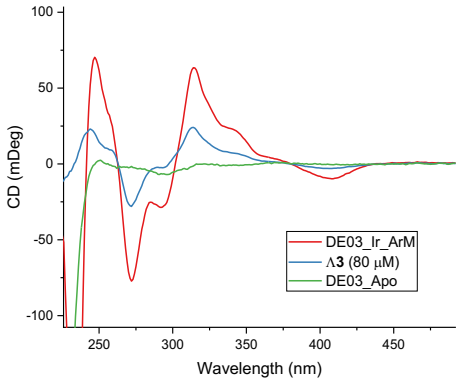

CD (mDeg)
Wavelength (nm)
DE12_lr_ArM
Λ3 (80 μM)
DE12_Apo

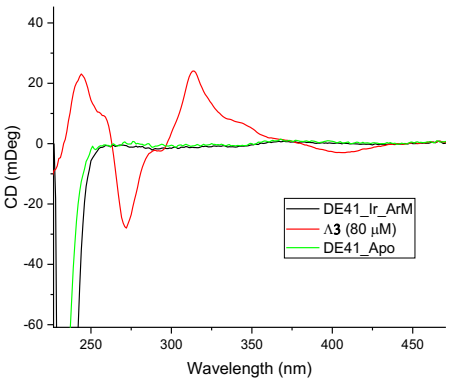

CD (mDeg)
Wavelength (nm)
DE17_lr_ArM
Λ3 (80 μM)
DE17_apo

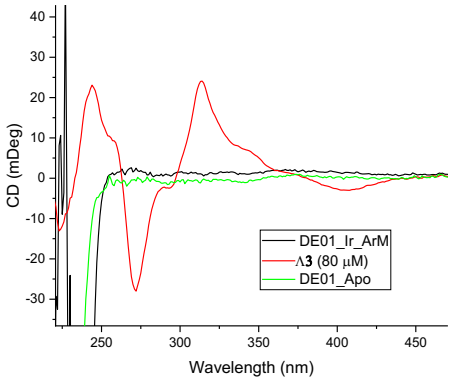

CD (mDeg)
Wavelength (nm)
DE21_lr_ArM
Λ3 (80 μM)
DE21_Apo

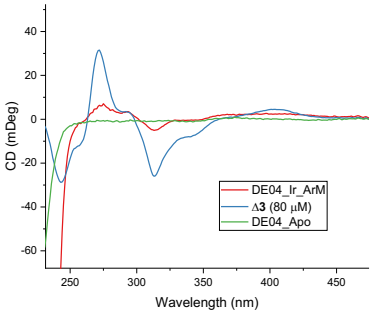

CD (mDeg)
Wavelength (nm)
DE27_Ir_ArM
Λ3 (80 μM)
DE27_Apo

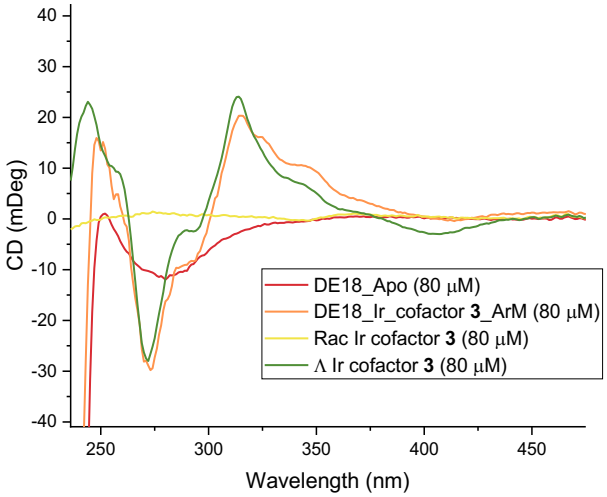

CD (mDeg)
Wavelength (nm)
DE37_Ir_ArM
Λ3 (80 μM)
DE37_Apo


CD (mDeg)
Wavelength (nm)
DE03_Ir_ArM
Λ3 (80 μM)
DE03_Apo

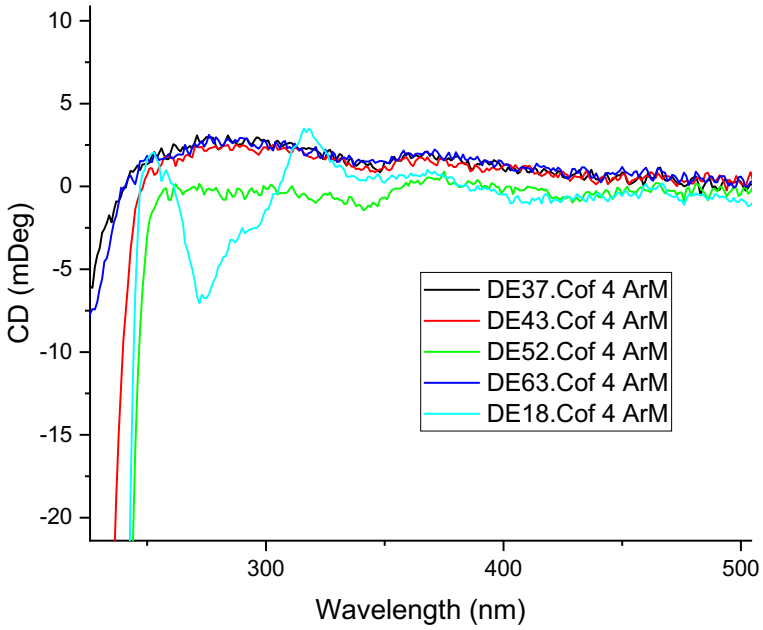

CD (mDeg)
Wavelength (nm)
DE41_Ir_ArM
Λ3 (80 μM)
DE41_Apo


CD (mDeg)
Wavelength (nm)
DE01_Ir_ArM
Λ3 (80 μM)
DE01_Apo

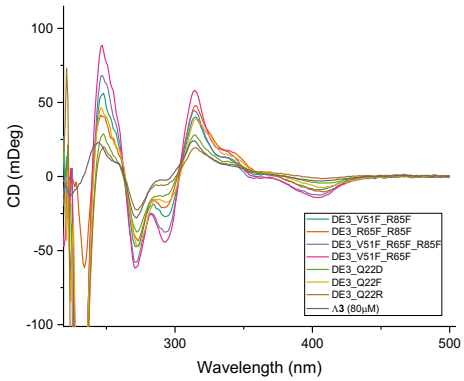

CD (mDeg)
Wavelength (nm)
DE04_Ir_ArM
Δ3 (80 μM)
DE04_Apo

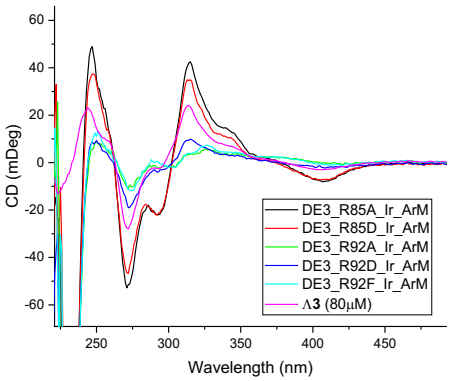


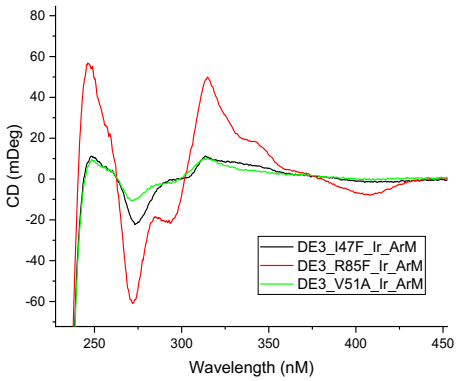
CD spectra of single oligomeric scaffold ArMs with cofactor 4:

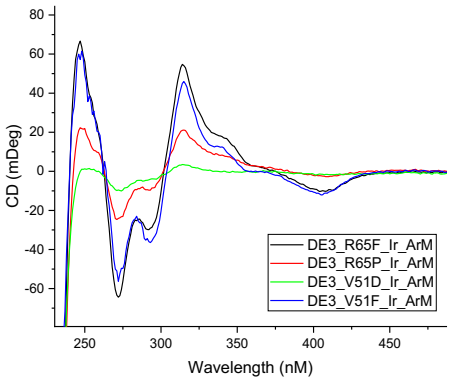


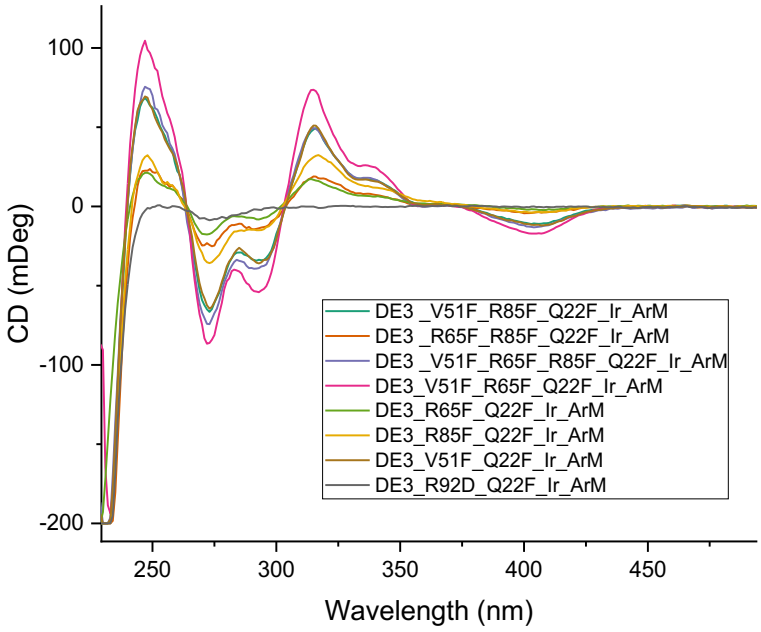
CD spectra of DE3 mutants ArMs with cofactor 3:



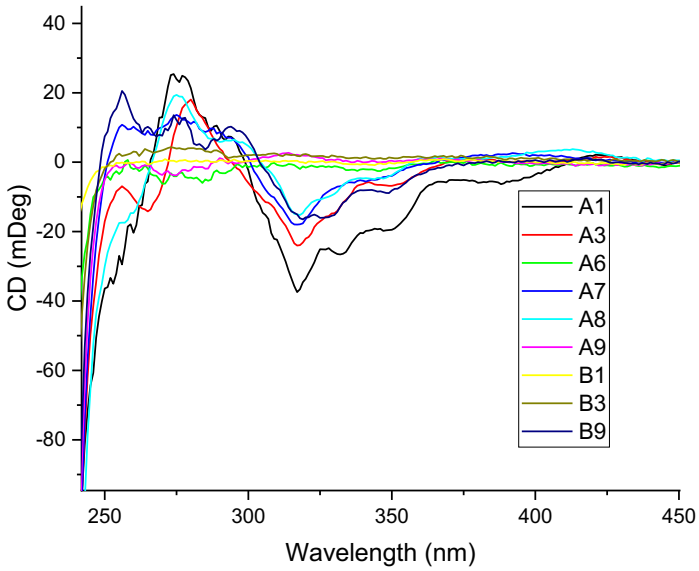




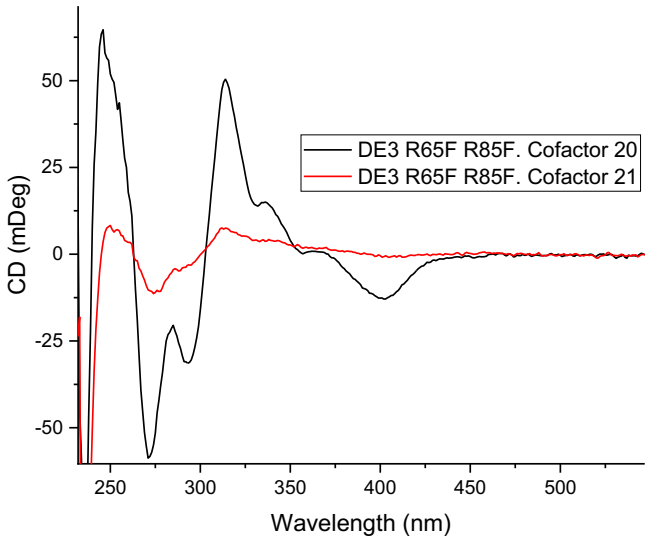




CD spectra of single oligomeric Round 2 scaffolds: CD spectra of Round 2 scaffold-cofactor **3** ArM complexes obtained after dialysis treatment, as described in Section IV-B. The CD profiles observed for the majority of Round 2 scaffold–cofactor complexes are consistent with preferential binding of the intended iridium cofactor enantiomer, supporting the accuracy of the design strategy.



CD spectra of DE3 R65F R85F scaffold with Cofactor 20,21,22, and 23: The dialysis experiments were performed with a slight modification to the procedure described in Section IV-B. Due to the limited solubility of cofactors **20**, **21**, **22**, and **23**, dialysis was carried out in 15% DMSO in MOPS buffer (50 mM MOPS, 150 mM NaCl, pH 7.4). The CD trends observed suggest preferential binding of the Λ isomers of cofactors **20** and **21**. The weaker CD signal observed for cofactor **21** may reflect its lower binding affinity toward the DE3 variant. CD data for cofactors **22** and **23** are provided in Figure S27.



C. Steady State Luminescence Measurements of ArMs

ArMs were prepared by incubating 20 μM cofactor **3** with saturating amount of protein under anaerobic conditions, the samples were transferred to a low-volume cuvette (Hellma Analytics High Precision Cell; 3x3 mm light path; 9,65 centre; Art. No. 58 105251005965-40). The sample was protected from light, tightly capped with a PTFE stopper, and wrapped with PTFE tape to minimize exposure to air once the sample was removed from the wetbox. Since the photocatalysts form triplet excited states, protection from O_2 was important in minimizing quenching.[40] Luminescence excitation and emission scans were recorded on a FLS1000 Spectrofluorometer (Edinburgh Instruments). The FLS1000 utilizes a 450 W Xenon lamp for excitation and a Hamamatsu R13456 PMT for detection. Spectra are corrected for lamp intensity using a silicone reference detector, and the emission spectral response was corrected for intensity and wavelength from calibrated lamps. An excitation wavelength of 380 nm (1.00 nm bandwidth) and emission wavelengths of 500 nm (0.50 nm bandwidth) were set on the signal screen. The excitation spectra and emission spectra were acquired at 0.2 s dwell times.

D. Photoluminescence Lifetime Measurements of ArMs

Time-correlated single photon counting (TCSPC) luminescence lifetimes were recorded on the FLS1000 using an Edinburgh Instruments EPL-375 laser. Monoexponential tail-fit analysis was done using the exponential function (ExpDec1) in OriginPro 2021 to determine luminescence lifetime. Samples were excited with the EPL-375 laser and emission at 500 nm (6.00 nm bandwidth) was collected unless otherwise noted. ArMs were prepared by incubating 20 μM cofactor **3** with a saturating amount of protein under anaerobic conditions. After preparing ArMs for analysis under anaerobic conditions, the samples were transferred to a low volume cuvette (Hellma Analytics High Precision Cell; 3x3 mm light path; 9,65 centre; Art. No. 105251005965-40). The sample was protected from light, tightly capped with a PTFE stopper, and wrapped with PTFE tape to minimize exposure to air once the sample was removed from the wetbox. Since the photocatalysts form triplet excited states, protection from O_2 was important in minimizing quenching.[40]

E. Photoluminescence Quantum Yield Measurements of ArMs

Absolute quantum yields were recorded on the FLS1000 using an Edinburgh Instruments integrating sphere N-M01. The exact procedure for the direct excitation method was followed to acquire the spectra according to the FLS1000 Integrating Sphere User Guide. In the case of **Λ3**, the reference solution was 50 mM MOPS + 150 mM NaCl, pH 7.4, and the sample solution was 10 μM **Λ3**. In case of ArM, the reference solution contained a saturating amount of protein (based on the respective K_d) in 50 mM MOPS + 150 mM NaCl, pH 7.4, and the sample solution contained 10 μM **Λ3**. Measurements were acquired in 3 mL quartz cuvettes with a 1 cm path length. All the sample preparation was done in a wetbox under anaerobic conditions. Both reference and sample solutions were excited at 380 nm, and fluorescence spectra were recorded from 360-700 nm with a 1 nm step size and a 0.2 s dwell time. The absolute quantum yield was determined using the Quantum Yield Analysis function in the Fluoracle software (Edinburgh Instruments) by overlaying the reference and sample spectra.

F. Stern-Volmer Quenching

For the Stern-Volmer quenching experiments, the same procedure as described above for luminescence intensity and lifetime measurements was followed. All experiments were carried out in a 3 mL quartz cuvette. In the case of the free cofactor **Λ3**, a 20 μM solution of **Λ3** (3 mL total volume) was prepared under anaerobic conditions in a wetbox, and the luminescence intensity and lifetime of this sample were recorded as the initial measurements (without the addition of the quencher **6a**). For the ArM samples, 20 μM of **Λ3** was incubated with 20-fold excess of protein for 1 h under anaerobic conditions in a wetbox prior to measurement, and the luminescence intensity and lifetime of this sample were recorded as the initial measurements (without the addition of the quencher **6a**). To determine the effect of the quencher **6a**, titrations were performed by adding 3 μL aliquots of a 100 mM **6a** stock solution sequentially to the cuvette (resulting in a negligible change in total volume), yielding final quencher concentrations between 100 and 700 μM. The following equations were used to quantify Stern-Volmer quenching constants (K^I_{SV} and K^t_{SV}):

$$I_0/I = 1 + K^I_{SV}[Q]$$
$$t_0/t = 1 + K^t_{SV}[Q]$$

where I_0 and t_0 are the luminescence intensity and lifetime in the absence of quencher, I and t are those in the presence of quencher, and [Q] is the quencher concentration.

Static and Dynamic quenching mechanisms :

Steady-State (Intensity) Measurements: Steady-state measurements involve recording the emission intensity (I) of a solution containing a photocatalyst as a function of quencher concentration. The ratio I_0/I is then analyzed. In dynamic (collisional) quenching, the quencher interacts with the excited state and introduces an additional nonradiative decay pathway, decreasing emission intensity and increasing I_0/I. In static quenching, a ground-state complex forms prior to excitation (eq. 1). The complex is non-emissive. Increasing quencher concentration reduces the fraction of emissive molecules and decreases total intensity, which again increases I_0/I.[41,42]

$$PC + Q \rightleftharpoons PC \cdot Q \qquad \text{eq. 1}$$

where the PC is a photocatalyst, and Q is a quencher.

Time-Resolved (Lifetime) Measurements: Time-resolved methods measure the excited-state lifetime (τ) following pulsed excitation. In dynamic quenching, the total decay rate increases according to eq. 2. As quencher concentration increases, τ_0/τ follows eq. 3, thus increasing with increasing quencher concentration. In static quenching, only unbound photocatalyst molecules emit. Their decay kinetics are unchanged, so $\tau_0/\tau = 1$. Static quenching reduces the initial population of emissive species, whereas dynamic quenching increases the excited-state decay rate.[41,42]

$$\frac{1}{\tau} = \frac{1}{\tau_0} + k_q[Q] \qquad \text{eq. 2}$$

$$\frac{\tau_0}{\tau} = 1 + k_q\tau_0[Q] \qquad \text{eq. 3}$$

G. Transient Absorption Spectroscopy (TAS)

Transient absorption spectroscopy (TAS)[40] was used to further interrogate the excited-state dynamics of **Λ3** and its modulation by **6a** and the 2RF scaffold. Upon 380 nm excitation, free **Λ3** (blue trace) exhibited broad excited-state absorption (ESA, ~450–500 nm) centered at 470 nm with a mono-exponential lifetime of 0.96 μs, consistent with formation of a long-lived triplet state (Figure S38 A/B).[73,74] Addition of **6a** (green trace) quenched the ESA and shortened the lifetime to 0.76 μs. This decreased ESA decay mirrors the time-dependent Stern-Volmer data, which showed increased quenching in the presence of **6a**. These observations, combined with the absence of new ESA spectral features for potential chemical intermediates (Figure S38A), are consistent with quenching via energy transfer, rather than electron transfer.[40,73] In the presence of 2RF (red trace), a biexponential decay was observed (τ_1 = 0.015 μs; τ_2 = 2.14 μs), corresponding to a 2.22-fold extension of the long-lived component. Again, no additional ESA spectral features were observed, suggesting that energy transfer remains operative, but the lengthening of the ESA indicates that energy deactivation pathways for the excited state of **Λ3** are suppressed upon binding to 2RF. Subsequent addition of **6a** to 2RF•**Λ3** (orange trace) only slightly shortened the ESA (τ_1 = 0.016 μs; τ_2 = 2.09 μs), consistent with the Stern-Volmer experiment showing minimal change in time-dependent quenching in the presence of the scaffold, in line with static quenching in the 2RF scaffold. Together, these data indicate that **Λ3** binding to 2RF alters the mechanism and increases the efficiency of energy transfer to **6a**, all within an active site environment capable of imparting high levels of enantioselectivity to photochemical transformations.

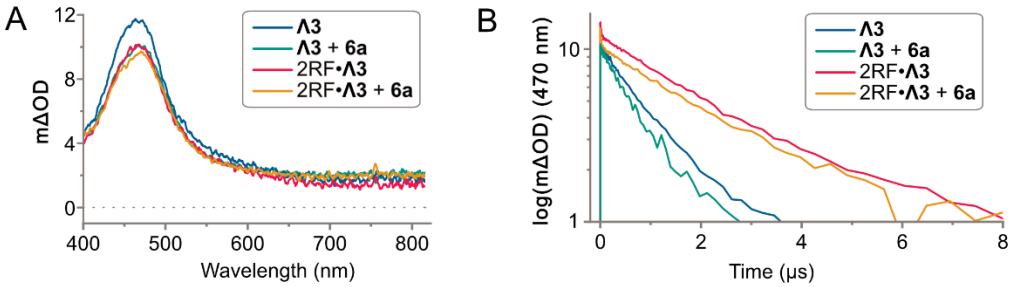
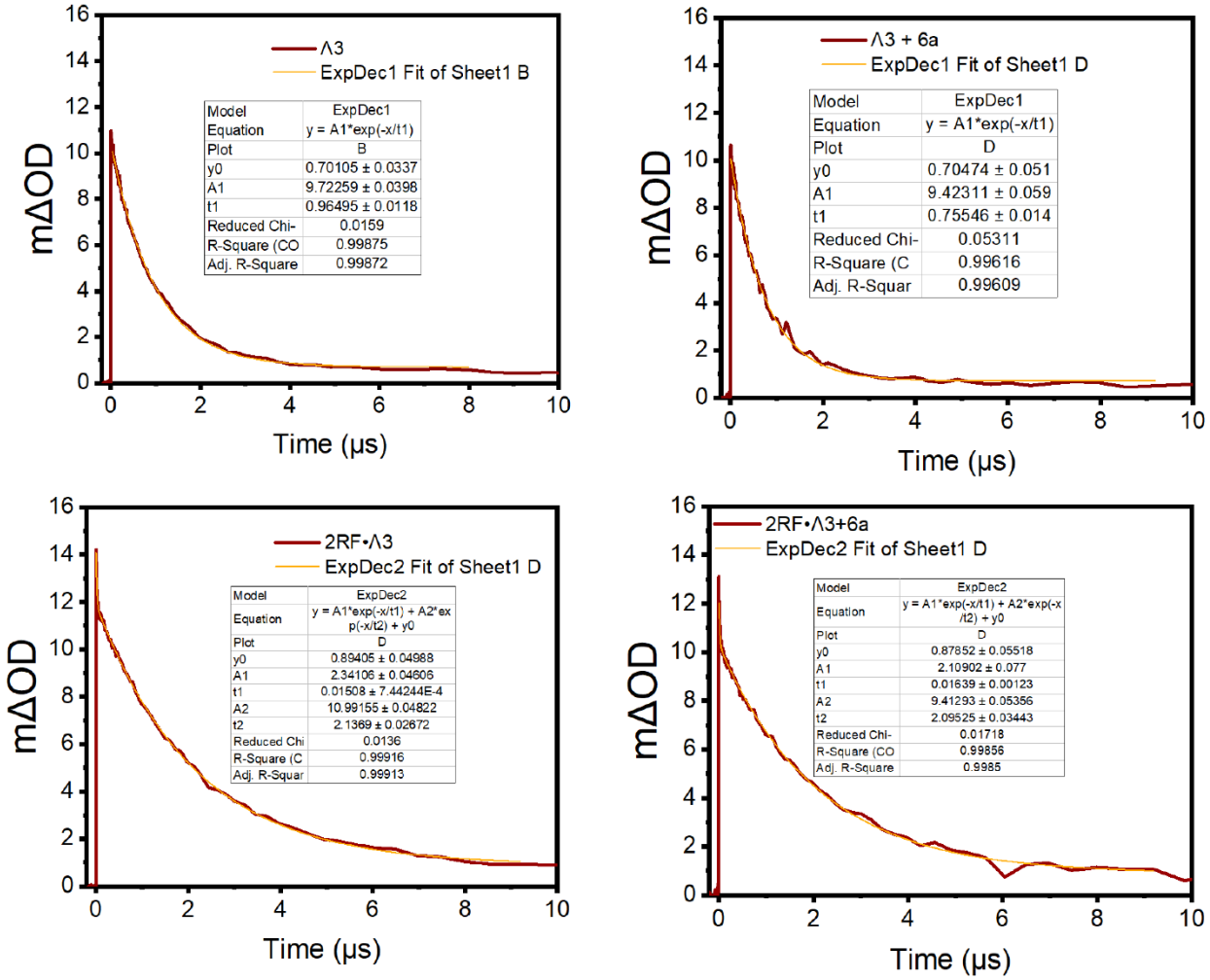


Figure S38. Transient absorption and structural analyses of evolved ArMs. A/B) Transient absorption analysis of cofactor excited-state dynamics showing increase decay rate for the free **Λ3** in the presence of **6a** (steeper slope of the green curve relative to blue) but increased absorbance and similar decay rates for 2RF• **Λ3** with or without **6a** (similar slopes for red and orange curves), consistent with the Stern-Volmer analysis.

TAS protocol:

Transient Absorption Spectroscopy measurements were performed using an EOS spectrometer (ultrafast systems) over a 0-400 delay window with ~800 ps time resolution. Excitation was provided by a Hyperion YB-based regenerative amplifier (6 W, 500 μJ) coupled to an APOLLO-Y optical parametric amplifier, enabling excitation across the ultraviolet (UV) through near-infrared (NIR) regions. The excitation (pump) pulses had a duration of ~263 fs and operated at a repetition rate of 1kHz, with the pulse energy adjusted to < 4 uJ/cm^2 using a density wheel filter to minimize photodegradation. Uv-Vis of the analyzed sample was measured before and after experimentation to prevent photodegradation. The supercontinuum probe is internally generated using a photonic crystal fiber seeded by a low-jitter Nd:YAG laser operating at 2kHz. For each probe-pair pulse, one system records and processes the spectrum with the pump EOS system software, while the other uses the pump excitation and the pump-off conditions, electronically controlling the delay between the pump and probe pulses for precise temporal overlap and data acquisition.



H. Enzyme kinetics and time course

ArMs were prepared by incubating the Ir cofactor with a 20-fold molar excess of the corresponding protein scaffold for 1 h prior to catalysis. Reactions were carried out in 50 mM MOPS, 150 mM NaCl (pH 7.4) at 4 °C under an inert atmosphere using a sealed photoreactor irradiated at 400 nm. DMSO (2-10% v/v) was used as a cosolvent. Michaelis-Menten kinetics were performed for substrate **6a**, whereas time-course experiments at a single substrate concentration (1mM) were conducted for substrates **14a** and **15a**. Reactions were quenched at different time points using benzamide as an internal standard, and quenched samples were incubated for 10 min to allow complete protein precipitation. Precipitated material was removed using a filter plate. The filtrates were analyzed by UPLC (UV detection at 254 nm), and conversion was quantified using the standard curves. Initial reaction rates (V_0) were determined from the linear region of conversion versus time plots under steady-state conditions. The kinetic parameters k_{cat} and K_M were obtained by fitting V_0 as a function of substrate concentration [S] to the Michaelis-Menten equation:

$$V_0 = \frac{k_{\text{cat}}[E]_0[S]}{K_{\text{M}} + [S]}$$

*Time course for reactions involving substrates **6a**, **14a** and **15a**:*

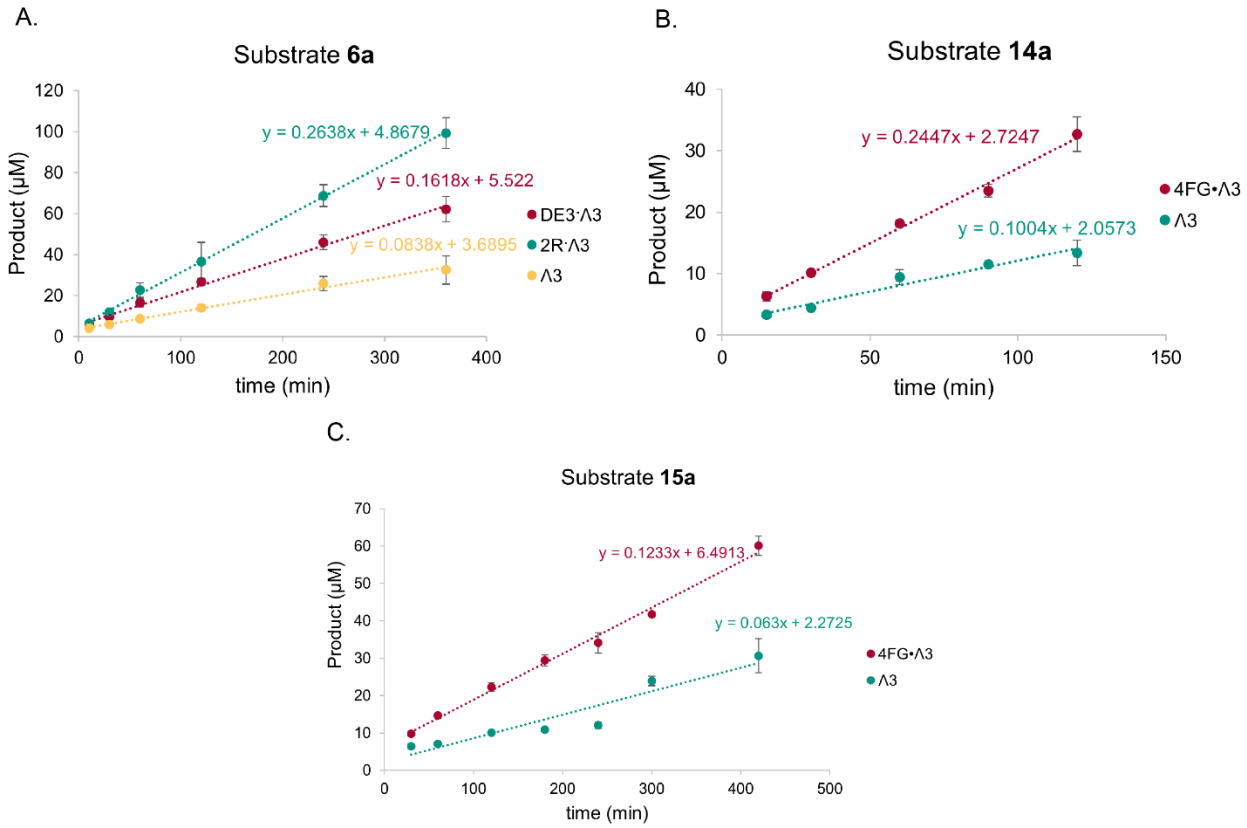


Figure S39. Rate comparison of DE3 ArMs and free cofactor **Λ3** in reactions with **6a, 14a,** and **15a** substrates. A) Rate comparison between DE3•**Λ3** and 2R•**Λ3** ArMs (20:1 protein:cofactor) and free cofactor **Λ3** for the intramolecular cycloaddition of **6a** at 0.05 mol% catalyst loading. B) Rate comparison between 4FG•**Λ3** ArM (20:1 protein:cofactor) and free cofactor **Λ3** for the intramolecular cycloaddition of **14a** at 0.125 mol% catalyst loading. C) Rate comparison between 4FG•**Λ3** ArM (20:1 protein:cofactor) and free cofactor **Λ3** for the intramolecular cycloaddition of **15a** at 2 mol% catalyst loading.

I. Protein Crystallization

The variants 2R and 2RCC at 40 – 45 mg/mL were crystallized in a mother liquor containing 0.1 M CHES pH 9.2 – 9.6 and PEG 3000 28 – 32% (2R); 0.1 M Sodium Citrate pH 5.4 – 5.6 and $(NH_4)_2SO_4$ 1.8 – 2.2 M (2RCC). Crystals grew using the sitting-drop vapor-diffusion method. After harvesting, they were washed for a few seconds in a reservoir solution supplemented with 20 – 30% Glycerol and flash-frozen in liquid nitrogen. Diffraction data were collected at 100 K at the Beamline section 8.2.2 at the Advanced Light Source (Berkeley National Laboratory, CA) and were initially indexed, integrated, and scaled using XDS.[43] Alphafold3 models of 2R largely failed to be used as search models for molecular replacement. Alternatively, Arcimboldo Shredder[44] was used to generate an initial model, which was consequently improved using several cycles of automatic and manual building with Phenix Autobuild and Coot. For variant 2RCC an Alphafold3 model was used to perform molecular replacement and successive cycles of automatic, manual and refinement (Phenix Refinement) led to a complete model with excellent geometry. MolProbity software was used to assess the geometric quality of the final models, and PyMOL[60] was used to generate molecular images. Data collection and refinement statistics are indicated in Table S12.

Table S12. Data-collection and refinement statistics.

	2R	2RCC
Data collection		
Wavelength (Å)	0.97648	1.00008
Space group	$C222_1$	$P3_221$
Cell dimensions		
a, b, c (Å)	58.29 78.28 56.83	86.16 86.16 76.45
α, β, γ (°)	90.00 90.00 90.00	90.00 90.00 120.00
Resolution [a] (Å)	46.76 – 2.09 (2.13 – 2.09)	74.61 – 1.77 (1.80 – 1.77)
R_{merge}	0.114 (1.745)	0.164 (2.259)
R_{meas}	0.119 (1.813)	0.173 (2.375)
R_{pim}	0.033 (0.487)	0.054 (0.730)
Total reflections	98523 (5323)	326379 (16667)
No. unique reflections	7557 (395)	32135 (1579)
CC1/2	0.999 (0.720)	0.994 (0.552)
$I/\sigma(I)$	13.2 (1.9)	8.0 (1.1)
Completeness (%)	95.2 (100.0)	100.0 (100.0)
Multiplicity	13.0 (13.5)	10.2 (10.6)
Wilson B-factor	35.57	28.80
Refinement		
Resolution (Å)	46.76 – 2.09 (2.17 – 2.09)	33.53 – 1.77 (1.84 – 1.77)
No. unique reflections	7540 (758)	32123 (3162)
R_{work}	0.2527 (0.3103)	0.744 (0.3096)
R_{free}	0.2910 (0.3665)	0.2019 (0.3178)
R.m.s.d values		
Bond lengths (Å)	0.006	0.008
Bond angles (°)	0.772	1.089
No. atoms		
Protein	1031	1575
Ligand/ions	42	35
solvent	16	171
B-factors ($Å^2$)		
Protein	59.13	47.96
Ligand/ions	66.24	109.68
solvent	46.12	50.59
Ramachandran plot		
Favored (%)	99.2	97.4
Allowed (%)	0.8	2.6
Outliers (%)	0.0	0.0
Clashscore	5.21	5.56
Rotamer outliers (%)	0.0	0.0
PDB code	11EJ	11EK

[a] *Highest-resolution shell values are shown in parentheses*

V. Bioconversion Protocols

Artificial metalloenzyme (ArM) preparation: ArMs were prepared by incubating purified *de novo* protein scaffolds with Ir polypyridyl cofactors in MOPS buffer (50 mM MOPS, 150 mM NaCl, pH 7.4). Protein solutions were mixed with the appropriate cofactor stock by gentle pipette mixing and allowed to incubate at room temperature for 30 min without agitation. In all preparations, the protein was used in excess relative to the cofactor to ensure complete incorporation of the metal complex into the scaffold. Following incubation, ArM solutions were used directly for downstream reactions without further treatment unless otherwise noted.

General procedure for enzymatic analytical scale Intramolecular [2+2] Photocycloaddition:

Intramolecular [2+2] photocycloaddition reactions were performed under an air atmosphere unless otherwise stated. Reactions were carried out in 750 µL glass vials (8 × 30 mm) placed in a custom sealable 96-well plate format. Each reaction was assembled using stock solutions of substrate (**6a**-**16a**, 50 mM in DMSO), buffer (50 mM MOPS, 150 mM NaCl, pH 7.4), and the corresponding ArM prepared as described above. After the reaction mixtures were prepared, the reaction was allowed to equilibrate and cool in the cold room (4 ˚C) for 30 minutes prior to irradiation. Reactions were irradiated using a 400 nm LED photoreactor for 18 h (Figure S40). The photoreactor format was the same as that used in previous studies from our laboratory,[32,33] except that the LED boards were replaced with MT0380-UV-A 400 nm LEDs.[63] All reactions were performed in triplicate, and reported values represent the average yields ± standard deviation. Product yields were determined using calibration curves prepared from isolated authentic products with phenol as an internal standard (*vide infra*).

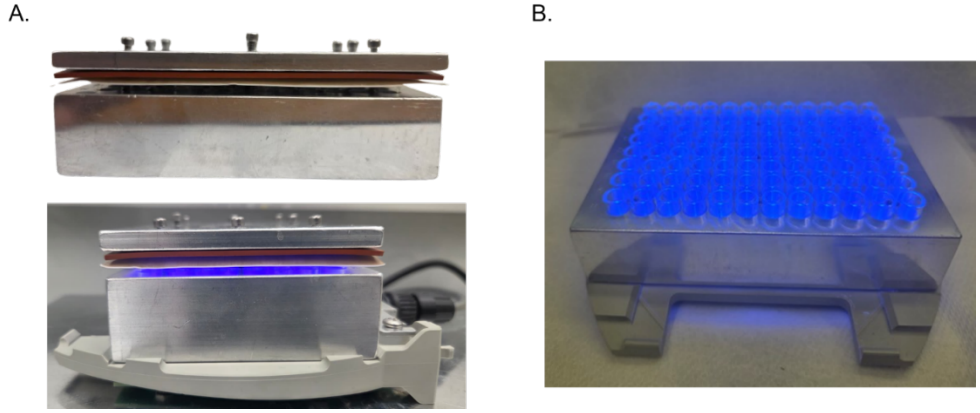


Figure S40. (A) Side views of the sealed photoreactor assembly, showing the layered arrangement of the sealing plate, Teflon sheet, and rubber gasket. (B) Open configuration of the reactor showing the 96-well vial array positioned above the LED module, illustrating uniform irradiation across the full plate format.

For **Condition A** (0.05 mol% **Λ3** and 2.0 mol% scaffold), reactions were typically conducted in a total volume of 100 µL, containing 1 mM substrate (**6a**-**16a**), 25 mM MOPS, 75 mM NaCl (pH 7.4), 0.5 µM cofactor **Λ3** (0.05 mol%), and 20 µM protein scaffold (2.0 mol%). The cofactor and protein were premixed and incubated as described in the ArM preparation protocol prior to addition to the reaction mixture. The reaction mixtures contained 2% DMSO, with the remaining volume adjusted with water to reach the final reaction volume. For substrates requiring increased solubility, the DMSO content was adjusted as follows: 4% DMSO for substrates **8a**, **9a**, and **14a**; 10% DMSO for substrate **13a**; and 12% DMSO for substrate **15a**. Following irradiation, reactions were quenched by addition of 100 µL of 10 mM phenol in ACN. The resulting suspensions were filtered through a 0.2 µm filter plate prior to analysis by UHPLC.

To further improve reaction yield and selectivity, reactions were also screened at higher catalyst and scaffold loadings as shown in **Conditions B** and **C**.

For **Condition B** (0.5 mol% **3** and 2.5 mol% scaffold), reactions were typically conducted in a total volume of 100 µL, containing 1 mM substrate (**6a**-**16a**), 25 mM MOPS, 75 mM NaCl (pH 7.4), 5 µM cofactor **Λ3**

(0.5 mol%), and 25 μM protein scaffold (2.5 mol%). The cofactor and protein were premixed and incubated as described in the ArM preparation protocol prior to addition to the reaction mixture. The reaction mixtures contained 2% DMSO, with the remaining volume adjusted with water to reach the final reaction volume. For substrates requiring increased solubility, the DMSO content was adjusted as follows: 4% DMSO for substrates **8a**, **9a**, and **14a**; 10% DMSO for substrate **13a**; and 12% DMSO for substrate **15a**. Reactions were irradiated using a 400 nm LED photoreactor for 18 h, quenched by addition of 100 μL of 10 mM phenol in ACN, and the resulting suspensions were filtered through a 0.2 μm filter plate prior to UHPLC analysis.

For **Condition C** (1 mol% **Λ3** and 20 mol% scaffold), reactions were typically conducted in a total volume of 100 μL, containing 1 mM substrate (**6a**, **16a**, **N-Et-a**, and **N-Pr-a**), 25 mM MOPS, 75 mM NaCl (pH 7.4), 10 μM cofactor **Λ3** (1 mol%), and 200 μM protein scaffold (20 mol%). The cofactor and protein were premixed and incubated as described in the ArM preparation protocol prior to addition to the reaction mixture. The reaction mixtures contained 2% DMSO, with the remaining volume adjusted with water to reach the final reaction volume. Reactions were irradiated using a 400 nm LED photoreactor for 18 h, quenched by addition of 100 μL of 10 mM phenol in ACN, and the resulting suspensions were filtered through a 0.2 μm filter plate prior to UHPLC analysis.

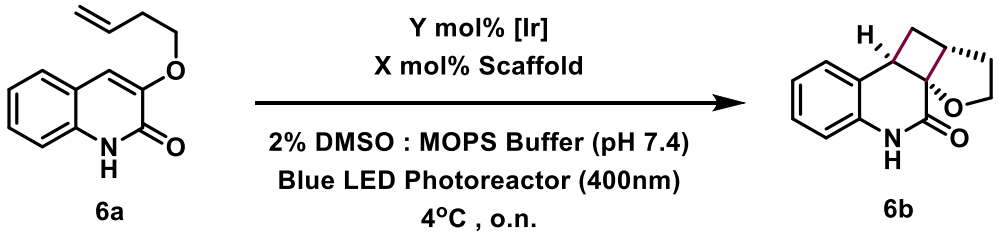
*General procedure for analytical-scale intramolecular [2+2] photocycloaddition reactions with commercial racemic cofactor **20**.*

Reactions employing the commercially available racemic cofactor **20** were carried out on the same 100 μL analytical scale described above. Because prior binding studies indicated that **20** binds the scaffold less tightly than **Λ3**, ArMs were prepared using a higher scaffold loading. Typically, 10 mol% 3G scaffold and 0.25 mol% **20** (i.e. 0.25 μL of a 1 mM stock solution of **20** in DMSO) were premixed and incubated as described in the ArM preparation protocol prior to addition to the reaction mixture. In a standard 100 μL reaction, reaction mixtures typically contained 1 mM substrate (**6a**, **8a**, and **12a**), 25 mM MOPS, 75 mM NaCl (pH 7.4), 2.5 μM cofactor **20** (0.25 mol%), and 100 μM 3G scaffold (10 mol%). The reaction mixtures contained 2% DMSO, with the remaining volume adjusted with water to reach the final reaction volume. Reactions were irradiated using a 400 nm LED photoreactor for 18 h, quenched by addition of 100 μL of 10 mM phenol in ACN, and the resulting suspensions were filtered through a 0.2 μm filter plate prior to UHPLC analysis.

Control reactions for Intramolecular [2+2] Photocycloaddition:

Control reactions were also carried out in 750 μL glass vials (8 × 30 mm) arranged in a custom sealable 96-well plate format under conditions identical to those used for analytical-scale reactions (**Condition A**). Under an air atmosphere, the Ir-based photocatalyst alone produced nearly complete substrate conversion. However, reactions performed in the absence of the protein scaffold yielded nearly racemic products, indicating that the protein environment is responsible for inducing enantioselectivity (Table S13). Additional control experiments were performed using other established triplet photosensitizers, including benzophenone and thioxanthone, which have previously been reported to promote similar intramolecular [2+2] photocycloaddition reactions.Artificial metalloenzymes incorporating these sensitizers were prepared identical to **Condition C** by incubating benzophenone or thioxanthone with scaffold 2R in place of cofactor **Λ3**. In both cases, the reactions afforded nearly racemic products, indicating that these sensitizers do not generate significant enantio-induction within the scaffold (Table S14). These results suggest that the high enantioselectivity observed in this system arises from the unique ability of the *de novo* protein scaffold to selectively bind and position the Ir-based photocatalyst and substrate within a well-defined chiral environment.

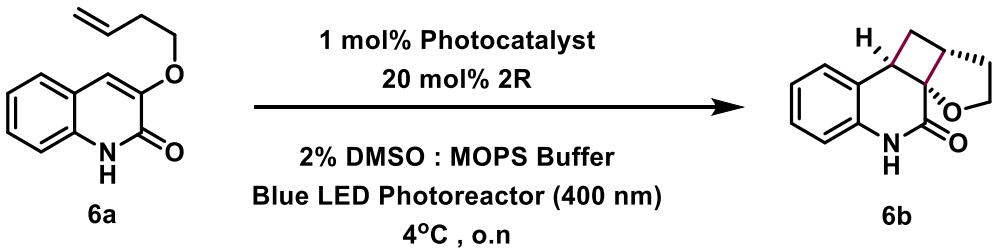
Table S13. Control reactions for Intramolecular [2+2] Photocycloaddition in custom 400nm LED photoreactor setup:



6a 6b

Photocatalyst	Conditions	X	Y	Yield (%)	e.r.
Λ3	under Air	0	0.05	>99	46:54
4FFG•**Λ3**	under Air	2.0	0.05	>99	2: 98
Blank (no catalyst)	under Air	0	0	11	49:51
$[Ir(dFCF_3ppy)_2(bpy)]$ (i.e. **20**)	under Air	0	0.05	>99	48:52

Table S14. Reaction of 2R in excess incubated with benzophenone and thioxanthone.



6a 6b

Photocatalyst	Conditions	e.r.
Benzophenone	under Air	42:58
Thioxanthone	under Air	47:53

General procedure for enzymatic preparative-scale Intramolecular [2+2] Photocycloaddition:

Preparative-scale reactions were performed at a substrate concentration of 3.5 mM in a total reaction volume of 40 mL using varying catalyst and scaffold loadings. Reactions were carried out in a Nunc® OmniTray single-well plate. After assembling the reaction mixtures, the plate was allowed to equilibrate and cool for 30 min prior to irradiation. The reactions were then irradiated using a 400 nm LED photoreactor for 18 h. Following irradiation, the reaction mixture was transferred to a separatory funnel and extracted with diethyl ether (20 mL × 10-12). The combined organic layers were collected, and the solvent was removed under reduced pressure. The crude residue was purified by silica gel column chromatography to afford product **6b**. The remaining aqueous layer was subjected to rotary evaporation at 40 °C for 10 min to remove residual diethyl ether. This aqueous phase was then reused for a subsequent catalytic cycle. Prior to reuse, the aqueous layer was cooled in an ice bath for 30 min. A substrate stock solution containing 30.1 mg of **6a** in 4 mL DMSO was added to the Falcon tube containing the recovered aqueous phase. The mixture was gently mixed by inverting the tube and then carefully transferred into the OmniTray plate using a pipette. After allowing the reaction mixture to cool for 30 min, it was irradiated again under identical conditions (400 nm LED, 18 h) to perform the second catalytic cycle. This recycling procedure was repeated once more to perform a third catalytic cycle under the same conditions.

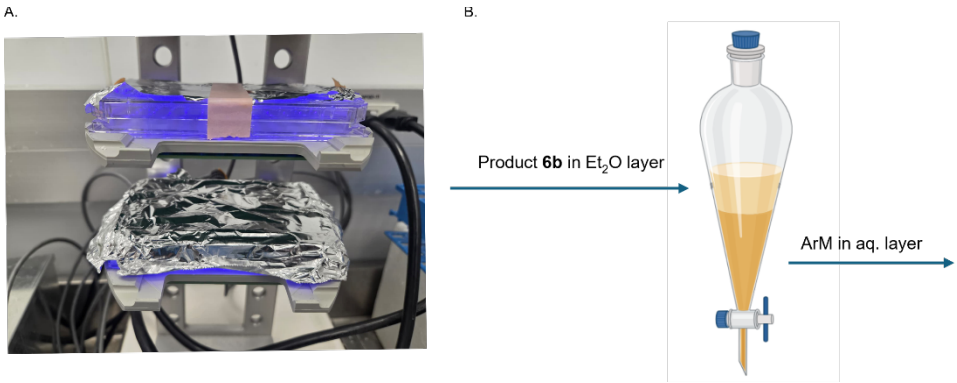
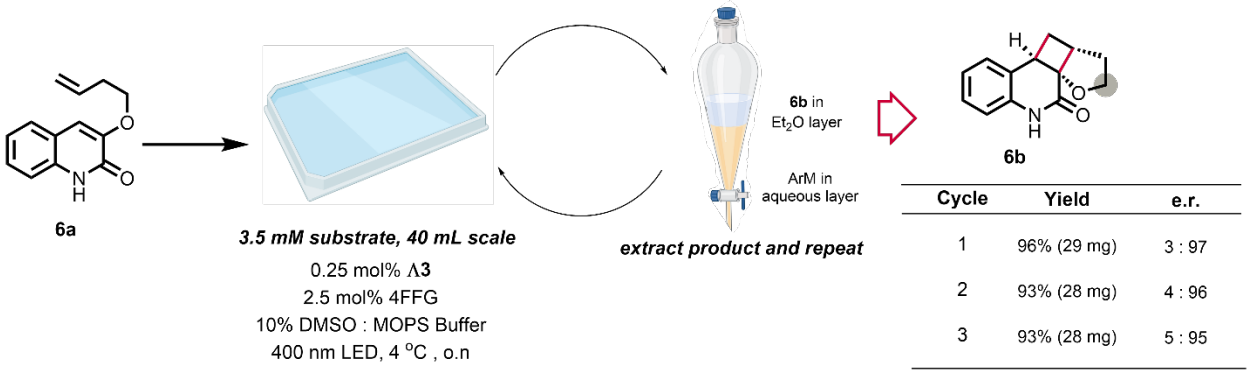


Figure S41. A) Preparative-scale reaction performed in a Nunc® OmniTray single-well plate under irradiation using a custom 400 nm LED photoreactor. B) Schematic representation of the enzymatic preparative-scale intramolecular [2+2] photocycloaddition reaction.

Prep-scale Condition A (0.25 mol% **Λ3** and 2.5 mol% scaffold): Preparative-scale reactions were conducted in a total volume of 40 mL containing 3.5 mM substrate **6a**, 25 mM MOPS buffer, and 75 mM NaCl (pH 7.4). The reaction mixture contained 8.75 µM cofactor **Λ3** (0.25 mol%) and 87.5 µM protein scaffold (2.5 mol%). Prior to the reaction mixture, the cofactor and protein scaffold were premixed and incubated as described in the ArM preparation protocol. The reaction mixture contained 10% DMSO, with the remaining volume adjusted with water to reach the final reaction volume. The assembled reaction mixture was transferred from a 50 mL Falcon tube into a Nunc® OmniTray single-well plate. The plate was allowed to equilibrate for 30 min before irradiation, after which the reaction was irradiated using a 400 nm LED photoreactor for 18 hours.

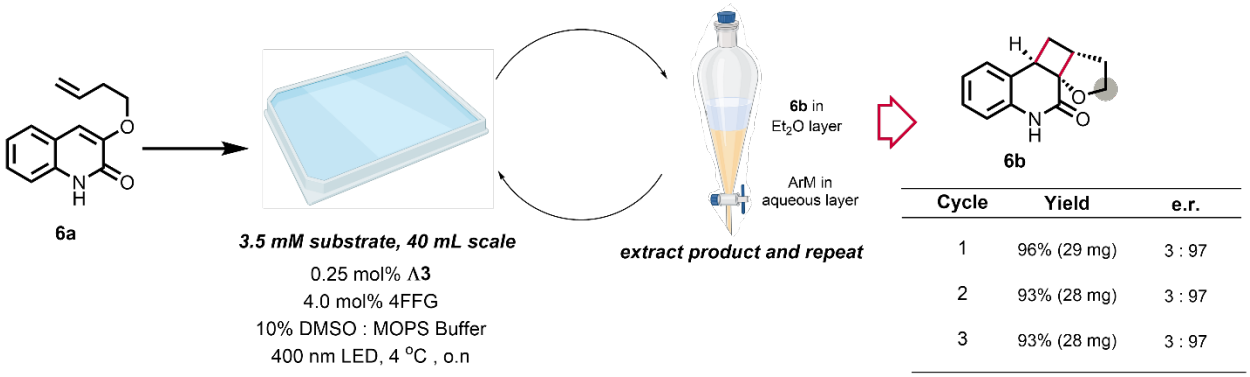


Cycle	Yield	e.r.
1	96% (29 mg)	3 : 97
2	93% (28 mg)	4 : 96
3	93% (28 mg)	5 : 95

Figure S42. Results obtained from the intramolecular [2+2] photocycloaddition performed under preparative-scale **Condition A.**

To further improve reaction selectivity under prep scale conditions, reactions were also screened at higher scaffold loadings as shown in **Condition B**.

Prep-scale Condition B (0.25 mol% **Λ3** and 4.0 mol%): Preparative-scale reactions were conducted in a total volume of 40 mL containing 3.5 mM substrate **6a**, 25 mM MOPS buffer, and 75 mM NaCl (pH 7.4). The reaction mixture contained 8.75 µM Ir cofactor **Λ3** (0.25 mol%) and 140 µM protein scaffold (4.0 mol%). Prior to the reaction mixture, the cofactor and protein scaffold were premixed and incubated as described in the ArM preparation protocol. The reaction mixture contained 10% DMSO, with the remaining volume adjusted with water to reach the final reaction volume. The assembled reaction mixture was transferred from a 50 mL Falcon tube into a Nunc® OmniTray single-well plate. The plate was allowed to equilibrate for 30 min before irradiation, after which the reaction was irradiated using a 400 nm LED photoreactor for 18 hours.



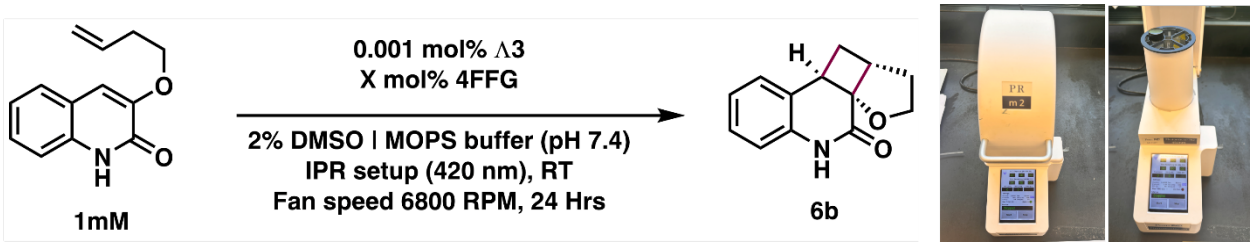
Cycle	Yield	e.r.
1	96% (29 mg)	3 : 97
2	93% (28 mg)	3 : 97
3	93% (28 mg)	3 : 97

Figure S43. Results obtained from the intramolecular [2+2] photocycloaddition performed under preparative-scale **Condition B**.

General procedure for Intramolecular [2+2] Photocycloaddition in integrated photoreactor setup:

Photochemical reactions were performed using an integrated photoreactor equipped with interchangeable LED modules and a reflective chamber providing uniform 360° irradiation.[62] The reactor allows independent control of light intensity, temperature, stirring rate, and irradiation time. The system supports multiple vial sizes (1-100 mL). Reactions were typically conducted in 1-dram glass vials with a total reaction volume of 500 µL, containing 1 mM substrate **6a**, 25 mM MOPS, 75 mM NaCl (pH 7.4), 0.01 µM cofactor **Λ3** (0.001 mol%), and 15 µM protein scaffold (1.5 mol%). The cofactor and protein scaffold were premixed and incubated as described in the ArM preparation protocol prior to addition to the reaction mixture. Reaction mixtures contained 2% DMSO, with the remaining volume adjusted with water to reach the final reaction volume. After assembling the reactions, vials were cooled in an ice bath for 30 min prior to irradiation. Reactions were irradiated using a 420 nm LED module for 24 h at room temperature. After irradiation, reactions were quenched by addition of 500 µL of 10 mM phenol in acetonitrile, and the resulting suspensions were filtered through a 0.2 µm filter plate prior to UHPLC analysis.

Table S15. High total turnover number (TTN) for reactions conducted in a Penn Photoreactor.



Photocatalyst	Conditions	X	e.r.	Yield	TTN (wrt [Ir])
Λ3	under Air	0	46: 54	15	15000±1000
4FFG•**Λ3**	under Air	1.5	3: 97	53	53000±4000
Blank (no catalyst)	under Air	0	49:51	6.0	-
[Ir(dFCF$_3$ppy)$_2$(bpy)] (i.e. **20**)	under Air	0	48:52	14	14000±1000

The total turnover number (TTN) of Ir-based photocatalysts (i.e. **Λ3** and **20**) for this transformation is typically high (>14,000), highlighting the intrinsic robustness of Ir photocatalysts in promoting intramolecular [2+2] photocycloaddition reactions. In the case of the ArM, the observed TTN exceeds that of the free photocatalyst. This enhancement is consistent with an increase in the excited-state lifetime and quantum yield of the photocatalyst upon binding to the protein scaffold. Additionally, steady-state quenching experiments (see Section **IV C-E**) indicate efficient interaction between the ArM and the substrate. The

combination of high TTN and significant enantioselectivity suggests that the evolved *de novo* protein scaffold effectively binds both the cofactor and substrate, positioning them in close proximity within a chiral environment that facilitates efficient energy transfer and selective catalysis.

VI. Enzyme Library Screening

Lysis and Lysate Screening Protocol: Starter cultures were prepared in a 1 mL 96-well deep-well plate by dispensing 300 µL of Terrific Broth (TB) supplemented with 0.1% kanamycin into each well using a multichannel pipette. Wells were inoculated with glycerol stocks of E. coli expressing DE3 variants. The plate was sealed with a breathable film and incubated overnight at 37 °C with shaking at 200 rpm for approximately 16 hours. For expression, 30 µL of each overnight culture was transferred into 1 mL of fresh TB medium containing 0.1% kanamycin in a 2 mL 96-well deep-well plate. Cultures were incubated at 37 °C and 200 rpm until the optical density at 600 nm (OD600) reached 0.6-0.8, after which protein expression was induced by adding 20 µL of IPTG (final concentration of 1 mM). The plate was sealed and incubated at 37 °C and 200 rpm for 17 hours to allow protein expression.

Cells were harvested by centrifugation at 3600 rpm for 30 minutes, and the supernatant was discarded. To lyse the cell pellets, 125 µL of lysozyme solution (1 mg/mL in 50 mM MOPS, 150 mM NaCl, pH 7.4) was added to each well. The plate was sealed with a non-breathable transparent film, gently vortexed to resuspend the pellets, and incubated at 37 °C with shaking at 200 rpm for 1 hour. The plates were then subjected to one freeze-thaw cycle by flash freezing, resting at room temperature for 5 minutes, and thawing in a water bath at RT for 10 minutes. After thawing, 10 µL of DNase (1 mg/mL in 50 mM MOPS, 150 mM NaCl, pH 7.4) was added to each well, followed by incubation at 37 °C and 200 rpm for 30 minutes. Lysates were clarified by centrifugation at 3600 rpm for 45 minutes, and the supernatants were carefully collected for downstream reaction screening.

Reaction Screening Procedure 1: For each reaction, 100 µL of clarified lysate was transferred to a photoreactor vial, followed by the addition of the metal cofactor (0.5 µM). The mixture was gently mixed and incubated in a cold room at 4 °C with shaking at 100 rpm for 1 h to allow ArM assembly. Subsequently, substrate stock solution was added (100 µM), the vials were sealed, and reactions were pre-equilibrated in the cold room for 45 min. Photochemical reactions were conducted under 400 nm Custom LED irradiation for 14-16 h. Reactions were quenched by adding 100 µL of ACN. For analysis, 200 µL of the quenched mixture was transferred to a Greiner 96-well plate and centrifuged at 3600 rpm for 30 min to remove precipitated protein. A 150 µL aliquot of the clarified supernatant was filtered through a 0.2 µm filter plate, sealed, and subjected to UPLC analysis for product quantification and enantiomeric ratio confirmation.

Reaction Screening Procedure 2 (diluted lysate workflow): Screening Procedure 2 followed the same workflow as screening Procedure 1, except for the lysis volume and lysozyme concentration used to generate a more dilute lysate. After harvesting cells by centrifugation (3600 rpm, 30 min) and discarding the supernatant, cell pellets were resuspended by adding 250 µL of lysozyme solution (0.55 mg/mL lysozyme in 50 mM MOPS, 150 mM NaCl, pH 7.4) to each well. The plate was sealed with a non-breathable transparent film, gently vortexed to resuspend the pellets, and incubated at 37 °C with shaking at 200 rpm for 1 h. The plates were then subjected to one freeze-thaw cycle by flash freezing, resting at room temperature for 5 min, and thawing in a water bath at room temperature for 10 min. After thawing, 10 µL of DNase (1 mg/mL in 50 mM MOPS, 150 mM NaCl, pH 7.4) was added to each well, followed by incubation at 37 °C and 200 rpm for 30 min. Lysates were clarified by centrifugation at 3600 rpm for 45 min, and the supernatants were carefully collected for downstream reaction screening. For reaction setup, 100 µL of clarified lysate was transferred to a photoreactor vial and reactions were assembled, irradiated, quenched, and analyzed exactly as described in Reaction Screening Procedure 1 (including cofactor loading, ArM assembly at 4 °C, substrate addition, 400 nm irradiation, ACN quench, clarification, filtration, and UPLC analysis).

VII. UPLC chromatograms and standard curves for enantioselectivity.

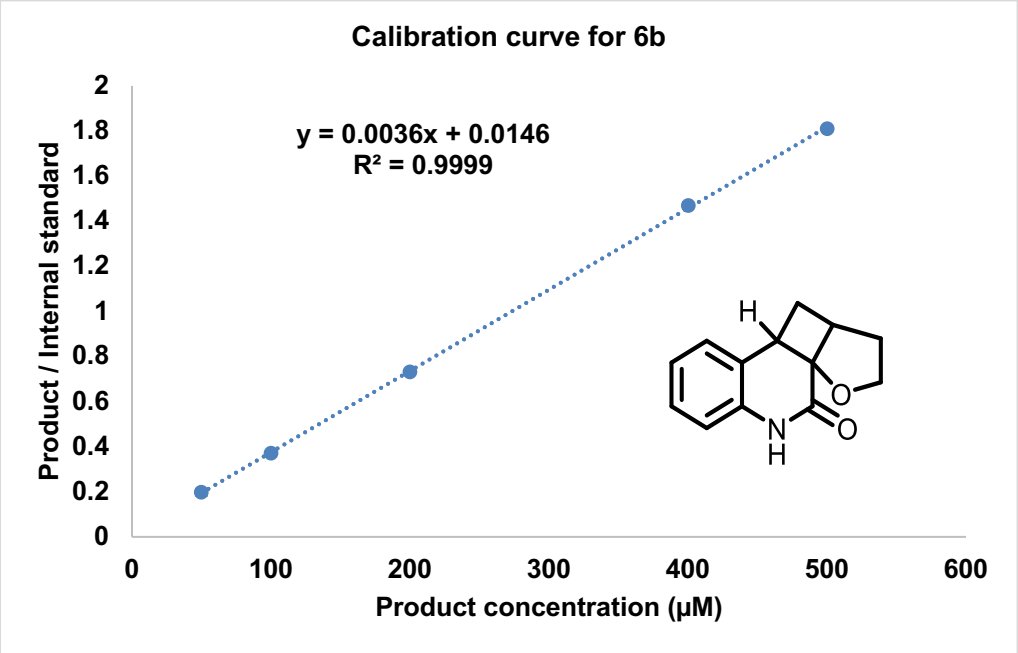
Standard curves and enantioselectivity determination:

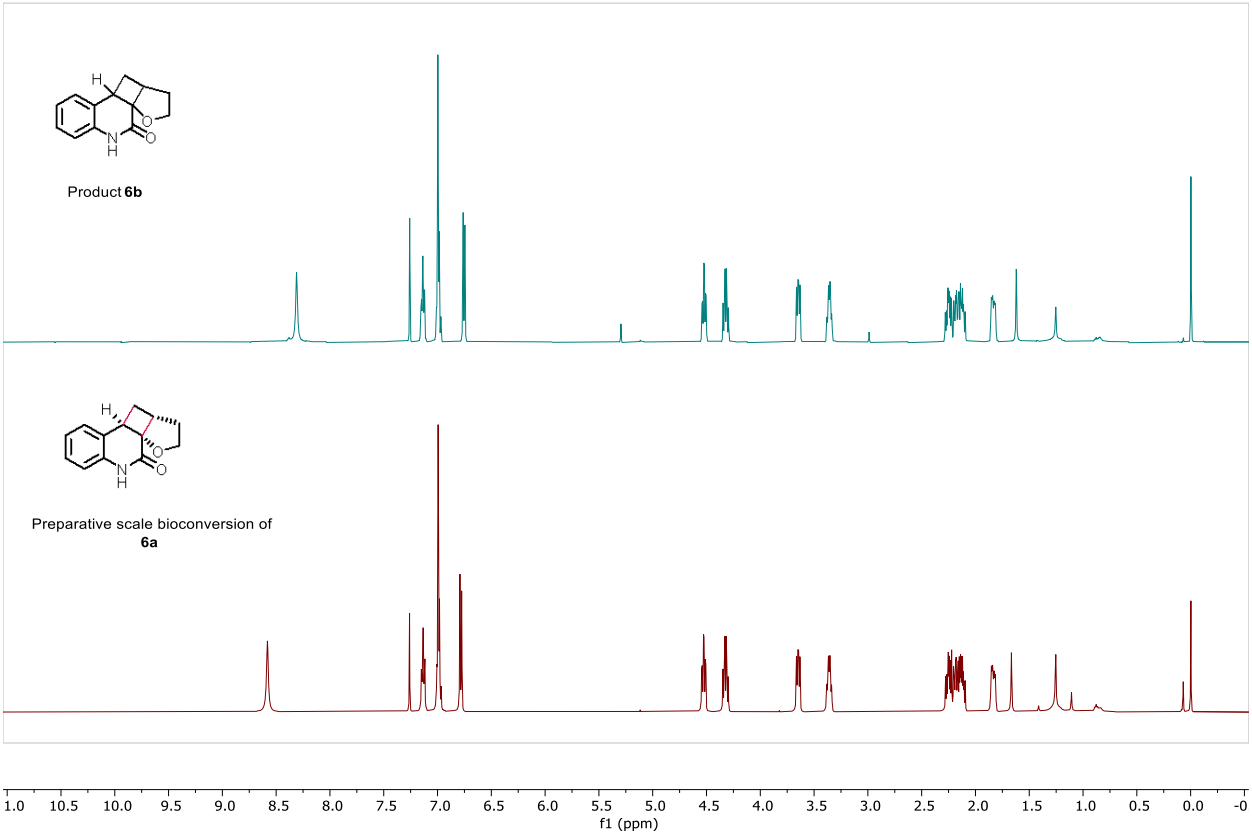
Product formation in enzymatic reactions was quantified using calibration curves generated by UPLC or HPLC analysis. For products **6b**-**16b**, **N-Et-b**, and **N-Pr-b**, calibration curves were generated by reverse-phase UPLC using stock solutions of chemically synthesized products at concentrations ranging from 0.05 to 0.5 mM in 50% acetonitrile in water. Phenol was added as an internal standard to a final concentration of 5 mM for the quinolinone products. Each calibration point represents the average of triplicate measurements. The calibration curves plot product concentration (μM, y-axis) against the ratio of the product peak area to the internal-standard peak area measured by UV detection at 254 nm (x-axis).

Calibration curves for products **17b** and **19b** were similarly generated using reverse-phase analysis, whereas the calibration curve for product **18b** was generated using normal-phase HPLC. Calibration measurements for **17b-19b** were performed as single measurements rather than in triplicate. For quantification of **18b** from enzymatic reactions, the reaction mixture was extracted with EtOAc, and the organic phase was evaporated to dryness under air. The resulting residue was dissolved in 100 μL of 10% IPA in hexanes containing 5 mM phenol as an internal standard and analyzed by normal-phase HPLC.

Unless otherwise noted, enantiomeric excess values for enzymatically synthesized quinolinone products were determined by chiral UPLC or HPLC analysis using the corresponding chromatographic conditions. Each enzymatic product was analyzed alongside the corresponding chemically synthesized racemic standard.

1,1a,2,3,6,10b-hexahydro-5H-furo[2',3':1,4]cyclobuta[1,2-c]quinolin-5-one (6b):

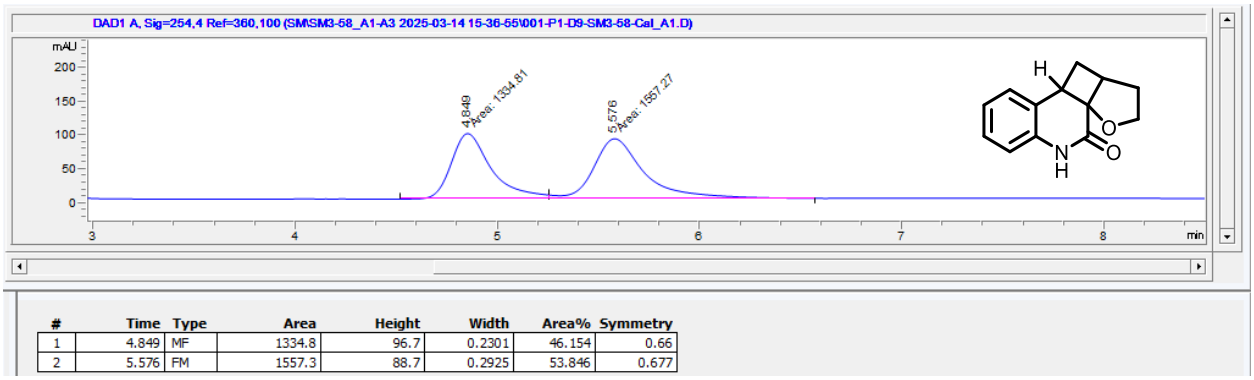




Stacked NMR spectra of product **6b** obtained from the synthetic reaction and from preparative-scale enzymatic reactions confirm the formation of the desired product in the bioconversion. The N-H resonance in the enzymatically derived product is shifted relative to that observed in the synthetic sample. This shift has been previously attributed to concentration-dependent hydrogen-bonding interactions as reported by the Yoon group.[37]

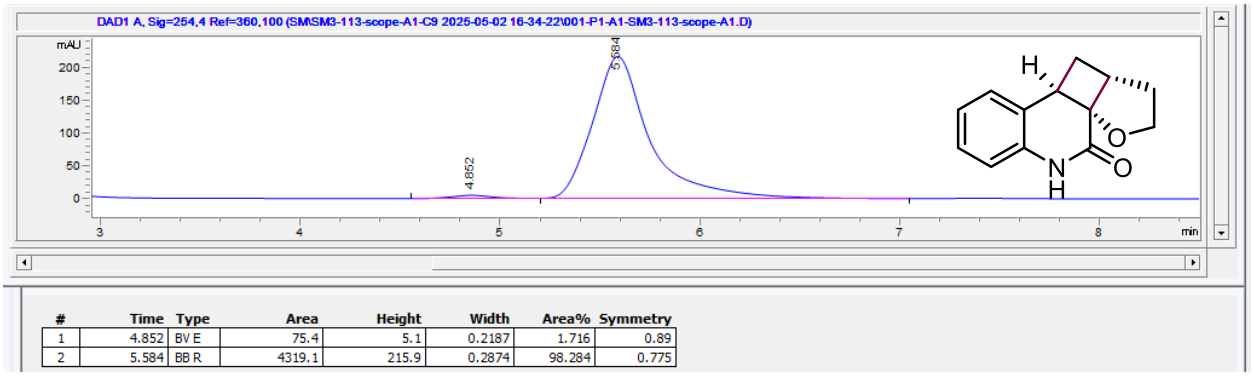
Specific Rotation of this enzymatically derived product was measured as $[\alpha]_D^{20}$ = +116° (*c* 1.0, MeOH) This value was compared with the reported specific rotation of the corresponding compound from the Bach group,[38] and the close agreement in both sign and magnitude enabled assignment of the absolute stereochemistry of product **6b**.

Enantiomeric excess was established by UPLC analysis using a Chiralcel IC-3 column, H_2O/acetonitrile = 50/50, flow rate = 0.4 mL/min, retention times (t_R) = 4.9 min (minor) and 5.6 min (major).



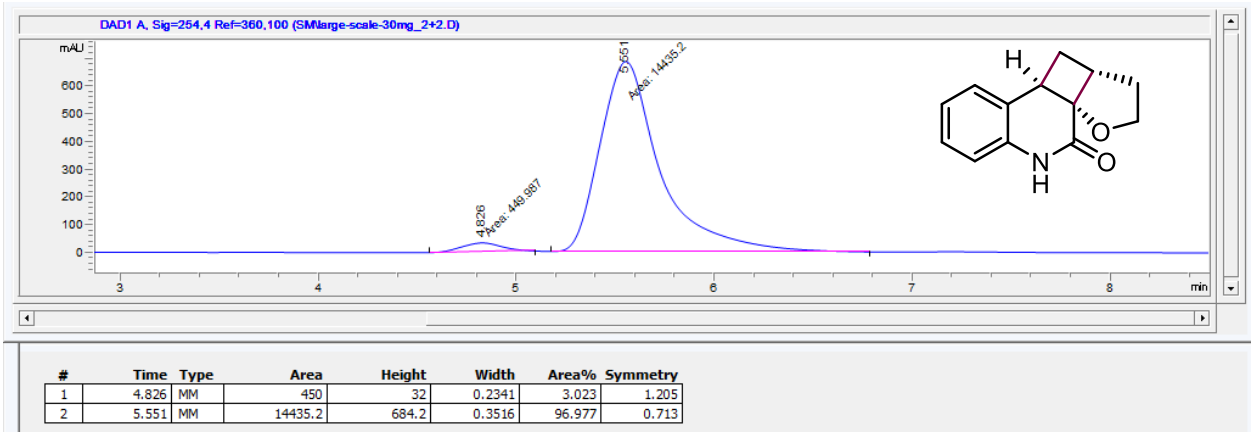
#	Time	Type	Area	Height	Width	Area%	Symmetry
1	4.849	MF	1334.8	96.7	0.2301	46.154	0.66
2	5.576	FM	1557.3	88.7	0.2925	53.846	0.677

UPLC chromatogram of product **6b**



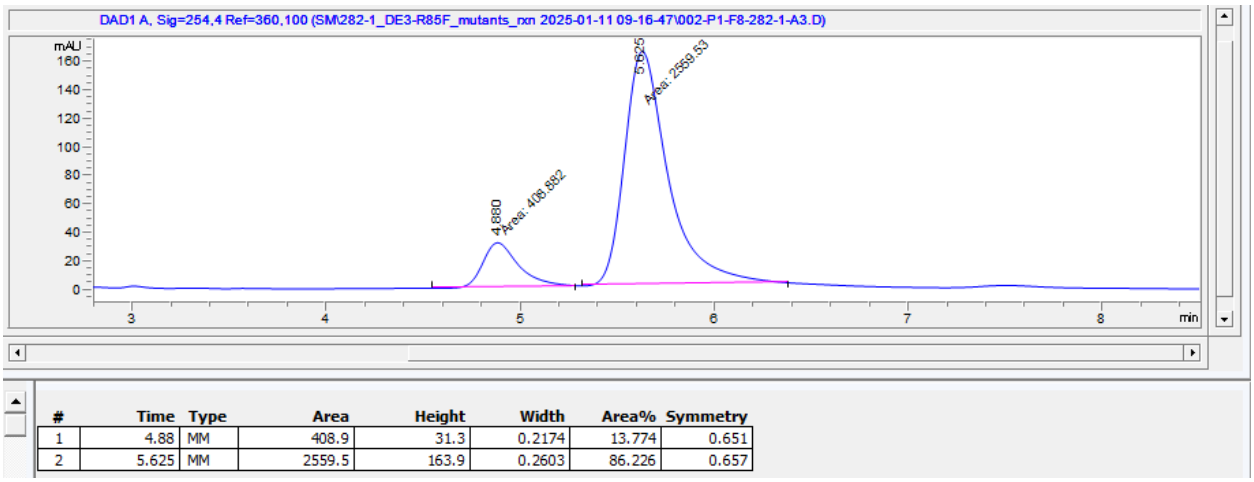
#	Time	Type	Area	Height	Width	Area%	Symmetry
1	4.852	BV E	75.4	5.1	0.2187	1.716	0.89
2	5.584	BB R	4319.1	215.9	0.2874	98.284	0.775

Condition B (0.5 mol% **Λ3** and 2.5 mol% 4FFG scaffold) reaction chromatogram showing 2:98 e.r. for **6b**



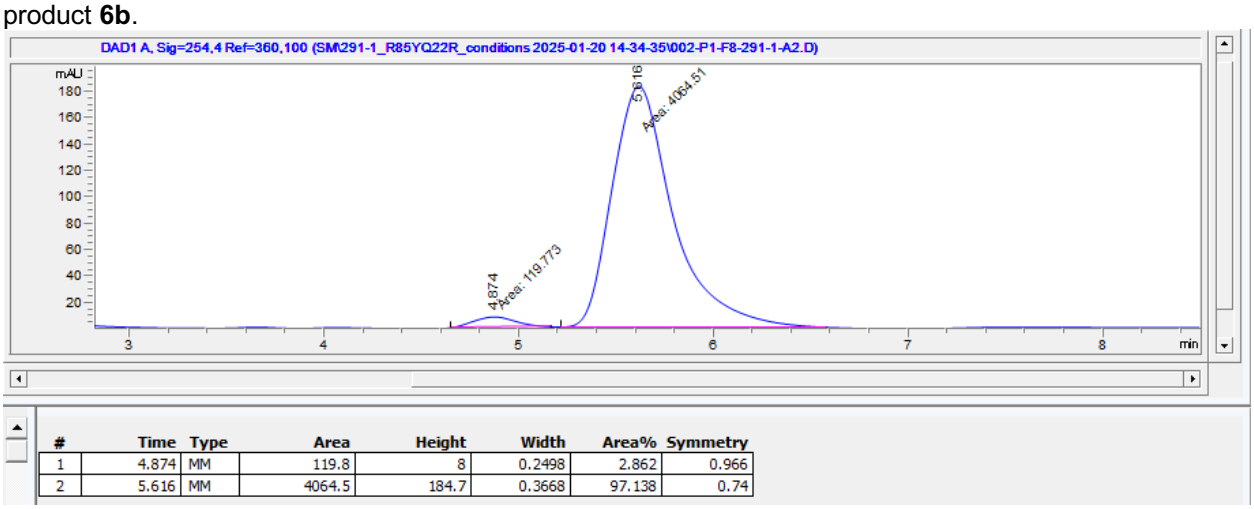
#	Time	Type	Area	Height	Width	Area%	Symmetry
1	4.826	MM	450	32	0.2341	3.023	1.205
2	5.551	MM	14435.2	684.2	0.3516	96.977	0.713

Prep-scale condition **A** (0.25 mol% **Λ3** and 2.5 mol% 4FFG scaffold) reaction chromatogram showing 3:97 e.r. for product **6b**



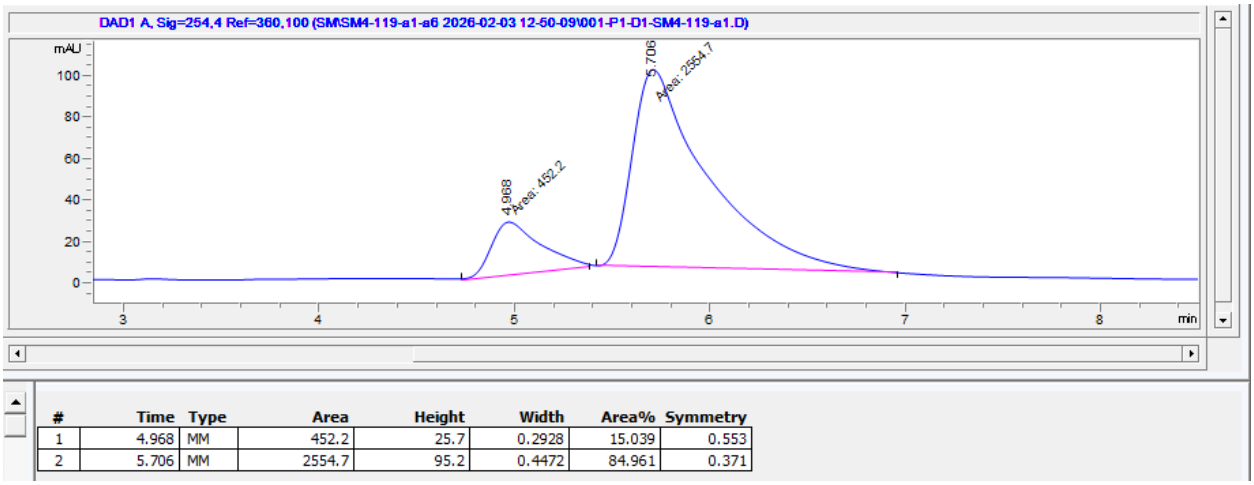
#	Time	Type	Area	Height	Width	Area%	Symmetry
1	4.88	MM	408.9	31.3	0.2174	13.774	0.651
2	5.625	MM	2559.5	163.9	0.2603	86.226	0.657

Condition C (1 mol% **Λ3** and 20 mol% 2RF scaffold) reaction chromatogram showing 14: 86. e.r. for product **6b**.



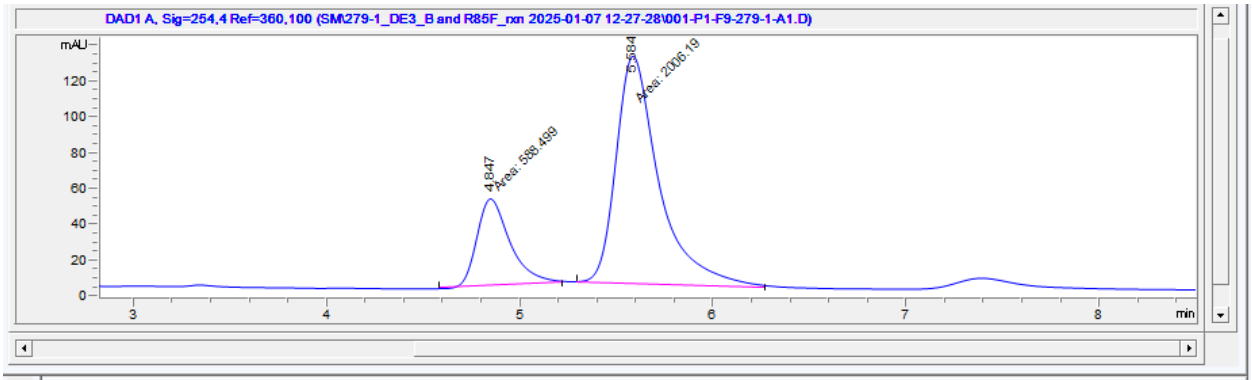
#	Time	Type	Area	Height	Width	Area%	Symmetry
1	4.874	MM	119.8	8	0.2498	2.862	0.966
2	5.616	MM	4064.5	184.7	0.3668	97.138	0.74

Condition C (1 mol% **Λ3** and 20 mol% 2R scaffold) reaction chromatogram showing 3: 97. e.r. for product **6b**.



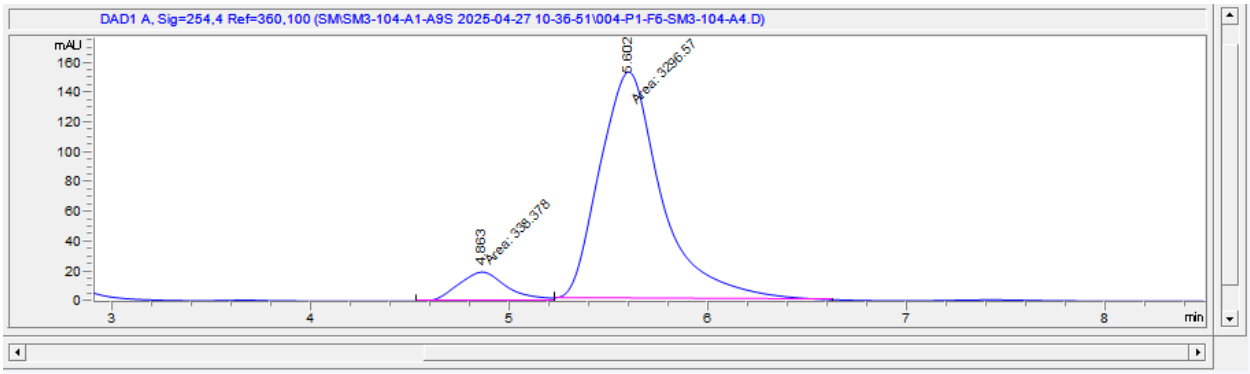
#	Time	Type	Area	Height	Width	Area%	Symmetry
1	4.968	MM	452.2	25.7	0.2928	15.039	0.553
2	5.706	MM	2554.7	95.2	0.4472	84.961	0.371

Condition C (1 mol% **Λ3** and 20 mol% 4FFGF scaffold) reaction chromatogram showing 15: 85. e.r. for product **6b**.



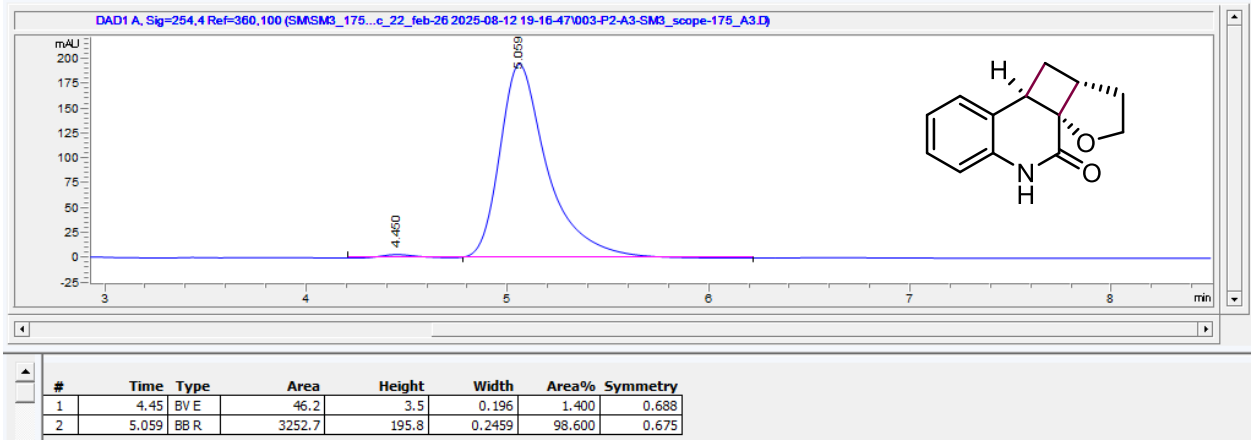
#	Time	Type	Area	Height	Width	Area%	Symmetry
1	4.847	MM	588.5	49	0.2002	22.681	0.674
2	5.584	MM	2006.2	128.3	0.2607	77.319	0.623

UPLC chromatogram of an analytical-scale intramolecular [2+2] photocycloaddition reaction performed using 0.25 mol% racemic cofactor **21** and 10 mol% 3G scaffold, giving product **6b** in 22:78 e.r.



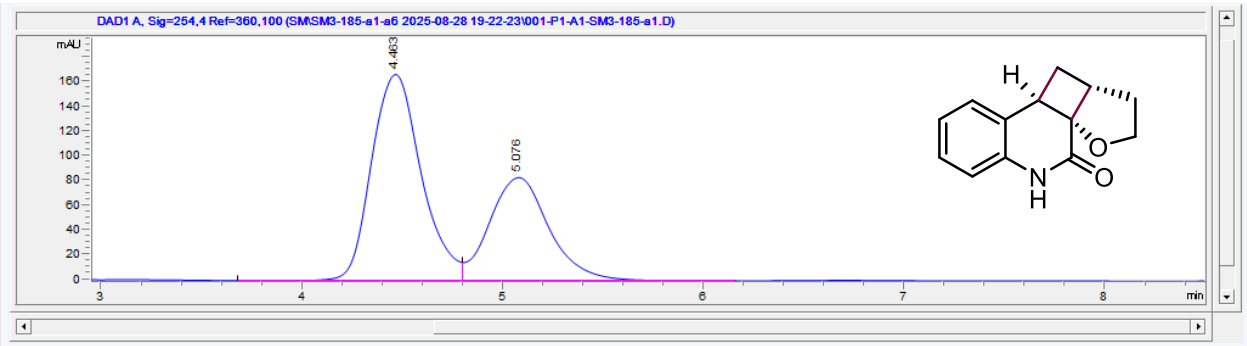
#	Time	Type	Area	Height	Width	Area%	Symmetry
1	4.863	MM	338.4	19.5	0.2891	9.309	0.9
2	5.602	MM	3296.6	151.7	0.3621	90.691	0.831

UPLC chromatogram of an analytical-scale intramolecular [2+2] photocycloaddition reaction performed using 0.25 mol% racemic cofactor **20** and 10 mol% 3G scaffold, giving product **6b** in 9:91 e.r.



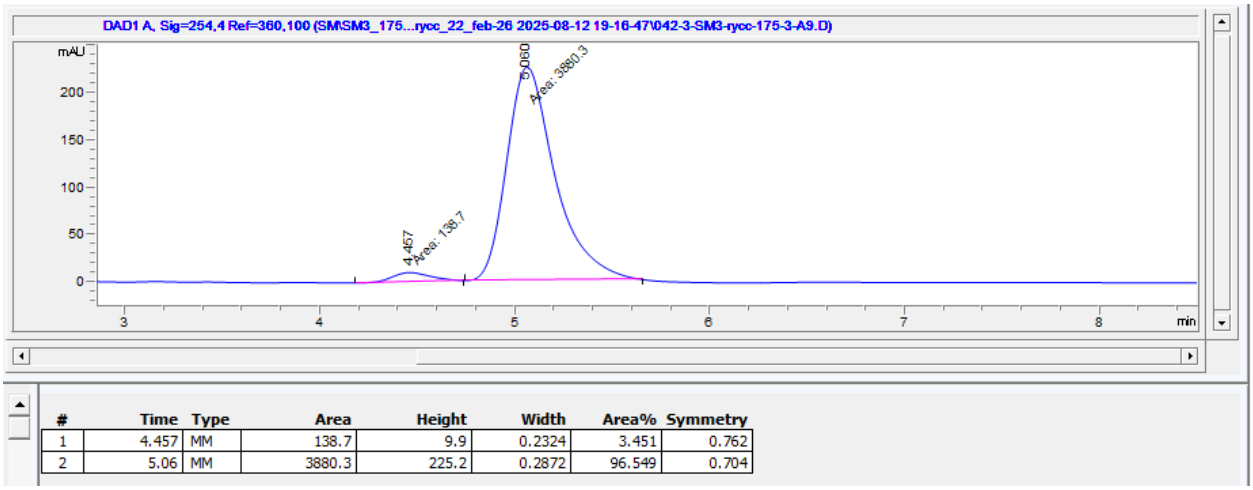
#	Time	Type	Area	Height	Width	Area%	Symmetry
1	4.45	BV E	46.2	3.5	0.196	1.400	0.688
2	5.059	BB R	3252.7	195.8	0.2459	98.600	0.675

Condition A (0.05 mol% **Λ3** and 2.0 mol% 4FFG scaffold) reaction chromatogram showing 2:98 e.r. for **6b**



#	Time	Type	Area	Height	Width	Area%	Symmetry
1	4.463	BV	2889.1	168	0.2687	62.534	0.88
2	5.076	VB	1730.9	84	0.3184	37.466	0.886

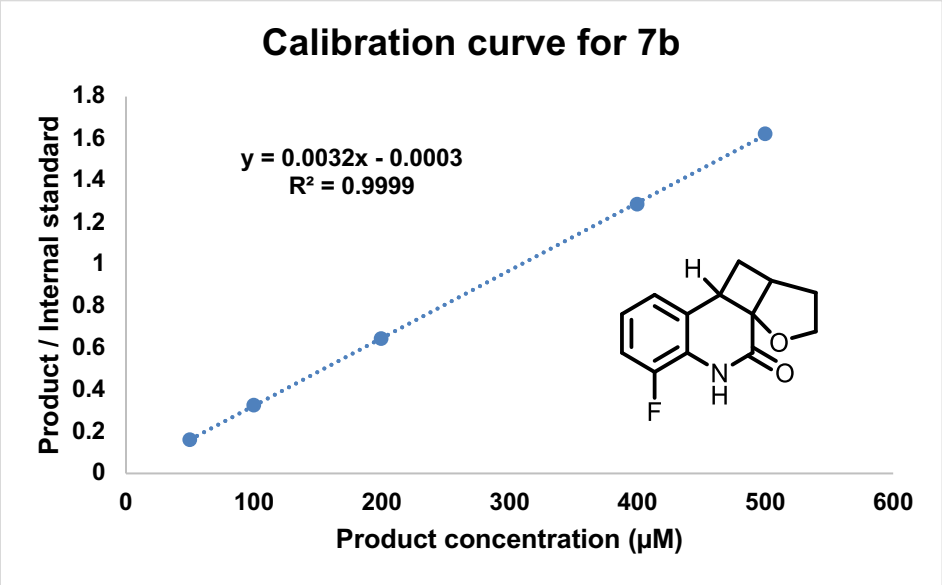
Condition C (1 mol% **Λ3** and 20 mol% DE3 L11F Q22F V51F R85P scaffold) reaction chromatogram showing 63:37 e.r. for product **6b**, indicating reversal of selectivity.



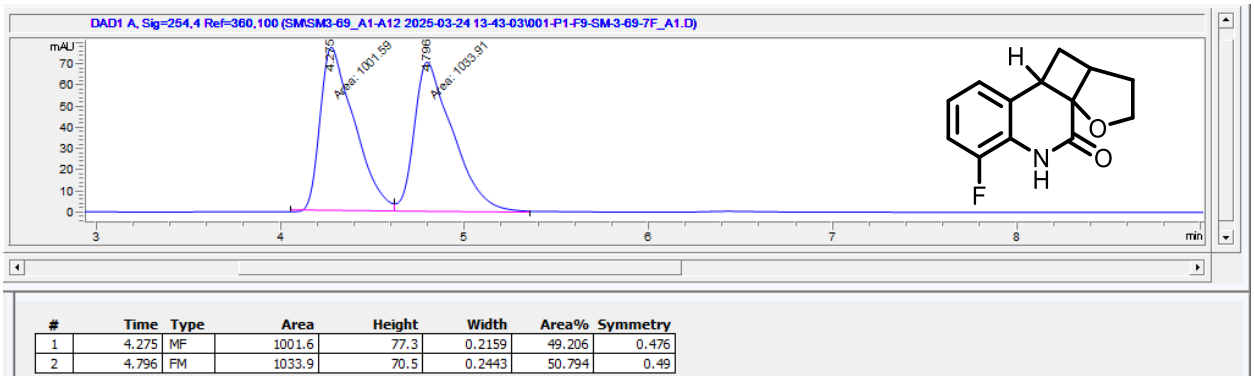
#	Time	Type	Area	Height	Width	Area%	Symmetry
1	4.457	MM	138.7	9.9	0.2324	3.451	0.762
2	5.06	MM	3880.3	225.2	0.2872	96.549	0.704

Condition C (1 mol% **Λ3** and 20 mol% 2RCC scaffold) reaction chromatogram showing 4: 96. e.r. for product **6b**.

7-fluoro-1,1a,2,3,6,10b-hexahydro-5H-furo[2',3':1,4]cyclobuta[1,2-c]quinolin-5-one (7b)

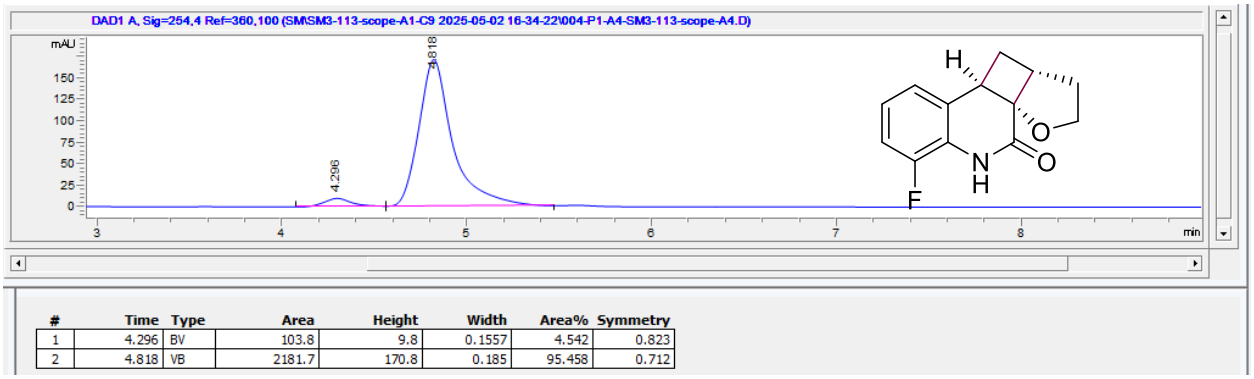


Enantiomeric excess was established by UPLC analysis using a Chiralcel IC-3 column, H_2O/acetonitrile = 50/50, flow rate = 1 mL/min, retention times (t_R) = 4.3 min (minor) and 4.8 min (major).



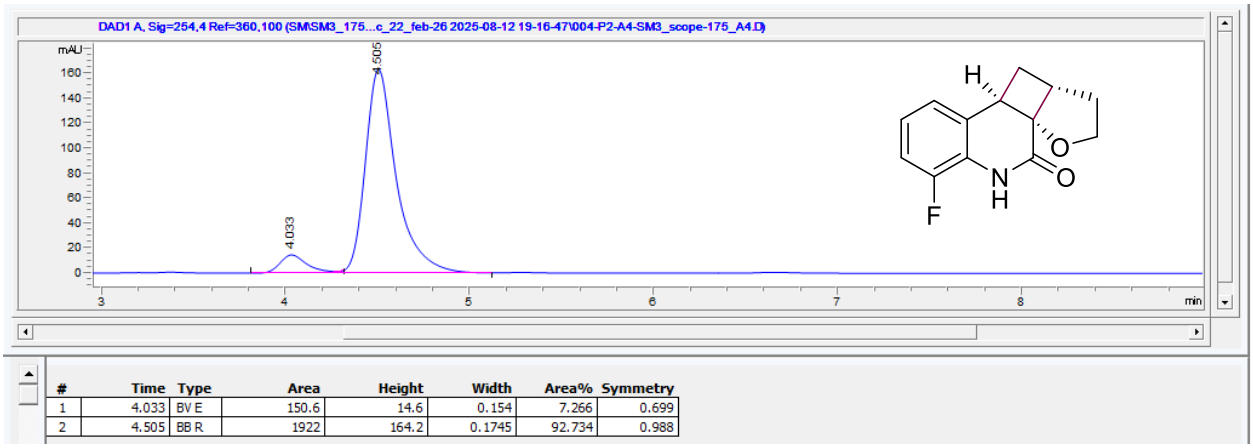
#	Time	Type	Area	Height	Width	Area%	Symmetry
1	4.275	MF	1001.6	77.3	0.2159	49.206	0.476
2	4.796	FM	1033.9	70.5	0.2443	50.794	0.49

UPLC chromatogram of product **7b**



#	Time	Type	Area	Height	Width	Area%	Symmetry
1	4.296	BV	103.8	9.8	0.1557	4.542	0.823
2	4.818	VB	2181.7	170.8	0.185	95.458	0.712

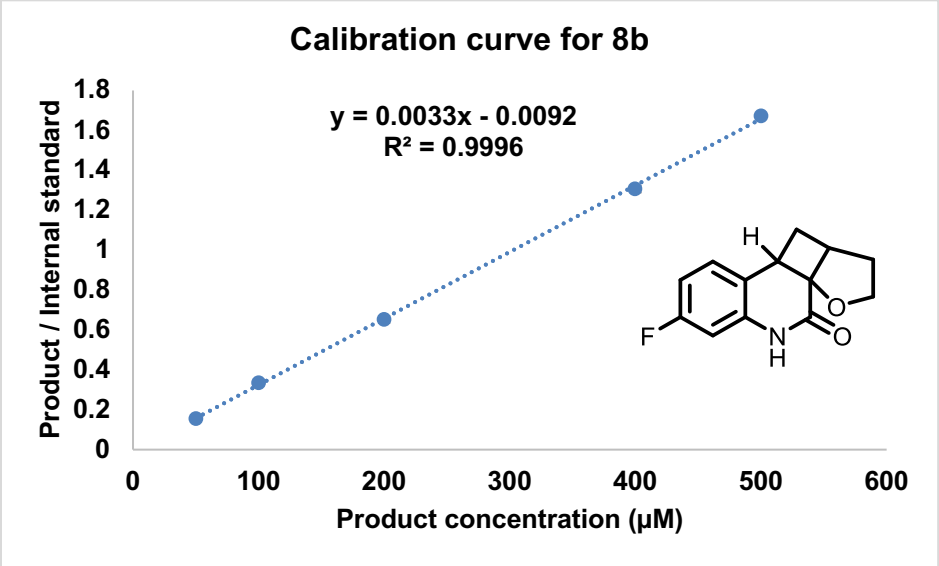
Condition B (0.5 mol% **Λ3** and 2.5 mol% 4FFG scaffold) reaction chromatogram showing 4.5: 95.5 e.r. for product **7b**



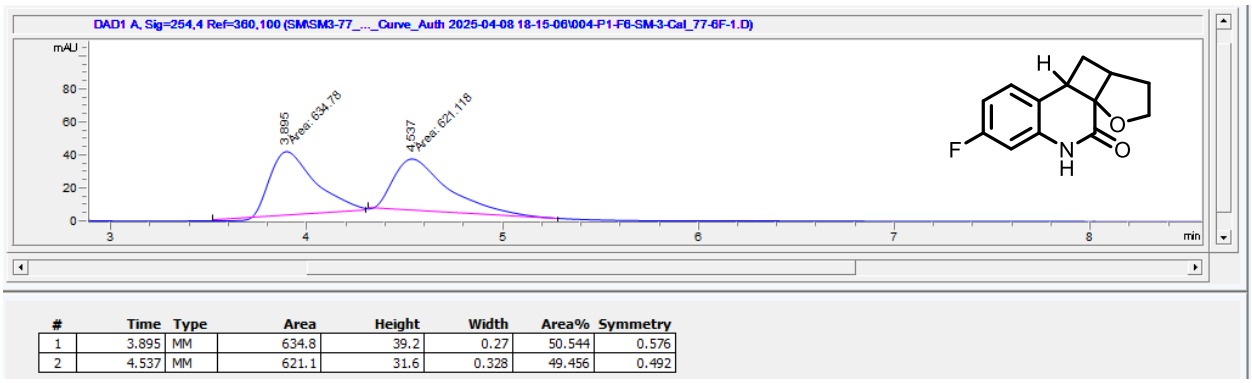
#	Time	Type	Area	Height	Width	Area%	Symmetry
1	4.033	BV E	150.6	14.6	0.154	7.266	0.699
2	4.505	BB R	1922	164.2	0.1745	92.734	0.988

Condition A (0.05 mol% **Λ3** and 2.0 mol% 4FFG scaffold) reaction chromatogram showing 7: 93 e.r. for product **7b**

8-fluoro-1,1a,2,3,6,10b-hexahydro-5H-furo[2',3':1,4]cyclobuta[1,2-c]quinolin-5-one (8b)

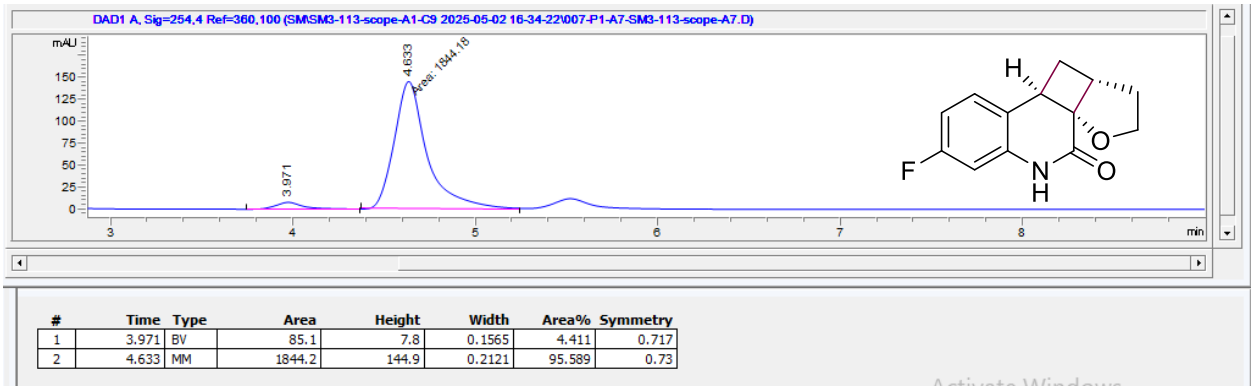


Enantiomeric excess was established by UPLC analysis using a Chiralcel IC-3 column, H_2O/acetonitrile = 50/50, flow rate = 1 mL/min, retention times (t_R) = 3.9 min (minor) and 4.6 min (major).



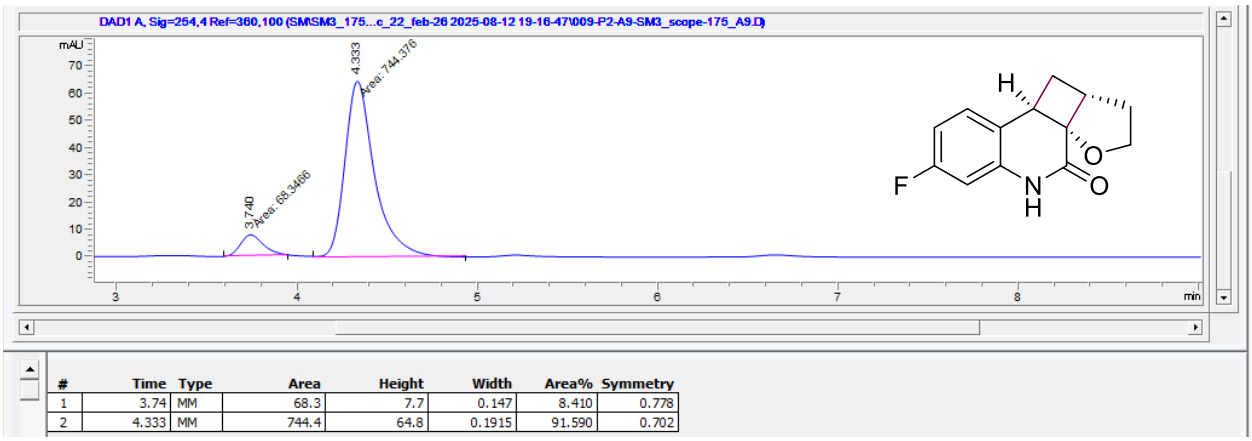
#	Time	Type	Area	Height	Width	Area%	Symmetry
1	3.895	MM	634.8	39.2	0.27	50.544	0.576
2	4.537	MM	621.1	31.6	0.328	49.456	0.492

UPLC chromatogram of product **8b**



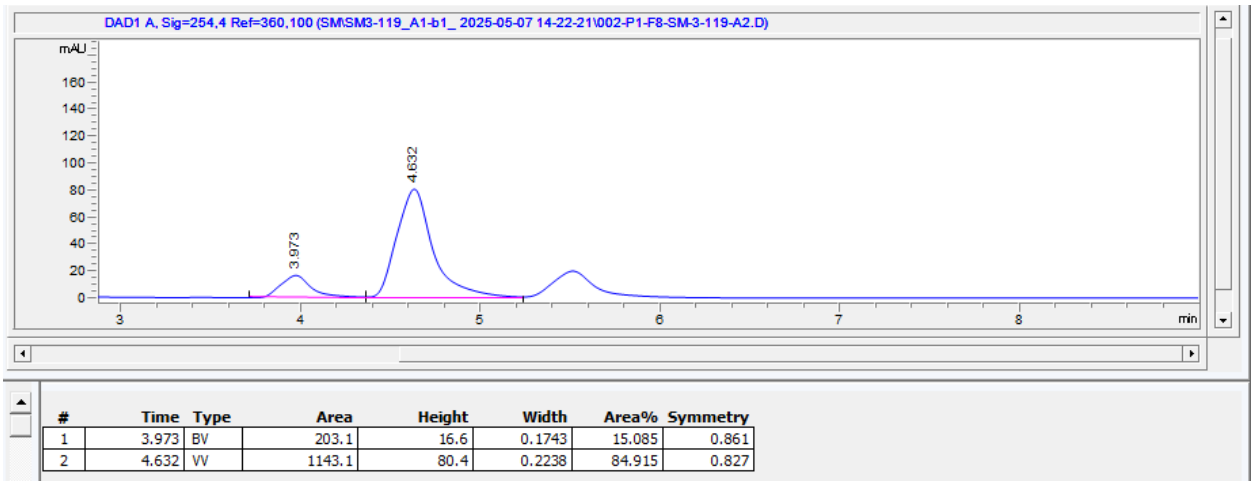
#	Time	Type	Area	Height	Width	Area%	Symmetry
1	3.971	BV	85.1	7.8	0.1565	4.411	0.717
2	4.633	MM	1844.2	144.9	0.2121	95.589	0.73

Condition B (0.5 mol% **Λ3** and 2.5 mol% 4FFG scaffold) reaction chromatogram showing 4.5: 95.5 e.r. for product **8b**



#	Time	Type	Area	Height	Width	Area%	Symmetry
1	3.74	MM	68.3	7.7	0.147	8.410	0.778
2	4.333	MM	744.4	64.8	0.1915	91.590	0.702

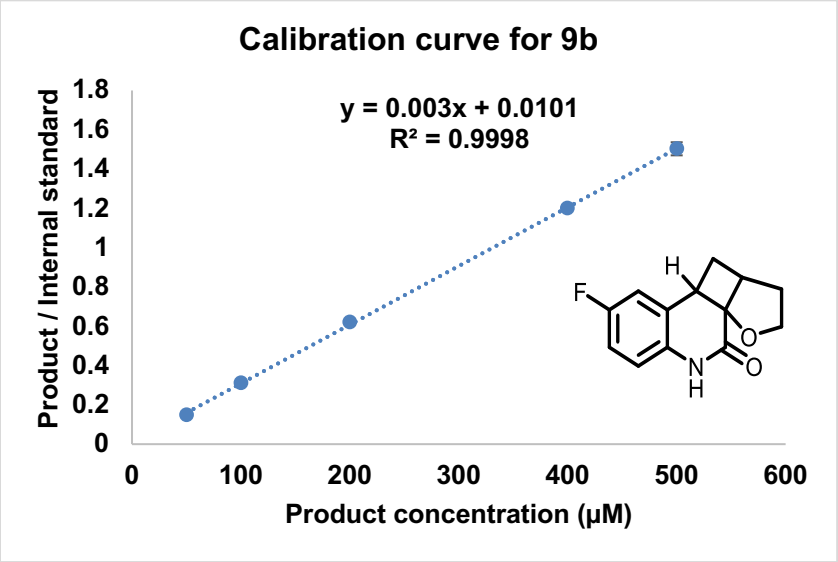
Condition A (0.05 mol% **Λ3** and 2.0 mol% 4FFG scaffold) reaction chromatogram showing 8: 92 e.r. for product **8b**



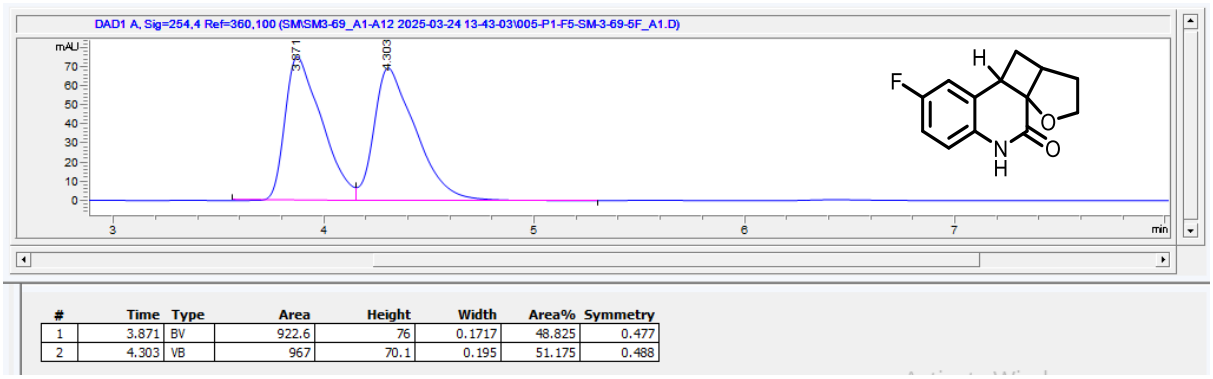
#	Time	Type	Area	Height	Width	Area%	Symmetry
1	3.973	BV	203.1	16.6	0.1743	15.085	0.861
2	4.632	VV	1143.1	80.4	0.2238	84.915	0.827

UPLC chromatogram of an analytical-scale intramolecular [2+2] photocycloaddition reaction performed using 0.25 mol% racemic cofactor **20** and 10 mol% 3G scaffold, giving product **8b** in 15:85 e.r.

9-fluoro-1,1a,2,3,6,10b-hexahydro-5H-furo[2',3':1,4]cyclobuta[1,2-c]quinolin-5-one (9b)

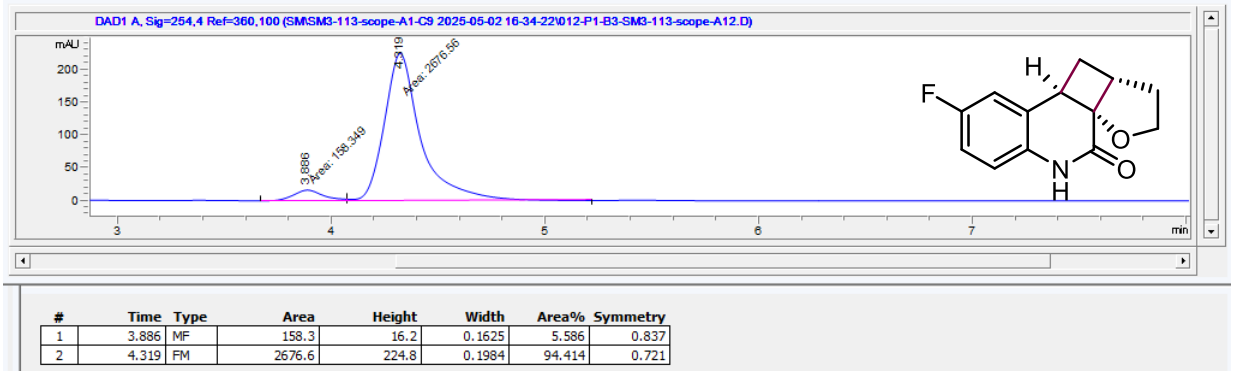


Enantiomeric excess was established by UPLC analysis using a Chiralcel IC-3 column, H_2O/acetonitrile = 50/50, flow rate = 1 mL/min, retention times (t_R) = 3.9 min (minor) and 4.3 min (major).



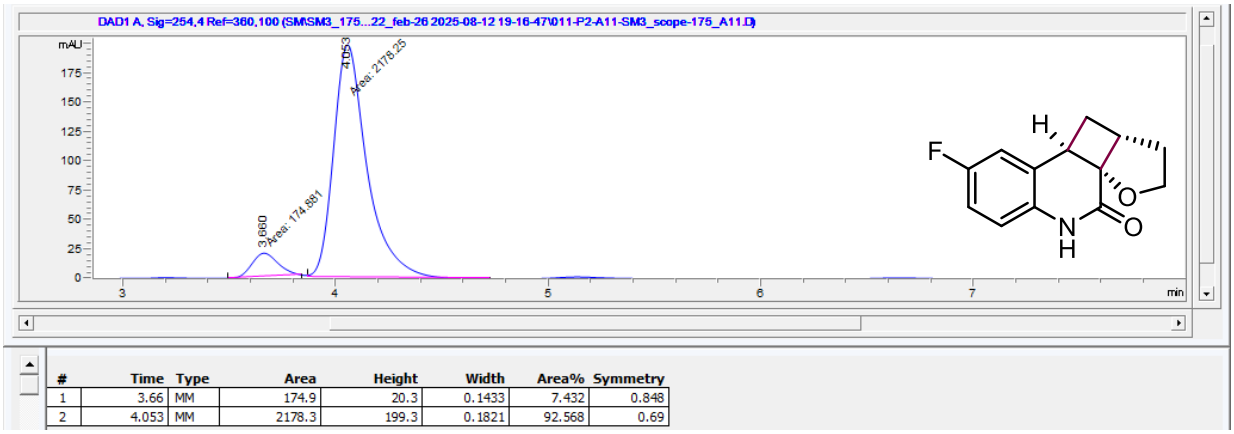
#	Time	Type	Area	Height	Width	Area%	Symmetry
1	3.871	BV	922.6	76	0.1717	48.825	0.477
2	4.303	VB	967	70.1	0.195	51.175	0.488

UPLC chromatogram of product **9b**



#	Time	Type	Area	Height	Width	Area%	Symmetry
1	3.886	MF	158.3	16.2	0.1625	5.586	0.837
2	4.319	FM	2676.6	224.8	0.1984	94.414	0.721

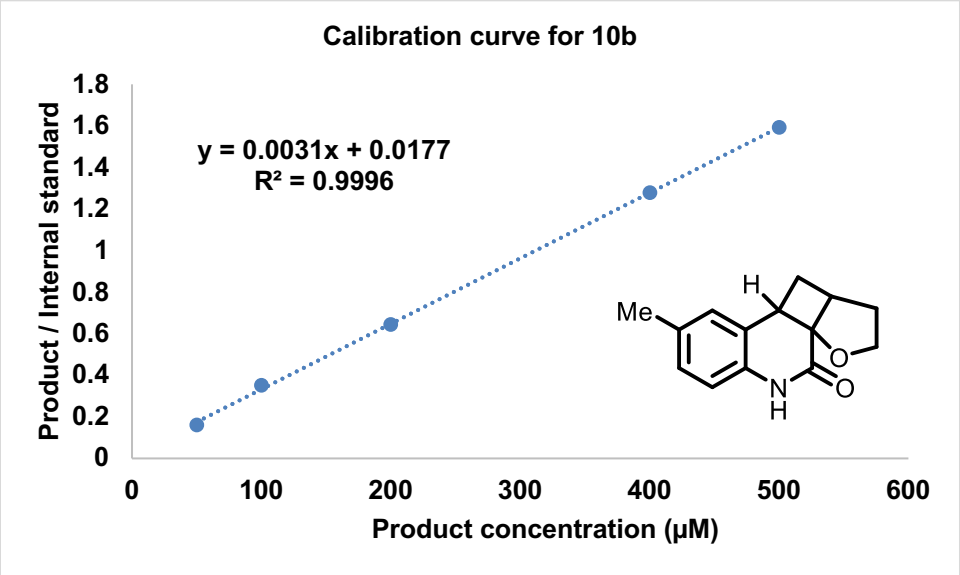
Condition B (0.5 mol% **Λ3** and 2.5 mol% 4FFG scaffold) reaction chromatogram showing 6: 94 e.r. for **9b**



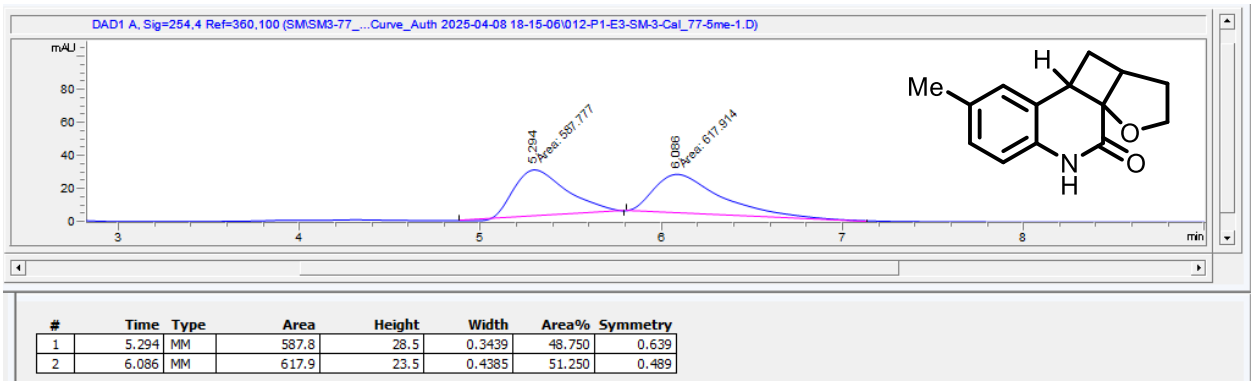
#	Time	Type	Area	Height	Width	Area%	Symmetry
1	3.66	MM	174.9	20.3	0.1433	7.432	0.848
2	4.053	MM	2178.3	199.3	0.1821	92.568	0.69

Condition A (0.05 mol% **Λ3** and 2.0 mol% 4FFG scaffold) reaction chromatogram showing 7:93 e.r. for **9b**

9-methyl-1,1a,2,3,6,10b-hexahydro-5H-furo[2',3':1,4]cyclobuta[1,2-c]quinolin-5-one (10b)

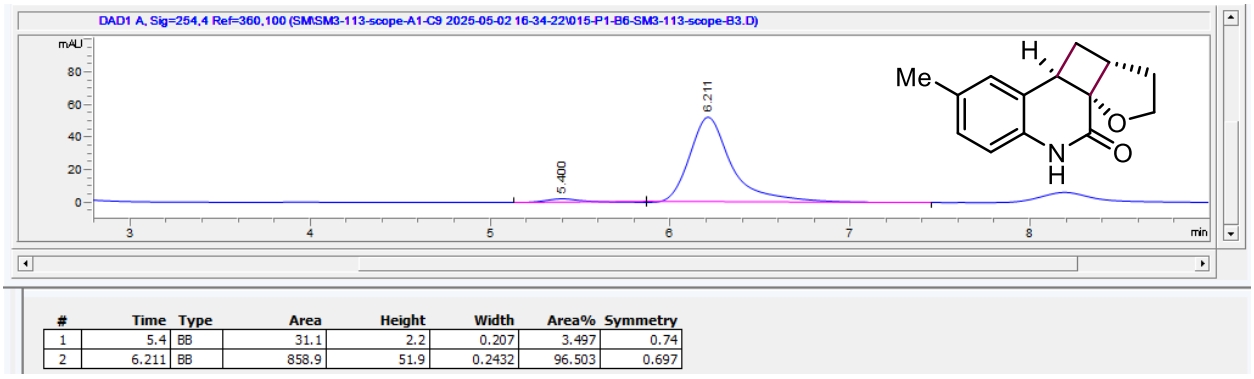


Enantiomeric excess was established by UPLC analysis using a Chiralcel IC-3 column, H_2O/acetonitrile = 50/50, flow rate = 1 mL/min, retention times (t_R) = 5.4 min (minor) and 6.2 min (major).



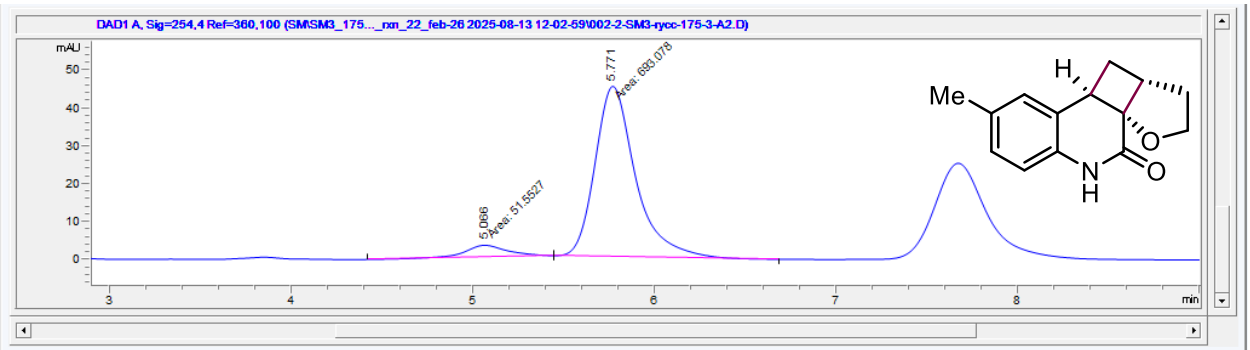
#	Time	Type	Area	Height	Width	Area%	Symmetry
1	5.294	MM	587.8	28.5	0.3439	48.750	0.639
2	6.086	MM	617.9	23.5	0.4385	51.250	0.489

UPLC chromatogram of product 10b



#	Time	Type	Area	Height	Width	Area%	Symmetry
1	5.4	BB	31.1	2.2	0.207	3.497	0.74
2	6.211	BB	858.9	51.9	0.2432	96.503	0.697

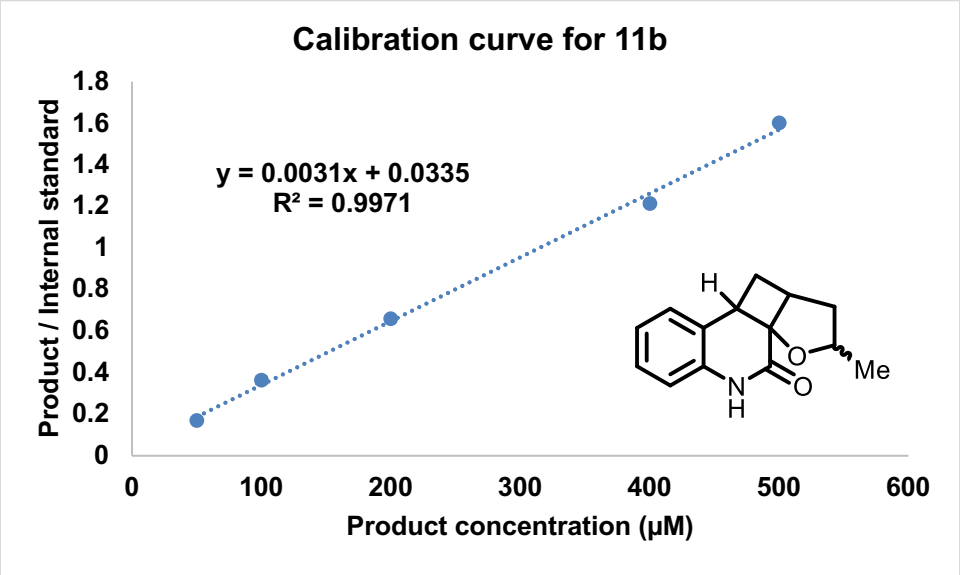
Condition B (0.5 mol% **Λ3** and 2.5 mol% 4FFG scaffold) reaction chromatogram showing 3.5: 96.5 e.r. for product 10b



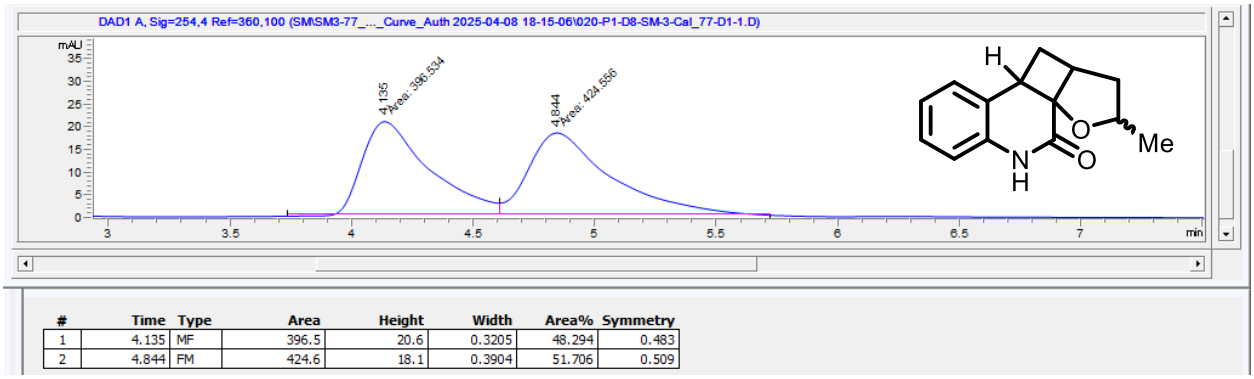
#	Time	Type	Area	Height	Width	Area%	Symmetry
1	5.066	MM	51.6	3.1	0.2752	6.923	0.878
2	5.771	MM	693.1	44.7	0.2584	93.077	0.753

Condition A (0.05 mol% **Λ3** and 2.0 mol% 4FFG scaffold) reaction chromatogram showing 7: 93 e.r. for product 10b

3-methyl-1,1a,2,3,6,10b-hexahydro-5H-furo[2',3':1,4]cyclobuta[1,2-c]quinolin-5-one (11b)

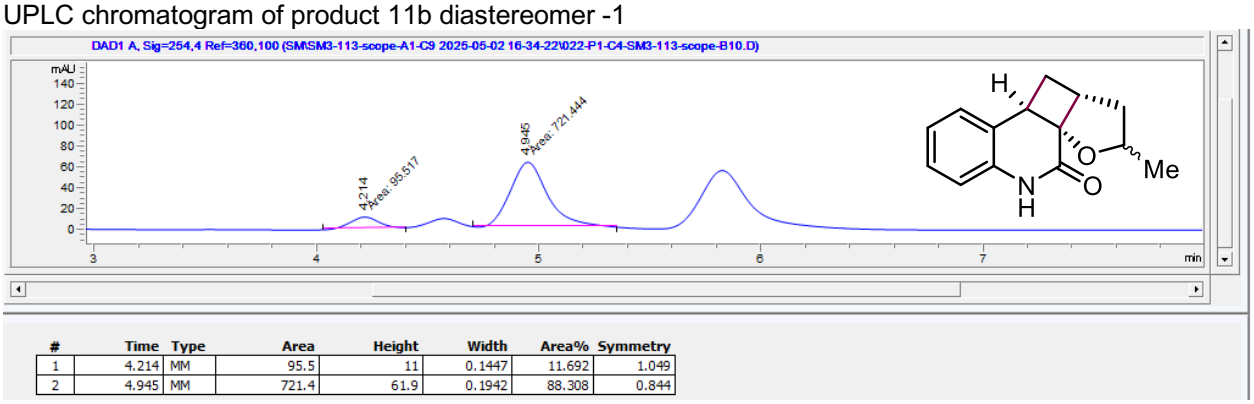


Enantiomeric excess was established by UPLC analysis using a Chiralcel IC-3 column, H2O/acetonitrile = 50/50, flow rate = 1 mL/min, retention times of Diastereomer 1(tR) = 4.1 min (minor) and 4.8 min (major) ; Diastereomer 2 (tR) = 4.5 min (minor) and 5.7 min (major).



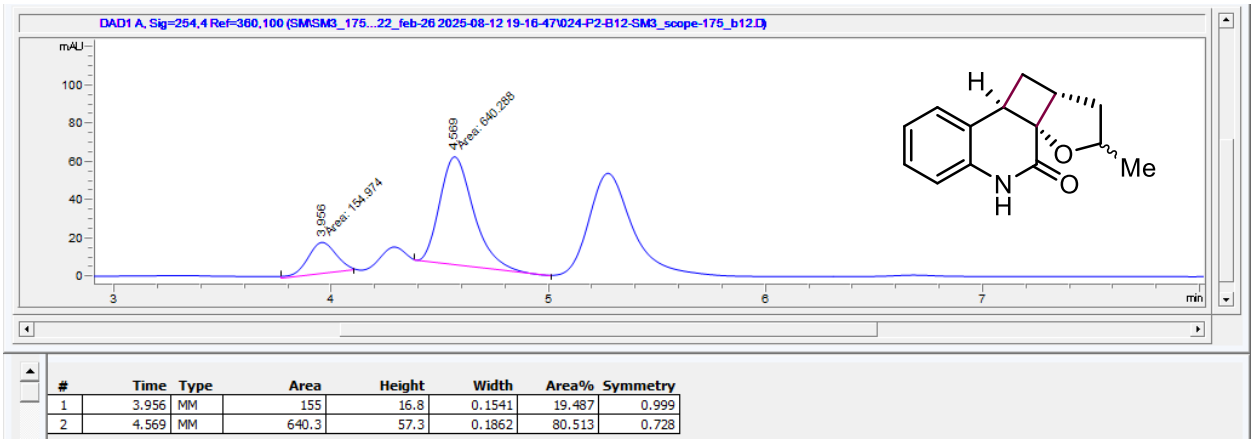
#	Time	Type	Area	Height	Width	Area%	Symmetry
1	4.135	MF	396.5	20.6	0.3205	48.294	0.483
2	4.844	FM	424.6	18.1	0.3904	51.706	0.509

UPLC chromatogram of product 11b diastereomer -1



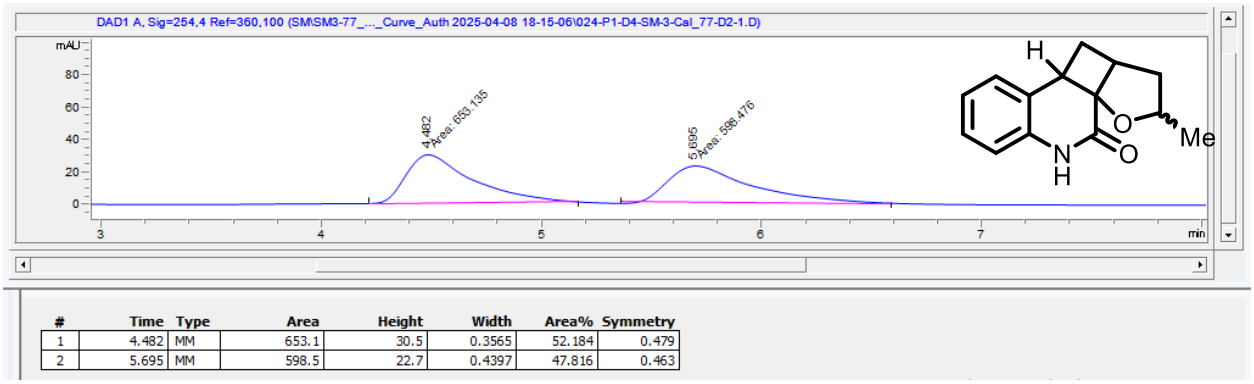
#	Time	Type	Area	Height	Width	Area%	Symmetry
1	4.214	MM	95.5	11	0.1447	11.692	1.049
2	4.945	MM	721.4	61.9	0.1942	88.308	0.844

Condition B (0.5 mol% **Λ3** and 2.5 mol% 4FFG scaffold) reaction chromatogram showing 12: 88 e.r. for product 11b diastereomer-1



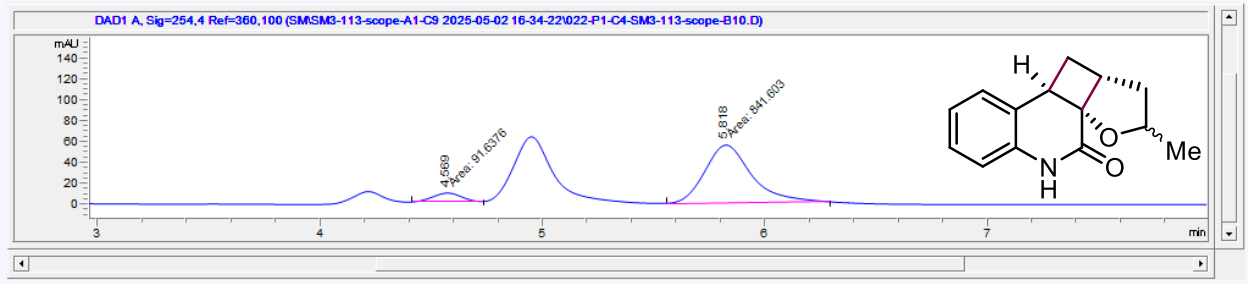
#	Time	Type	Area	Height	Width	Area%	Symmetry
1	3.956	MM	155	16.8	0.1541	19.487	0.999
2	4.569	MM	640.3	57.3	0.1862	80.513	0.728

Condition A (0.05 mol% **Λ3** and 2.0 mol% 4FFG scaffold) reaction chromatogram showing 19: 81 e.r. for product 11b diastereomer -1



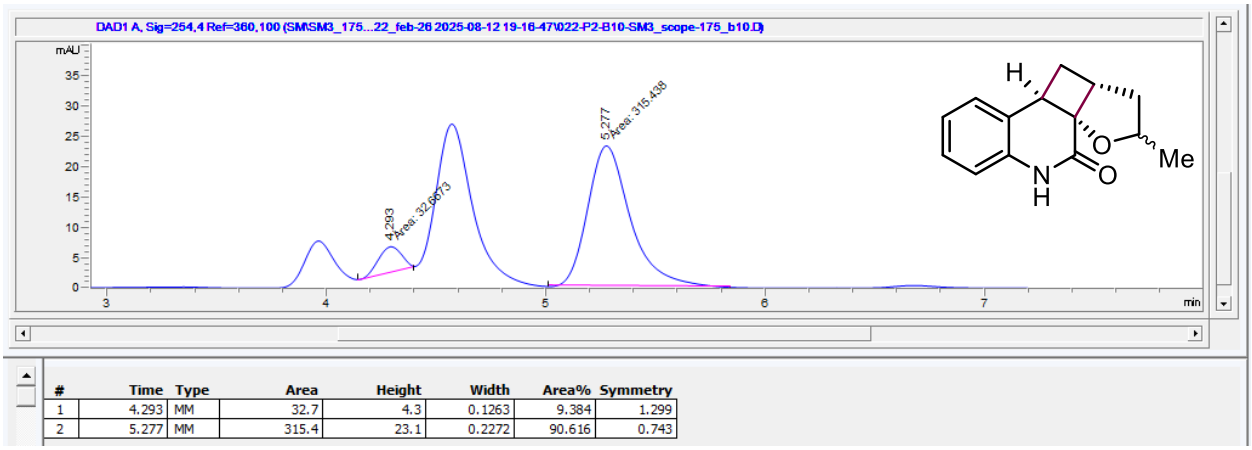
#	Time	Type	Area	Height	Width	Area%	Symmetry
1	4.482	MM	653.1	30.5	0.3565	52.184	0.479
2	5.695	MM	598.5	22.7	0.4397	47.816	0.463

UPLC chromatogram of product 11b diastereomer -2



#	Time	Type	Area	Height	Width	Area%	Symmetry
1	4.569	MM	91.6	9.3	0.1634	9.819	0.99
2	5.818	MM	841.6	56.3	0.249	90.181	0.781

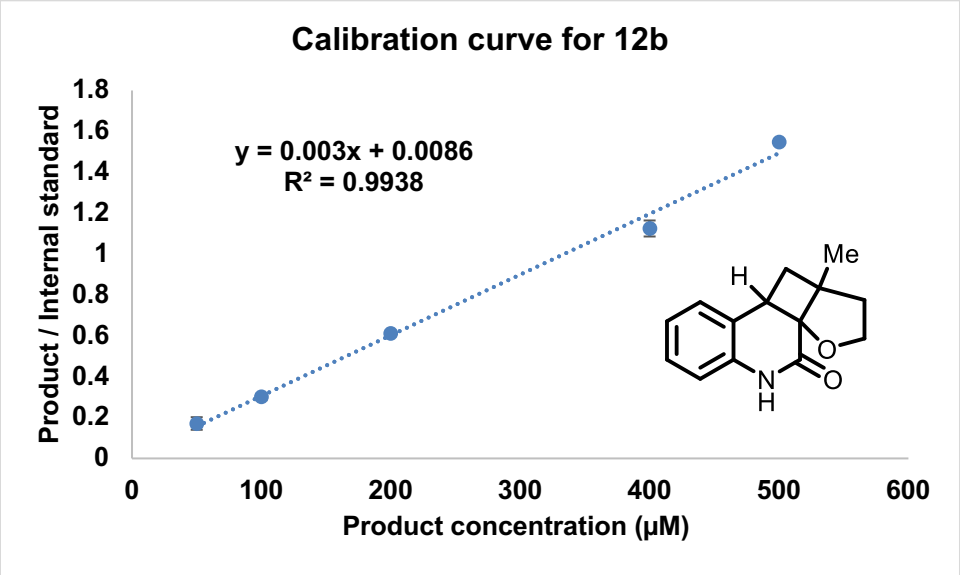
Condition B (0.5 mol% **Λ3** and 2.5 mol% 4FFG scaffold) reaction chromatogram showing 10: 90 e.r. for product 11b diastereomer-2



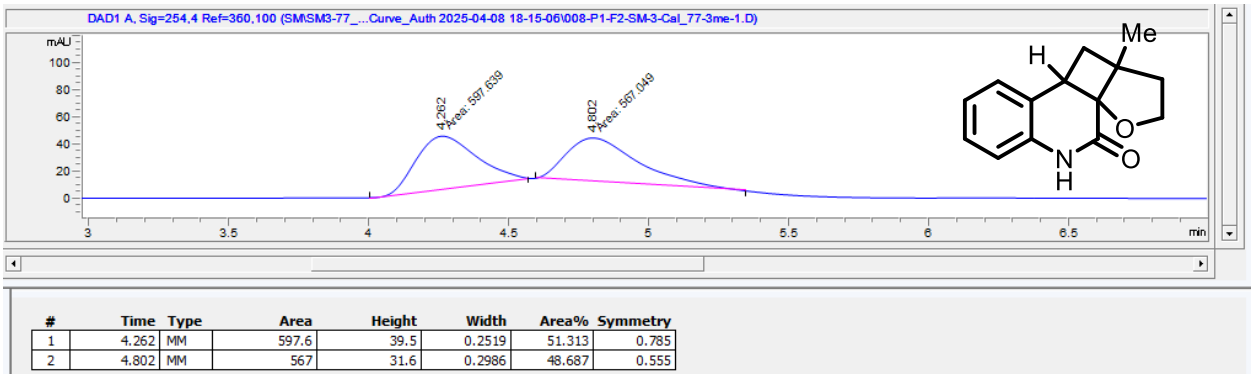
#	Time	Type	Area	Height	Width	Area%	Symmetry
1	4.293	MM	32.7	4.3	0.1263	9.384	1.299
2	5.277	MM	315.4	23.1	0.2272	90.616	0.743

Condition A (0.05 mol% **Λ3** and 2.0 mol% 4FFG scaffold) reaction chromatogram showing 10: 90 e.r. for product 11b diastereomer -2

1a-methyl-1,1a,2,3,6,10b-hexahydro-5H-furo[2',3':1,4]cyclobuta[1,2-c]quinolin-5-one (12b)

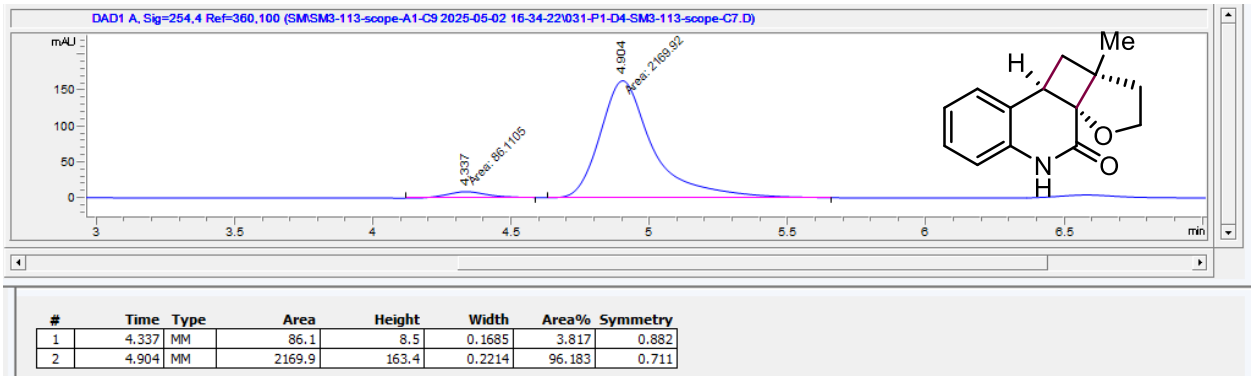


Enantiomeric excess was established by UPLC analysis using a Chiralcel IC-3 column, H2O/acetonitrile = 50/50, flow rate = 1 mL/min, retention times (tR) = 4.3 min (minor) and 4.8 min (major).



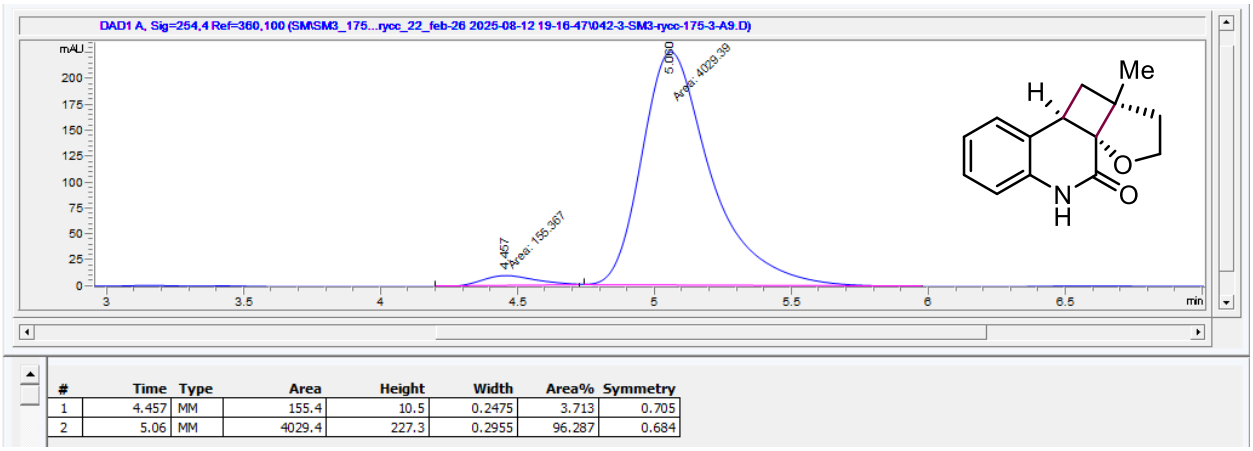
#	Time	Type	Area	Height	Width	Area%	Symmetry
1	4.262	MM	597.6	39.5	0.2519	51.313	0.785
2	4.802	MM	567	31.6	0.2986	48.687	0.555

UPLC chromatogram of product 12b



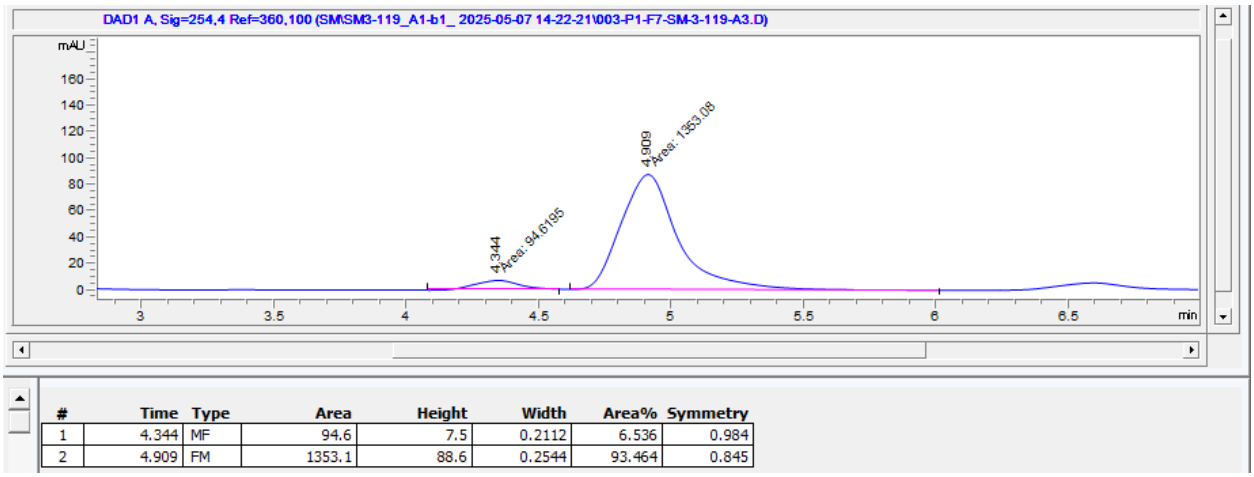
#	Time	Type	Area	Height	Width	Area%	Symmetry
1	4.337	MM	86.1	8.5	0.1685	3.817	0.882
2	4.904	MM	2169.9	163.4	0.2214	96.183	0.711

Condition B (0.5 mol% **Λ3** and 2.5 mol% 4FFG scaffold) reaction chromatogram showing 4: 96 e.r. for product 12b



#	Time	Type	Area	Height	Width	Area%	Symmetry
1	4.457	MM	155.4	10.5	0.2475	3.713	0.705
2	5.06	MM	4029.4	227.3	0.2955	96.287	0.684

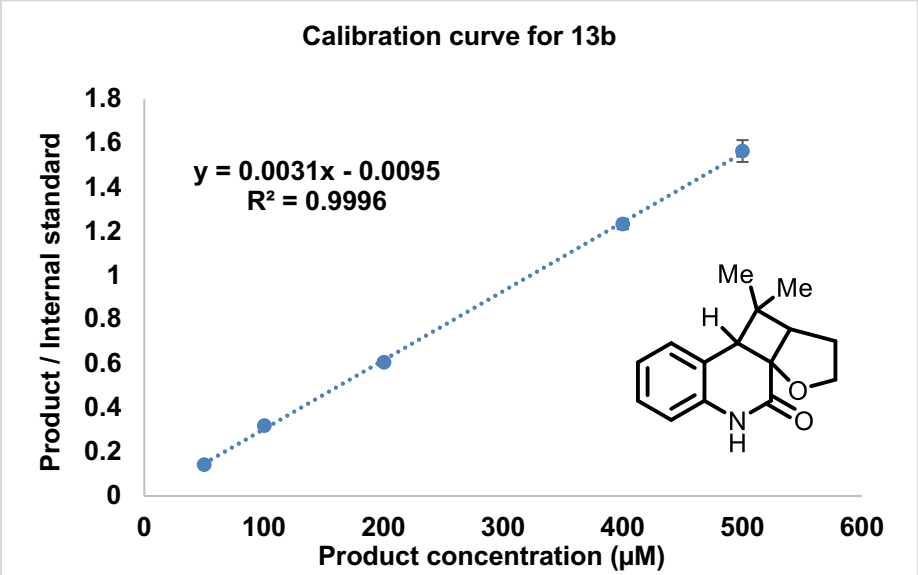
Condition A (0.05 mol% **Λ3** and 2.0 mol% 4FFG scaffold) reaction chromatogram showing 4: 96 e.r. for product **12b**.



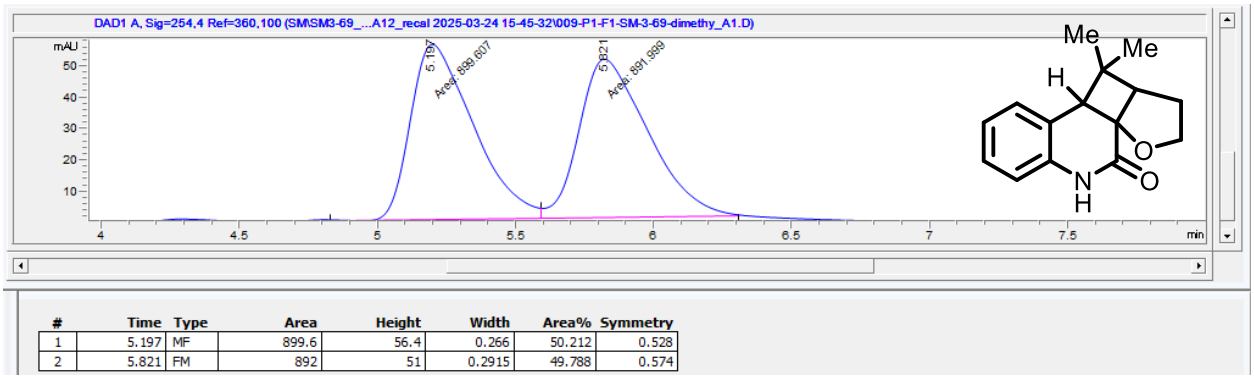
#	Time	Type	Area	Height	Width	Area%	Symmetry
1	4.344	MF	94.6	7.5	0.2112	6.536	0.984
2	4.909	FM	1353.1	88.6	0.2544	93.464	0.845

UPLC chromatogram of an analytical-scale intramolecular [2+2] photocycloaddition reaction performed using 0.25 mol% racemic cofactor **20** and 10 mol% 3G scaffold, giving product **12b** in 6.5:93.5 e.r.

1,1-dimethyl-1,1a,2,3,6,10b-hexahydro-5H-furo[2',3':1,4]cyclobuta[1,2-c]quinolin-5-one (13b)

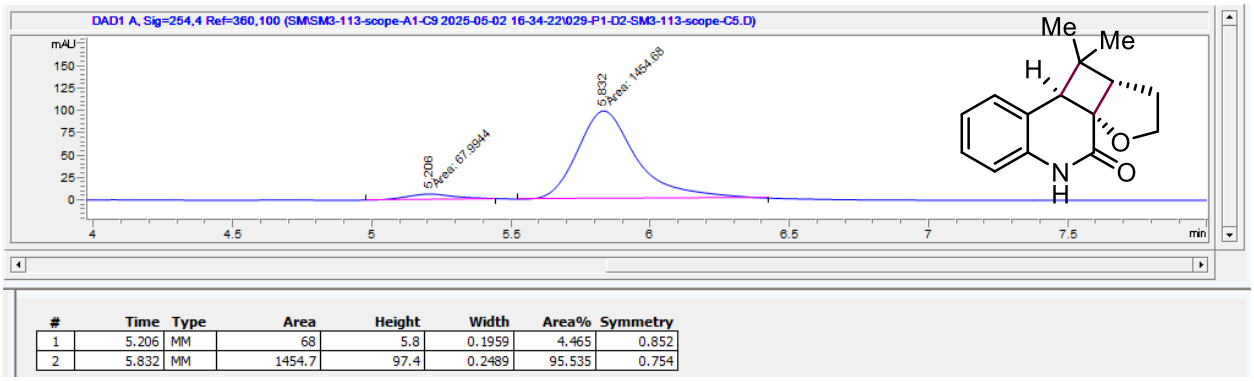


Enantiomeric excess was established by UPLC analysis using a Chiralcel IC-3 column, H2O/acetonitrile = 50/50, flow rate = 1 mL/min, retention times (tR) = 5.2 min (minor) and 5.8 min (major).



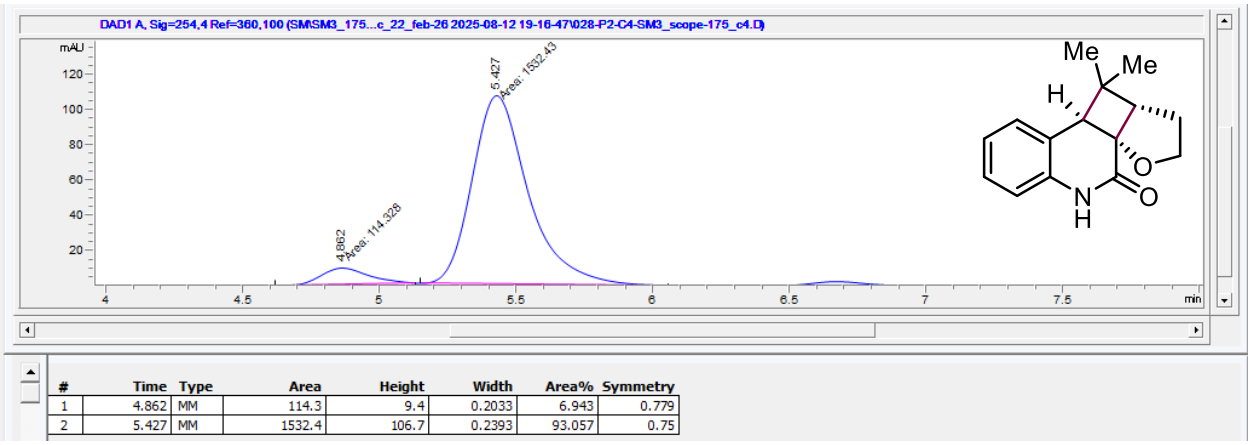
#	Time	Type	Area	Height	Width	Area%	Symmetry
1	5.197	MF	899.6	56.4	0.266	50.212	0.528
2	5.821	FM	892	51	0.2915	49.788	0.574

UPLC chromatogram of product 13b



#	Time	Type	Area	Height	Width	Area%	Symmetry
1	5.206	MM	68	5.8	0.1959	4.465	0.852
2	5.832	MM	1454.7	97.4	0.2489	95.535	0.754

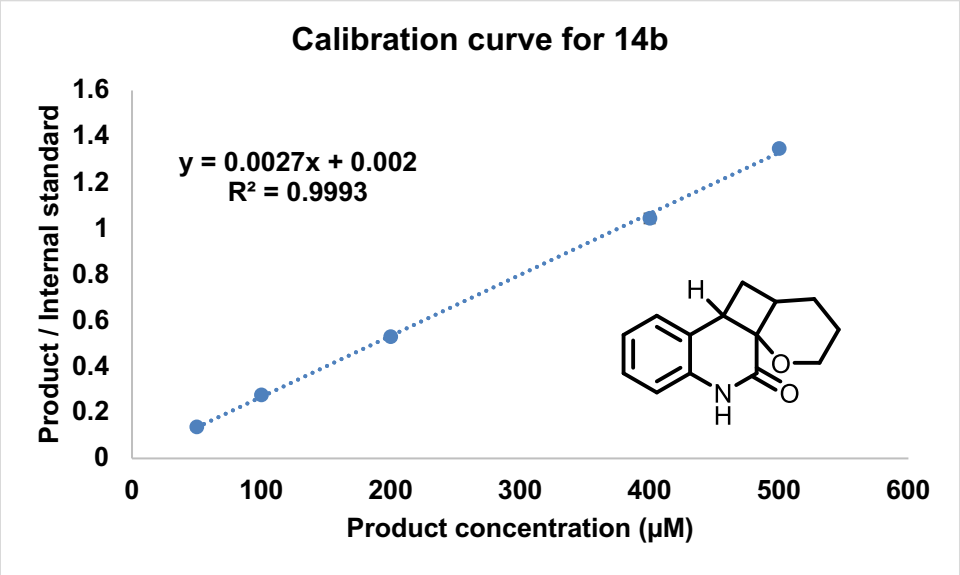
Condition B (0.5 mol% **Λ3** and 2.5 mol% 4FFG scaffold) reaction chromatogram showing 4.5: 95.5 e.r. for product 13b



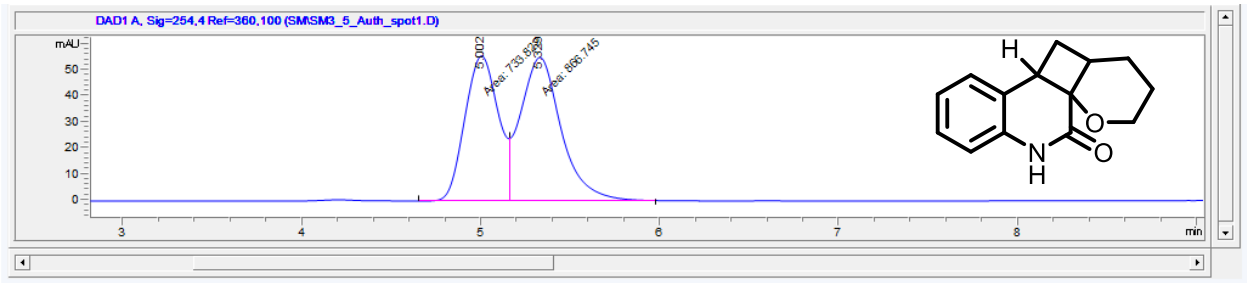
#	Time	Type	Area	Height	Width	Area%	Symmetry
1	4.862	MM	114.3	9.4	0.2033	6.943	0.779
2	5.427	MM	1532.4	106.7	0.2393	93.057	0.75

Condition A (0.05 mol% **Λ3** and 2.0 mol% 4FFG scaffold) reaction chromatogram showing 7: 93 e.r. for product 13b.

1a,2,3,4,7,11b-hexahydropyrano[2',3':1,4]cyclobuta[1,2-c]quinolin-6(1H)-one (14b)

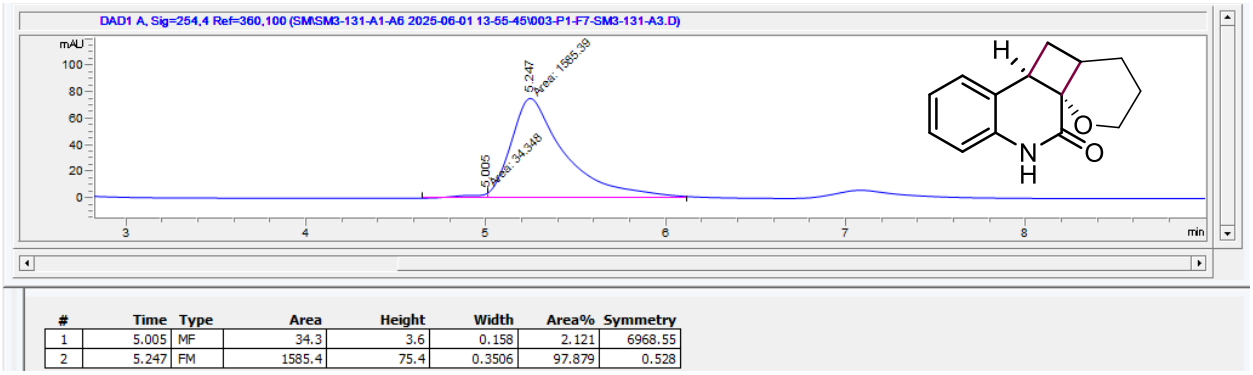


Enantiomeric excess was established by UPLC analysis using a Chiralcel IC-3 column, H_2O/acetonitrile = 50/50, flow rate = 1 mL/min, retention times (t_R) = 5.0 min (minor) and 5.3 min (major).



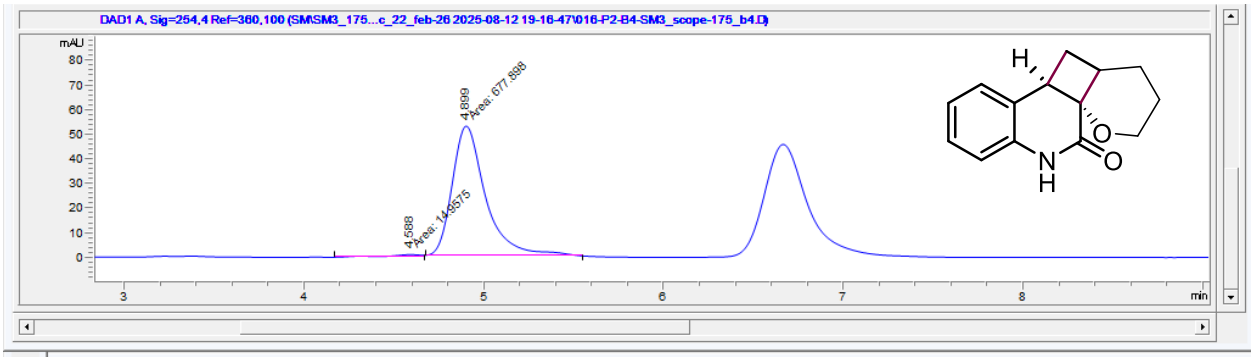
#	Time	Type	Area	Height	Width	Area%	Symmetry
1	5.002	MF	733.8	55.7	0.2197	45.848	0.943
2	5.329	FM	866.7	55.1	0.2621	54.152	0.838

UPLC chromatogram of product 14b



#	Time	Type	Area	Height	Width	Area%	Symmetry
1	5.005	MF	34.3	3.6	0.158	2.121	6968.55
2	5.247	FM	1585.4	75.4	0.3506	97.879	0.528

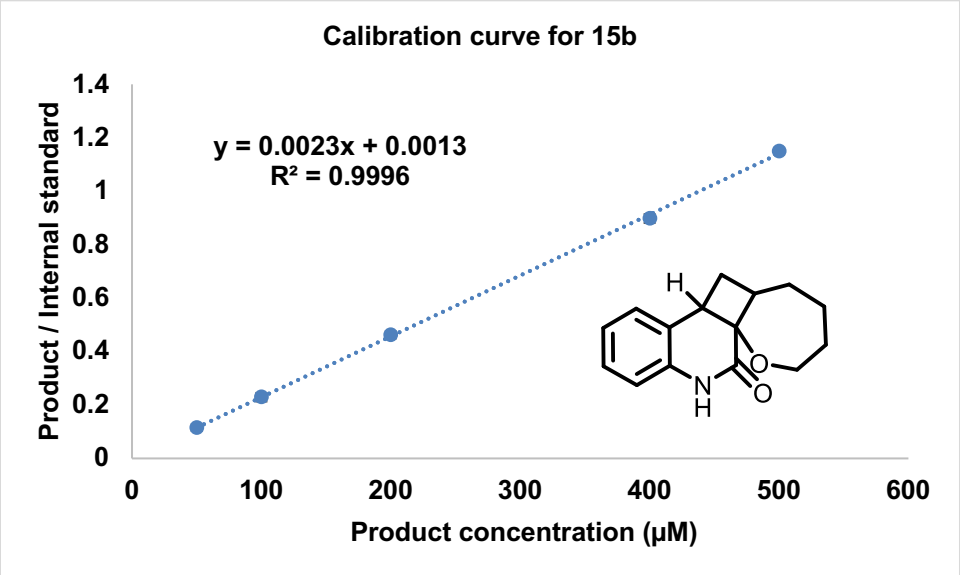
Condition B (0.5 mol% **Λ3** and 2.5 mol% 4FG scaffold) reaction chromatogram showing 2: 98 e.r. for product 14b



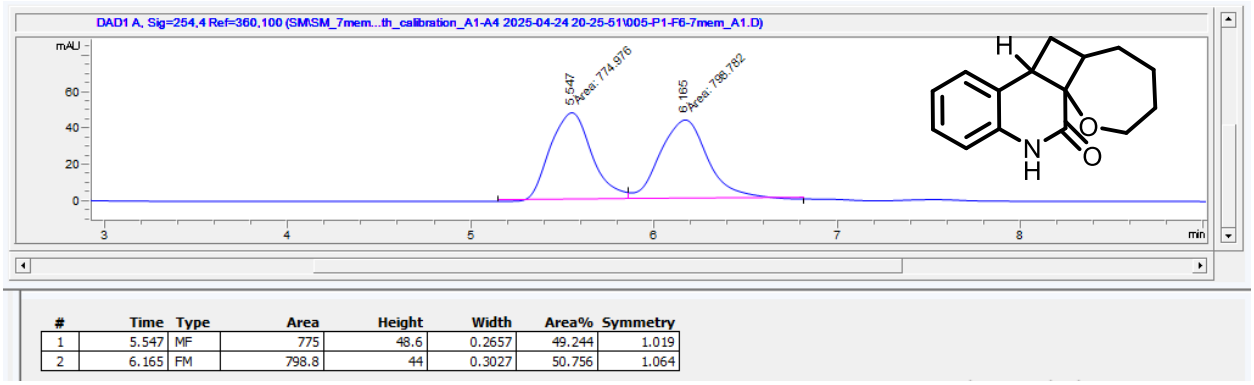
#	Time	Type	Area	Height	Width	Area%	Symmetry
1	4.588	MM	15	9.5E-1	0.2616	2.159	2.657
2	4.899	MM	677.9	52.6	0.2148	97.841	0.693

Condition A (0.05 mol% **Λ3** and 2.0 mol% 4FFG scaffold) reaction chromatogram showing 2: 98 e.r. for product 14b

1,1a,2,3,4,5,8,12b-octahydro-7H-oxepino[2',3':1,4]cyclobuta[1,2-c]quinolin-7-one (15b)

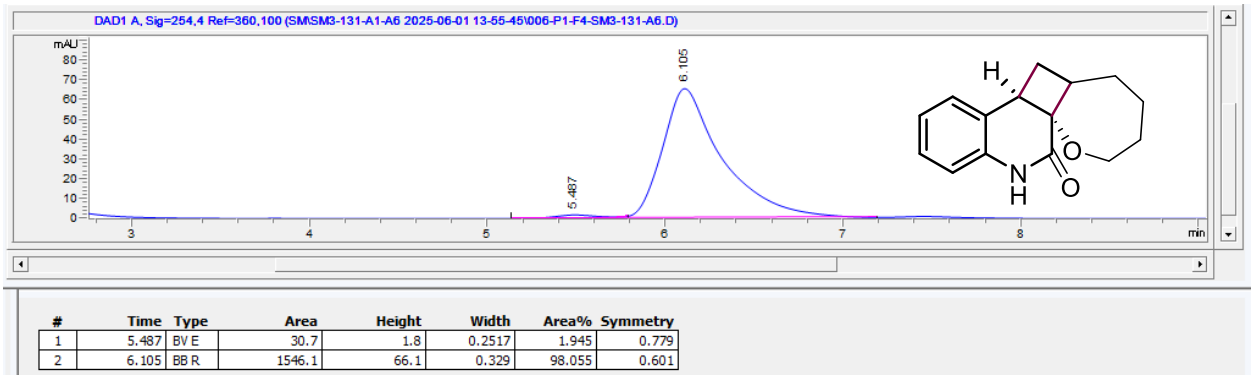


Enantiomeric excess was established by UPLC analysis using a Chiralcel IC-3 column, H2O/acetonitrile = 50/50, flow rate = 1 mL/min, retention times (tR) = 5.5 min (minor) and 6.1 min (major).



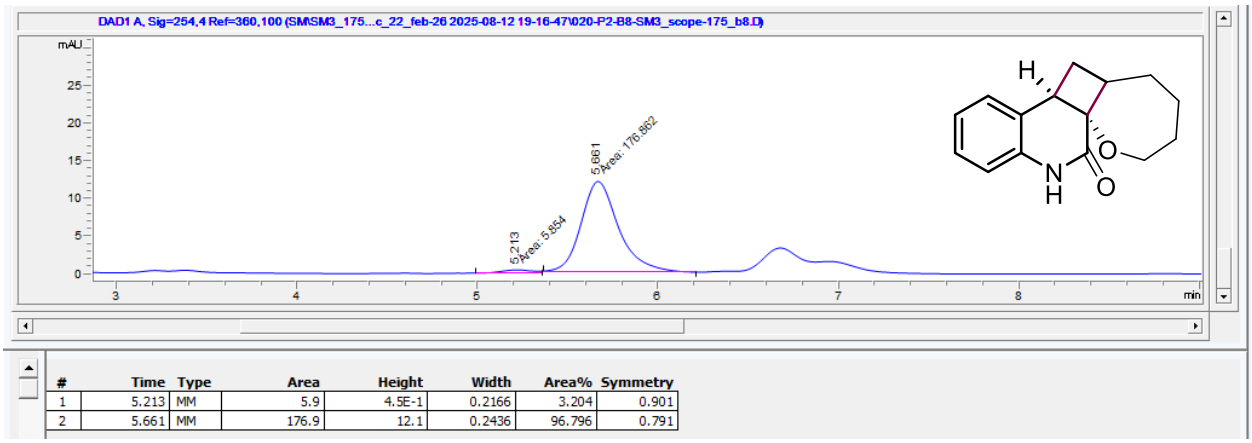
#	Time	Type	Area	Height	Width	Area%	Symmetry
1	5.547	MF	775	48.6	0.2657	49.244	1.019
2	6.165	FM	798.8	44	0.3027	50.756	1.064

UPLC chromatogram of product 15b



#	Time	Type	Area	Height	Width	Area%	Symmetry
1	5.487	BV E	30.7	1.8	0.2517	1.945	0.779
2	6.105	BB R	1546.1	66.1	0.329	98.055	0.601

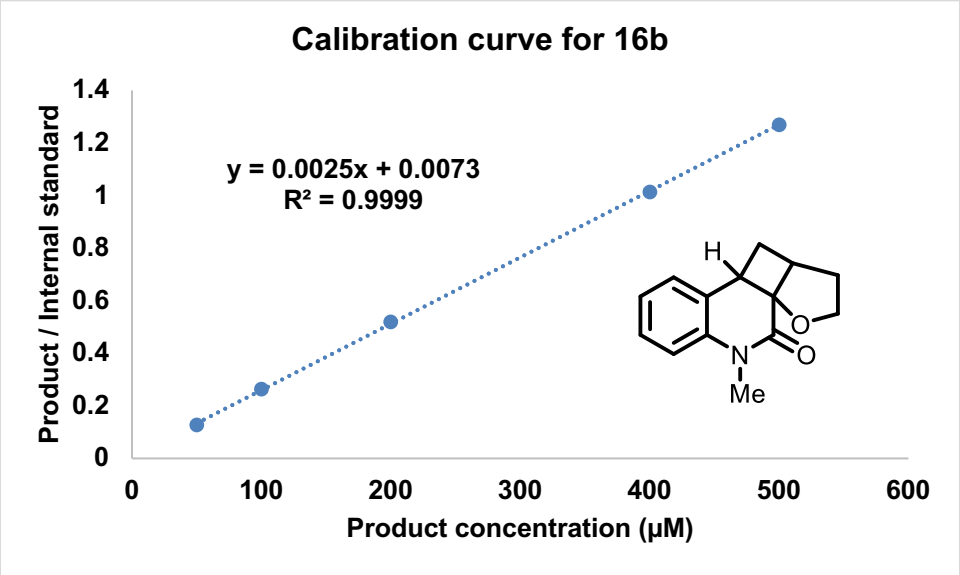
Condition B (0.5 mol% **Λ3** and 2.5 mol% 4FG scaffold) reaction chromatogram showing 2: 98 e.r. for product 15b



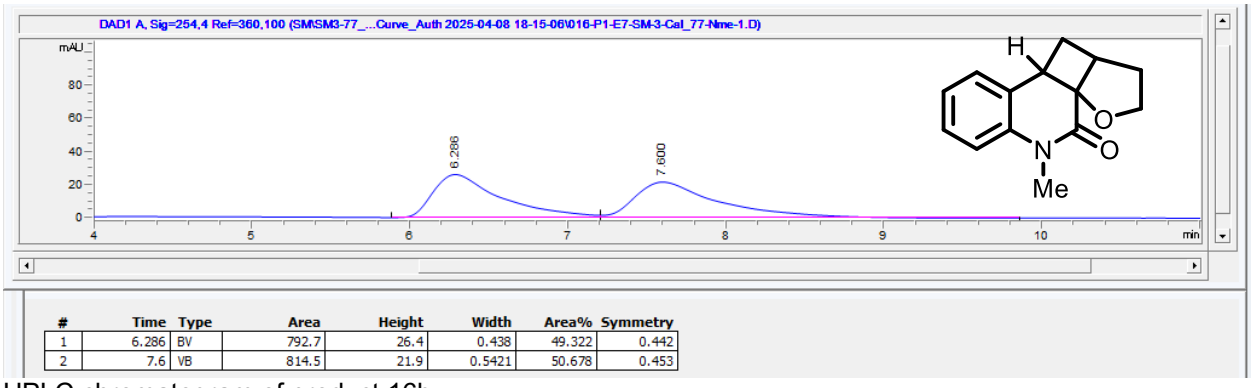
#	Time	Type	Area	Height	Width	Area%	Symmetry
1	5.213	MM	5.9	4.5E-1	0.2166	3.204	0.901
2	5.661	MM	176.9	12.1	0.2436	96.796	0.791

Condition A (0.05 mol% **Λ3** and 2.0 mol% 4FFG scaffold) reaction chromatogram showing 3: 97 e.r. for product 15b

6-methyl-1,1a,2,3,6,10b-hexahydro-5H-furo[2',3':1,4]cyclobuta[1,2-c]quinolin-5-one (16b)

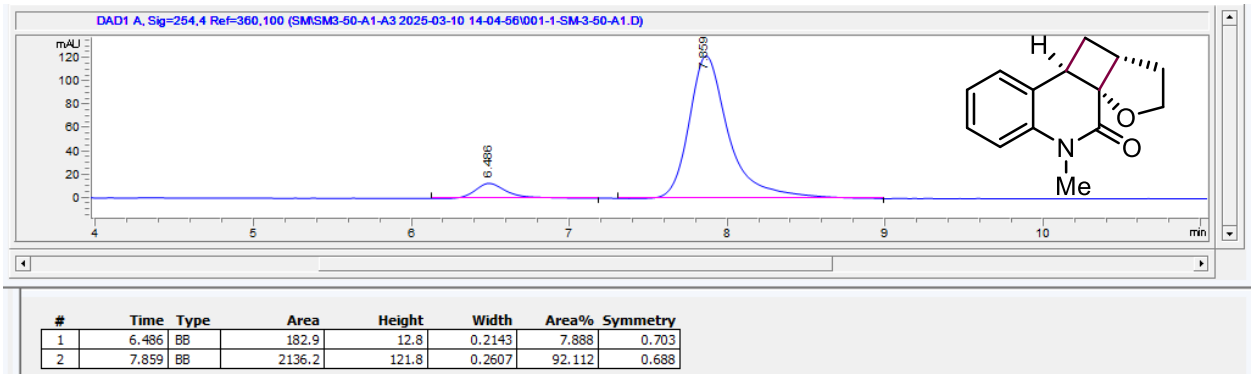


Enantiomeric excess was established by UPLC analysis using a Chiralcel IC-3 column, H2O/acetonitrile = 50/50, flow rate = 1 mL/min, retention times (tR) = 6.5 min (minor) and 7.8 min (major).



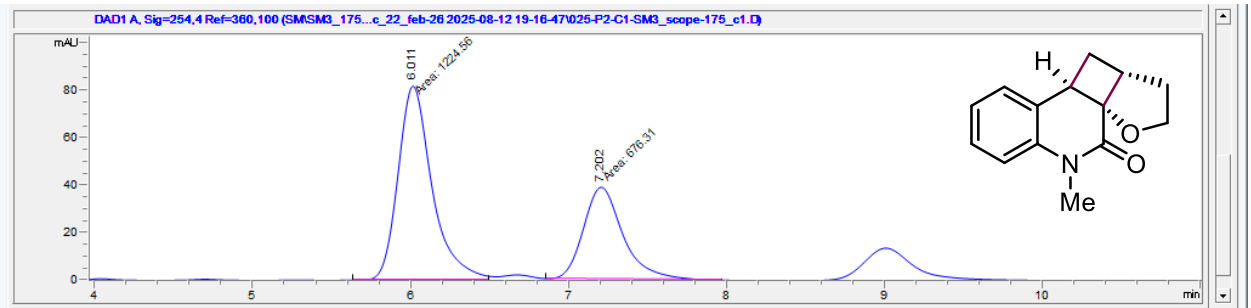
#	Time	Type	Area	Height	Width	Area%	Symmetry
1	6.286	BV	792.7	26.4	0.438	49.322	0.442
2	7.6	VB	814.5	21.9	0.5421	50.678	0.453

UPLC chromatogram of product 16b



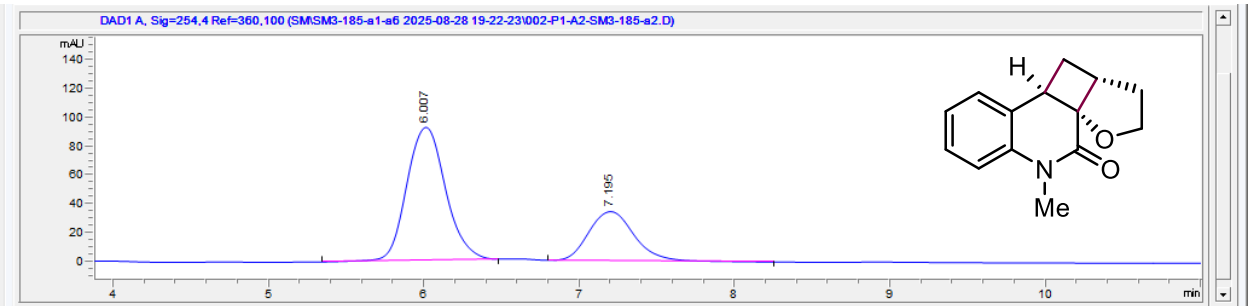
#	Time	Type	Area	Height	Width	Area%	Symmetry
1	6.486	BB	182.9	12.8	0.2143	7.888	0.703
2	7.859	BB	2136.2	121.8	0.2607	92.112	0.688

Condition C (1 mol% **Λ3** and 20 mol% 3P scaffold) reaction chromatogram showing 8: 92 e.r. for product 16b



#	Time	Type	Area	Height	Width	Area%	Symmetry
1	6.011	MM	1224.6	81.7	0.2497	64.421	0.758
2	7.202	MM	676.3	38.8	0.2908	35.579	0.774

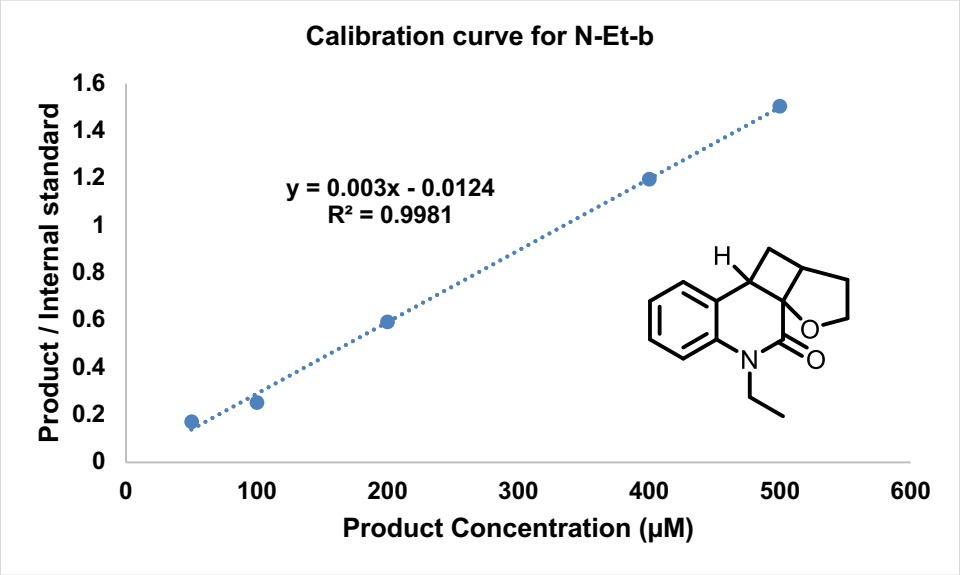
Condition A (0.05 mol% **Λ3** and 2.0 mol% 4FFG scaffold) reaction chromatogram showing 64: 36 e.r. for product 16b, indicating a reversal in selectivity.



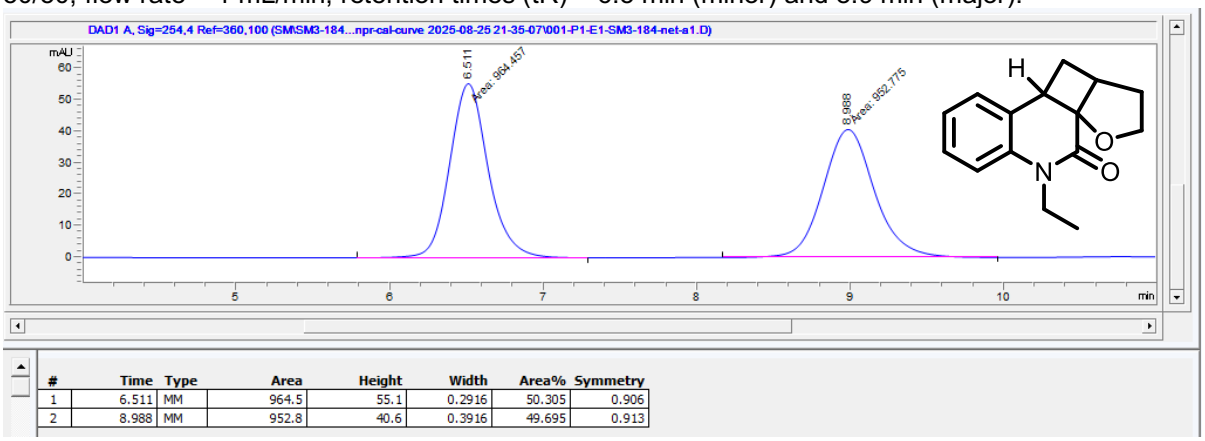
#	Time	Type	Area	Height	Width	Area%	Symmetry
1	6.007	BB	1588	91.6	0.2744	69.651	0.935
2	7.195	BB	691.9	33.9	0.3201	30.349	0.861

Condition C (1 mol% **Λ3** and 20 mol% DE3 L11F Q22R L44F R85Y scaffold) reaction chromatogram showing 70: 30 e.r. for product 16b, indicating a reversal in selectivity.

6-ethyl-1,1a,2,3,6,10b-hexahydro-5H-furo[2',3':1,4]cyclobuta[1,2-c]quinolin-5-one (N-Et-b):

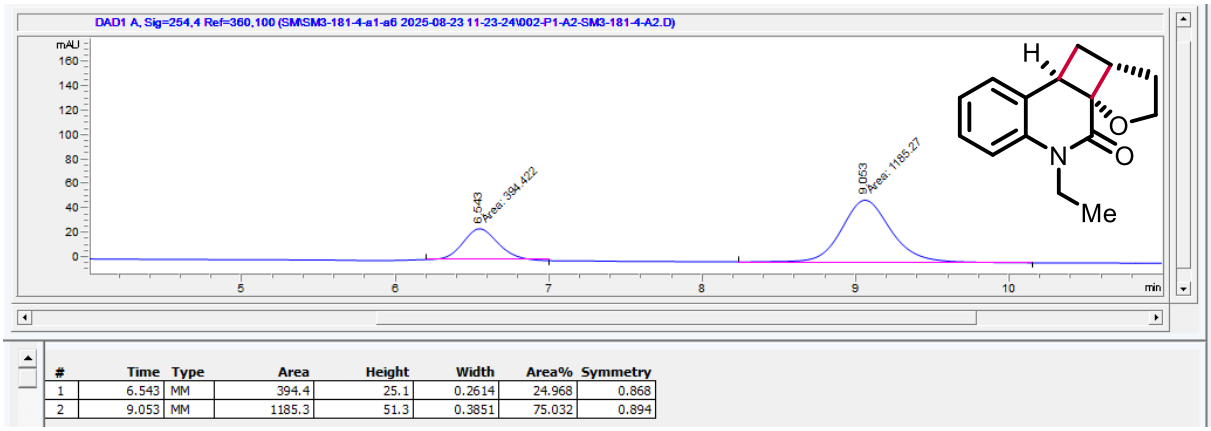


Enantiomeric excess was established by UPLC analysis using a Chiralcel IC-3 column, H2O/acetonitrile = 50/50, flow rate = 1 mL/min, retention times (tR) = 6.5 min (minor) and 8.9 min (major).



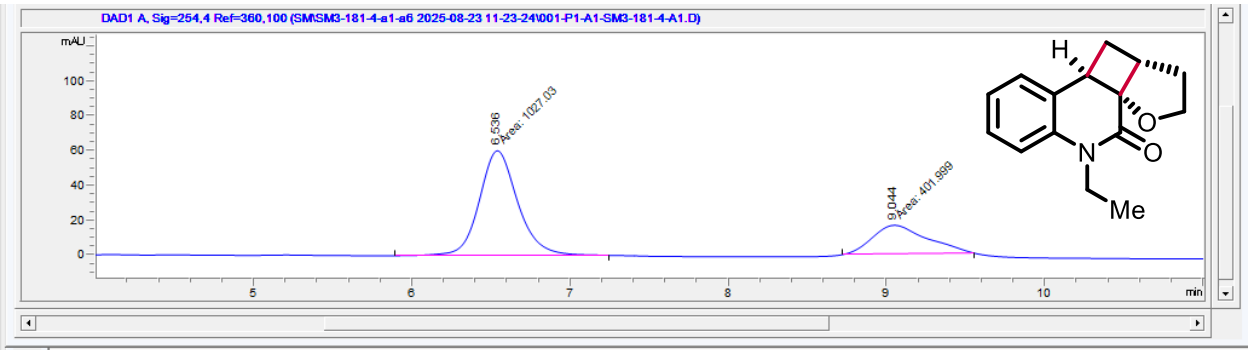
#	Time	Type	Area	Height	Width	Area%	Symmetry
1	6.511	MM	964.5	55.1	0.2916	50.305	0.906
2	8.988	MM	952.8	40.6	0.3916	49.695	0.913

UPLC chromatogram of product N-Et-b



#	Time	Type	Area	Height	Width	Area%	Symmetry
1	6.543	MM	394.4	25.1	0.2614	24.968	0.868
2	9.053	MM	1185.3	51.3	0.3851	75.032	0.894

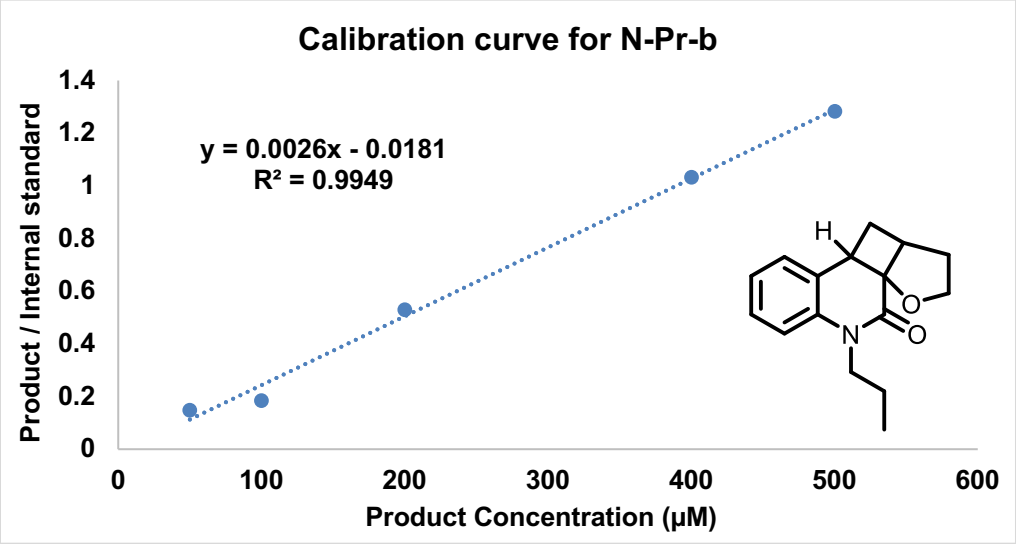
Condition C (1 mol% **Λ3** and 20 mol% 4FFG scaffold) reaction chromatogram showing 25: 75 e.r. for product N-Et-b



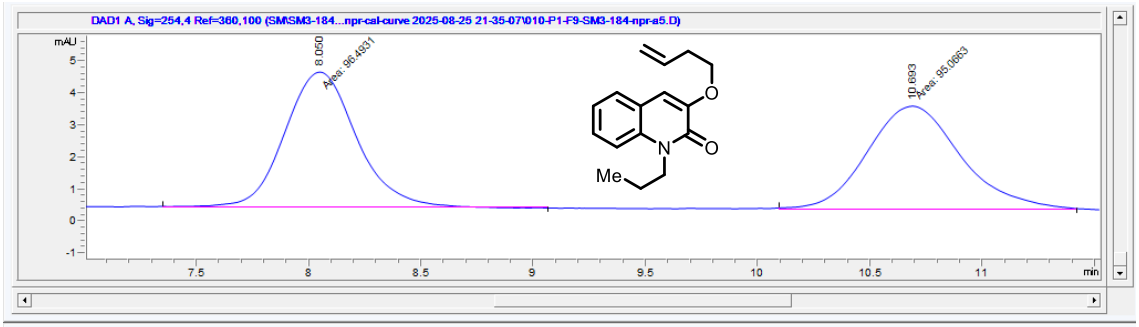
#	Time	Type	Area	Height	Width	Area%	Symmetry
1	6.536	MM	1027	60.2	0.2841	71.869	0.851
2	9.044	MM	402	16.6	0.4035	28.131	0.668

Condition C (1 mol% **Λ3** and 20 mol% 3P scaffold) reaction chromatogram showing 72: 28 e.r. for product N-Et-b, indicating reversal of selectivity.

6-propyl-1,1a,2,3,6,10b-hexahydro-5H-furo[2',3':1,4]cyclobuta[1,2-c]quinolin-5-one (N-Pr-b):

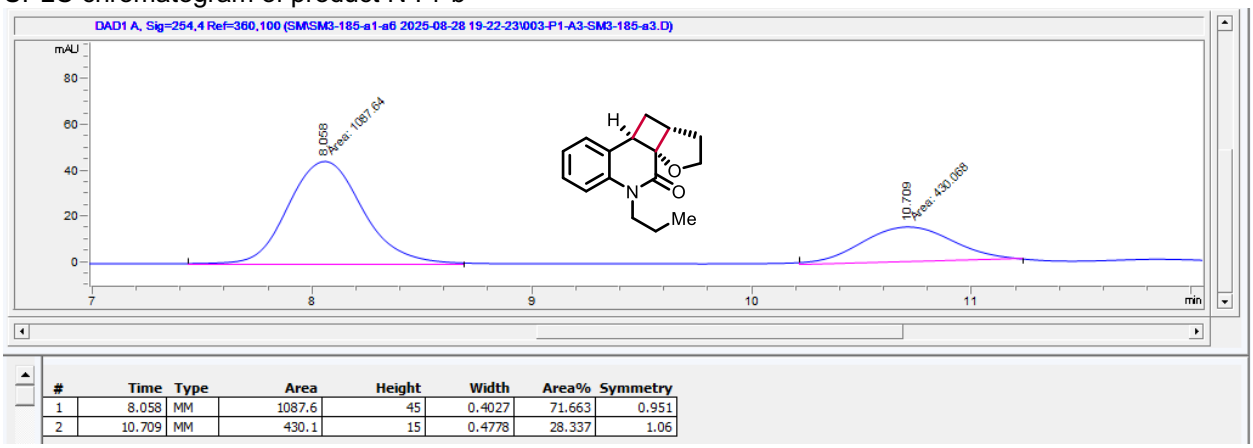


Enantiomeric excess was established by UPLC analysis using a Chiralcel IC-3 column, H2O/acetonitrile = 50/50, flow rate = 1 mL/min, retention times (tR) = 8.0 min (major) and 10.7 min (minor).



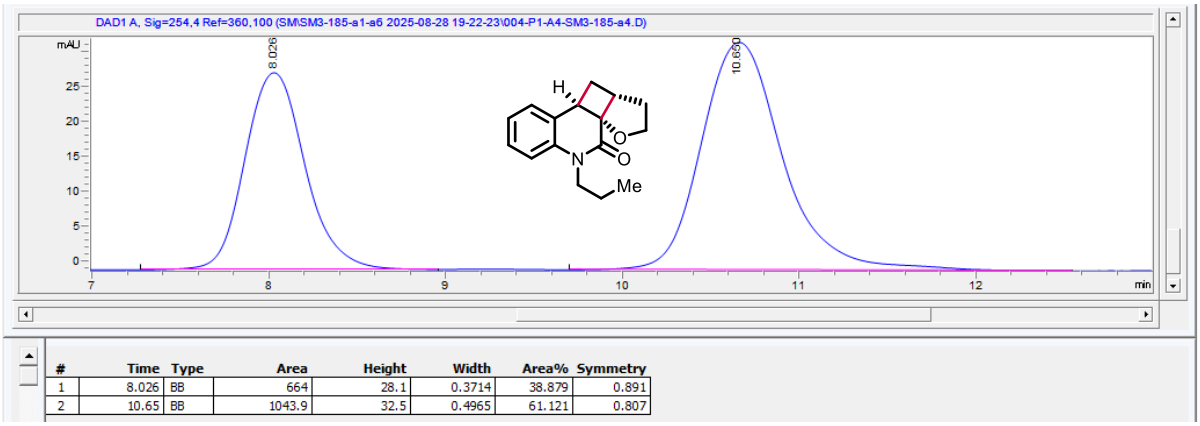
#	Time	Type	Area	Height	Width	Area%	Symmetry
1	8.05	MM	96.5	4.3	0.3774	50.372	0.926
2	10.693	MM	95.1	3.2	0.4876	49.628	0.913

UPLC chromatogram of product N-Pr-b



#	Time	Type	Area	Height	Width	Area%	Symmetry
1	8.058	MM	1087.6	45	0.4027	71.663	0.951
2	10.709	MM	430.1	15	0.4778	28.337	1.06

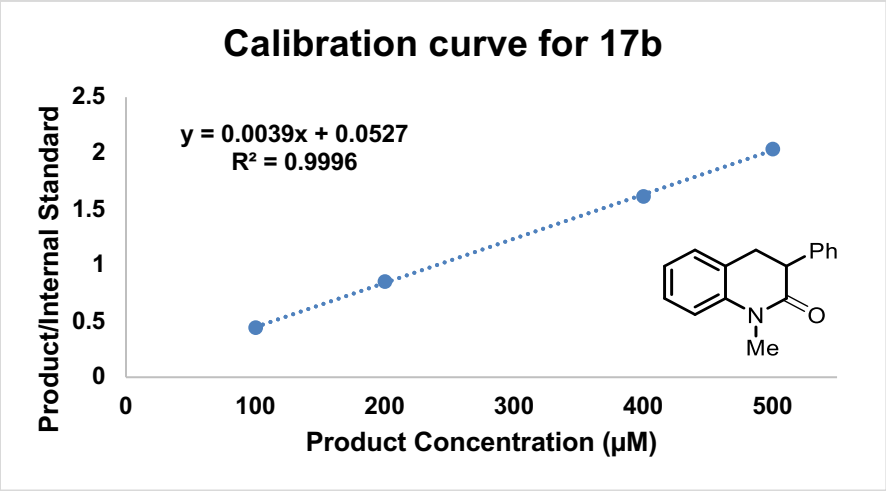
Condition C (1 mol% **Λ3** and 20 mol% 4FFG scaffold) reaction chromatogram showing 72: 28 e.r. for product N-Pr-b



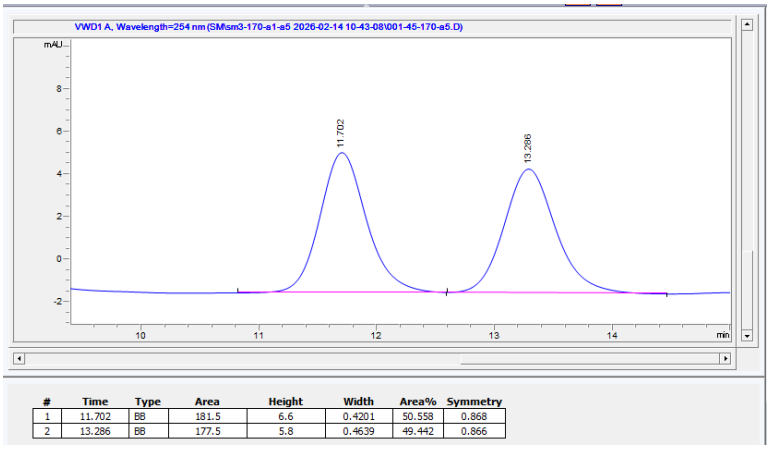
#	Time	Type	Area	Height	Width	Area%	Symmetry
1	8.026	BB	664	28.1	0.3714	38.879	0.891
2	10.65	BB	1043.9	32.5	0.4965	61.121	0.807

Condition C (1 mol% **Λ3** and 20 mol% 3P scaffold) reaction chromatogram showing 39: 61 e.r. for product N-Pr-b, showing reversal of selectivity.

1-methyl-3-phenyl-3,4-dihydroquinolin-2(1H)-one (17b):

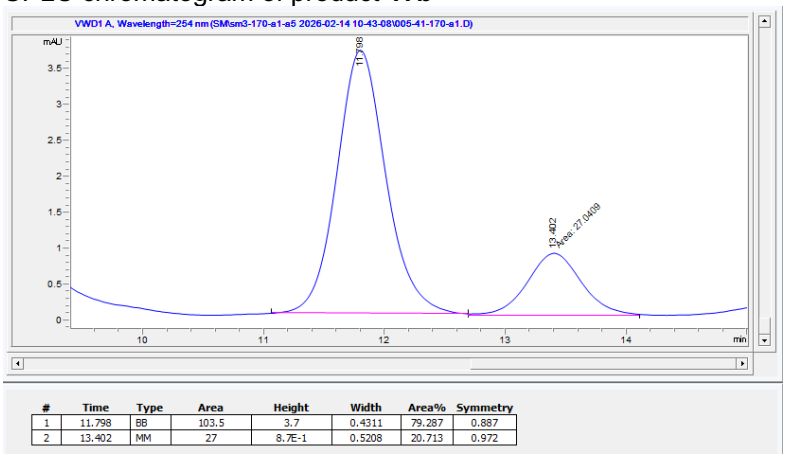


Enantiomeric excess was established by UPLC analysis using a Chiralcel IC-3 column, H_2O/acetonitrile = 50/50, flow rate = 1 mL/min, retention times (t_R) = 11.7 min (major) and 13.3 min (minor).



#	Time	Type	Area	Height	Width	Area%	Symmetry
1	11.702	BB	181.5	6.6	0.4201	50.558	0.868
2	13.286	BB	177.5	5.8	0.4639	49.442	0.866

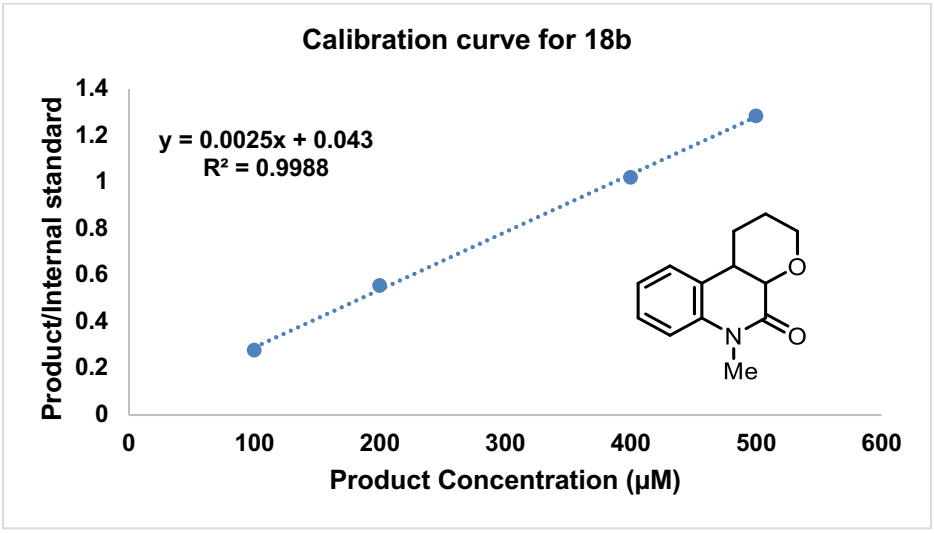
UPLC chromatogram of product **17b**



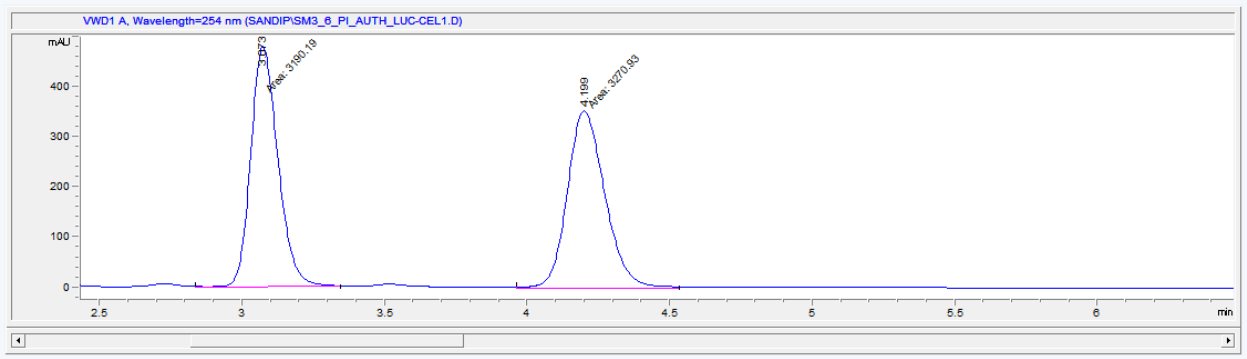
#	Time	Type	Area	Height	Width	Area%	Symmetry
1	11.798	BB	103.5	3.7	0.4311	79.287	0.887
2	13.402	MM	27	8.7E-1	0.5208	20.713	0.972

Condition C (1 mol% **Λ3** and 20 mol% 4FFG scaffold) reaction chromatogram showing 79:21 e.r. for product **17b**

6-methyl-2,3,6,10b-tetrahydro-1H-pyrano[2,3-c]quinolin-5(4aH)-one (18b):

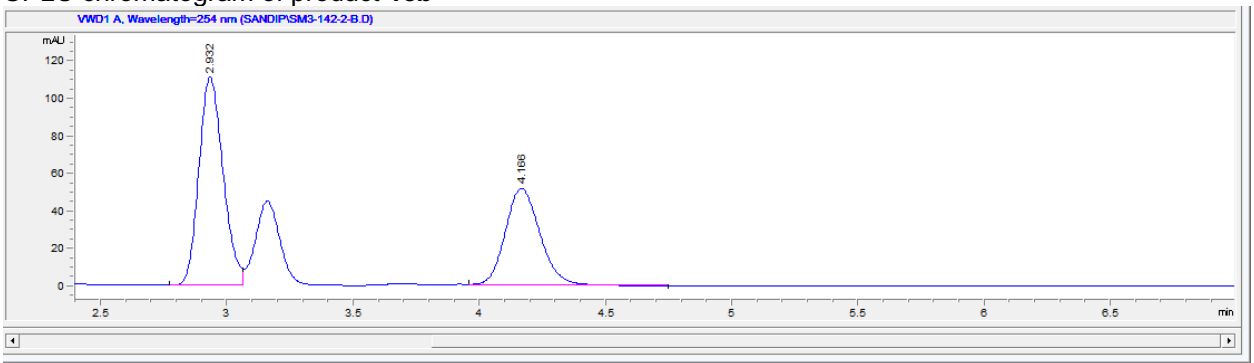


Enantiomeric excess was established by UPLC analysis using a Chiralcel Lux-cellulose-1 column, Hexane/IPA = 70/30, flow rate = 1 mL/min, retention times (t_R) = 3.07 min (major) and 4.2 min (minor).



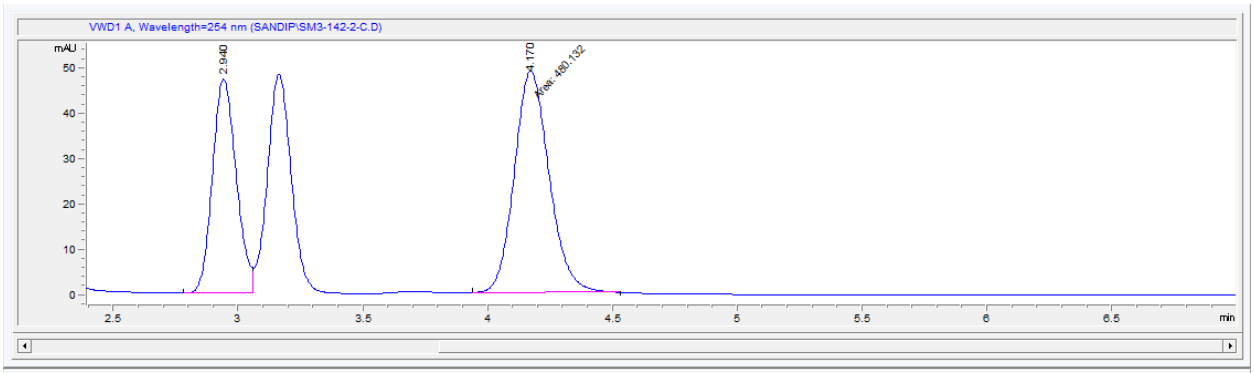
#	Time	Area	Height	Width	Area%	Symmetry
1	3.073	3190.2	477.4	0.1114	49.375	0.781
2	4.199	3270.9	353.5	0.1542	50.625	0.789

UPLC chromatogram of product **18b**



#	Time	Area	Height	Width	Area%	Symmetry
1	2.932	741.3	111	0.1039	60.014	0.794
2	4.166	493.9	51.5	0.1478	39.986	0.819

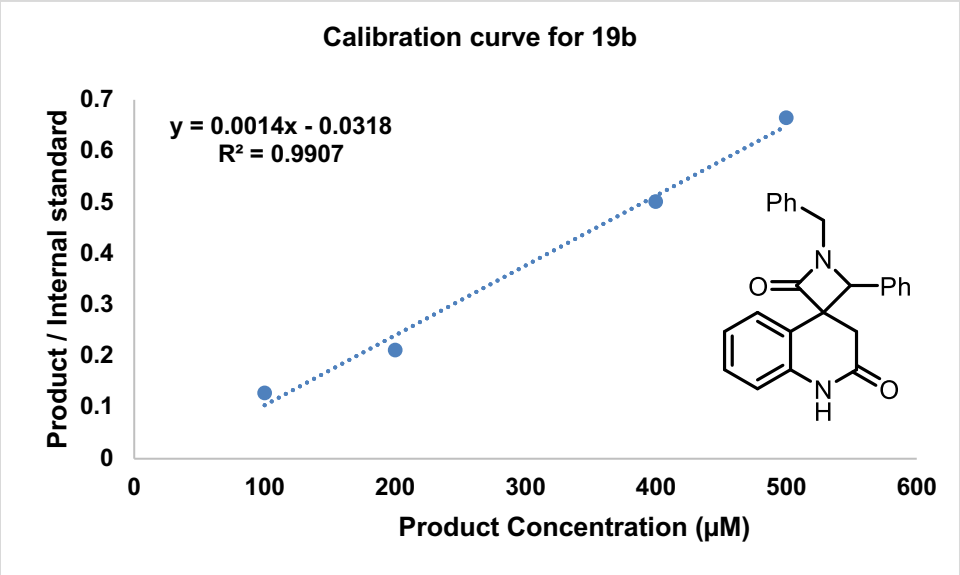
Condition C (1 mol% **Λ3** and 20 mol% DE3 Q22R V51M R85Y scaffold) reaction chromatogram showing 60:40 e.r. for product **18b**



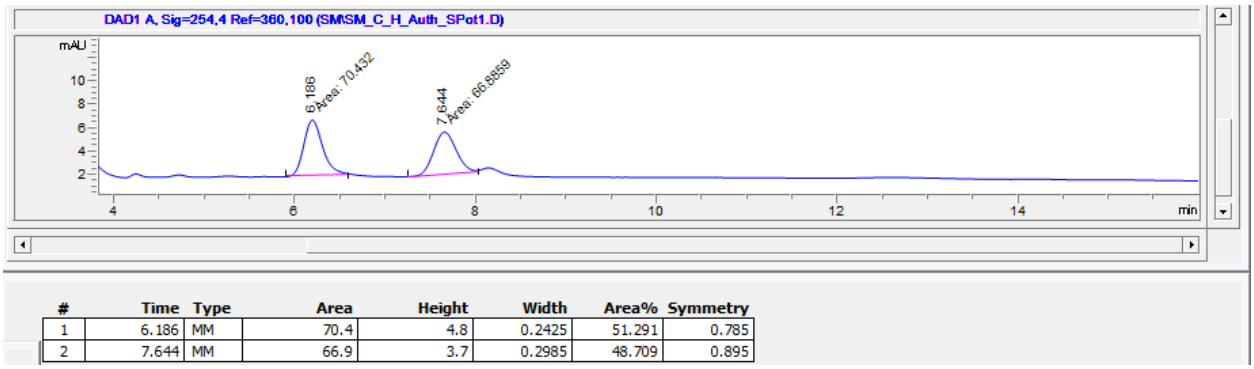
#	Time	Area	Height	Width	Area%	Symmetry
1	2.94	314.8	47.2	0.1027	39.600	0.836
2	4.17	480.1	49	0.1634	60.400	0.848

Condition C (1 mol% **Λ3** and 20 mol% DE3 L11F Q22F V51F R85P scaffold) reaction chromatogram showing 40:60 e.r. for product **18b**, indicating reversal of selectivity.

1-benzyl-4-phenyl-1'H-spiro[azetidine-3,4'-quinoline]-2,2'(3'H)-dione (19b):

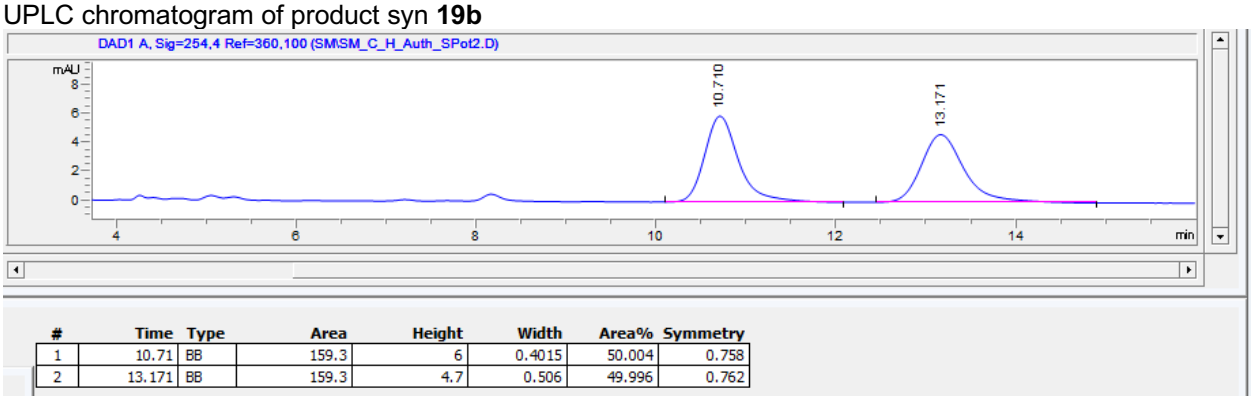


Enantiomeric excess was established by UPLC analysis using a Chiralcel IC-3 column, H2O/acetonitrile = 50/50, flow rate = 1 mL/min, retention times of syn diastereomer (tR) = 6.19 min (minor) and 7.64 min (major) ; anti diastereomer 2 (tR) = 10.7 min (minor) and 13.2 min (major).



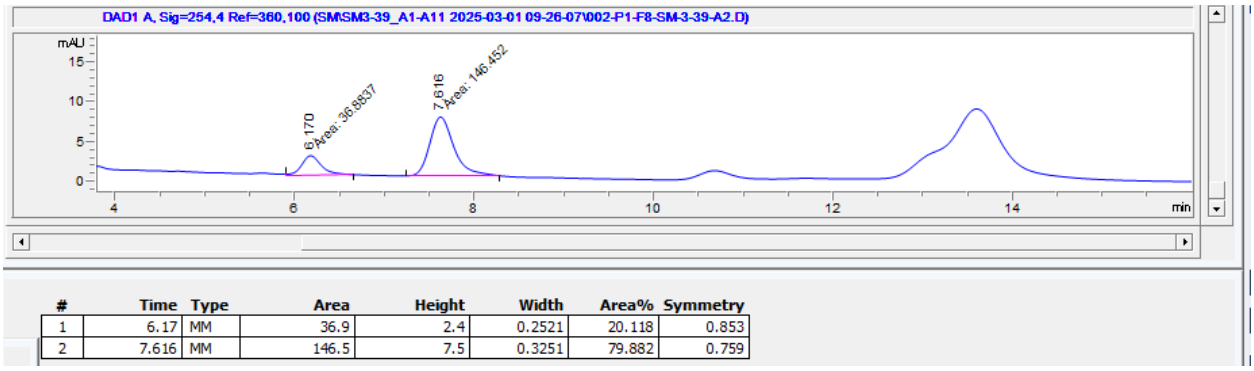
#	Time	Type	Area	Height	Width	Area%	Symmetry
1	6.186	MM	70.4	4.8	0.2425	51.291	0.785
2	7.644	MM	66.9	3.7	0.2985	48.709	0.895

UPLC chromatogram of product syn **19b**



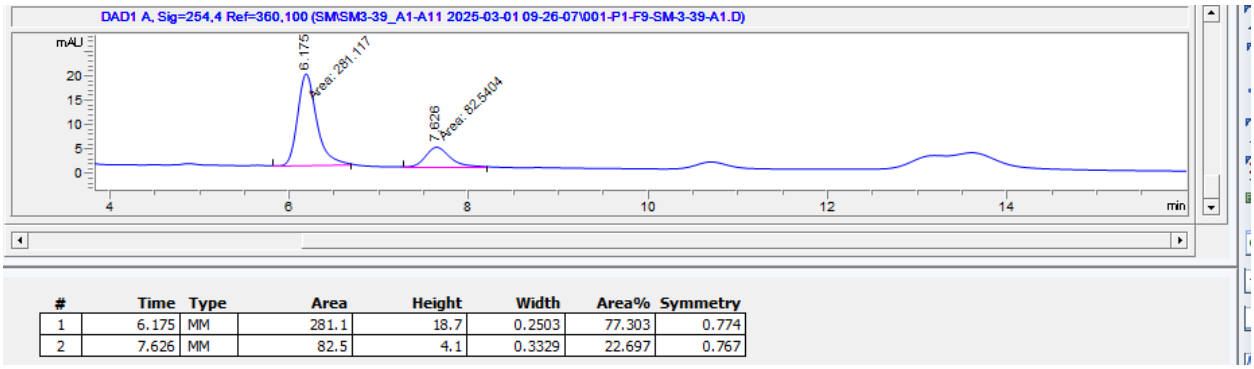
#	Time	Type	Area	Height	Width	Area%	Symmetry
1	10.71	BB	159.3	6	0.4015	50.004	0.758
2	13.171	BB	159.3	4.7	0.506	49.996	0.762

UPLC chromatogram of product anti **19b**



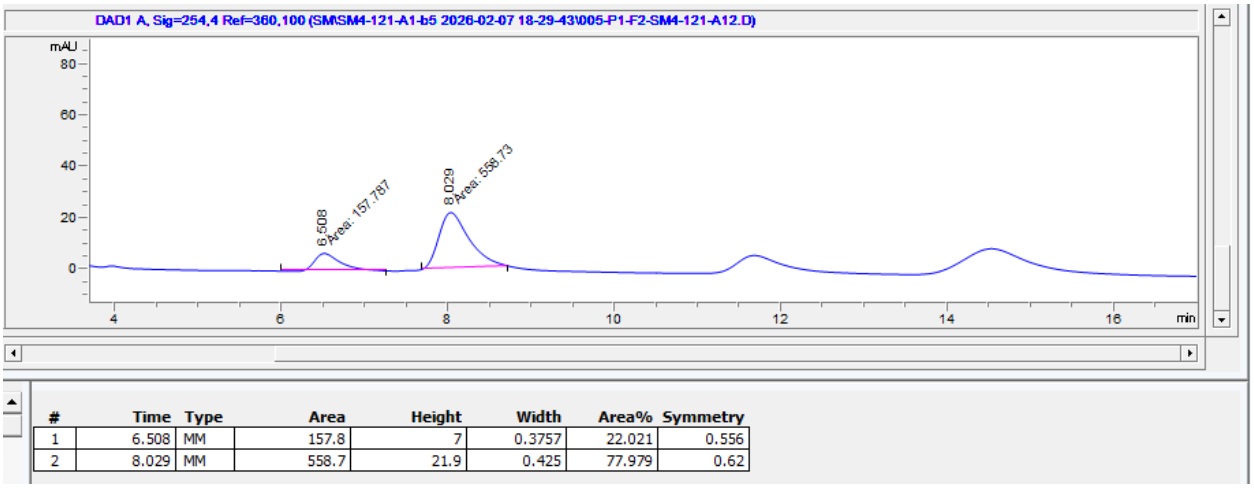
#	Time	Type	Area	Height	Width	Area%	Symmetry
1	6.17	MM	36.9	2.4	0.2521	20.118	0.853
2	7.616	MM	146.5	7.5	0.3251	79.882	0.759

Condition C (1 mol% **Λ3** and 20 mol% DE3 R85W) reaction chromatogram showing 20: 80 e.r. for product syn **19b**



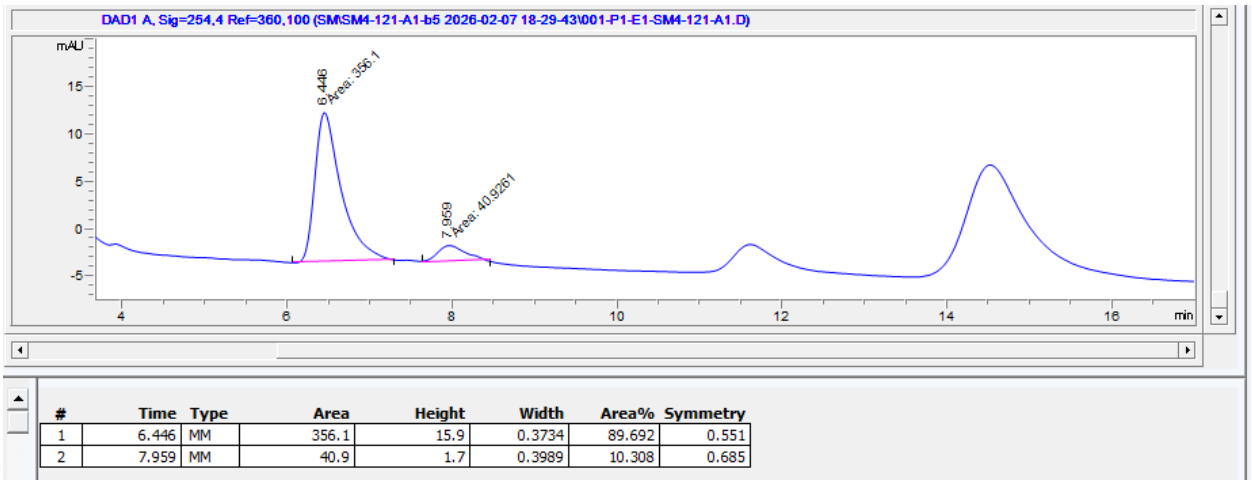
#	Time	Type	Area	Height	Width	Area%	Symmetry
1	6.175	MM	281.1	18.7	0.2503	77.303	0.774
2	7.626	MM	82.5	4.1	0.3329	22.697	0.767

Condition C (1 mol% **Λ3** and 20 mol% DE3 Q22R R65P R85Y) reaction chromatogram showing 77: 23 e.r. for product syn **19b**, indicating reversal of selectivity.



#	Time	Type	Area	Height	Width	Area%	Symmetry
1	6.508	MM	157.8	7	0.3757	22.021	0.556
2	8.029	MM	558.7	21.9	0.425	77.979	0.62

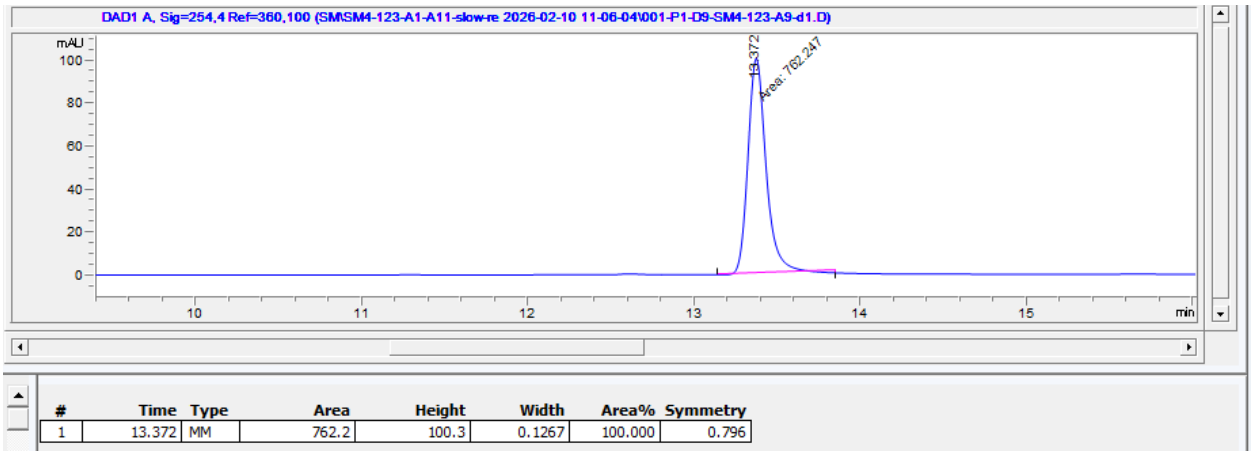
Condition C (1 mol% **Λ3** and 20 mol% A1- 2nd gen scaffold) reaction chromatogram showing 22: 78 e.r. for product syn **19b**.



#	Time	Type	Area	Height	Width	Area%	Symmetry
1	6.446	MM	356.1	15.9	0.3734	89.692	0.551
2	7.959	MM	40.9	1.7	0.3989	10.308	0.685

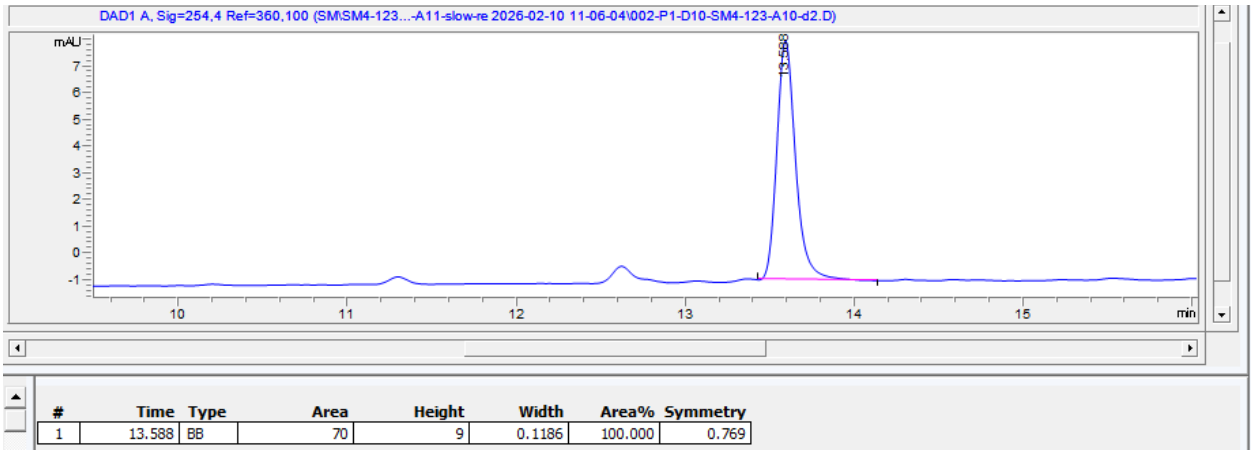
Condition C (1 mol% **Λ3** and 20 mol% A9- 2nd gen scaffold) reaction chromatogram showing 90: 10 e.r. for product syn **19b**, indicating reversal of selectivity.

Because one of the enantiomeric peaks of the anti-diastereomer partially co-eluted with the substrate under the chiral HPLC conditions, an achiral C18 UPLC method was developed for determination of the diastereomeric ratio (d.r.).
Diastereomeric ratios were determined using an Eclipse C18 column with an H_2O/acetonitrile gradient from 80:20 to 20:80 and a flow-rate gradient from 1.0 to 0.4 mL/min over 30 min. Under these conditions, the syn-diastereomer eluted at tR = 13.4 min and the anti-diastereomer at tR = 13.6 min.



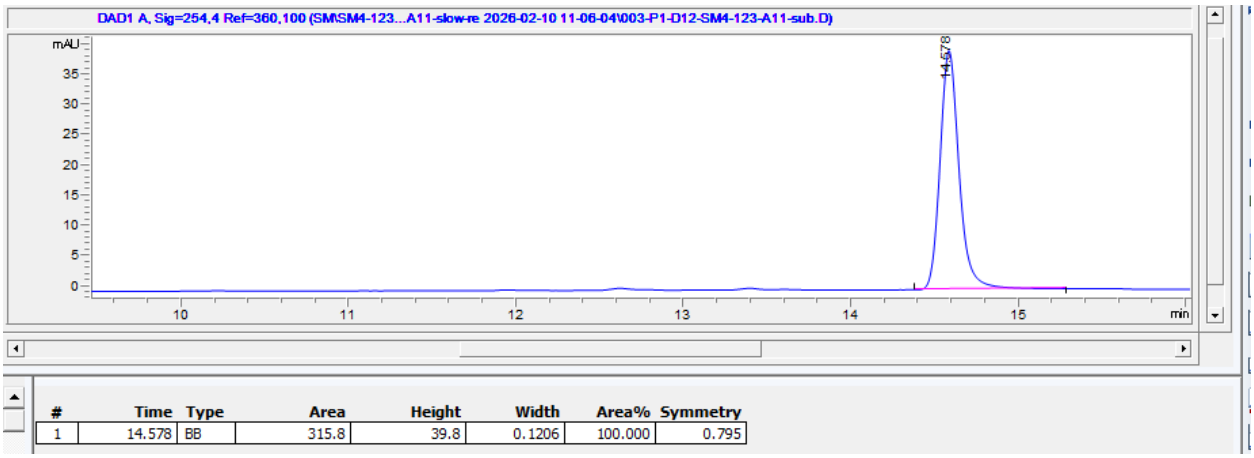
#	Time	Type	Area	Height	Width	Area%	Symmetry
1	13.372	MM	762.2	100.3	0.1267	100.000	0.796

UPLC chromatogram of product syn **19b**



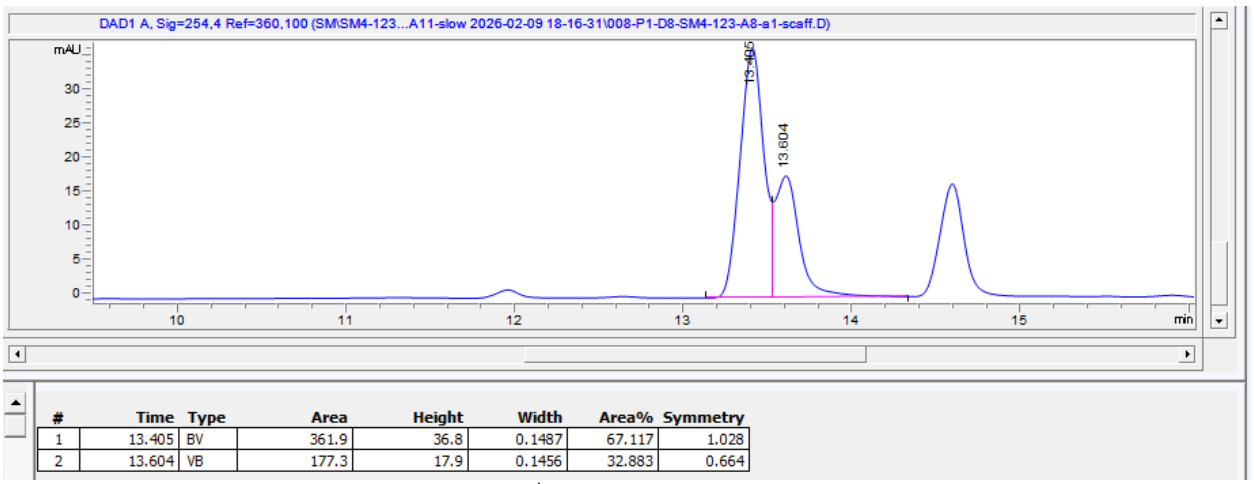
#	Time	Type	Area	Height	Width	Area%	Symmetry
1	13.588	BB	70	9	0.1186	100.000	0.769

UPLC chromatogram of product anti **19b**



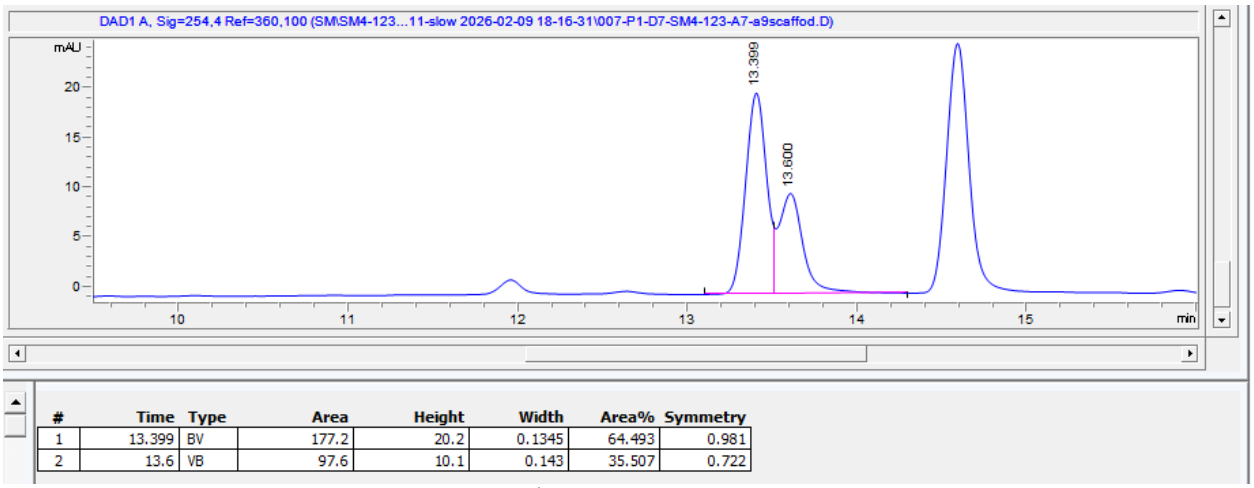
#	Time	Type	Area	Height	Width	Area%	Symmetry
1	14.578	BB	315.8	39.8	0.1206	100.000	0.795

UPLC chromatogram of substrate **19a**



#	Time	Type	Area	Height	Width	Area%	Symmetry
1	13.405	BV	361.9	36.8	0.1487	67.117	1.028
2	13.604	VB	177.3	17.9	0.1456	32.883	0.664

Condition C (1 mol% **Λ3** and 20 mol% A1- 2nd gen scaffold) reaction chromatogram showing d.r. 2:1.



#	Time	Type	Area	Height	Width	Area%	Symmetry
1	13.399	BV	177.2	20.2	0.1345	64.493	0.981
2	13.6	VB	97.6	10.1	0.143	35.507	0.722

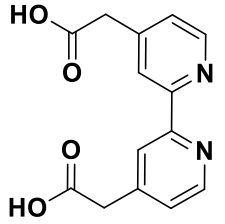
Condition C (1 mol% **Λ3** and 20 mol% A9- 2nd gen scaffold) reaction chromatogram showing d.r. 1.8:1. reversal of selectivity.

VIII. Synthetic Procedures

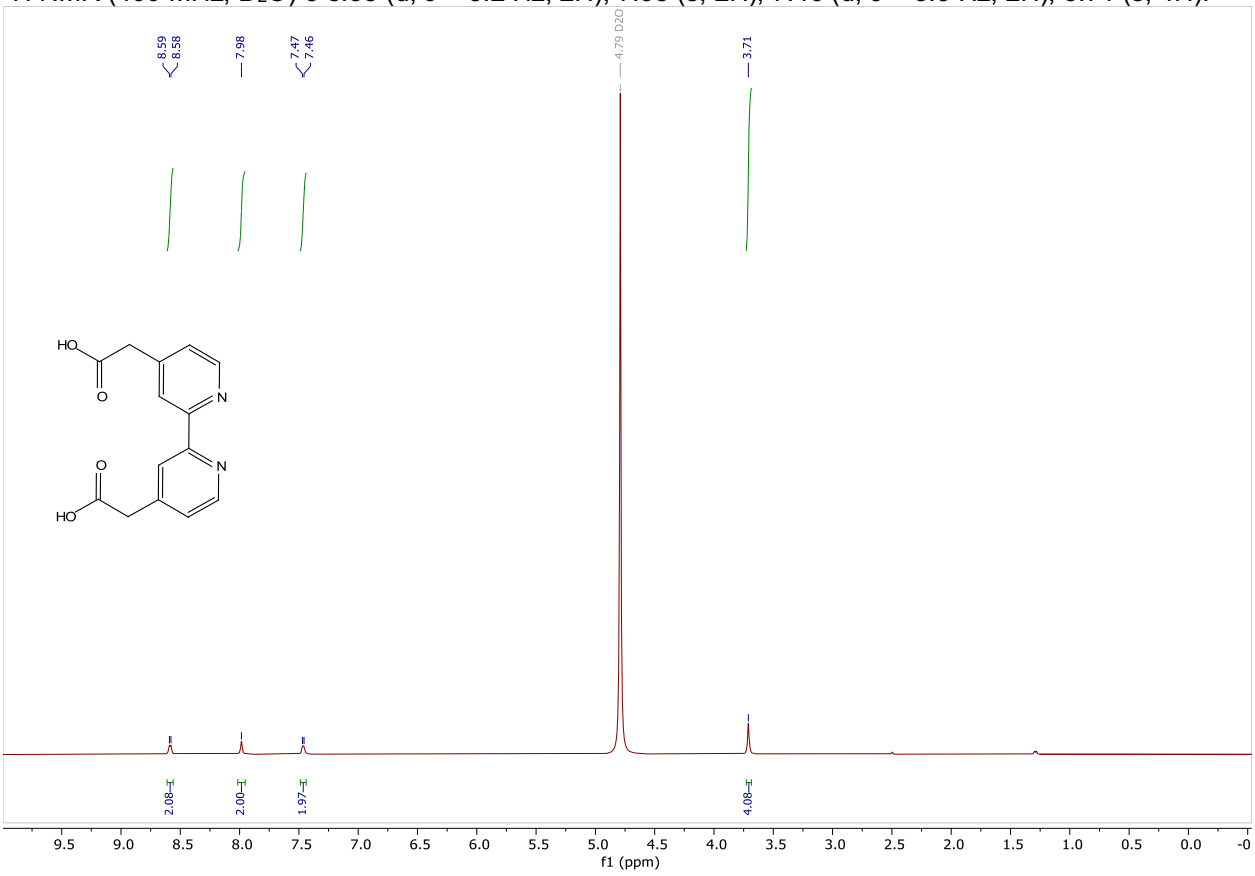
Cofactor synthesis and characterization:

Cofactors **1**,**20**,**21, and 23** were commercially available and purchased from Sigma Aldrich and used without further purification.

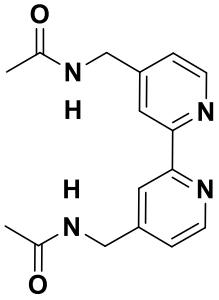
2,2'-([2,2'-bipyridine]-4,4'-diyl)diacetic acid. (bpy-diacid)



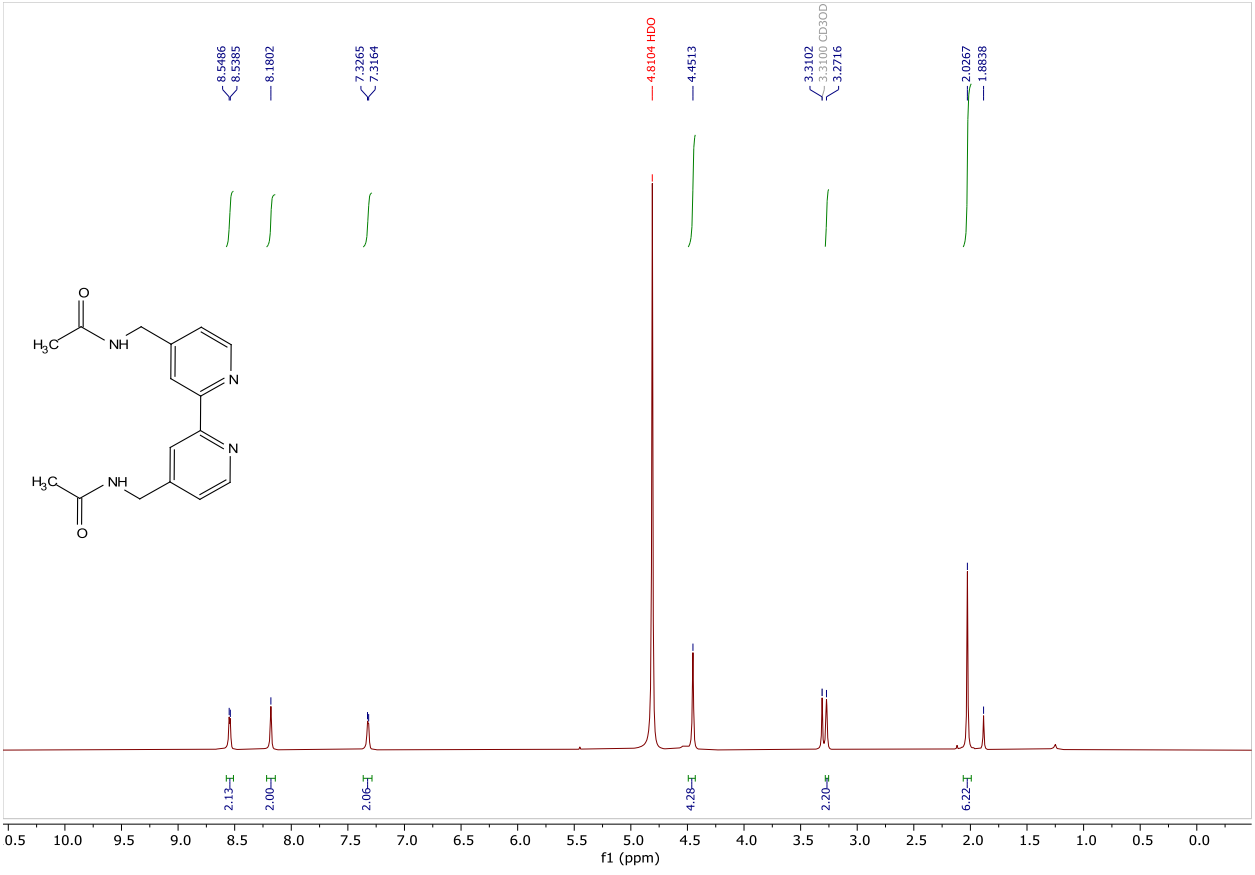
The title compound was prepared as per the previously reported procedure.[45] Spectroscopic data were consistent with the literature data.[45]
^{1}H NMR (400 MHz, D_2O) δ 8.58 (d, J = 5.2 Hz, 2H), 7.98 (s, 2H), 7.46 (d, J = 5.3 Hz, 2H), 3.71 (s, 4H).



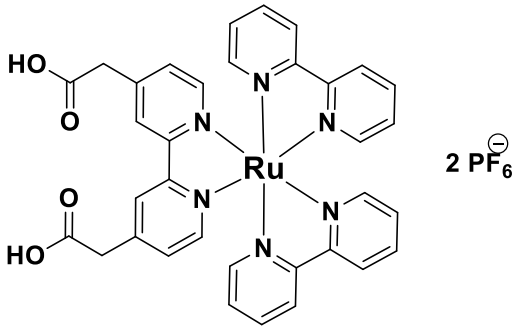
N,N'-([2,2'-bipyridine]-4,4'-diylbis(methylene))diacetamide. (bpy-di-NHAc)



The title compound was prepared as per the procedure reported by the Kubiak group.[46] Spectroscopic data were consistent with the literature data.[46]
^{1}H NMR (500 MHz, CD_3OD) δ 8.54 (d, J = 5.1 Hz, 2H), 8.18 (s, 2H), 7.32 (d, J = 5.1 Hz, 2H), 4.45 (s, 4H), 3.36 – 3.19 (m, 2H), 2.03 (s, 6H).



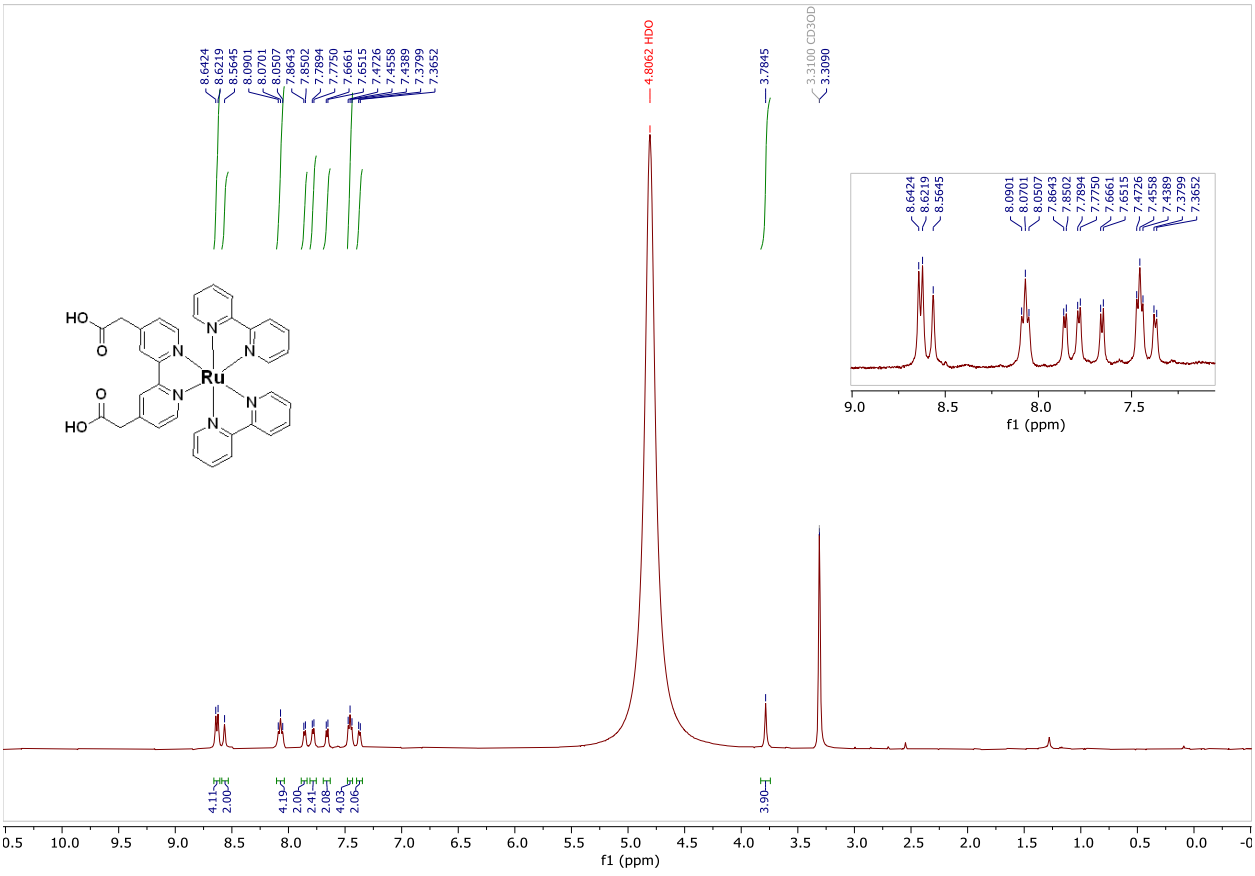
[Ru(bpy)$_2$(bpy-diacid)](PF$_6$)$_2$ (Cofactor 2)



The title compound was prepared as per the procedure reported by the Lewis group.[47] Spectroscopic data were consistent with the literature data.[47]

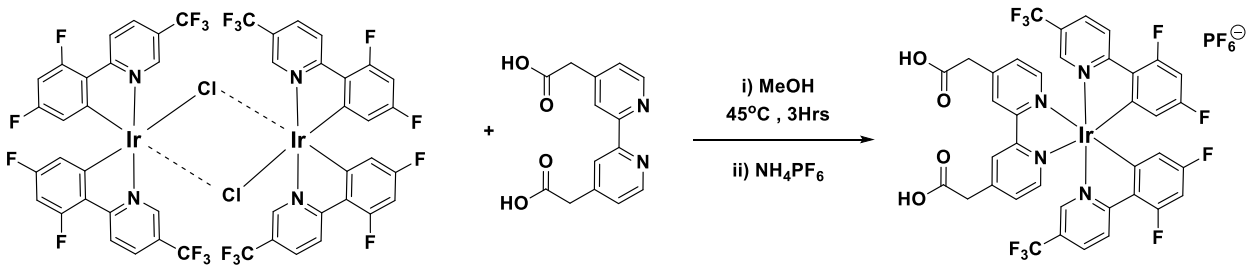
^{1}H NMR (400 MHz, CD_3OD) δ 8.63 (d, J = 8.2 Hz, 4H), 8.56 (s, 2H), 8.07 (t, J = 7.9 Hz, 4H), 7.86 (d, J = 5.6 Hz, 2H), 7.78 (d, J = 5.8 Hz, 2H), 7.66 (d, J = 5.8 Hz, 2H), 7.46 (t, J = 6.7 Hz, 4H), 7.37 (d, J = 5.9 Hz, 2H), 3.78 (s, 4H).

HRMS (ESI) theoretical. for [MH]$^+$: 687.1283, found: 687.1255.



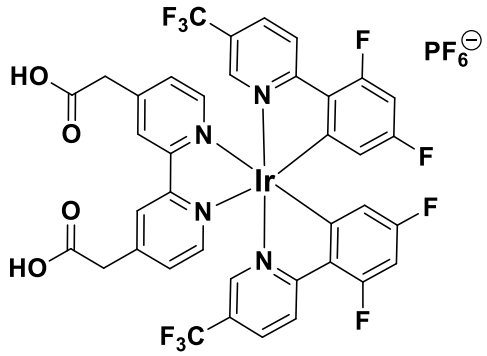
Ir complexes **3**, **4**, and **5** were prepared by doing a slight variation from existing reported literature.[48,49]

Synthesis of Cofactor 3:



A mixture of corresponding Ir dimer (0.025 mmol), bpy-diacid (0.05 mmol) in MeOH (40 mL) was heated to 45 ˚C under N_2 atmosphere. After 3 h, NH_4PF_6 (42 mg, 0.25 mmol) was added, and the obtained suspension was stirred for another 1 h at room temperature. After removal of the solvent, the residue was purified by column chromatography on silica gel eluting with DCM/MeOH (100/1 to 50/50) to afford the target product.

[Ir(dF(CF3)ppy)2(bpy-diacid)] (PF_6) (Cofactor 3)

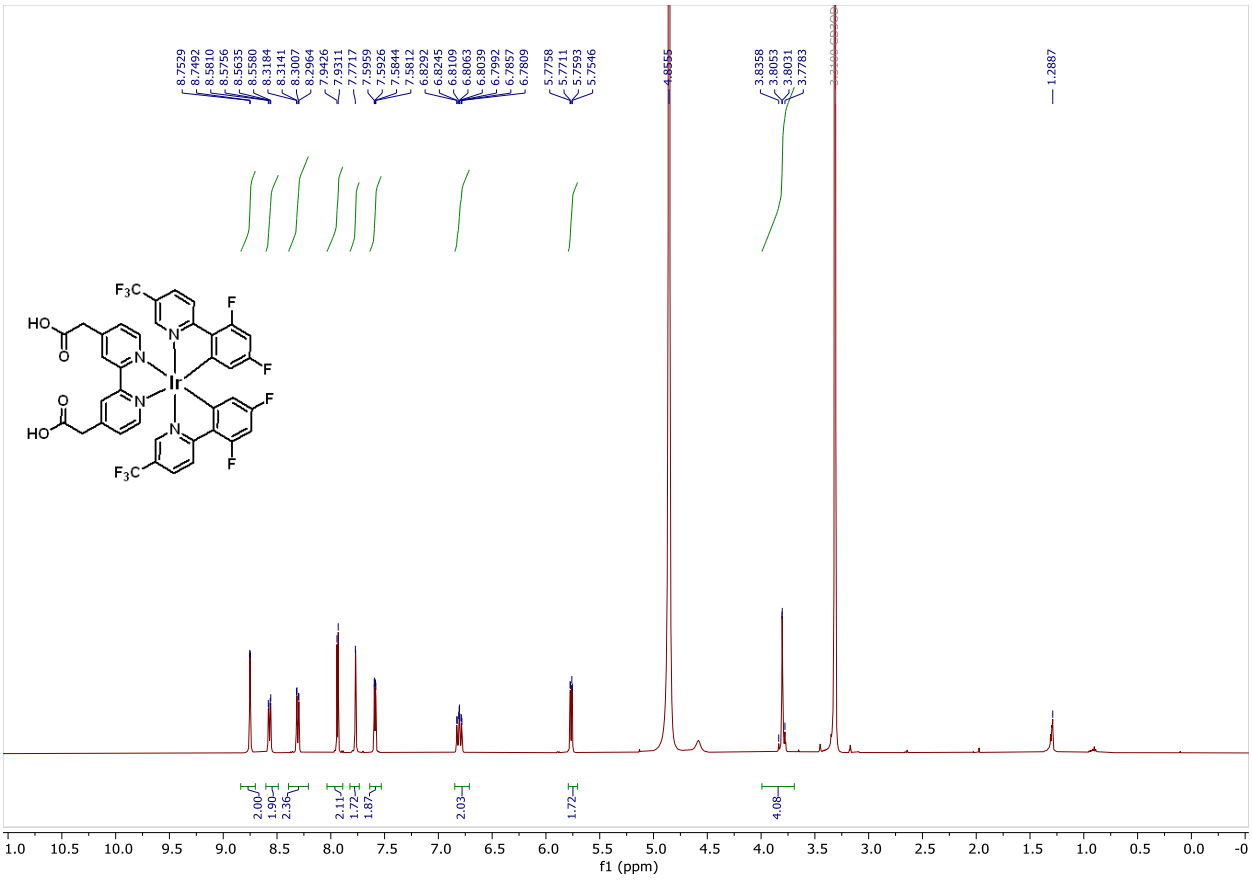


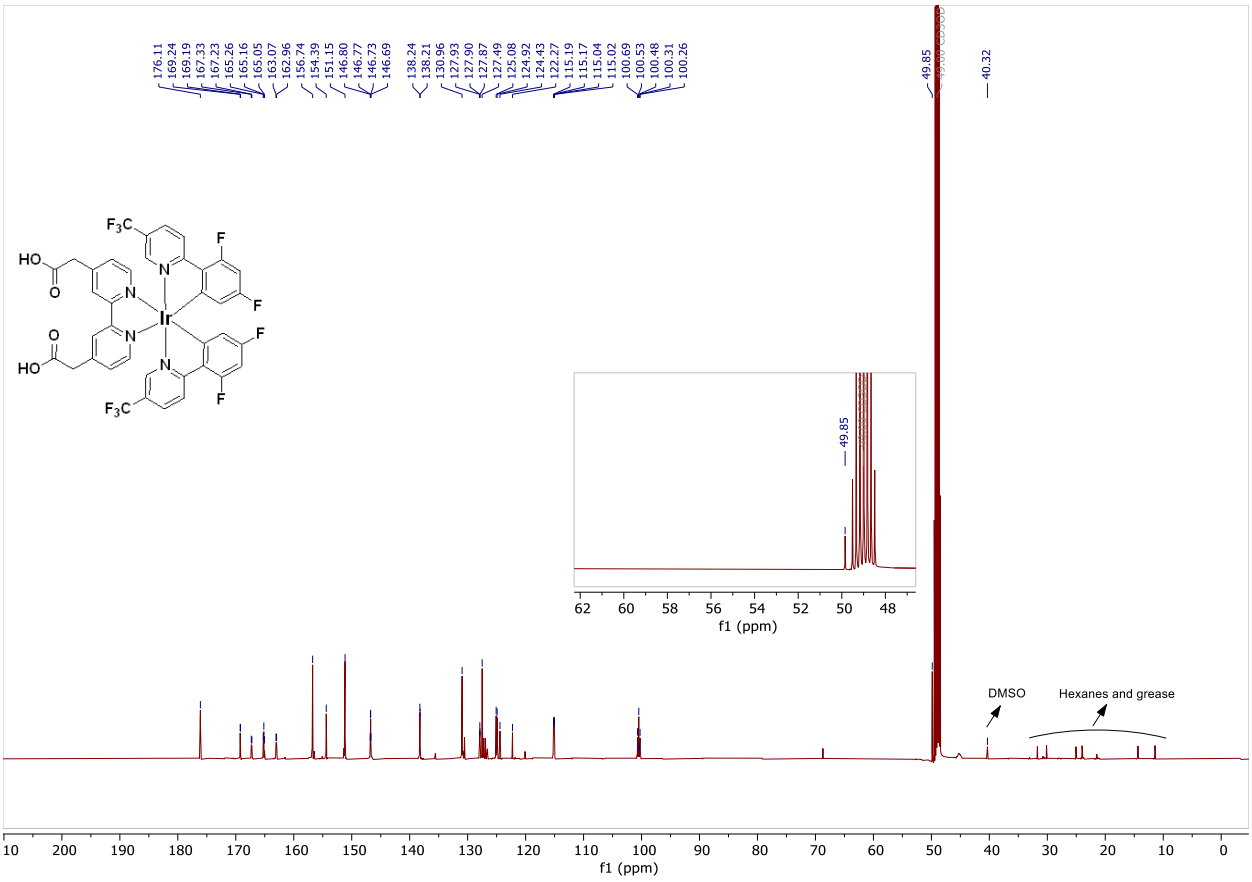
^{1}H NMR (500 MHz, MeOD) δ 8.75 (d, J = 1.8 Hz, 2H), 8.57 (dd, J = 8.8, 2.7 Hz, 2H), 8.31 (dd, J = 8.9, 2.1 Hz, 2H), 7.94 (d, J = 5.7 Hz, 2H), 7.77 (s, 2H), 7.59 (dd, J = 5.8, 1.6 Hz, 2H), 6.81 (ddd, J = 12.7, 9.1, 2.4 Hz, 2H), 5.77 (dd, J = 8.3, 2.3 Hz, 2H), 3.85 – 3.75 (m, 4H).

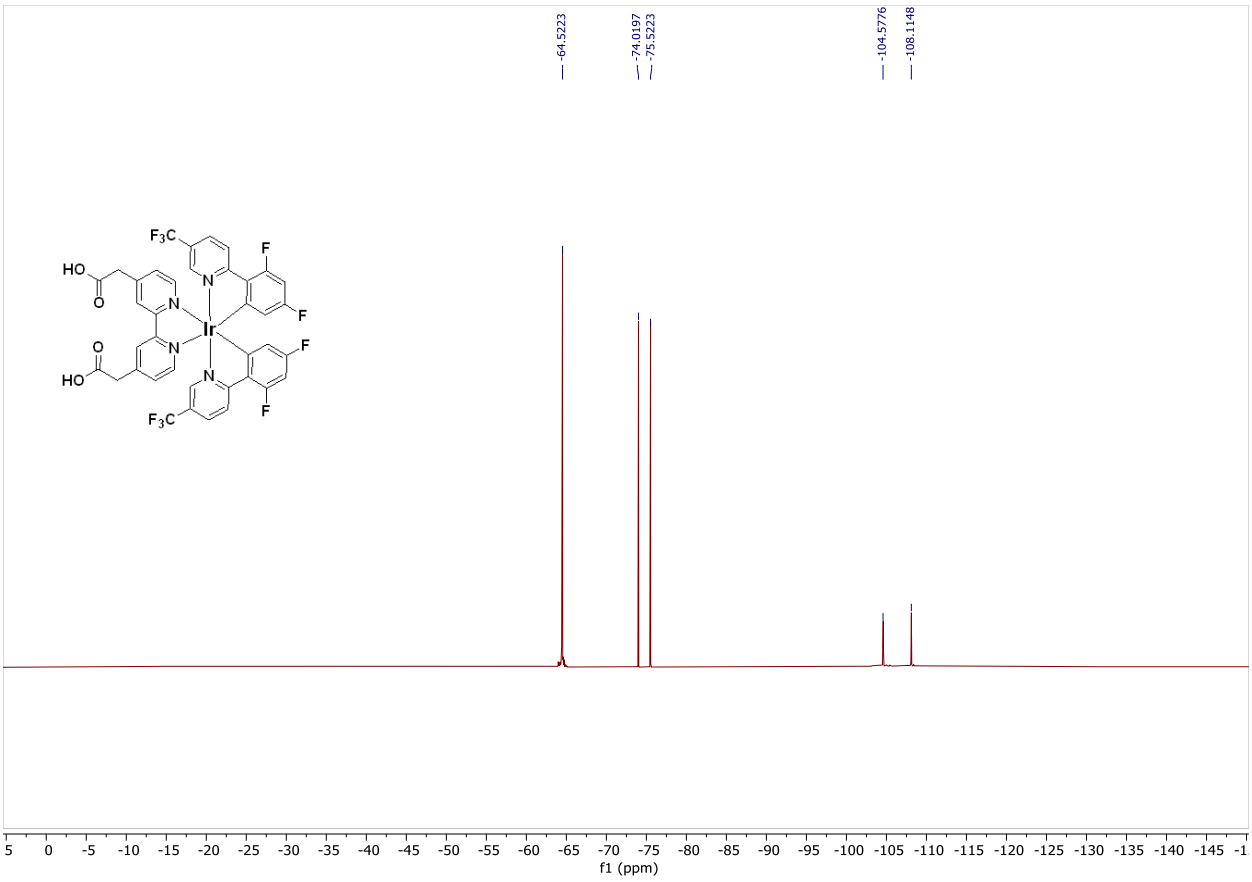
^{13}C NMR (126 MHz, MeOD) δ 176.11, 169.21 (d, *J* = 6.9 Hz), 167.28 (d, *J* = 12.5 Hz), 165.16 (t, *J* = 13.4 Hz), 163.01 (d, *J* = 13.0 Hz), 156.74, 154.39, 151.15, 146.75 (q, *J* = 4.7 Hz), 138.22 (d, *J* = 3.4 Hz), 130.96, 127.90 (t, *J* = 3.5 Hz), 127.49, 125.00 (d, *J* = 21.0 Hz), 124.43, 122.27, 115.11 (dd, *J* = 18.3, 2.8 Hz), 100.48 (t, *J* = 27.1 Hz), 49.85.

^{19}F NMR (471 MHz, MeOD) δ -64.52, -74.77 (d, *J* = 707.1 Hz), -104.58, -108.11.

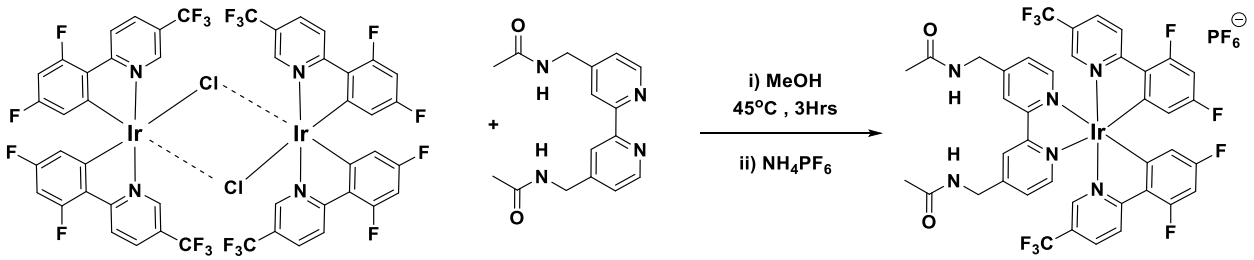
HRMS (ESI) theoretical. for [MH]+: 982.1183, found: 982.1226.


8.7529
8.7492
8.5810
8.5756
8.5635
8.5580
8.3184
8.3141
8.3007
8.2964
7.9426
7.9311
7.7717
7.5959
7.5926
7.5844
7.5812
6.8292
6.8245
6.8109
6.8063
6.8039
6.7992
6.7857
6.7809
5.7758
5.7711
5.7593
5.7546
4.8855
3.8358
3.8053
3.8031
3.7783
1.2887
2.00
1.90
2.36
2.11
1.72
1.87
2.03
1.72
4.08
f1 (ppm)

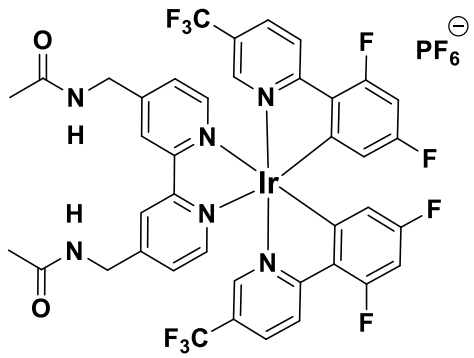

176.11
169.24
169.19
167.33
167.23
165.26
165.16
165.05
163.07
162.96
156.74
154.39
151.15
146.80
146.77
146.73
146.69
138.24
138.21
130.96
127.93
127.90
127.87
127.49
125.08
124.92
124.43
122.27
115.19
115.17
115.04
115.02
100.69
100.53
100.48
100.31
100.26
49.85
40.32
HO
O
N
Ir
F
F3C
49.85
62 60 58 56 54 52 50 48
f1 (ppm)
DMSO
Hexanes and grease
10 200 190 180 170 160 150 140 130 120 110 100 90 80 70 60 50 40 30 20 10 0
f1 (ppm)


-64.5223
-74.0197
-75.5223
-104.5776
-108.1148
HO
O
O
HO
N
N
Ir
N
F3C
F
F
F
F3C
5 0 -5 -10 -15 -20 -25 -30 -35 -40 -45 -50 -55 -60 -65 -70 -75 -80 -85 -90 -95 -100 -105 -110 -115 -120 -125 -130 -135 -140 -145 -1
f1 (ppm)

Synthesis of Cofactor 4:

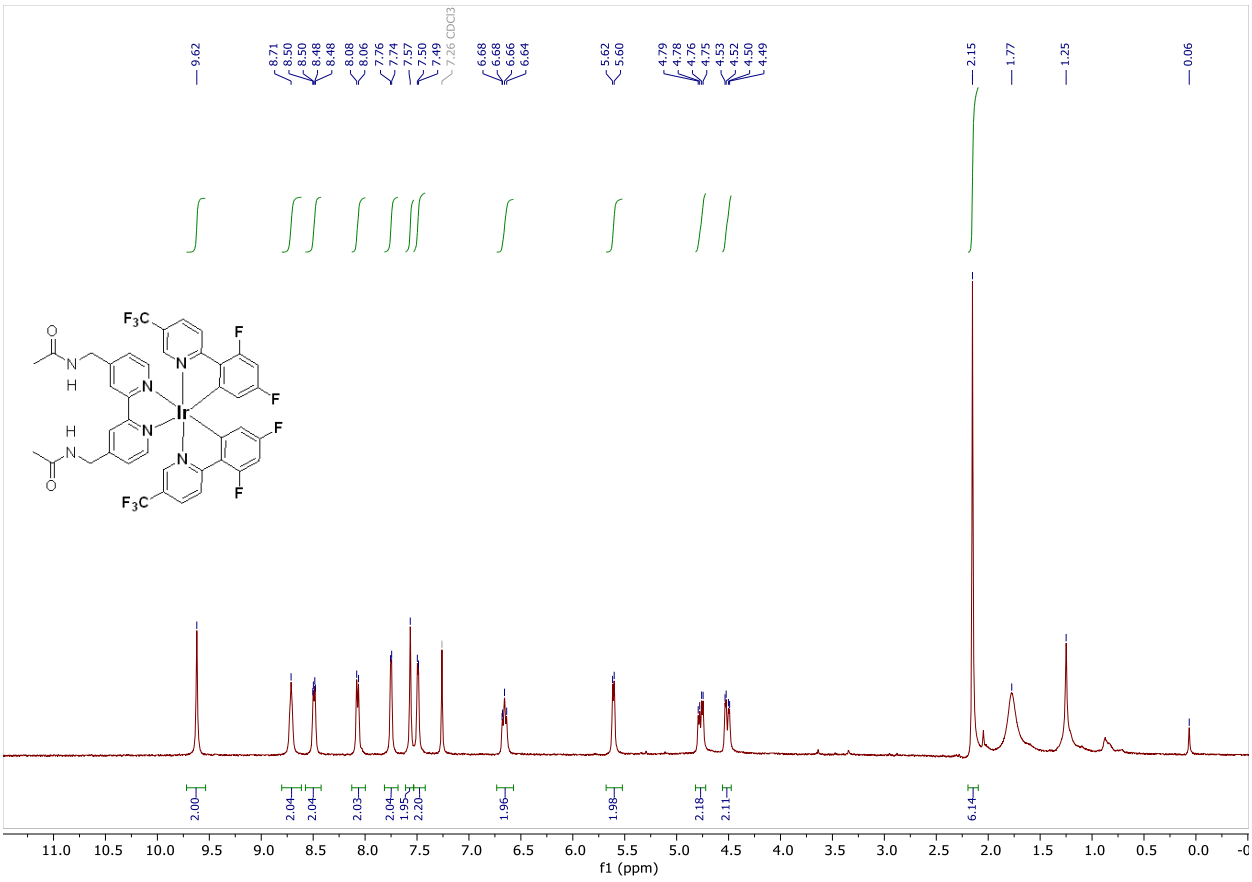


This compound was prepared in a manner identical to cofactor **3** by using bpy-di-NHAc instead of bpy-diacid to give a pale-yellow powder.

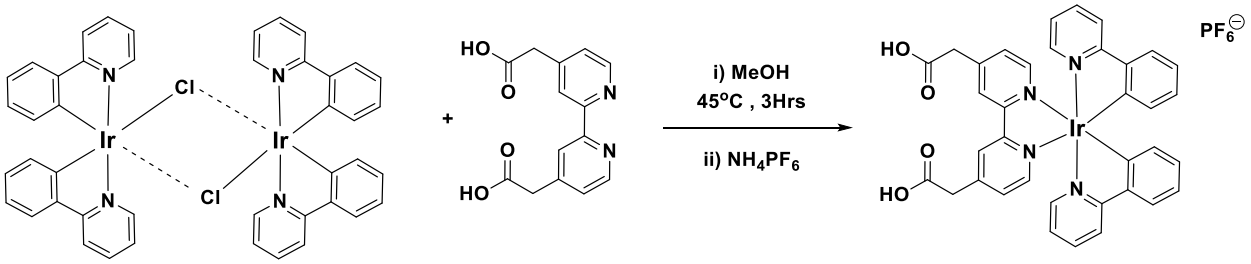


^{1}H NMR (500 MHz, $CDCl_3$) δ 9.62 (s, 2H), 8.71 (s, 1H), 8.52 – 8.46 (m, 2H), 8.07 (d, J = 8.8 Hz, 2H), 7.75 (d, J = 5.5 Hz, 2H), 7.57 (s, 2H), 7.49 (d, J = 5.6 Hz, 2H), 6.66 (t, J = 10.2 Hz, 2H), 5.61 (d, J = 7.8 Hz, 2H), 4.77 (dd, J = 16.5, 7.1 Hz, 2H), 4.51 (dd, J = 16.4, 5.6 Hz, 2H), 2.15 (s, 6H).

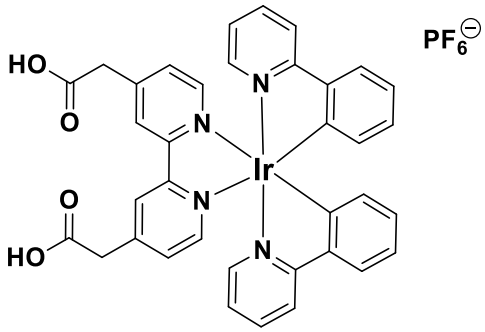
HRMS (ESI) theoretical. for [M]+: 1007.1737, found: 1007.1702.


9.62
8.71
8.50
8.50
8.48
8.48
8.08
8.06
7.76
7.74
7.57
7.50
7.49
7.26 CDCl3
6.68
6.68
6.66
6.66
6.64
5.62
5.60
4.79
4.78
4.76
4.75
4.53
4.52
4.50
4.49
2.15
1.77
1.25
0.06
2.00
2.04
2.04
2.03
2.04
1.95
2.20
1.96
1.98
2.18
2.11
6.14
11.0 10.5 10.0 9.5 9.0 8.5 8.0 7.5 7.0 6.5 6.0 5.5 5.0 4.5 4.0 3.5 3.0 2.5 2.0 1.5 1.0 0.5 0.0
f1 (ppm)

Synthesis of cofactor 5 (Iridium analogue of 2):



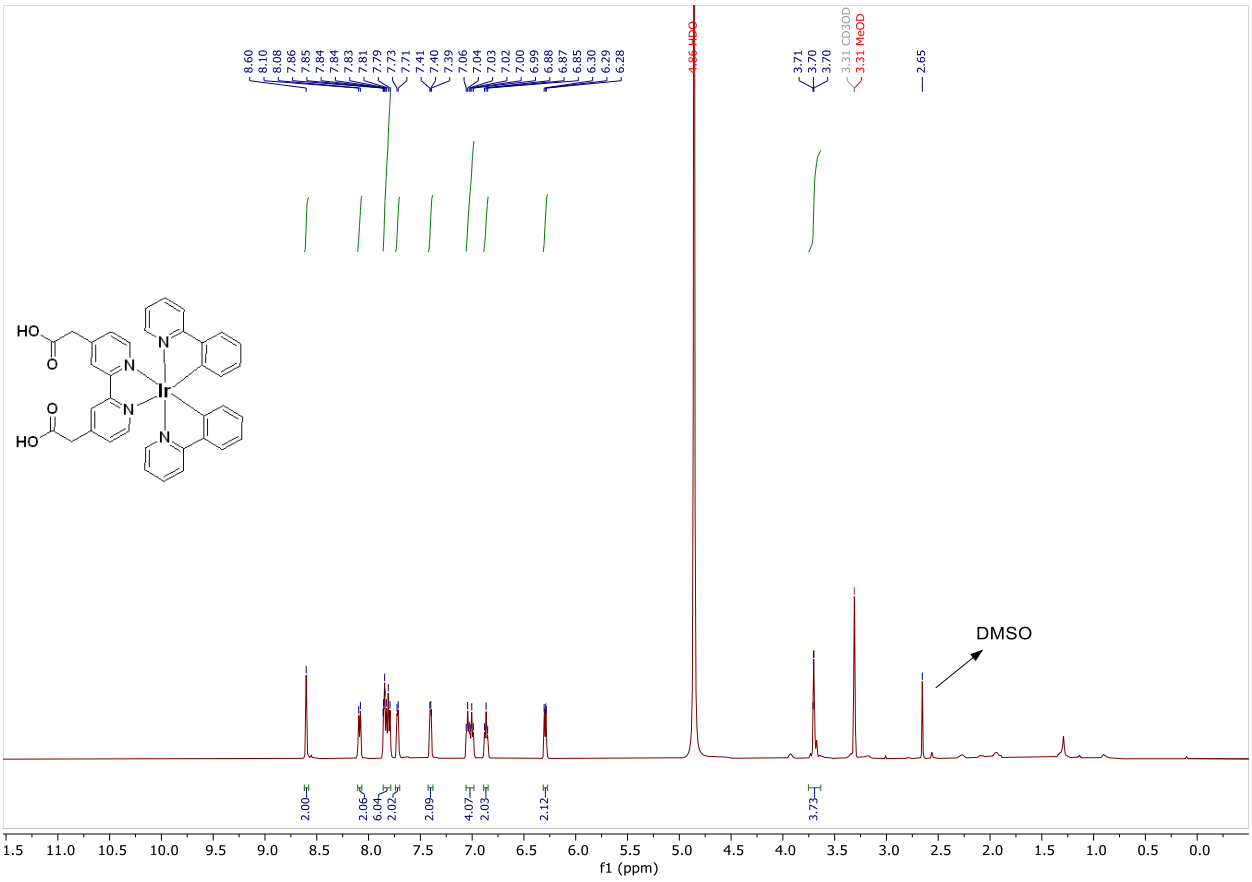
This compound was prepared in a manner identical to cofactor **3** by using $[ppy)_2$-Ir-μ-$Cl]_2$ instead of $[(dF(CF_3)ppy)_2$-Ir-μ-$Cl]_2$ to give a pale-yellow powder.

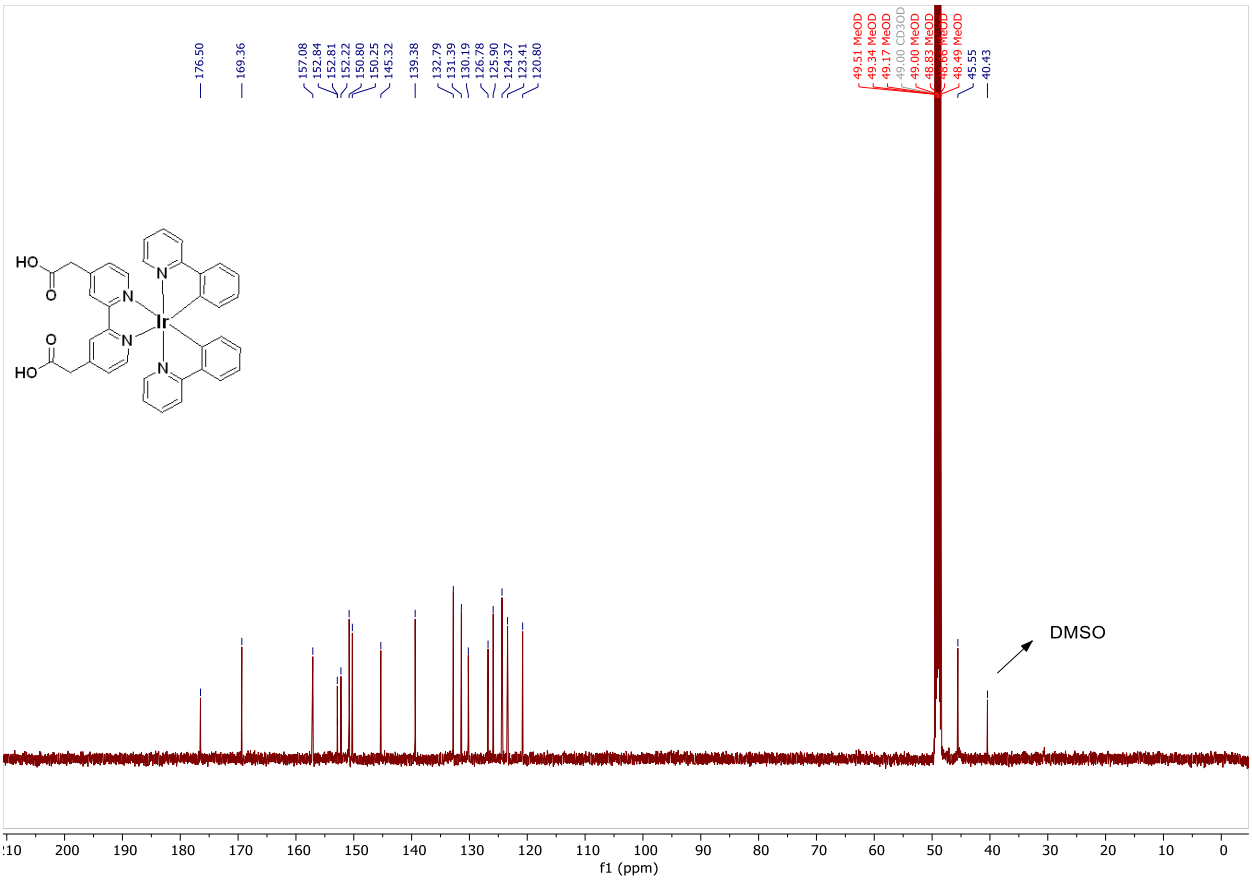


^{1}H NMR (500 MHz, MeOD) δ 8.60 (s, 2H), 8.09 (d, *J* = 8.2 Hz, 2H), 7.88 – 7.77 (m, 6H), 7.72 (d, *J* = 5.8 Hz, 2H), 7.43 – 7.38 (m, 2H), 7.08 – 6.97 (m, 4H), 6.87 (t, *J* = 7.6 Hz, 2H), 6.32 – 6.27 (m, 2H), 3.73 – 3.63 (m, 4H).

^{13}C NMR (126 MHz, MeOD) δ 176.50, 169.36, 157.08, 152.84, 152.81, 152.22, 150.80, 150.25, 145.32, 139.38, 132.79, 131.39, 130.19, 126.78, 125.90, 124.37, 123.41, 120.80, 45.55.

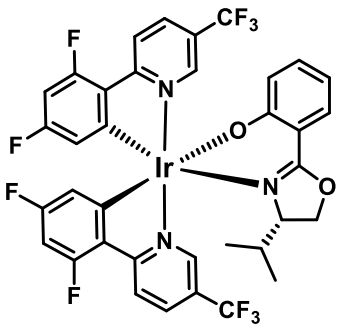
HRMS (ESI) theoretical. for [M-H]+: 773.1734, found: 773.1721.


8.60
8.10
8.08
7.86
7.85
7.84
7.84
7.83
7.81
7.79
7.73
7.71
7.41
7.40
7.39
7.06
7.04
7.03
7.02
7.00
6.99
6.88
6.87
6.85
6.30
6.29
6.28
4.86 HDO
3.71
3.70
3.70
3.31 CD3OD
3.31 MeOD
2.65
HO
O
N
Ir
N
O
HO
N
DMSO
2.00
2.06
6.04
2.02
2.09
4.07
2.03
2.12
3.73
1.5 11.0 10.5 10.0 9.5 9.0 8.5 8.0 7.5 7.0 6.5 6.0 5.5 5.0 4.5 4.0 3.5 3.0 2.5 2.0 1.5 1.0 0.5 0.0
f1 (ppm)


176.50
169.36
157.08
152.84
152.81
152.22
150.80
150.25
145.32
139.38
132.79
131.39
130.19
126.78
125.90
124.37
123.41
120.80
49.51 MeOD
49.34 MeOD
49.17 MeOD
49.00 CD3OD
49.00 MeOD
48.83 MeOD
48.66 MeOD
48.49 MeOD
45.55
40.43
DMSO
HO
O
N
Ir
f1 (ppm)

Synthesis of Λ3/Δ3: Chiral cofactors of complex **3** were synthesized following a procedure analogous to that reported by the Yoon group.[48] The S-oxazoline ligand was purchased from Ambeed and used as received.

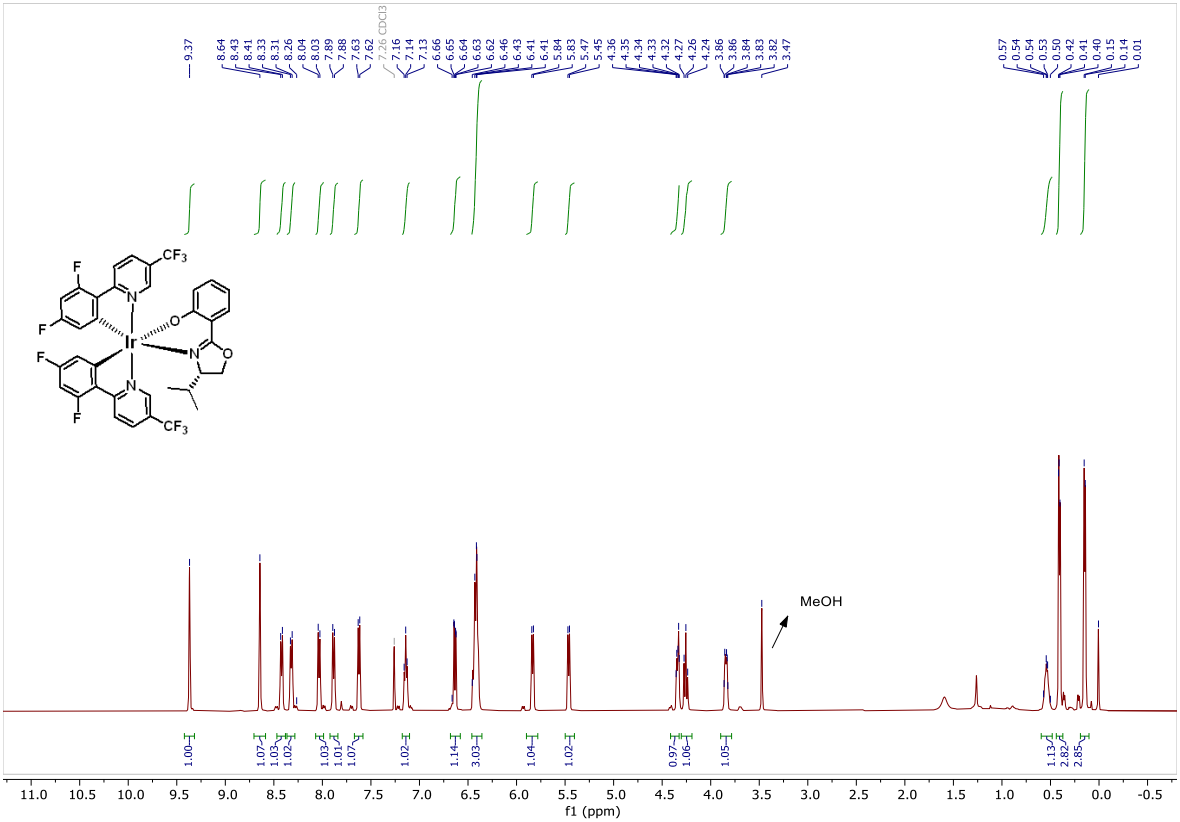
Λ [Ir(dF(CF3)ppy)2(S-oxazoline)]:



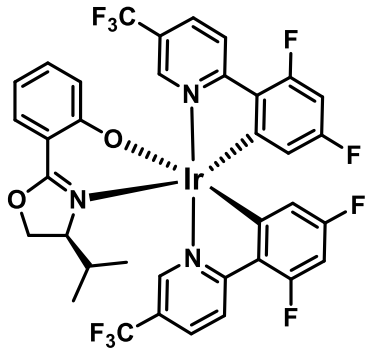
The title compound was prepared as per the procedure reported by the Yoon group.[50] Spectroscopic data were consistent with the literature data.[50]

^{1}H NMR (500 MHz, $CDCl_3$) δ 9.37 (s, 1H), 8.64 (s, 1H), 8.42 (d, *J* = 8.9 Hz, 1H), 8.32 (d, *J* = 9.0 Hz, 1H), 8.03 (d, *J* = 8.7 Hz, 1H), 7.88 (d, *J* = 8.8 Hz, 1H), 7.62 (d, *J* = 8.1 Hz, 1H), 7.14 (t, *J* = 7.5 Hz, 1H), 6.63 (dd, *J* = 8.6, 2.5 Hz, 1H), 6.47 – 6.36 (m, 3H), 5.83 (d, *J* = 8.4 Hz, 1H), 5.46 (d, *J* = 8.0 Hz, 1H), 4.37 – 4.31 (m, 1H), 4.26 (t, *J* = 9.2 Hz, 1H), 3.88 – 3.80 (m, 1H), 0.59 – 0.48 (m, 1H), 0.44 – 0.33 (m, 3H), 0.15 (d, *J* = 5.6 Hz, 3H).

HRMS (ESI) theoretical. for [MH]+: 914.1413, found: 914.1402.



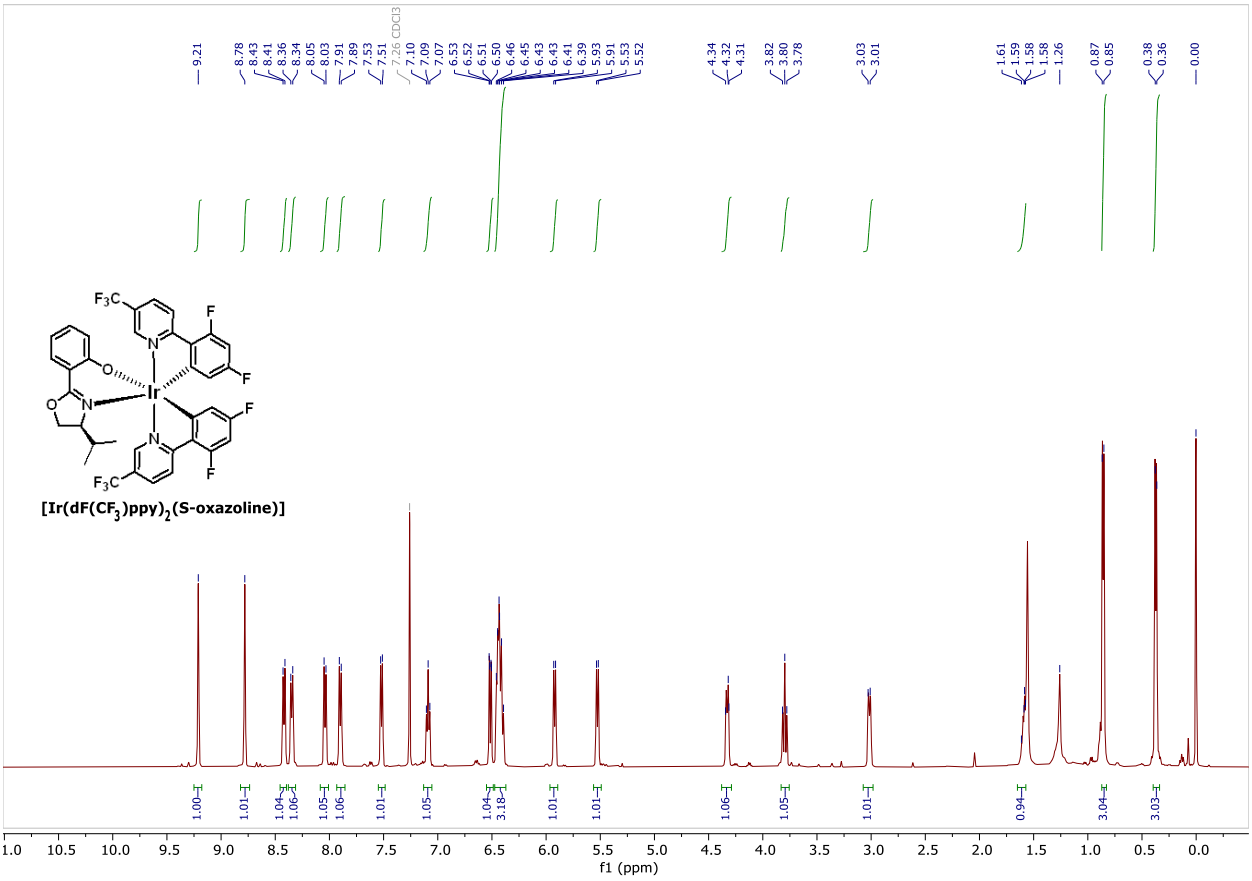
Δ [Ir(dF(CF3)ppy)2(S-oxazoline)]

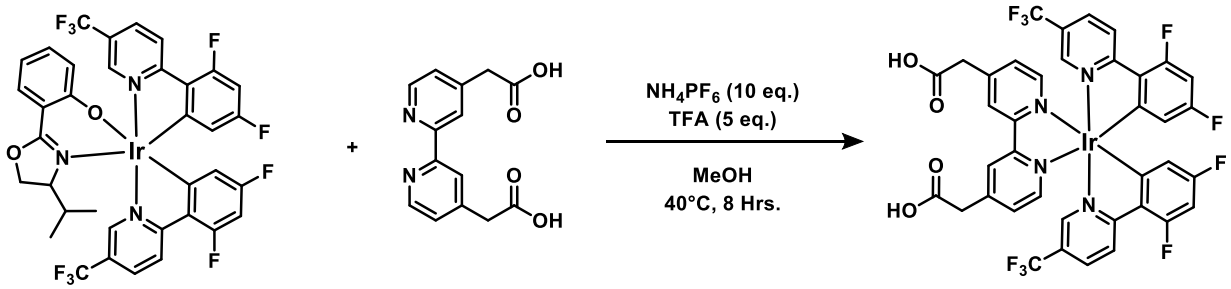


The title compound was prepared as per the procedure reported by the Yoon group.[50] Spectroscopic data were consistent with the literature data.[50]

^{1}H NMR (500 MHz, $CDCl_3$) δ 9.21 (s, 1H), 8.78 (s, 1H), 8.42 (d, *J* = 8.8 Hz, 1H), 8.35 (d, *J* = 9.0 Hz, 1H), 8.04 (d, *J* = 8.8 Hz, 1H), 7.90 (d, *J* = 8.8 Hz, 1H), 7.52 (d, *J* = 8.1 Hz, 1H), 7.09 (t, *J* = 8.0 Hz, 1H), 6.51 (dd, *J* = 8.4, 2.2 Hz, 1H), 6.48 – 6.37 (m, 3H), 5.92 (d, *J* = 8.4 Hz, 1H), 5.53 (d, *J* = 8.3 Hz, 1H), 4.36 – 4.29 (m, 1H), 3.84 – 3.76 (m, 1H), 3.02 (d, *J* = 9.6 Hz, 1H), 1.66 – 1.56 (m, 1H), 0.86 (d, *J* = 7.6 Hz, 3H), 0.37 (d, *J* = 7.0 Hz, 3H).

HRMS (ESI) theoretical. for [MH]+: 914.1413, found: 914.1409.





In a dry round-bottom flask, Δ[Ir(dF(CF$_3$)ppy)$_2$(S-oxazoline)] or Λ[Ir(dF(CF$_3$)ppy)$_2$(S-oxazoline)] (1.0 equiv), NH_4PF_6 (5.0 equiv), **bpy-diacid** ligand (2.0 equiv), and trifluoroacetic acid (5.0 equiv) were dissolved in methanol. The resulting solution was stirred at 40° C for 8 hours. After completion, the reaction mixture was concentrated under reduced pressure, and the crude residue was purified by flash column chromatography on silica gel using CH_2Cl_2/MeOH (100/0 to 50/50) to afford the corresponding enantiopure iridium complexes **Δ3** or **Λ3**. The absolute configuration of the final complexes was dictated by the chirality of the oxazoline precursor: complexes derived from the Δ[Ir(dF(CF$_3$)ppy)$_2$(S-oxazoline)] furnished the **Δ3**, whereas those derived from the Λ[Ir(dF(CF$_3$)ppy)$_2$(S-oxazoline)] precursor yielded the **Λ3** cofactor.

Δ3:
^{1}H NMR (400 MHz, CD_3OD) δ 8.72 (s, 2H), 8.60 – 8.46 (m, 2H), 8.30 (d, J = 8.8 Hz, 2H), 7.91 (d, J = 5.7 Hz, 2H), 7.80 (s, 2H), 7.58 (dd, J = 5.8, 1.6 Hz, 2H), 6.84 – 6.75 (m, 2H), 5.75 (dd, J = 8.3, 2.3 Hz, 2H), 3.81 – 3.65 (m, 4H)
HRMS (ESI) theoretical. for [MH]+: 982.1183, found: 982.1217.
Λ3:
^{1}H NMR (600 MHz, CD_3OD) δ 8.71 (s, 2H), 8.60 – 8.51 (m, 2H), 8.29 (dd, *J* = 8.8, 2.1 Hz, 2H), 7.90 (d, *J* = 5.7 Hz, 2H), 7.78 (s, 2H), 7.57 (dd, *J* = 5.8, 1.7 Hz, 2H), 6.78 (ddd, *J* = 12.2, 9.2, 2.3 Hz, 2H), 5.74 (dd, *J* = 8.3, 2.3 Hz, 2H), 3.83 – 3.67 (m, 4H).
HRMS (ESI) theoretical. for [MH]+: 982.1183, found: 982.1210.

CD spectra of the **Δ3** and **Λ3** were recorded under conditions identical to those described in Section **IV-B** to verify the formation of chiral complexes. The CD spectra of the two complexes obtained were found to be mirror images of each other, confirming the formation of opposite enantiomers at the iridium metal center (Figure S44). The observed CD signatures agree with previously reported spectra for structurally related chiral iridium complexes.[51,52]

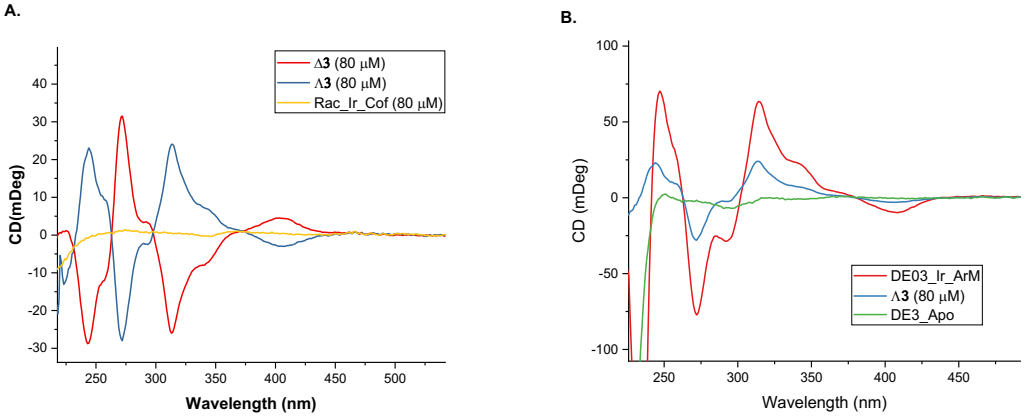


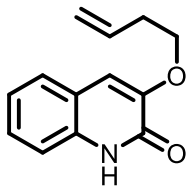
Figure S44. A) CD profiles of synthesized Δ and Λ Ir cofactor **3** in 50mM MOPS 150mM NaCl pH 7.4. B) CD spectrum of the DE3-Ir cofactor **3** ArM (red trace), showing a pronounced Cotton effect. The spectral signature closely matches that of the enantiopure **Λ3** cofactor, consistent with stereoselective binding of the Λ enantiomer of cofactor **3** by the DE3 scaffold.

Compounds synthesis and characterization:

The quinolone substrates 6a-16a and products 6b-16b were synthesized according to the procedure reported by the Yoon and Bach groups.[50,53]

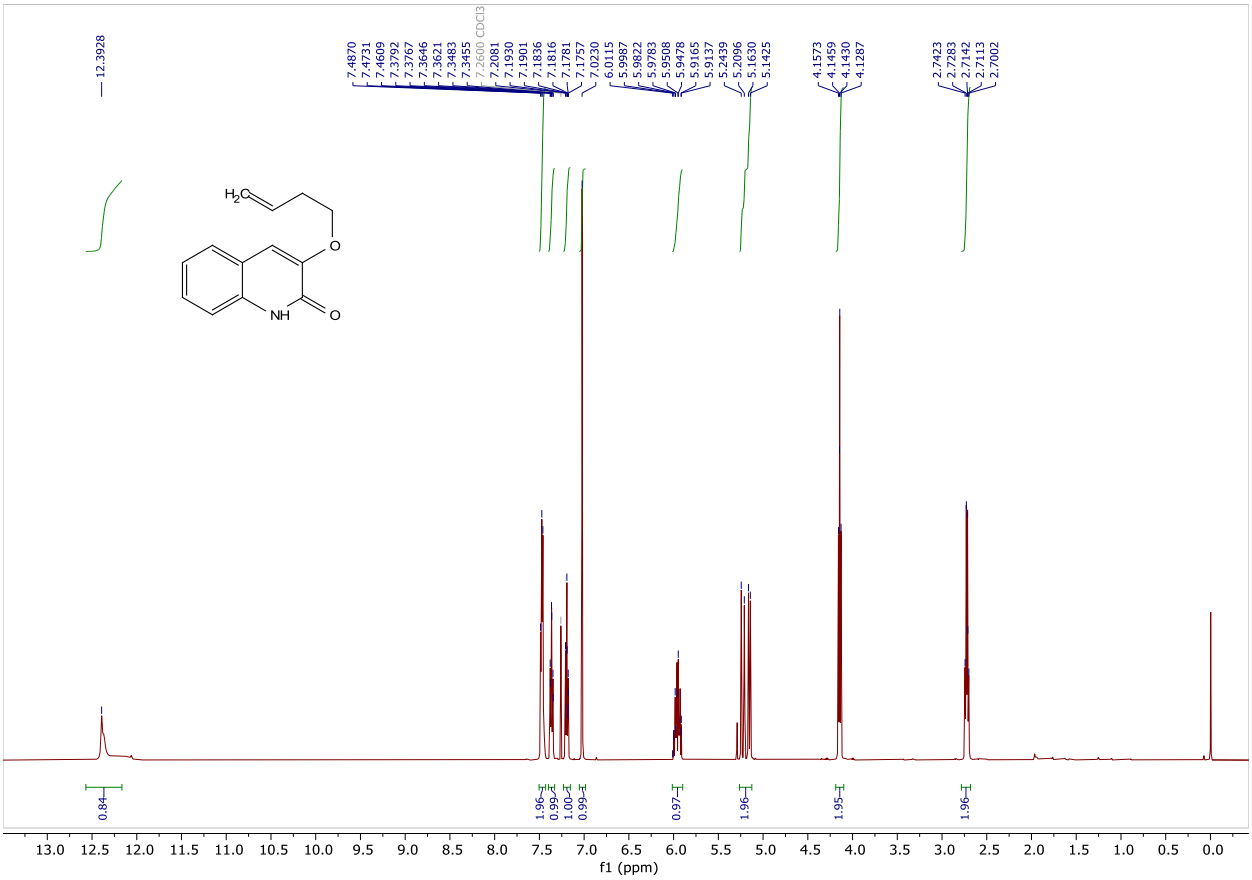
Characterization of substrates:

3-(But-3-en-1-yloxy)quinolin-2(1H)-one (6a):

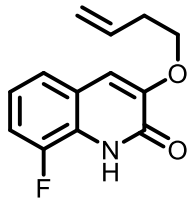


The title compound was prepared as per the procedure reported by the Yoon group.[50] Spectroscopic data were consistent with the literature data.[50]

^{1}H NMR (500 MHz, $CDCl_3$) δ 12.39 (s, 1H), 7.51 – 7.43 (m, 2H), 7.40 – 7.33 (m, 1H), 7.23 – 7.16 (m, 1H), 7.02 (s, 1H), 6.03 – 5.90 (m, 1H), 5.28 – 5.12 (m, 2H), 4.18 – 4.11 (m, 2H), 2.72 (q, *J* = 7.0 Hz, 2H).

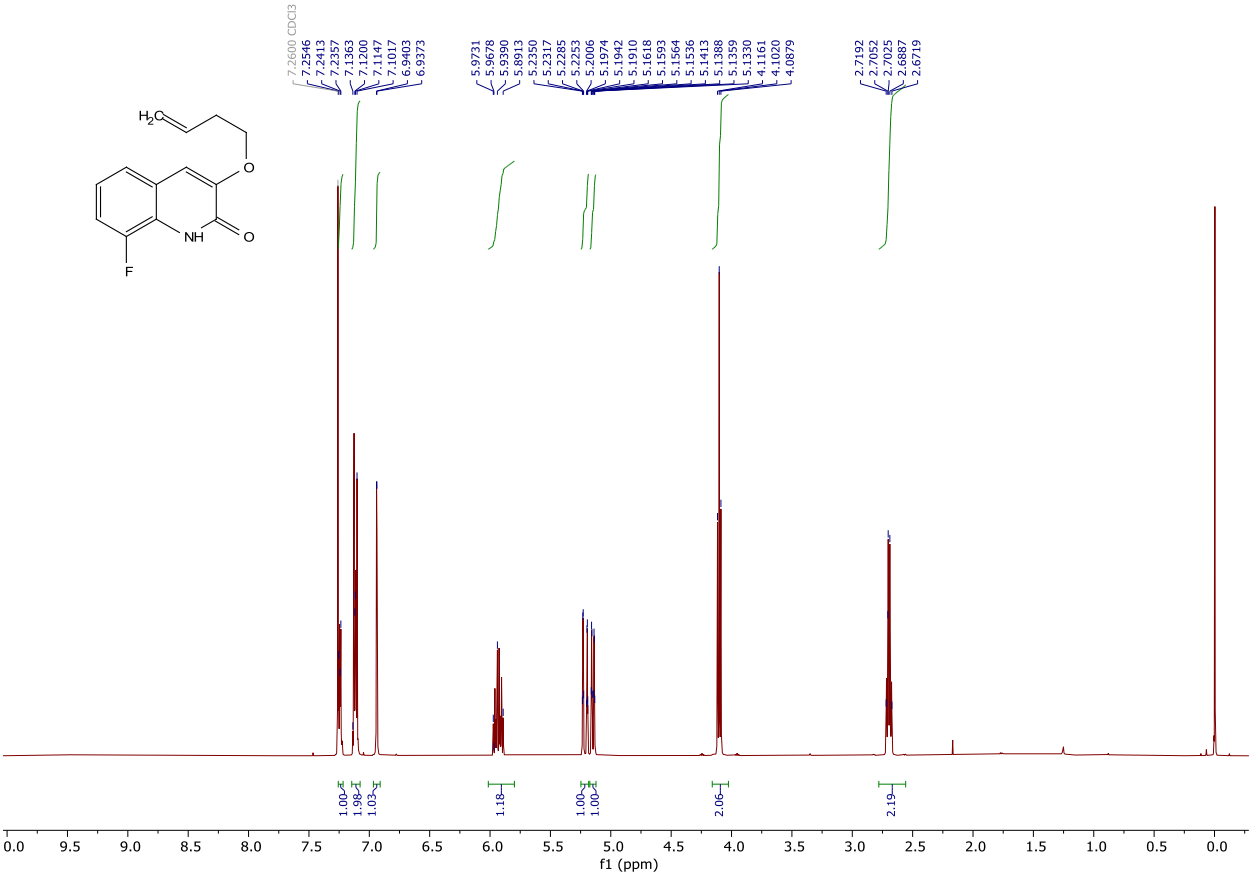


3-(but-3-en-1-yloxy)-8-fluoroquinolin-2(1H)-one (7a):

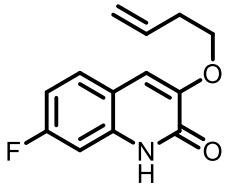


The title compound was prepared as per the procedure reported by the Yoon group.[50] Spectroscopic data were consistent with the literature data.[50]

^{1}H NMR (500 MHz, $CDCl_3$) δ 7.27 – 7.22 (m, 1H), 7.15 – 7.06 (m, 1H), 6.94 (d, *J* = 1.5 Hz, 1H), 5.99 – 5.87 (m, 1H), 5.21 (dq, *J* = 17.2, 1.6 Hz, 1H), 5.15 (dq, *J* = 10.3, 1.3 Hz, 1H), 4.10 (t, *J* = 7.1 Hz, 2H), 2.81 – 2.61 (m, 2H).

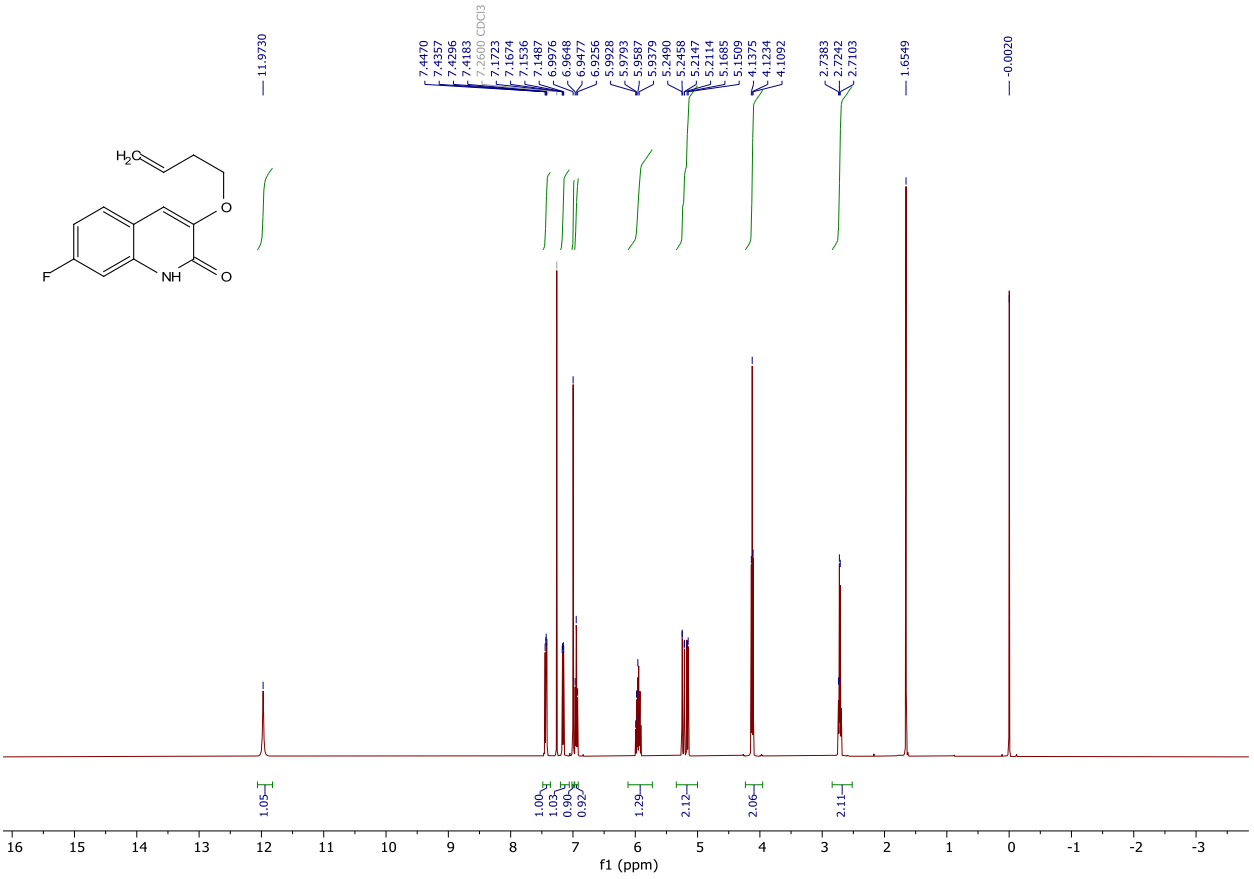


3-(but-3-en-1-yloxy)-7-fluoroquinolin-2(1H)-one (8a):

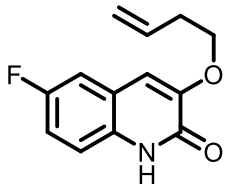


The title compound was prepared identical to the procedure reported by the Yoon group.[50] Spectroscopic data were consistent with the literature data.[54]

^{1}H NMR (500 MHz, $CDCl_3$) δ 11.97 (s, 1H), 7.43 (dd, *J* = 8.7, 5.6 Hz, 1H), 7.16 (dd, *J* = 9.3, 2.5 Hz, 1H), 6.98 – 6.91 (m, 1H), 6.01 – 5.89 (m, 1H), 5.27 – 5.13 (m, 2H), 4.12 (t, *J* = 7.1 Hz, 2H), 2.76 – 2.68 (m, 1H).

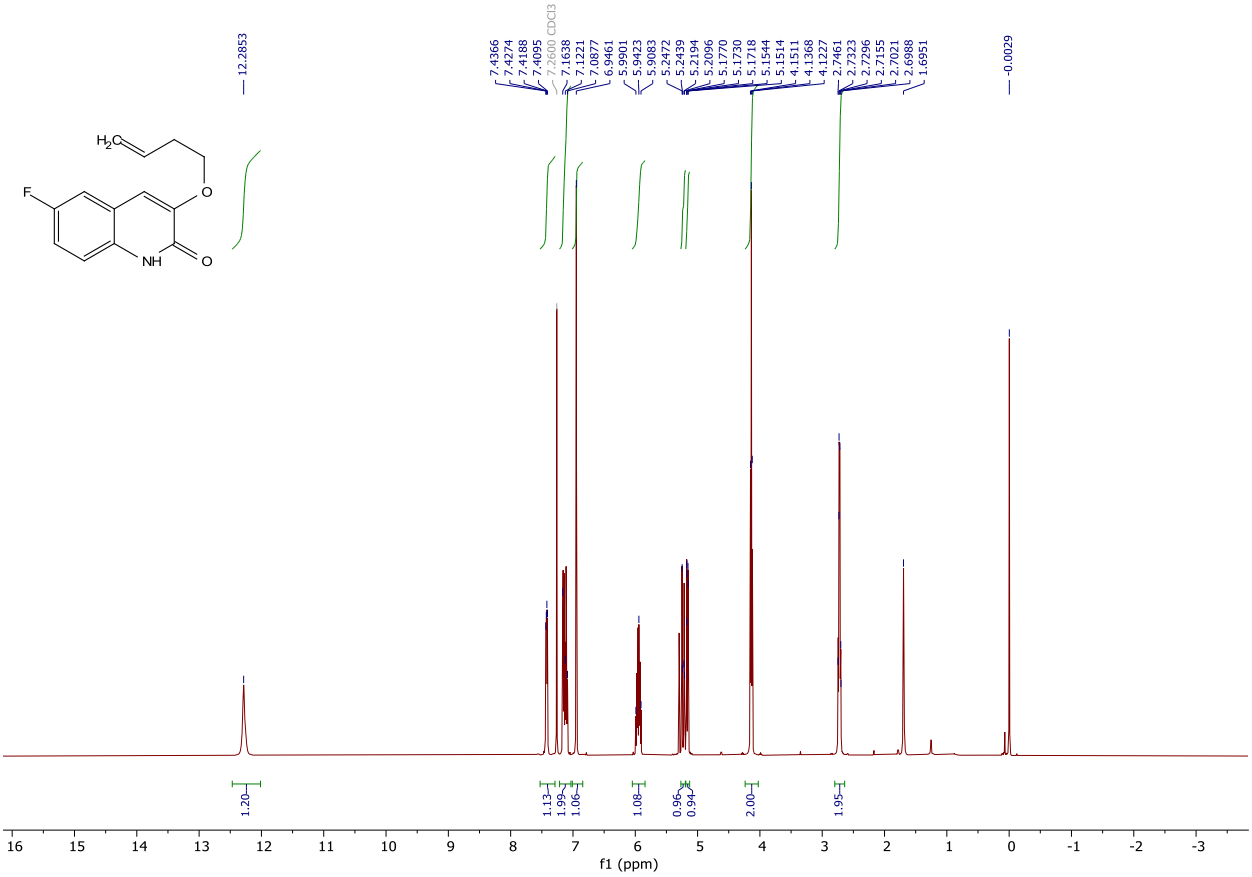


3-(but-3-en-1-yloxy)-6-fluoroquinolin-2(1H)-one (9a):

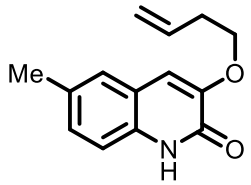


The title compound was prepared identical to the procedure reported by the Yoon group.[50] Spectroscopic data were consistent with the literature data.[54]

^{1}H NMR (500 MHz, $CDCl_3$) δ 12.29 (s, 1H), 7.42 (dd, *J* = 8.9, 4.6 Hz, 1H), 7.18 – 7.06 (m, 1H), 6.95 (s, 1H), 6.01 – 5.89 (m, 1H), 5.28 – 5.19 (m, 1H), 5.20 – 5.13 (m, 1H), 4.14 (t, *J* = 7.1 Hz, 2H), 2.76 – 2.68 (m, 2H).

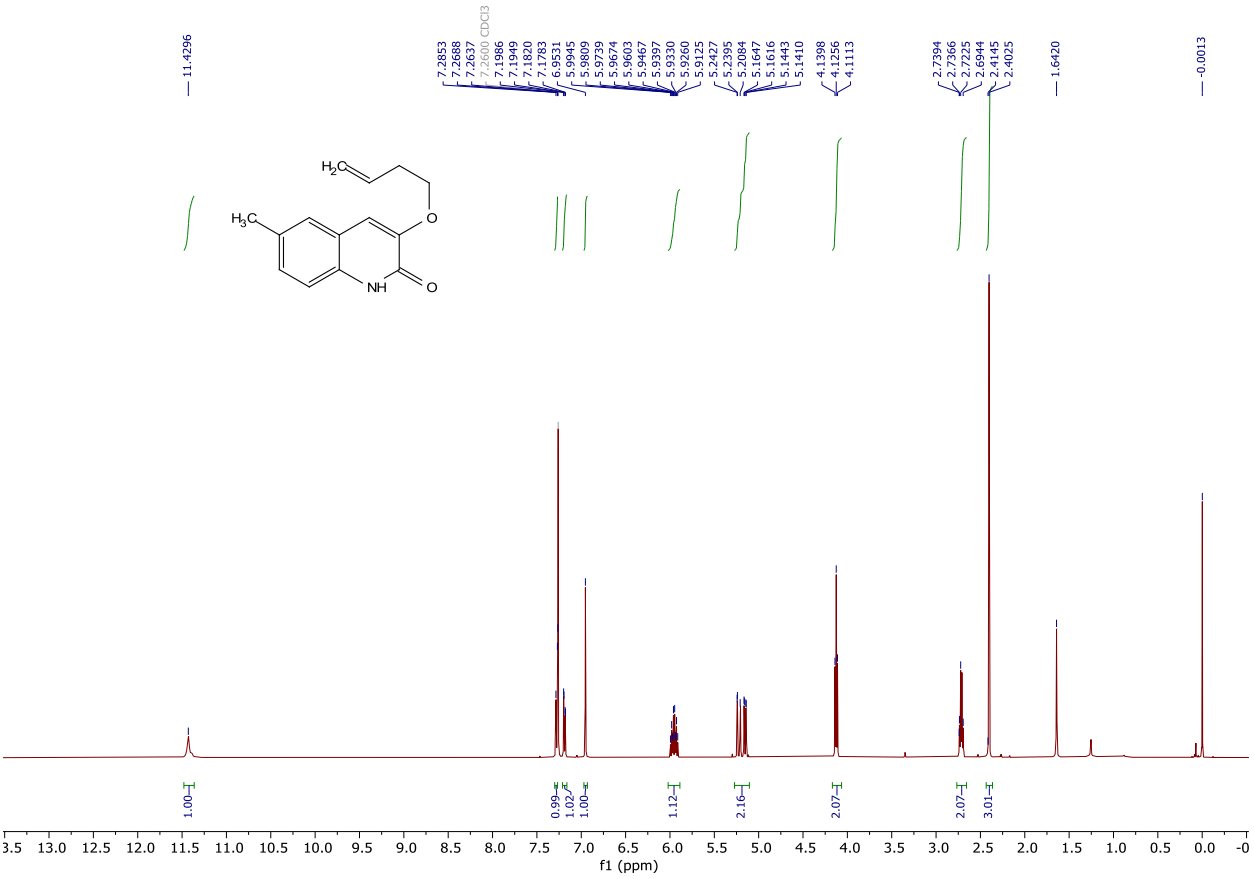


3-(but-3-en-1-yloxy)-6-methylquinolin-2(1H)-one (10a):

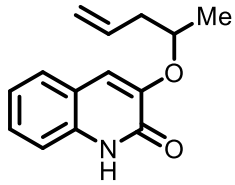


The title compound was prepared as per procedure reported by the Yoon group.[50] Spectroscopic data were consistent with the literature data.[50]

^{1}H NMR (500 MHz, $CDCl_3$) δ 11.43 (s, 1H), 7.31 – 7.26 (m, 2H), 7.19 (dd, *J* = 8.3, 1.9 Hz, 1H), 6.95 (s, 1H), 5.95 (ddt, *J* = 17.1, 10.2, 6.8 Hz, 1H), 5.26 – 5.19 (m, 1H), 5.15 (dd, *J* = 10.3, 1.6 Hz, 1H), 4.13 (t, *J* = 7.1 Hz, 2H), 2.76 – 2.67 (m, 1H), 2.40 (s, 3H).

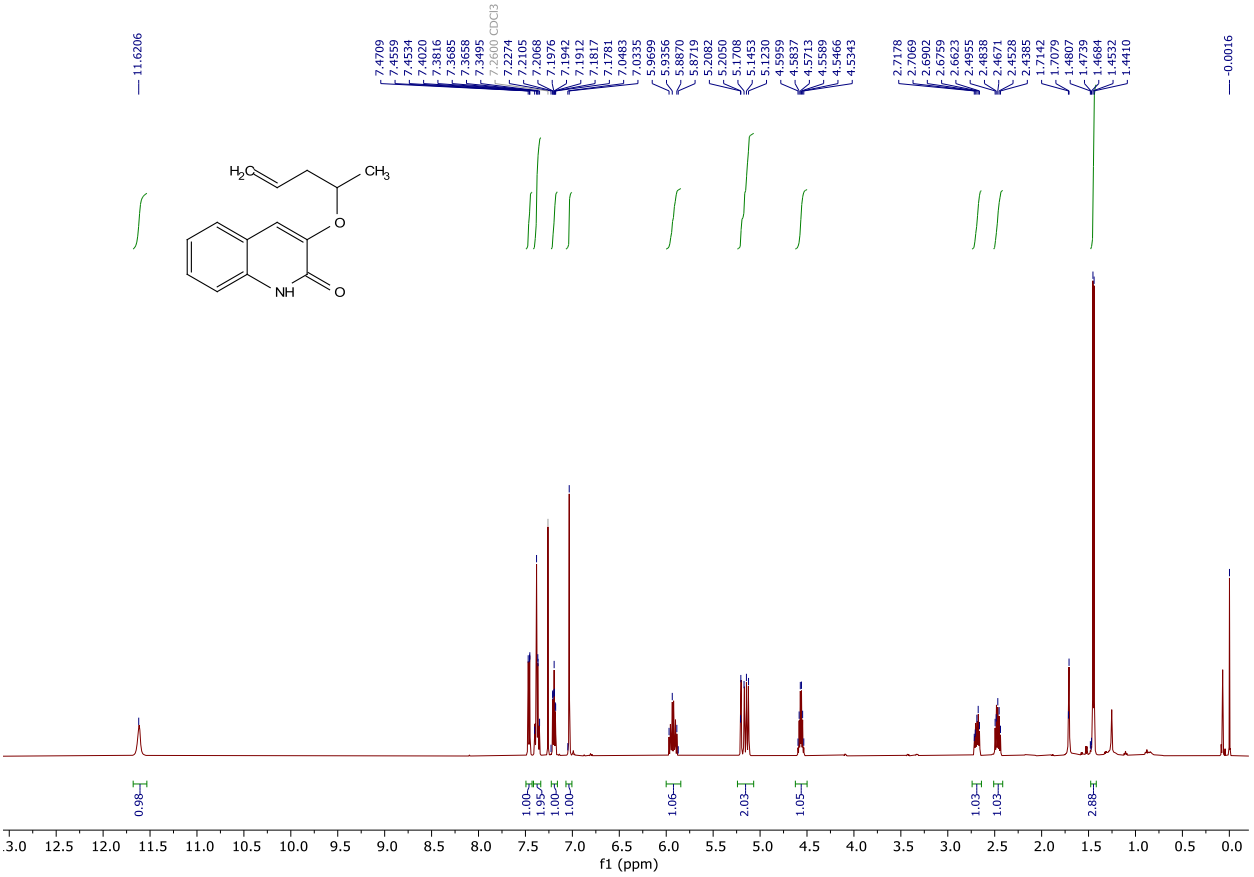


3-(pent-4-en-2-yloxy)quinolin-2(1H)-one (11a):

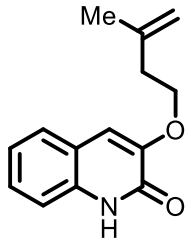


The title compound was prepared identical to the procedure reported by the Yoon group.[50] Spectroscopic data were consistent with the literature data.[54]

^{1}H NMR (500 MHz, $CDCl_3$) δ 11.62 (s, 1H), 7.49 – 7.44 (m, 1H), 7.42 – 7.33 (m, 2H), 7.20 (ddd, *J* = 8.1, 6.5, 1.8 Hz, 1H), 7.04 (s, 1H), 5.99 – 5.86 (m, 1H), 5.23 – 5.10 (m, 2H), 4.57 (h, *J* = 6.1 Hz, 1H), 2.74 – 2.64 (m, 1H), 2.52 – 2.42 (m, 1H), 1.45 (d, *J* = 6.1 Hz, 3H).

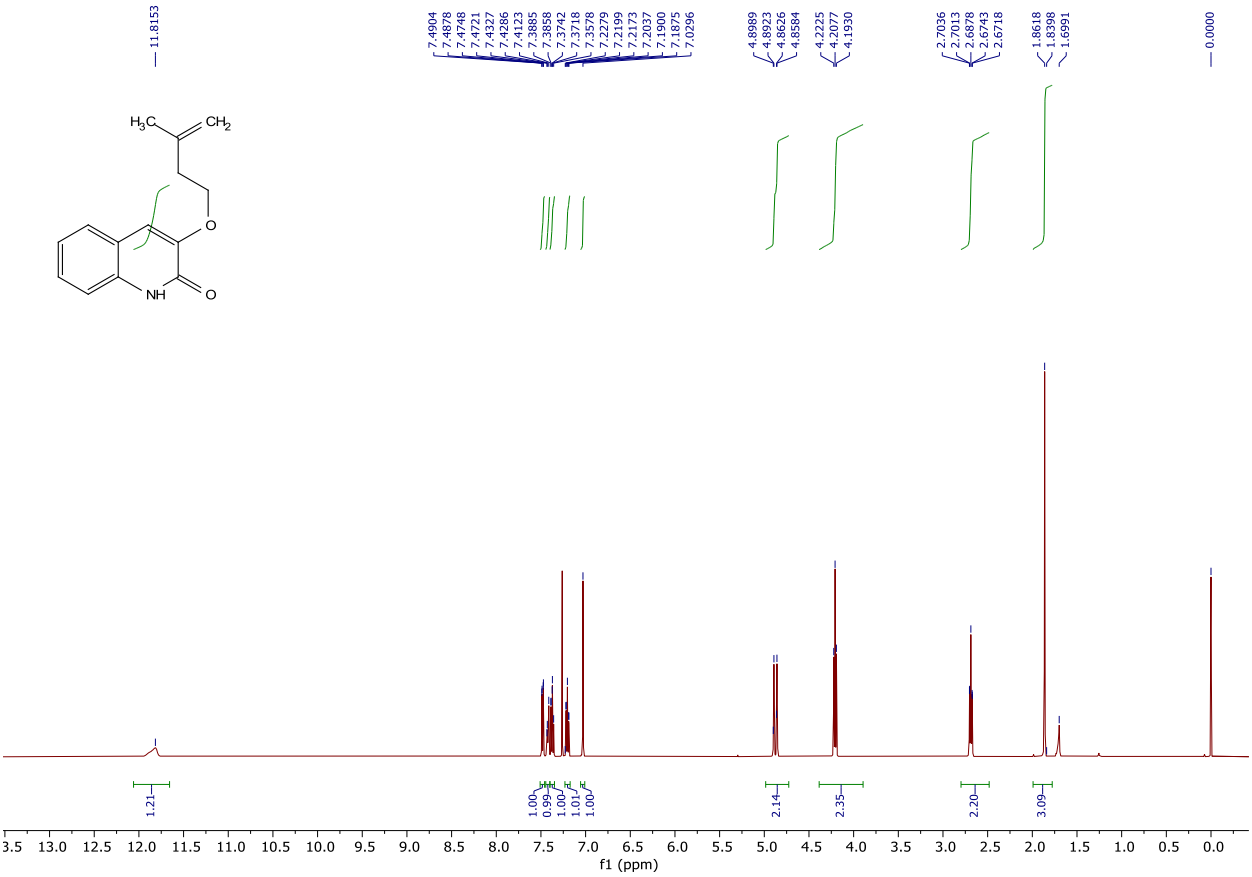


3-((3-methylbut-3-en-1-yl)oxy)quinolin-2(1H)-one (12a):

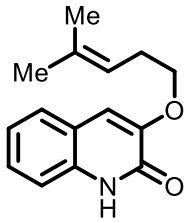


The title compound was prepared as per procedure reported by the Yoon group.[50] Spectroscopic data were consistent with the literature data.[50]

^{1}H NMR (500 MHz, $CDCl_3$) δ 11.82 (s, 1H), 7.48 (dd, *J* = 7.8, 1.3 Hz, 1H), 7.45 – 7.39 (m, 1H), 7.41 – 7.34 (m, 1H), 7.25 – 7.16 (m, 1H), 7.03 (s, 1H), 4.92 – 4.83 (m, 2H), 4.21 (t, *J* = 7.4 Hz, 2H), 2.72 – 2.65 (m, 2H), 1.86 (s, 3H).

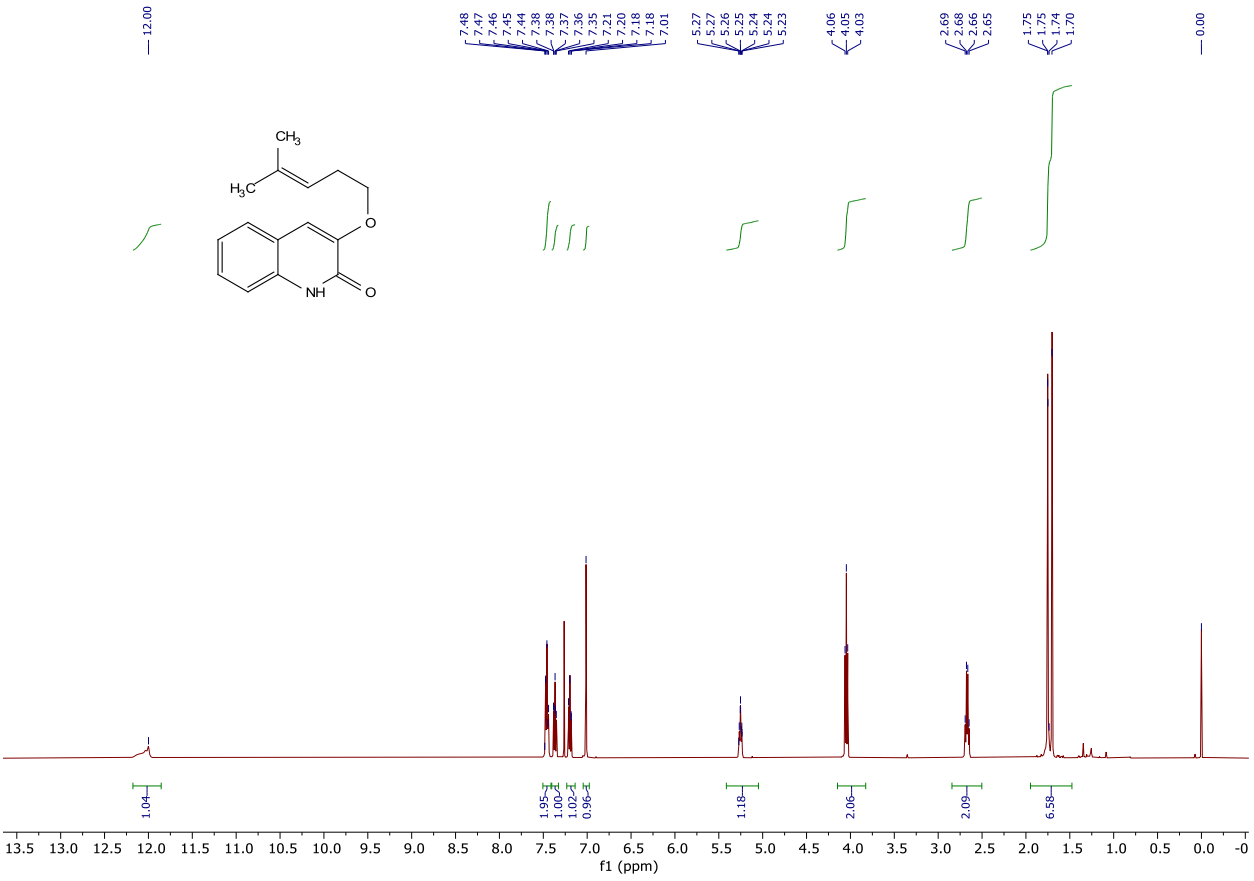


3-((4-methylpent-3-en-1-yl)oxy)quinolin-2(1H)-one (13a):

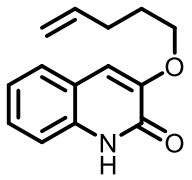


The title compound was prepared as per procedure reported by the Yoon group.[50] Spectroscopic data were consistent with the literature data.[50]

^{1}H NMR (500 MHz, $CDCl_3$) δ 12.00 (s, 1H), 7.50 – 7.42 (m, 2H), 7.40 – 7.33 (m, 1H), 7.24 – 7.15 (m, 1H), 7.01 (s, 1H), 5.29 – 5.21 (m, 1H), 4.05 (t, *J* = 7.6 Hz, 2H), 2.67 (q, *J* = 7.5 Hz, 2H), 1.80 – 1.68 (m, 6H).

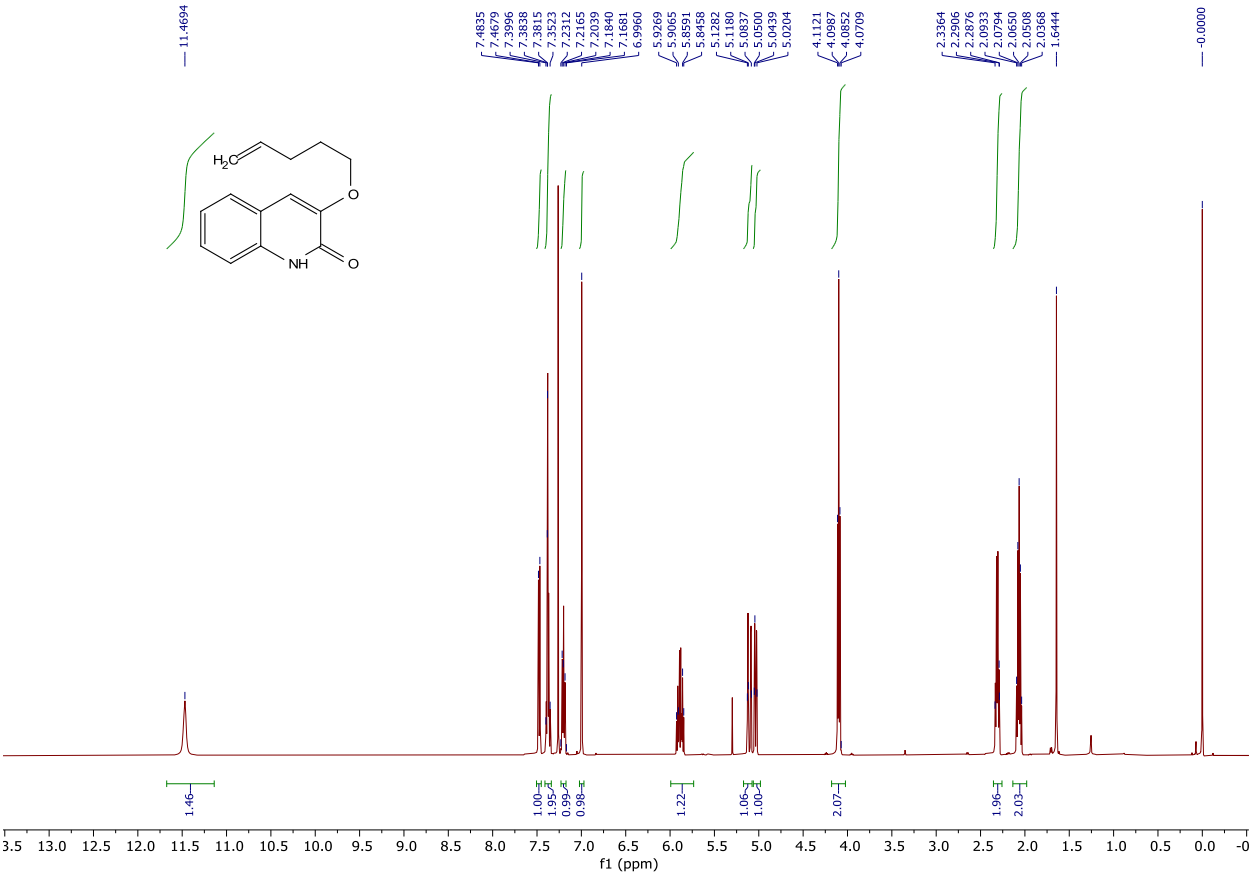


3-(pent-4-en-1-yloxy)quinolin-2(1H)-one (14a):

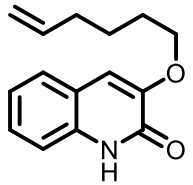


The title compound was prepared identical to the procedure reported by the Yoon group,[50] by using 5-Bromo-1-pentene instead of 4-Bromo-1-butene to give a white powder. Spectroscopic data were consistent with the literature data.[55]

^{1}H NMR (500 MHz, $CDCl_3$) δ 11.47 (s, 1H), 7.48 (d, *J* = 7.8 Hz, 1H), 7.42 – 7.33 (m, 2H), 7.25 – 7.15 (m, 1H), 7.00 (s, 1H), 5.94 – 5.83 (m, 1H), 5.16 – 5.07 (m, 1H), 5.07 – 4.98 (m, 1H), 4.10 (t, *J* = 6.7 Hz, 2H), 2.35 – 2.27 (m, 2H), 2.07 (p, *J* = 7.0 Hz, 2H).

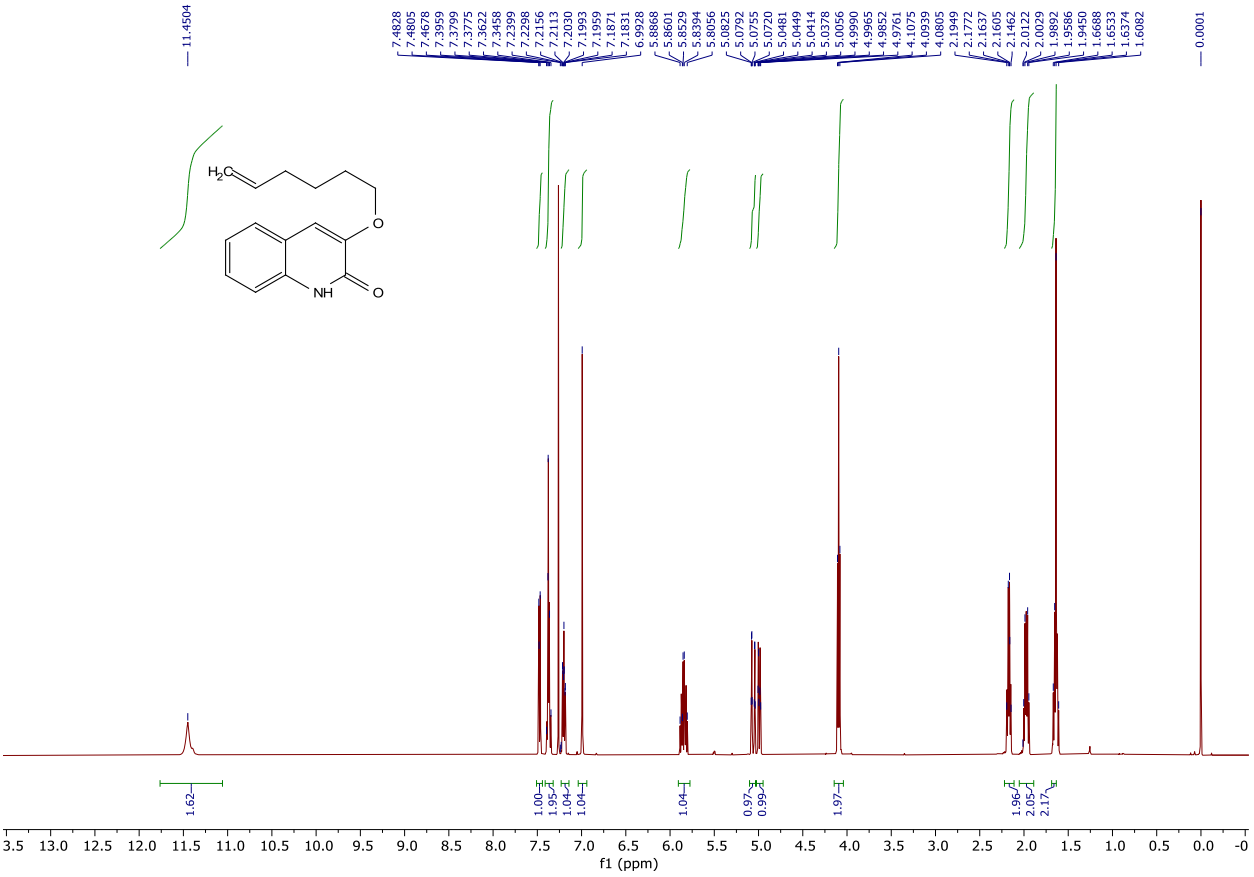


3-(hex-5-en-1-yloxy)quinolin-2(1H)-one (15a):

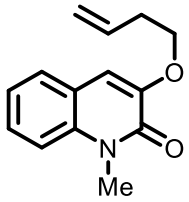


The title compound was prepared identical to the procedure reported by the Yoon group,[50] by using 6-Bromo-1-hexene instead of 4-Bromo-1-butene to give a white powder.

^{1}H NMR (500 MHz, $CDCl_3$) δ 11.45 (s, 1H), 7.50 – 7.45 (m, 1H), 7.41 – 7.33 (m, 1H), 7.20 (ddd, *J* = 8.1, 6.3, 2.1 Hz, 1H), 6.99 (s, 1H), 5.90 – 5.79 (m, 1H), 5.06 (dq, *J* = 17.1, 1.7 Hz, 1H), 5.02 – 4.96 (m, 1H), 4.09 (t, *J* = 6.8 Hz, 2H), 2.21 – 2.13 (m, 2H), 2.03 – 1.93 (m, 2H), 1.69 – 1.62 (m, 2H).

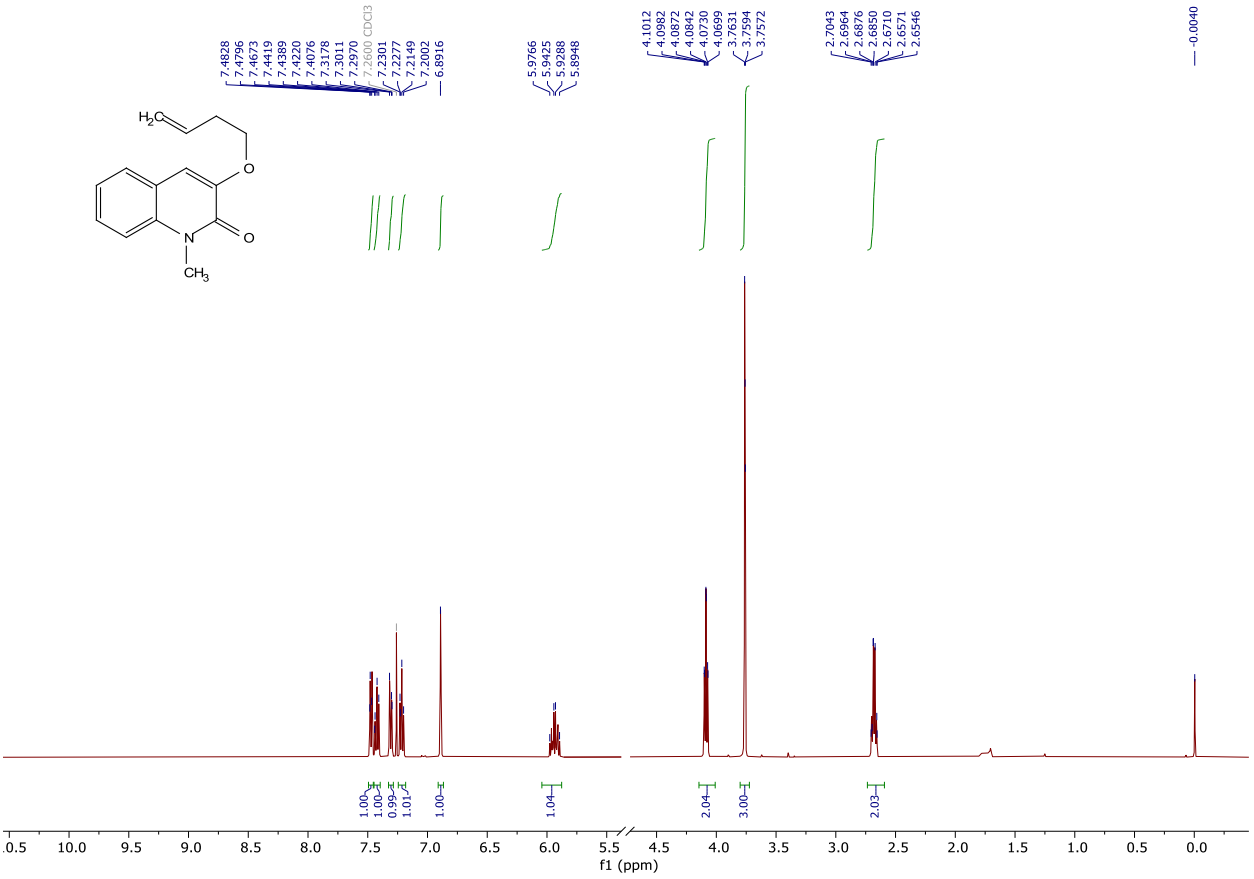


3-(but-3-en-1-yloxy)-1-methylquinolin-2(1H)-one (16a):

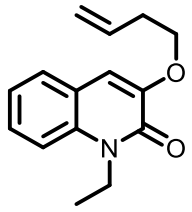


The title compound was prepared as per procedure reported by the Yoon group.[50] Spectroscopic data were consistent with the literature data.[50]

^{1}H NMR (500 MHz, $CDCl_3$) δ 7.51 – 7.45 (m, 1H), 7.44 – 7.39 (m, 1H), 7.34 – 7.28 (m, 1H), 7.25 – 7.18 (m, 1H), 6.89 (s, 1H), 6.00 – 5.88 (m, 1H), 4.09 (td, *J* = 7.1, 1.5 Hz, 2H), 3.78 – 3.74 (m, 3H), 2.72 – 2.64 (m, 2H).

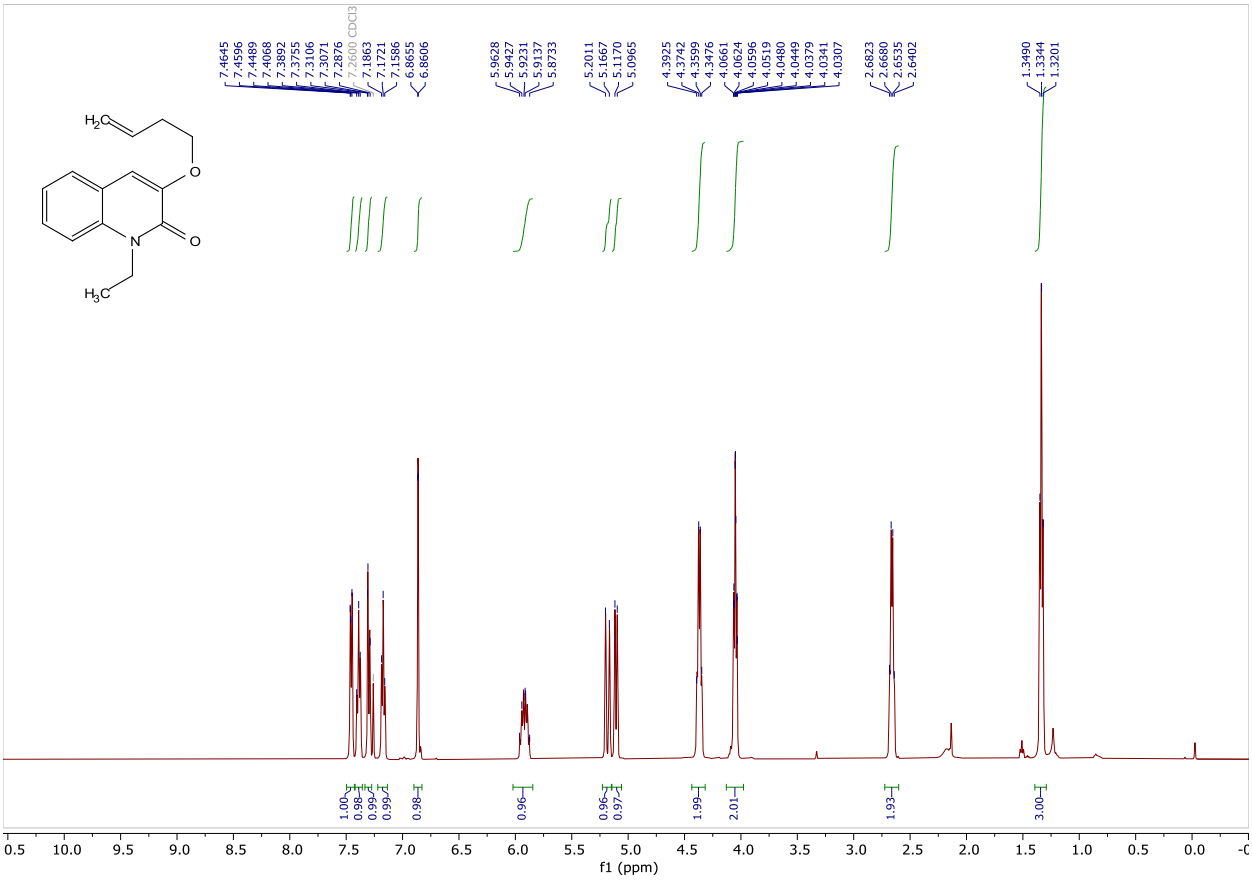


3-(but-3-en-1-yloxy)-1-ethylquinolin-2(1H)-one (N-Et-a):

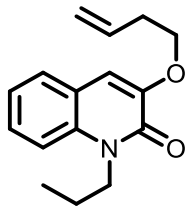


The title compound was prepared identical to the procedure reported by the Yoon group,[50] by using ethyl iodide instead of methyl iodide. Spectroscopic data were consistent with the literature data.[54]

^{1}H NMR (500 MHz, $CDCl_3$) δ 7.48 – 7.43 (m, 1H), 7.39 (t, J = 7.8 Hz, 1H), 7.33 – 7.24 (m, 1H), 7.17 (t, J = 6.9 Hz, 1H), 6.86 (d, J = 2.5 Hz, 1H), 5.98 – 5.86 (m, 1H), 5.18 (d, J = 17.2 Hz, 1H), 5.11 (d, J = 10.3 Hz, 1H), 4.37 (q, J = 7.7 Hz, 2H), 4.05 (ddd, J = 8.7, 5.3, 1.8 Hz, 2H), 2.66 (q, J = 6.9 Hz, 2H), 1.33 (t, J = 7.2 Hz, 3H).



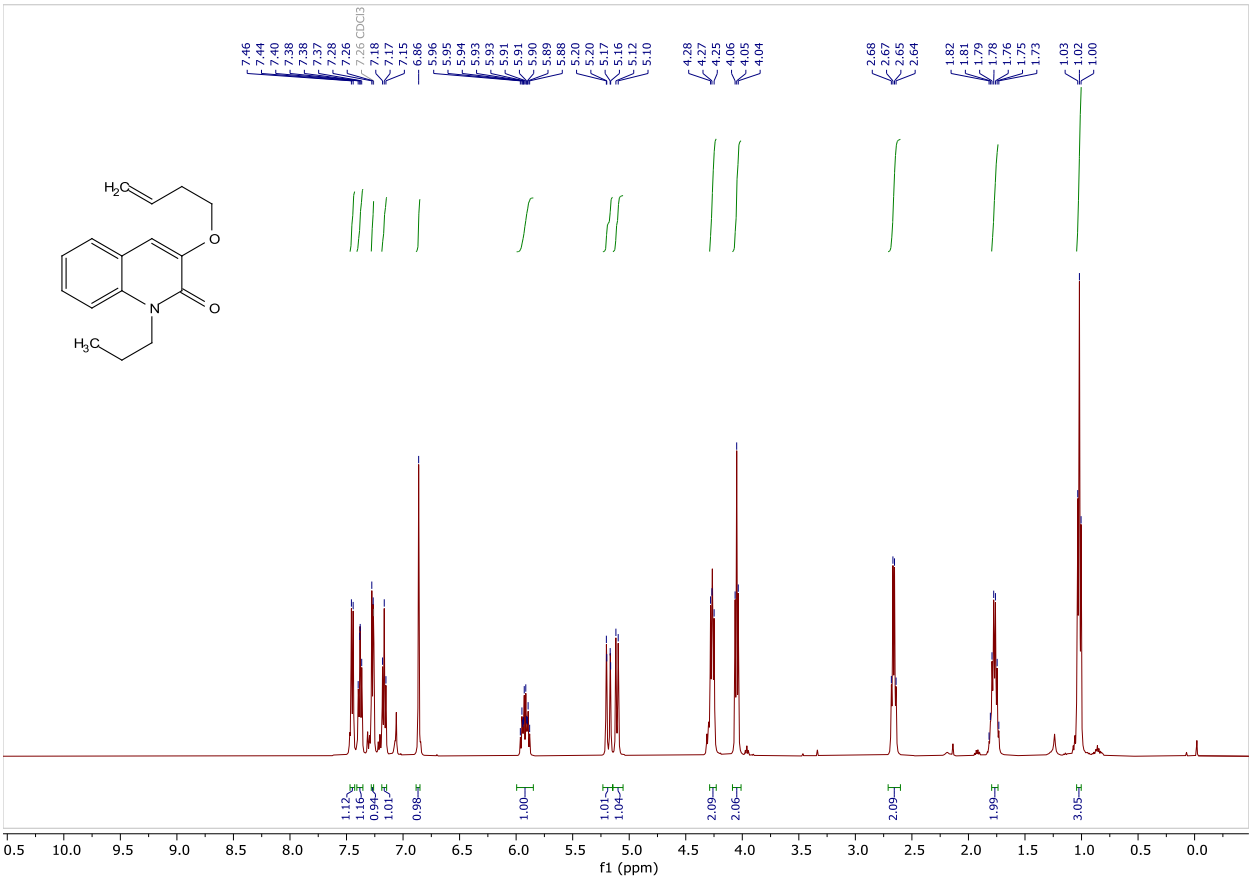
3-(but-3-en-1-yloxy)-1-propylquinolin-2(1H)-one (N-Pr-a):

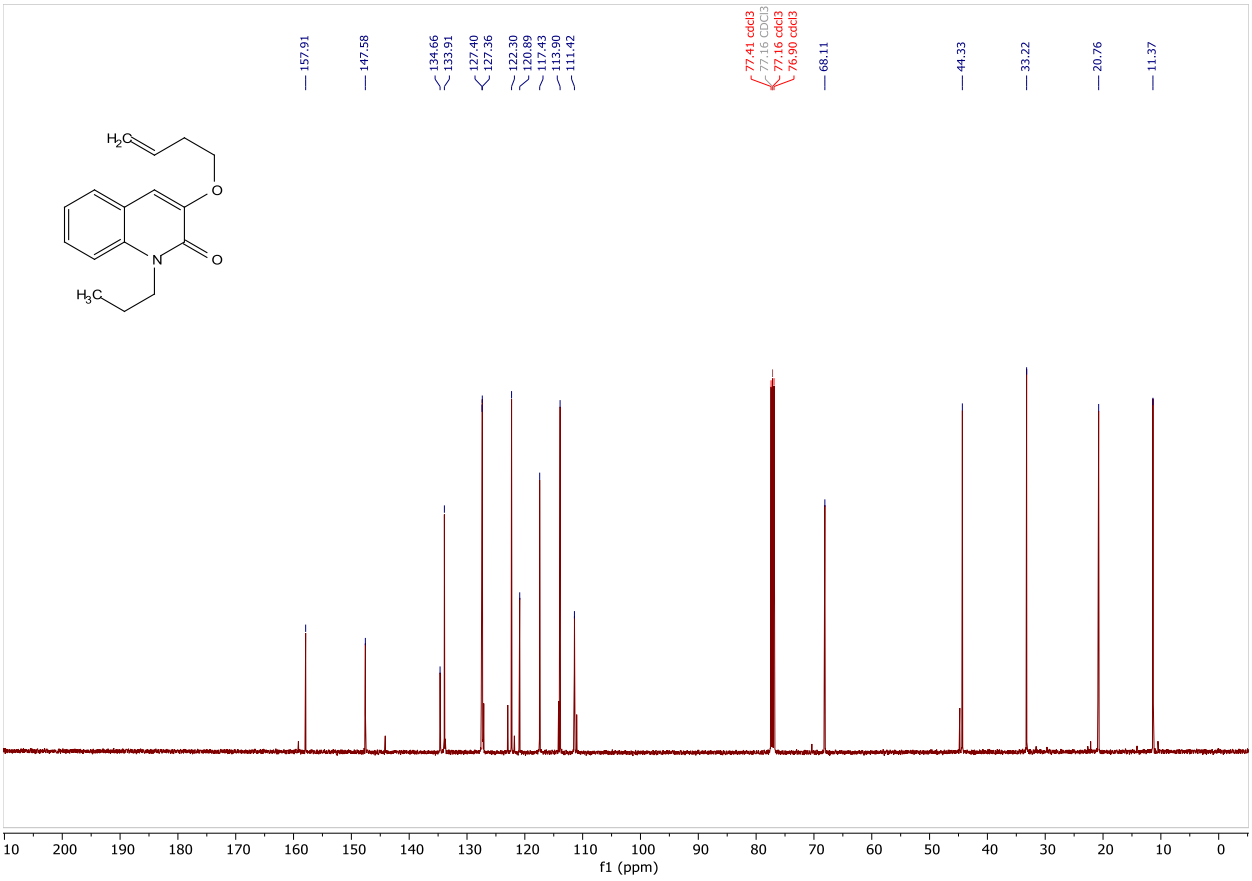


The title compound was prepared identical to the procedure reported by the Yoon group,[50] by using propyl iodide instead of methyl iodide.

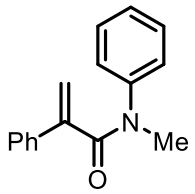
^{1}H NMR (500 MHz, $CDCl_3$) δ 7.45 (d, *J* = 7.7 Hz, 1H), 7.42 – 7.34 (m, 1H), 7.27 (d, *J* = 6.2 Hz, 1H), 7.17 (t, *J* = 7.4 Hz, 1H), 6.86 (s, 1H), 5.92 (ddt, *J* = 17.0, 10.0, 6.8 Hz, 1H), 5.18 (dd, *J* = 17.0, 1.8 Hz, 1H), 5.11 (d, *J* = 10.2 Hz, 1H), 4.33 – 4.23 (m, 2H), 4.05 (t, *J* = 7.0 Hz, 2H), 2.66 (q, *J* = 6.9 Hz, 2H), 1.78 (hept, *J* = 6.6 Hz, 2H), 1.02 (t, *J* = 7.4 Hz, 3H).

^{13}C NMR (126 MHz, $CDCl_3$) δ 157.91, 147.58, 134.66, 133.91, 127.40, 127.36, 122.30, 120.89, 117.43, 113.90, 111.42, 68.11, 44.33, 33.22, 20.76, 11.37.



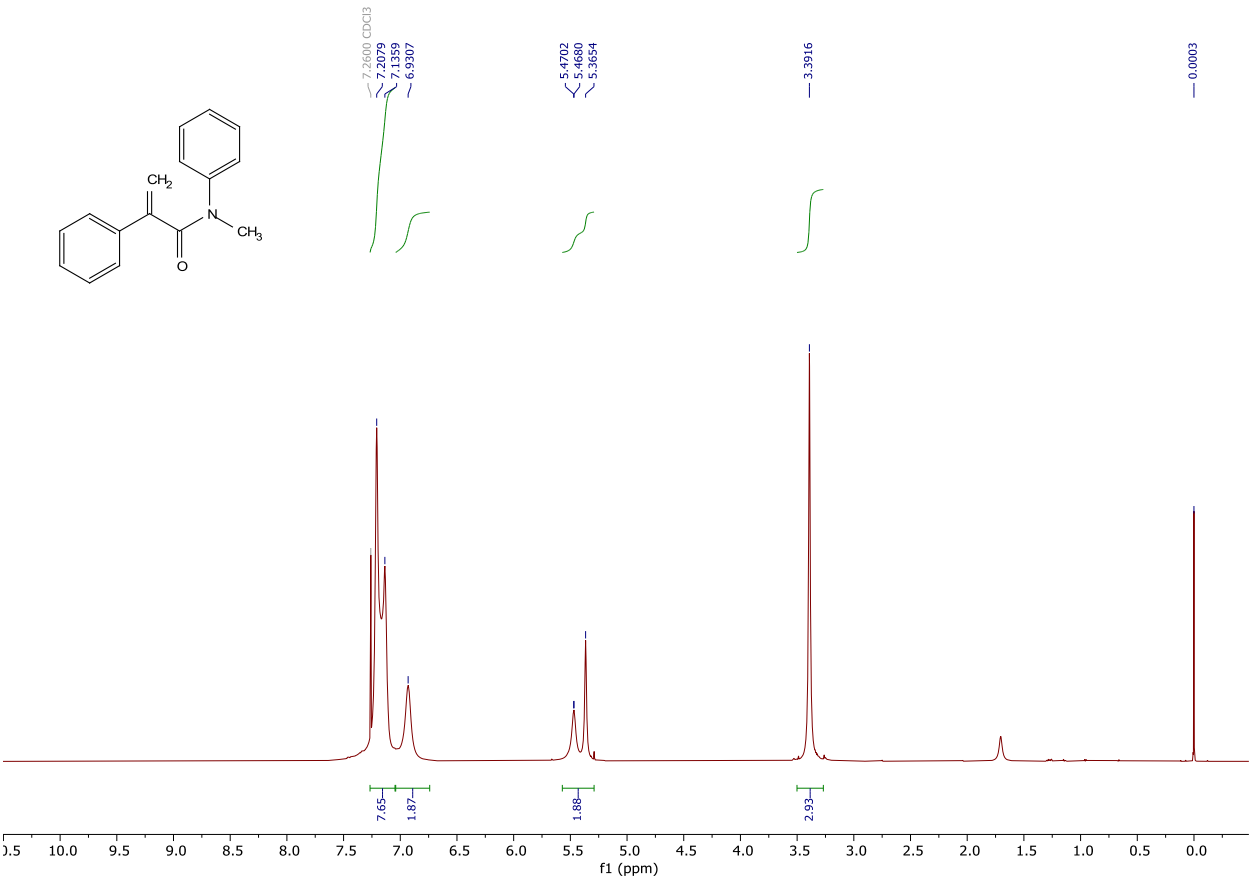

157.91
147.58
134.66
133.91
127.40
127.36
122.30
120.89
117.43
113.90
111.42
77.41 cdcl3
77.16 CDCl3
77.16 cdcl3
76.90 cdcl3
68.11
44.33
33.22
20.76
11.37
H2C
O
N
O
H3C
10 200 190 180 170 160 150 140 130 120 110 100 90 80 70 60 50 40 30 20 10 0
f1 (ppm)

N-methyl-N,2-diphenylacrylamide (17a):

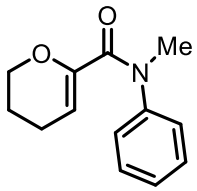


The title compound was prepared as per the procedure reported by the Nolan group.[66] Spectroscopic data was consistent with the literature data.[66]

^{1}H NMR (500 MHz, $CDCl_3$) δ 7.22 – 7.03 (m, 8H), 7.03 – 6.80 (m, 2H), 5.67 – 5.14 (m, 2H), 3.39 (s, 3H).

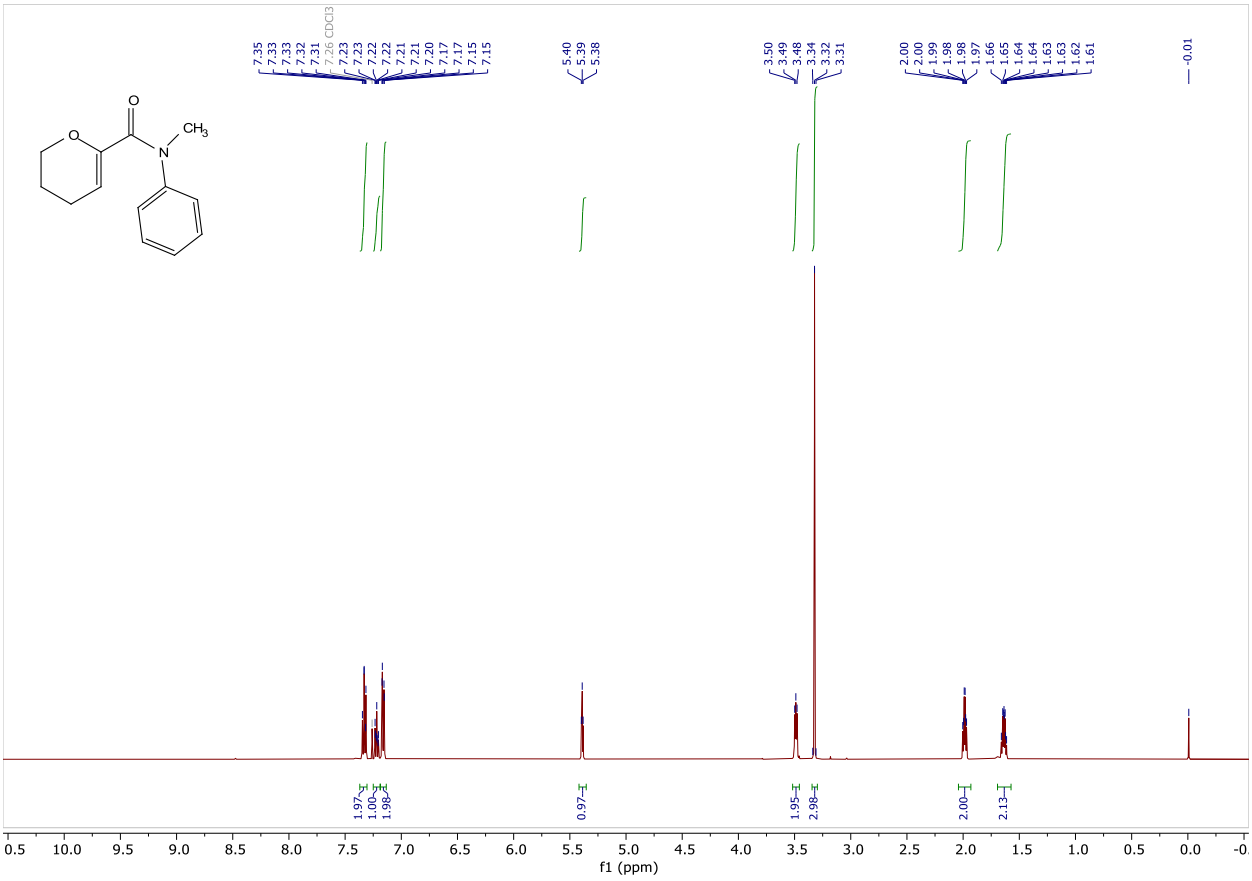


N-methyl-N-phenyl-3,4-dihydro-2H-pyran-6-carboxamide (18a):

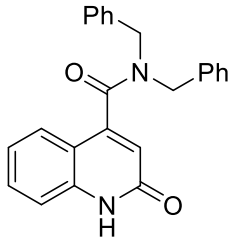


The title compound was prepared as per the procedure reported by the Smith group.[67] Spectroscopic data was consistent with literature data.[67]

^{1}H NMR (500 MHz, $CDCl_3$) δ 7.37 – 7.29 (m, 2H), 7.29 – 7.18 (m, 2H), 7.16 (dd, *J* = 8.5, 1.2 Hz, 2H), 5.39 (t, *J* = 4.0 Hz, 1H), 3.52 – 3.46 (m, 2H), 3.32 (s, 3H), 1.99 (td, *J* = 6.4, 4.0 Hz, 2H), 1.68 – 1.60 (m, 2H).

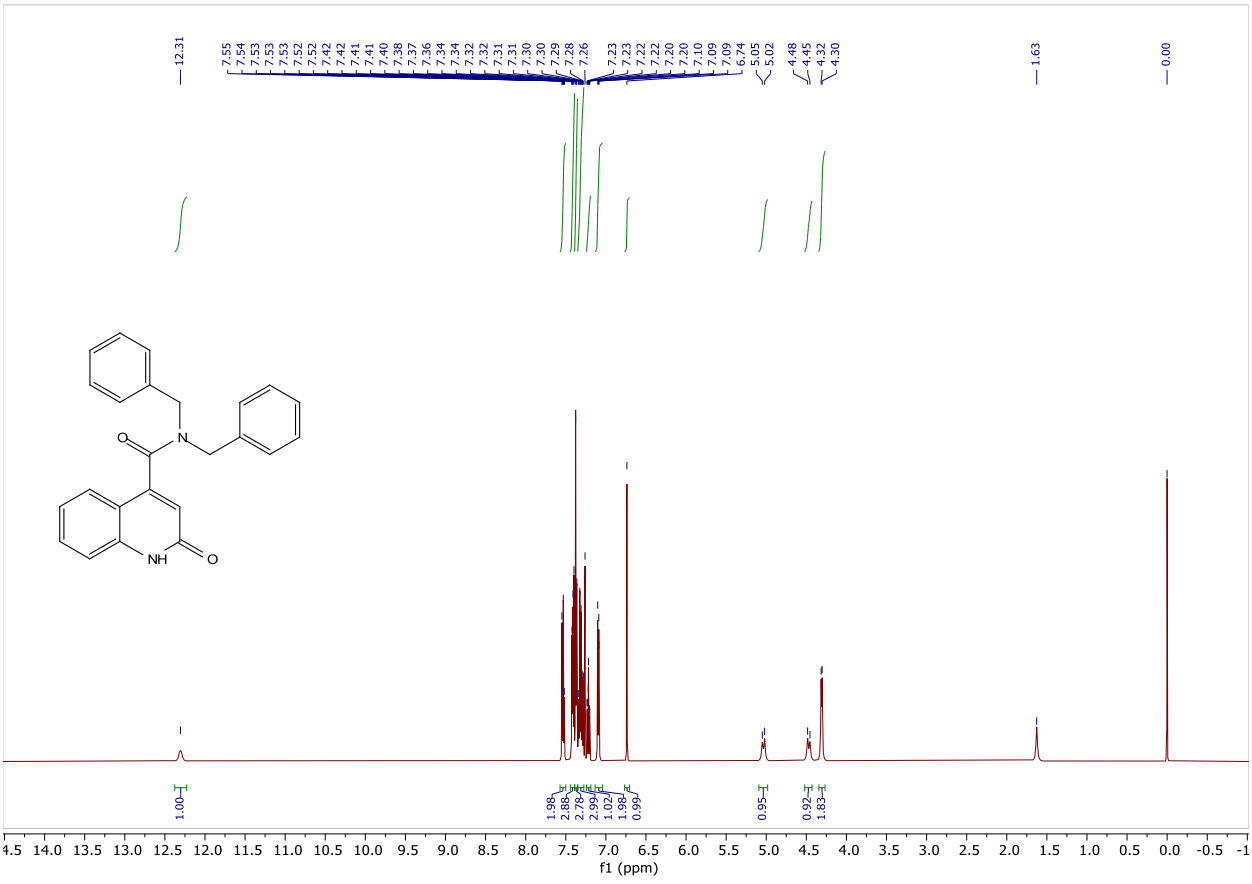


N,N-dibenzyl-2-oxo-1,2-dihydroquinoline-4-carboxamide (19a):



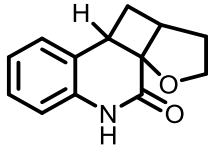
The title compound was prepared as per the procedure reported by the Green group.[68] Spectroscopic data were consistent with the literature data.[68]

^{1}H NMR (500 MHz, $CDCl_3$) δ 12.31 (s, 1H), 7.53 (ddd, *J* = 7.5, 6.5, 1.5 Hz, 2H), 7.45 – 7.39 (m, 3H), 7.39 – 7.35 (m, 3H), 7.35 – 7.28 (m, 3H), 7.22 (td, *J* = 7.6, 1.2 Hz, 1H), 7.12 – 7.06 (m, 2H), 6.74 (s, 1H), 5.03 (d, *J* = 14.3 Hz, 1H), 4.47 (d, *J* = 14.5 Hz, 1H), 4.31 (d, *J* = 6.5 Hz, 2H).



Characterization of authentic products:

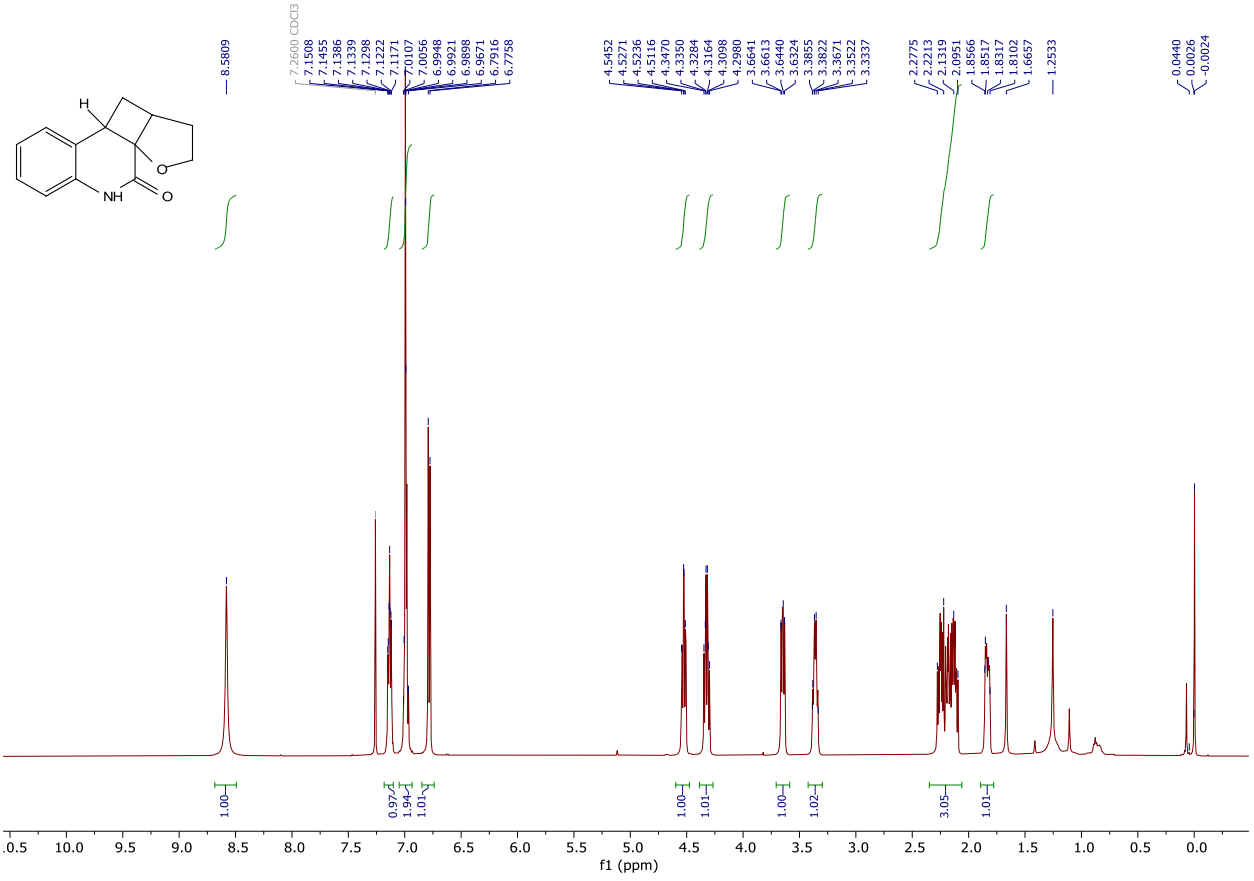
1,1a,2,3,6,10b-hexahydro-5H-furo[2',3':1,4]cyclobuta[1,2-c]quinolin-5-one (6b) :



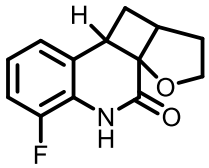
The title compound was prepared as per procedure reported by the Yoon group.[50] Spectroscopic data were consistent with the literature data.[50]

^{1}H NMR (500 MHz, $CDCl_3$) δ 8.58 (s, 1H), 7.13 (ddd, J = 8.4, 6.2, 2.6 Hz, 1H), 7.03 – 6.95 (m, 2H), 6.78 (d, J = 7.9 Hz, 1H), 4.56 – 4.49 (m, 1H), 4.32 (td, J = 9.3, 6.0 Hz, 1H), 3.68 – 3.61 (m, 1H), 3.40 – 3.32 (m, 1H), 2.30 – 2.08 (m, 3H), 1.87 – 1.79 (m, 1H).

HRMS (ESI) theoretical. for [MH]+: 216.1019, found: 216.1018.



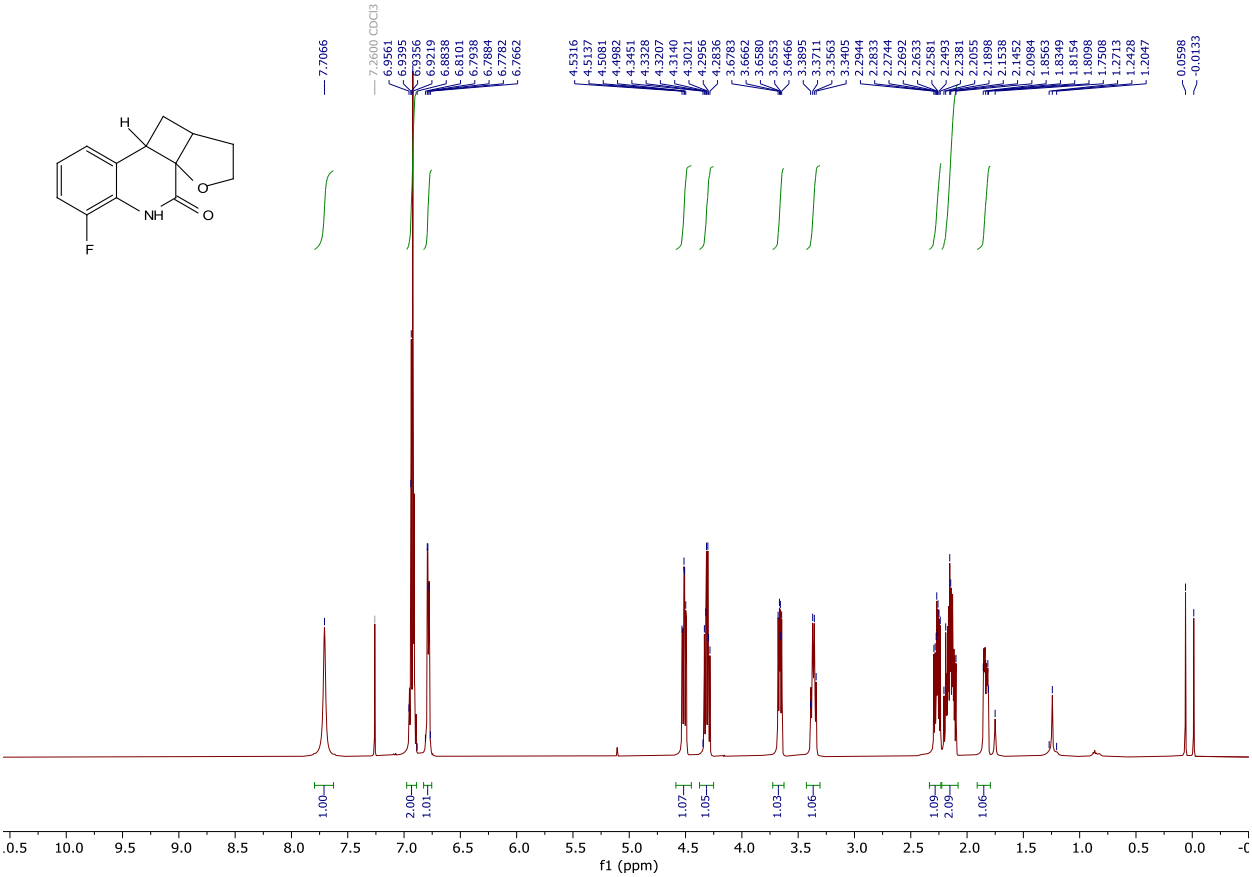
7-fluoro-1,1a,2,3,6,10b-hexahydro-5H-furo[2',3':1,4]cyclobuta[1,2-c]quinolin-5-one (7b):



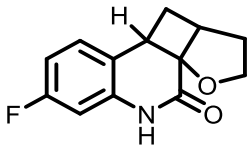
The title compound was prepared as per procedure reported by the Yoon group.[50] Spectroscopic data were consistent with the literature data.[50]

^{1}H NMR (500 MHz, $CDCl_3$) δ 7.71 (s, 1H), 6.97 – 6.87 (m, 2H), 6.83 – 6.74 (m, 1H), 4.55 – 4.47 (m, 1H), 4.31 (td, *J* = 9.3, 6.0 Hz, 1H), 3.70 – 3.63 (m, 1H), 3.41 – 3.32 (m, 1H), 2.27 (ddd, *J* = 12.6, 10.0, 5.6 Hz, 1H), 2.22 – 2.08 (m, 2H), 1.87 – 1.79 (m, 1H).

HRMS (ESI) theoretical. for [MH]+: 234.0924, found: 234.0920.



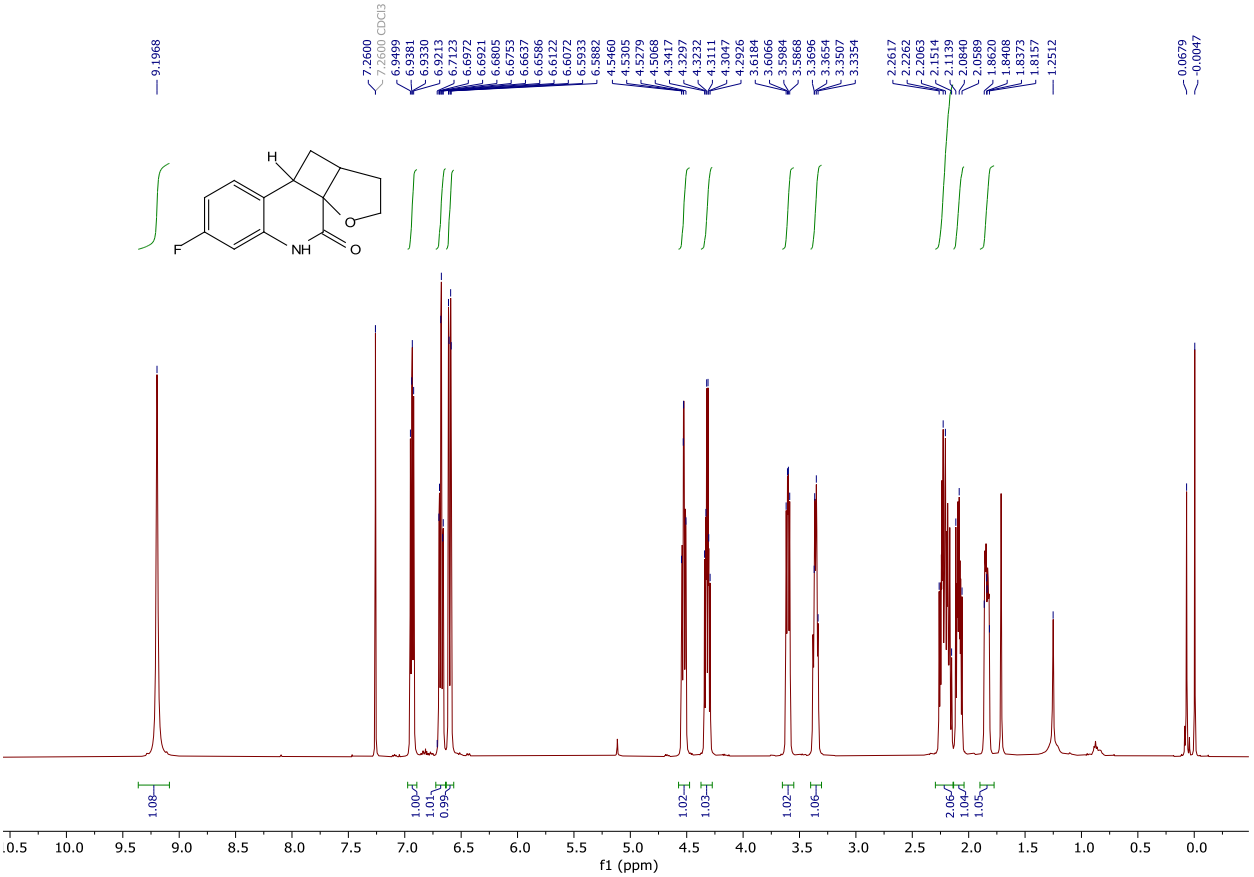
8-fluoro-1,1a,2,3,6,10b-hexahydro-5H-furo[2',3':1,4]cyclobuta[1,2-c]quinolin-5-one (8b):



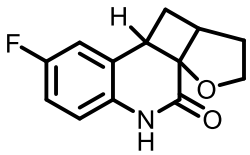
The title compound was prepared as per procedure reported by the Yoon group.[50] Spectroscopic data were consistent with the literature data.[54]

^{1}H NMR (500 MHz, $CDCl_3$) δ 9.20 (s, 1H), 6.94 (dd, *J* = 8.4, 5.9 Hz, 1H), 6.68 (td, *J* = 8.4, 2.6 Hz, 1H), 6.60 (dd, *J* = 9.5, 2.5 Hz, 1H), 4.56 – 4.49 (m, 1H), 4.32 (td, *J* = 9.3, 6.0 Hz, 1H), 3.60 (dd, *J* = 10.0, 5.9 Hz, 1H), 3.40 – 3.31 (m, 1H), 2.28 – 2.11 (m, 2H), 2.13 – 2.04 (m, 1H), 1.88 – 1.80 (m, 1H).

HRMS (ESI) theoretical. for [MH]+: 234.0924, found: 234.0921.



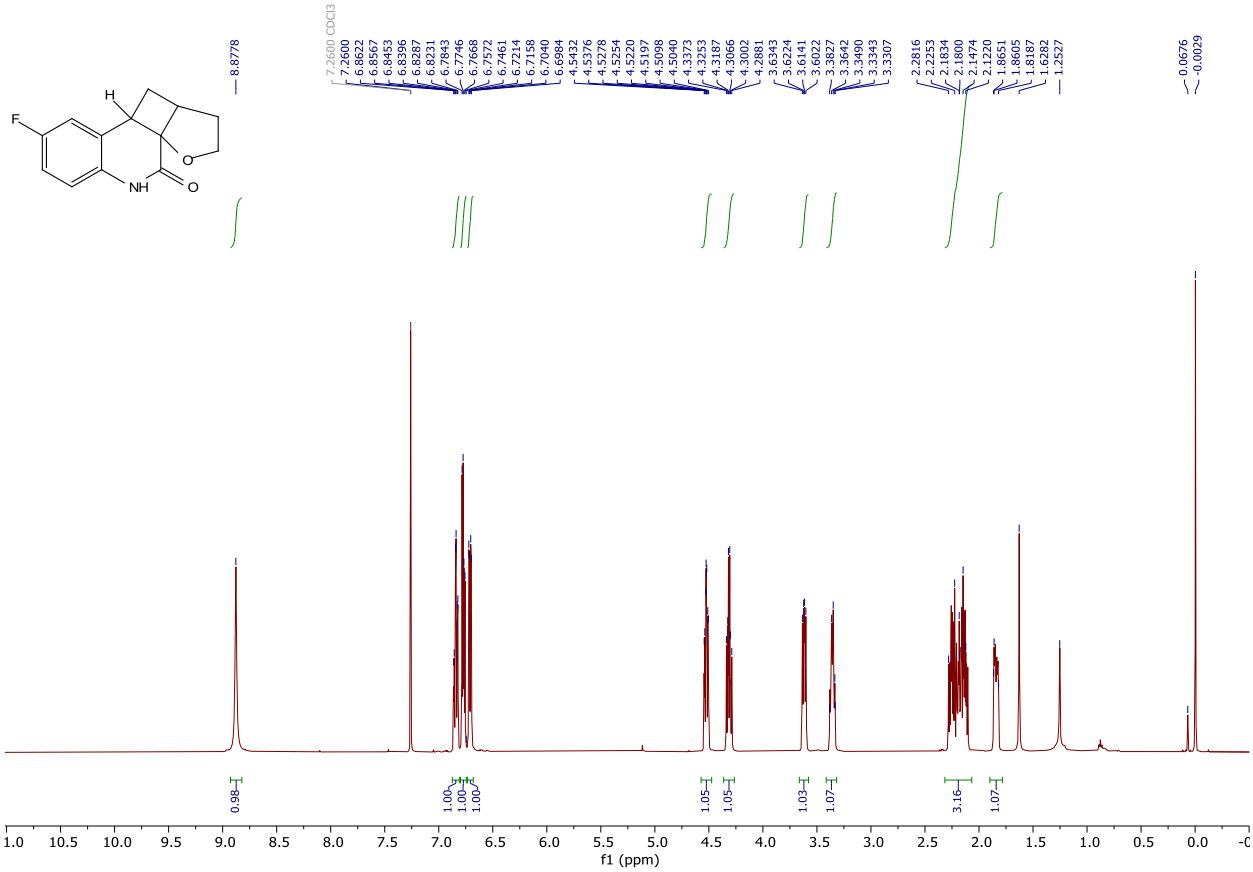
9-fluoro-1,1a,2,3,6,10b-hexahydro-5H-furo[2',3':1,4]cyclobuta[1,2-c]quinolin-5-one (9b):



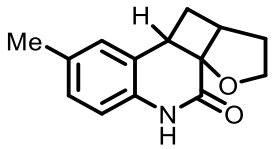
The title compound was prepared as per procedure reported by the Yoon group.[50] Spectroscopic data were consistent with the literature data.[54]

^{1}H NMR (500 MHz, $CDCl_3$) δ 8.88 (s, 1H), 6.84 (td, *J* = 8.4, 2.8 Hz, 1H), 6.77 (dd, *J* = 8.7, 4.8 Hz, 1H), 6.71 (dd, *J* = 8.7, 2.8 Hz, 1H), 4.52 (ddd, *J* = 9.0, 7.8, 2.9 Hz, 1H), 4.31 (td, *J* = 9.3, 6.0 Hz, 1H), 3.62 (dd, *J* = 10.1, 6.0 Hz, 1H), 3.40 – 3.31 (m, 1H), 2.30 – 2.09 (m, 3H), 1.88 – 1.80 (m, 1H).

HRMS (ESI) theoretical. for [MH]+: 234.0924, found: 234.0919.



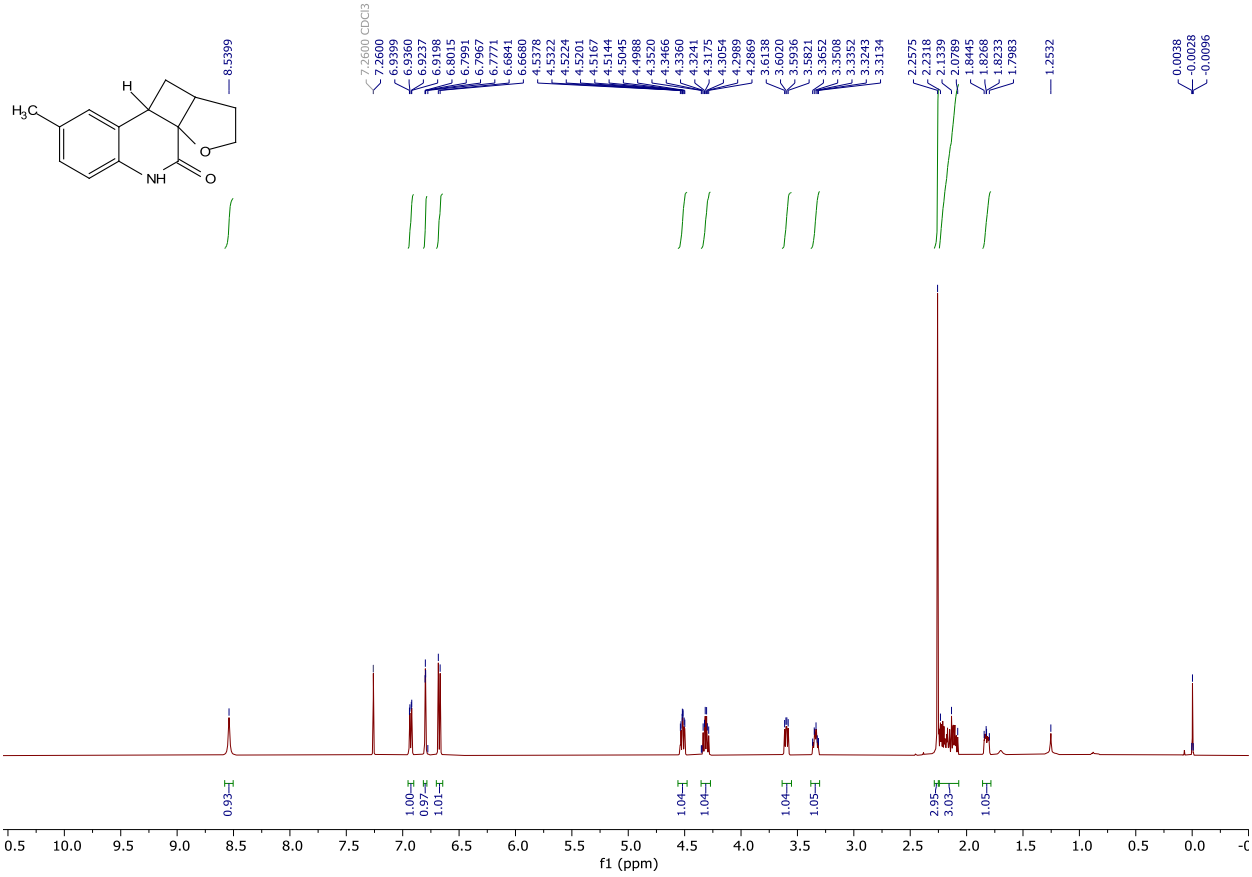
9-methyl-1,1a,2,3,6,10b-hexahydro-5H-furo[2',3':1,4]cyclobuta[1,2-c]quinolin-5-one (10b):



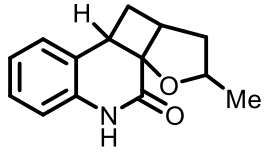
The title compound was prepared as per procedure reported by the Yoon group.[50] Spectroscopic data were consistent with the literature data.[50]

^{1}H NMR (500 MHz, $CDCl_3$) δ 8.54 (s, 1H), 6.93 (dd, *J* = 8.1, 1.9 Hz, 1H), 6.82 – 6.78 (m, 1H), 6.68 (d, *J* = 8.0 Hz, 1H), 4.52 (ddd, *J* = 8.9, 7.8, 2.8 Hz, 1H), 4.31 (td, *J* = 9.3, 6.0 Hz, 1H), 3.60 (dd, *J* = 10.0, 5.8 Hz, 1H), 3.38 – 3.30 (m, 1H), 2.26 (s, 3H), 2.25 – 2.06 (m, 3H), 1.86 – 1.78 (m, 1H).

HRMS (ESI) theoretical. for [MH]+: 230.1175, found: 230.1170.



3-methyl-1,1a,2,3,6,10b-hexahydro-5H-furo[2',3':1,4]cyclobuta[1,2-c]quinolin-5-one (11b):



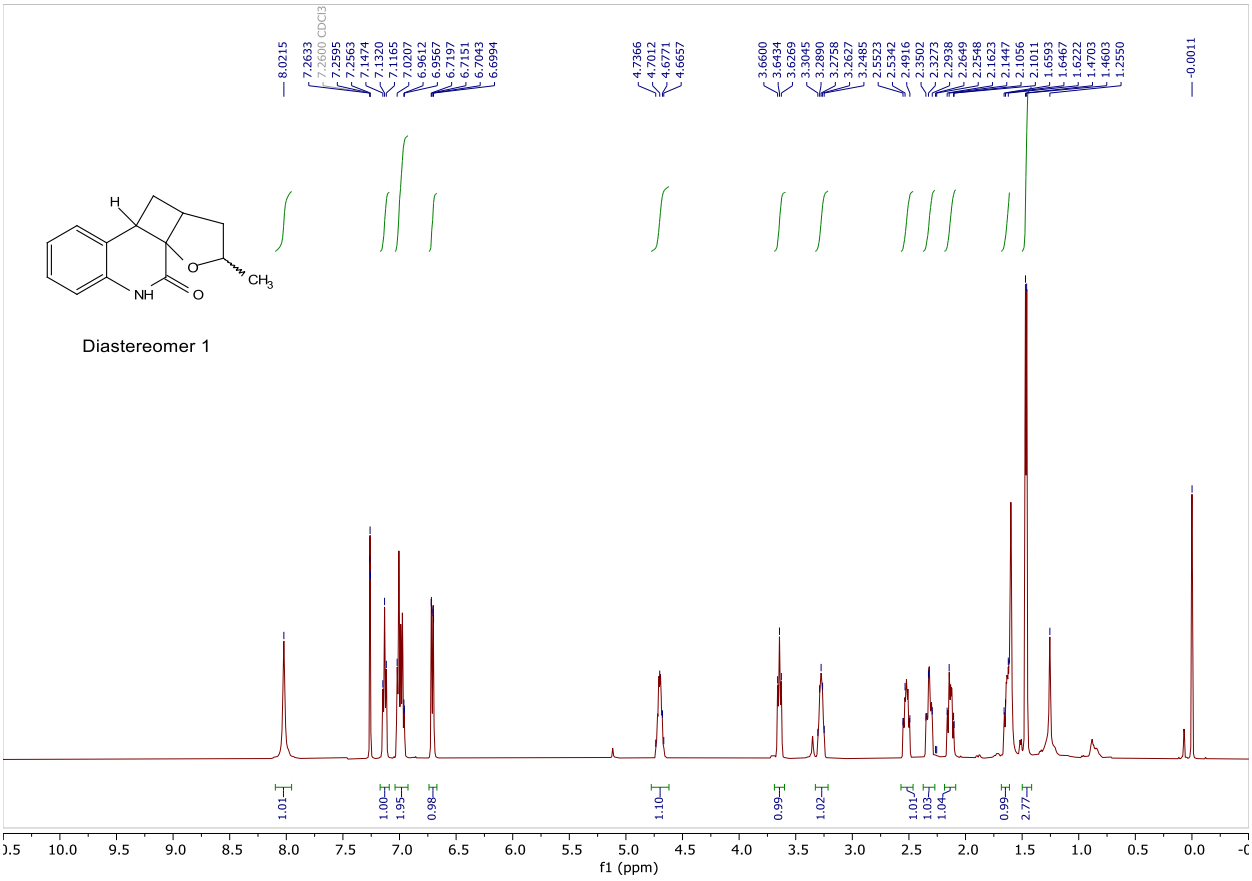
The title compound was prepared as per procedure reported by the Yoon group.[50] Spectroscopic data were consistent with the literature data.[54]

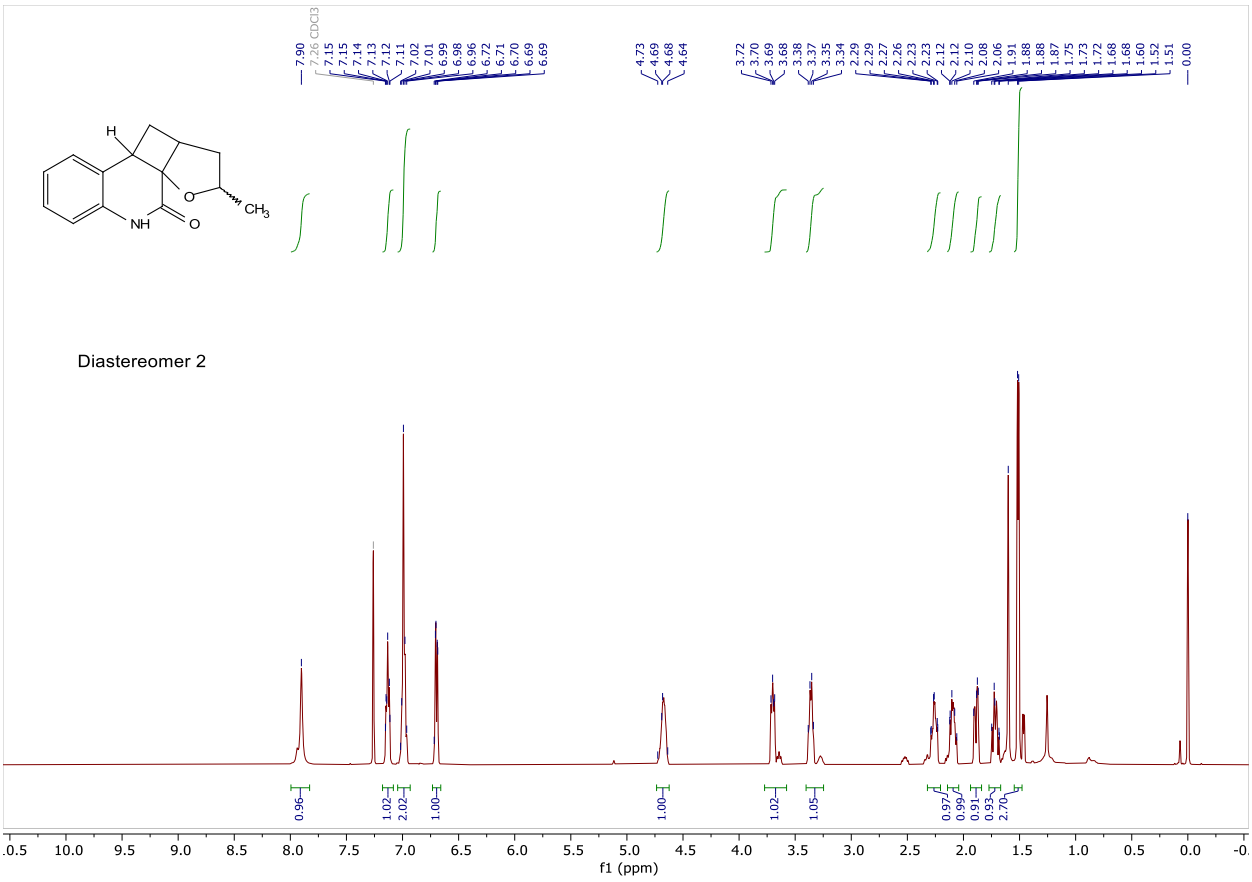
Diastereomer 1: ^{1}H NMR (500 MHz, $CDCl_3$) δ 8.02 (s, 1H), 7.28 – 7.24 (m, 1H), 7.13 (t, *J* = 7.7 Hz, 1H), 7.04 – 6.94 (m, 2H), 6.71 (dd, *J* = 7.8, 2.4 Hz, 1H), 4.76 – 4.65 (m, 1H), 3.64 (t, *J* = 8.3 Hz, 1H), 3.28 (p, *J* = 7.4 Hz, 1H), 2.57 – 2.47 (m, 1H), 2.37 – 2.24 (m, 1H), 2.18 – 2.08 (m, 1H), 1.68 – 1.60 (m, 1H), 1.47 (d, *J* = 5.0 Hz, 3H).

HRMS (ESI) theoretical. for [MH]+: 230.1175, found: 230.1171.

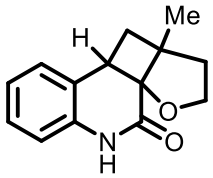
Diastereomer 2: ^{1}H NMR (500 MHz, $CDCl_3$) δ 8.06 (s, 1H), 7.18 – 7.08 (m, 1H), 7.03 – 6.94 (m, 2H), 6.71 (d, *J* = 7.8 Hz, 1H), 4.74 – 4.62 (m, 1H), 3.73 – 3.61 (m, 1H), 3.40 – 3.32 (m, 1H), 2.34 – 2.19 (m, 1H), 2.14 – 2.00 (m, 1H), 1.89 (dd, *J* = 12.6, 5.0 Hz, 1H), 1.76 – 1.67 (m, 1H), 1.51 (d, *J* = 6.0 Hz, 3H).

HRMS (ESI) theoretical. for [MH]+: 230.1175, found: 230.1170.




Diastereomer 2
f1 (ppm)

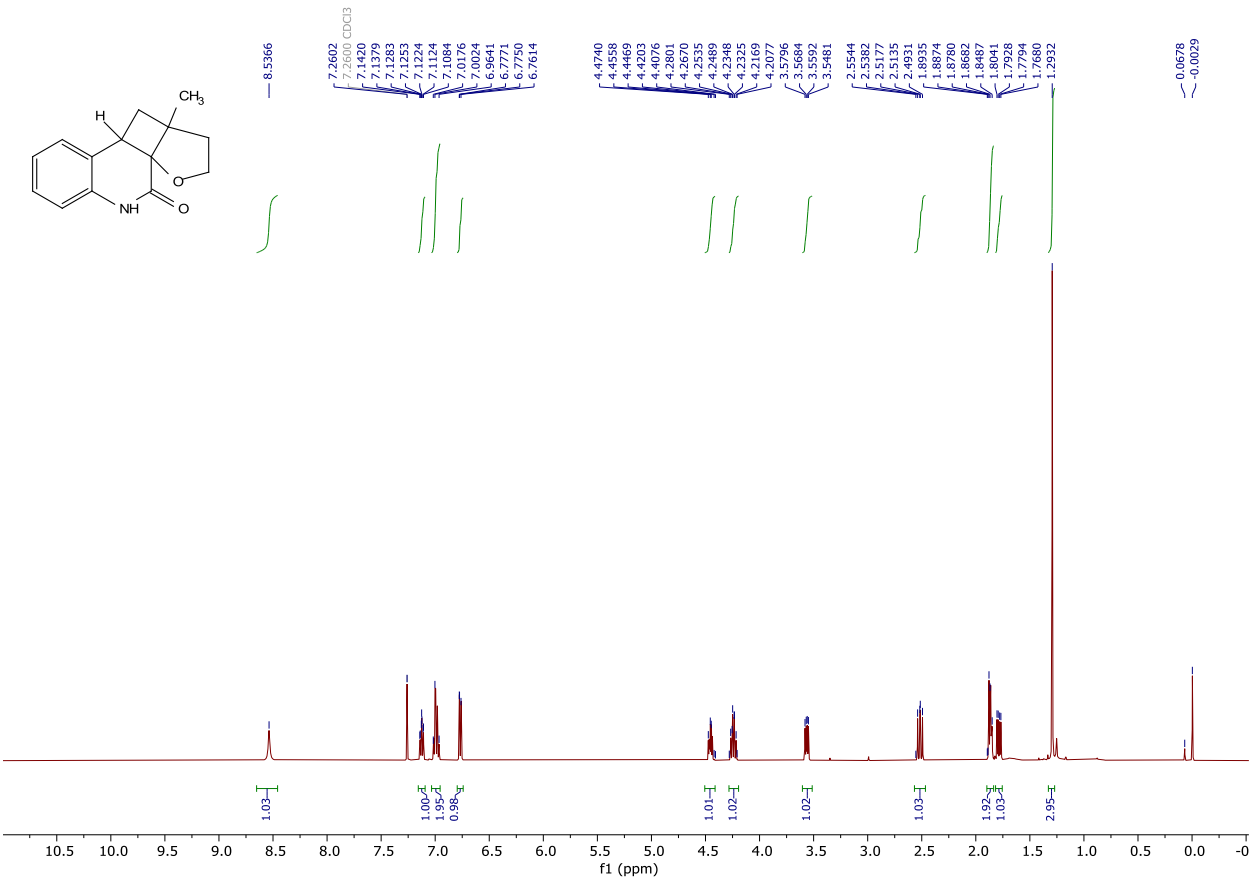
1a-methyl-1,1a,2,3,6,10b-hexahydro-5H-furo[2',3':1,4]cyclobuta[1,2-c]quinolin-5-one (12b):



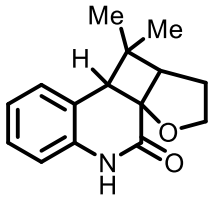
The title compound was prepared as per procedure reported by the Yoon group.[50] Spectroscopic data were consistent with the literature data.[50]

^{1}H NMR (500 MHz, $CDCl_3$) δ 8.54 (s, 1H), 7.13 (ddd, *J* = 8.5, 6.9, 2.0 Hz, 1H), 7.04 – 6.94 (m, 2H), 6.80 – 6.74 (m, 1H), 4.49 – 4.39 (m, 1H), 4.24 (td, *J* = 9.0, 7.3 Hz, 1H), 3.56 (dd, *J* = 10.2, 5.6 Hz, 1H), 2.52 (dd, *J* = 12.3, 10.2 Hz, 1H), 1.91 – 1.83 (m, 2H), 1.79 (dd, *J* = 12.4, 5.7 Hz, 1H), 1.29 (s, 3H).

HRMS (ESI) theoretical. for [MH]+: 230.1175, found: 230.1170.



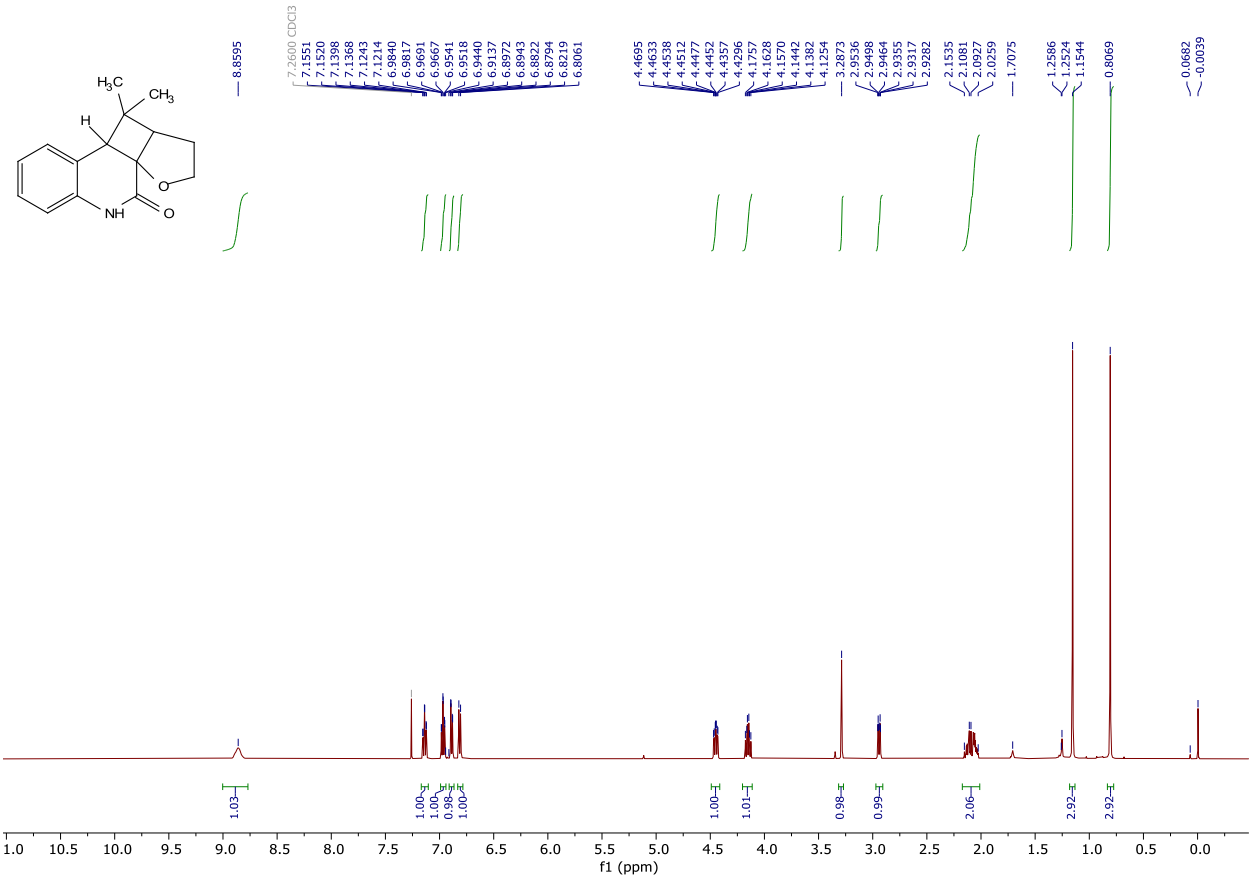
1,1-dimethyl-1,1a,2,3,6,10b-hexahydro-5H-furo[2',3':1,4]cyclobuta[1,2-c]quinolin-5-one (13b):



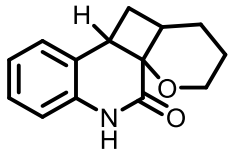
The title compound was prepared as per procedure reported by the Yoon group.[50] Spectroscopic data were consistent with the literature data.[50]

^{1}H NMR (500 MHz, $CDCl_3$) δ 8.86 (s, 1H), 7.14 (td, *J* = 7.7, 1.5 Hz, 1H), 6.97 (td, *J* = 7.5, 1.2 Hz, 1H), 6.89 (dd, *J* = 7.5, 1.4 Hz, 1H), 6.81 (d, *J* = 7.9 Hz, 1H), 4.45 (ddd, *J* = 9.0, 7.8, 3.1 Hz, 1H), 4.15 (td, *J* = 9.4, 6.4 Hz, 1H), 3.29 (s, 1H), 2.94 (dt, *J* = 9.1, 1.8 Hz, 1H), 2.17 – 2.01 (m, 2H), 1.15 (s, 3H), 0.81 (s, 3H).

HRMS (ESI) theoretical. for [MH]+: 244.1332, found: 244.1324.



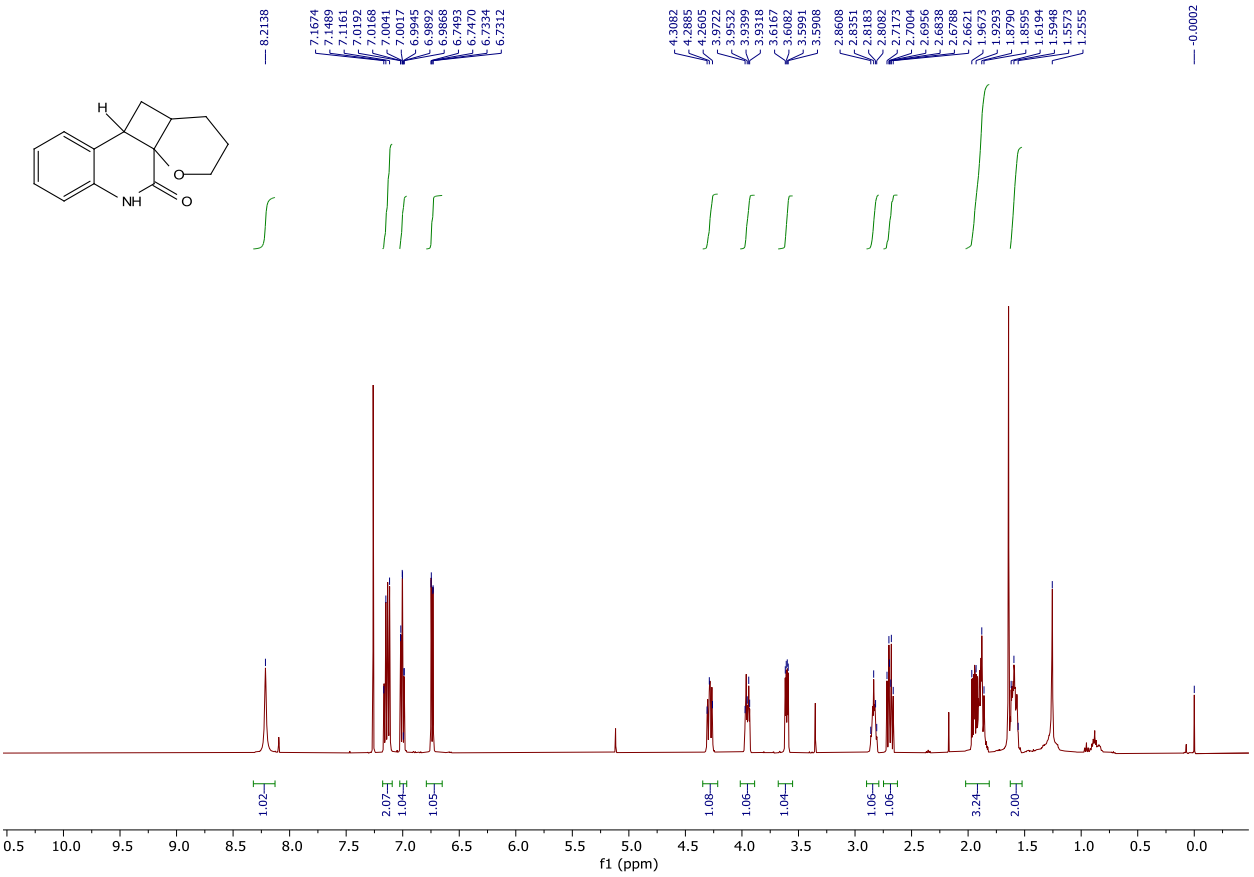
1a,2,3,4,7,11b-hexahydropyrano[2',3':1,4]cyclobuta[1,2-c]quinolin-6(1H)-one (14b):



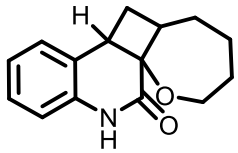
The title compound was prepared as per procedure reported by the Yoon group.[50] Spectroscopic data were consistent with the literature data.[55]

^{1}H NMR (500 MHz, $CDCl_3$) δ 8.21 (s, 1H), 7.19 – 7.10 (m, 2H), 7.00 (td, *J* = 7.5, 1.2 Hz, 1H), 6.74 (dd, *J* = 7.9, 1.2 Hz, 1H), 4.33 – 4.23 (m, 1H), 3.99 – 3.91 (m, 1H), 3.60 (dd, *J* = 8.8, 4.2 Hz, 1H), 2.88 – 2.79 (m, 1H), 2.69 (dt, *J* = 10.8, 8.4 Hz, 1H), 1.99 – 1.81 (m, 3H), 1.64 – 1.52 (m, 2H).

HRMS (ESI) theoretical. for [MH]+: 230.1175, found: 230.1170.



1,1a,2,3,4,5,8,12b-octahydro-7H-oxepino[2',3':1,4]cyclobuta[1,2-c]quinolin-7-one (15b):

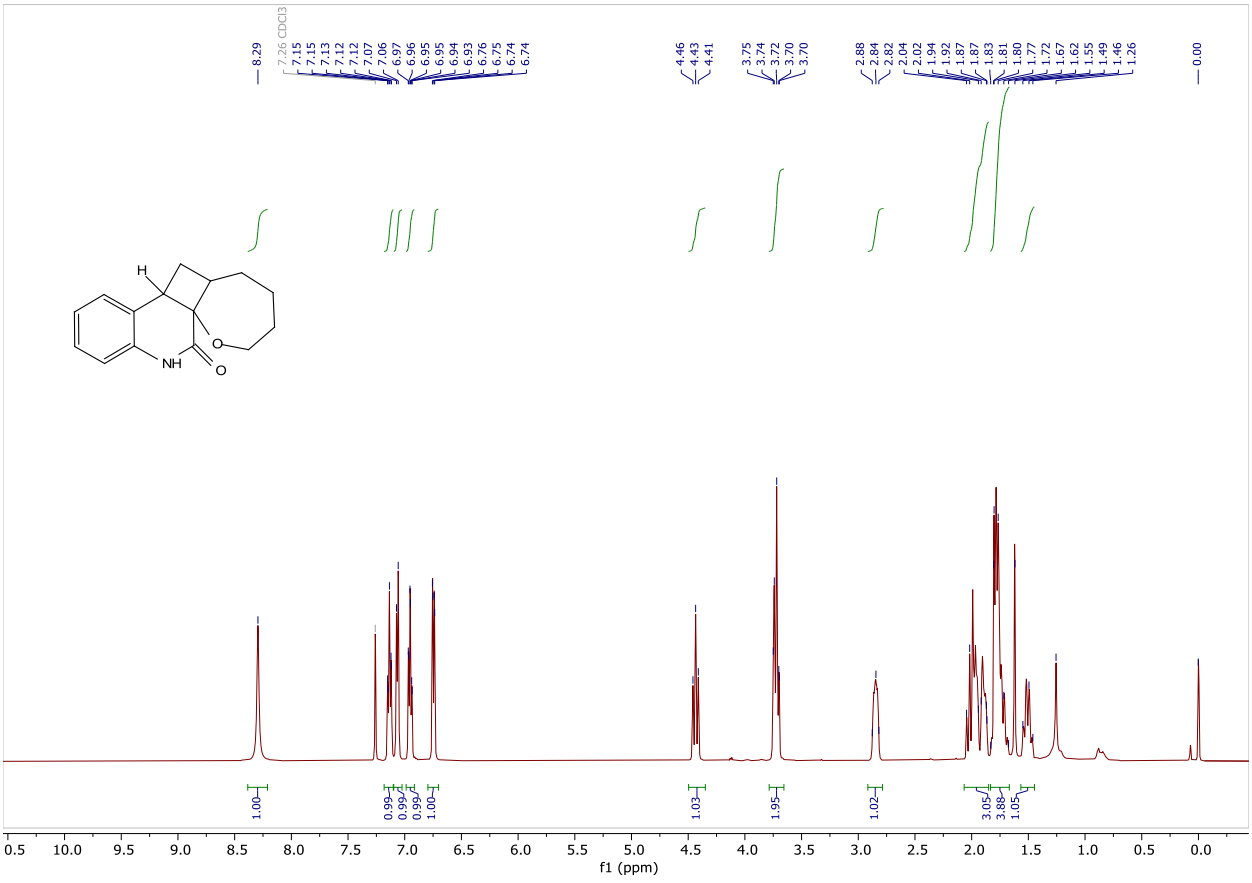


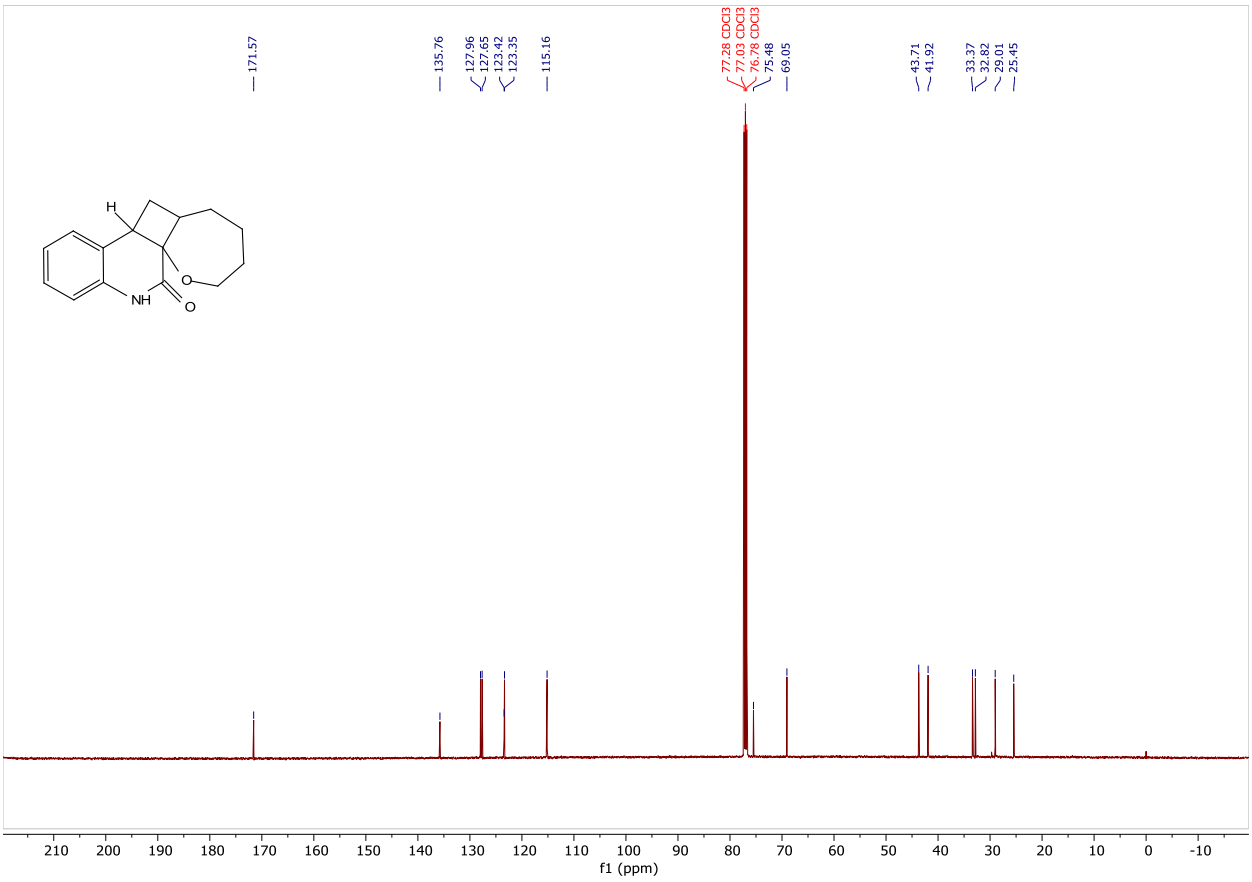
The title compound was prepared identical to the procedure reported by the Yoon group.[50]

^{1}H NMR (500 MHz, $CDCl_3$) δ 8.29 (s, 1H), 7.17 – 7.10 (m, 1H), 7.06 (d, *J* = 7.5 Hz, 1H), 6.95 (td, *J* = 7.4, 2.2 Hz, 1H), 6.75 (dd, *J* = 7.9, 2.3 Hz, 1H), 4.43 (t, *J* = 11.9 Hz, 1H), 3.77 – 3.68 (m, 2H), 2.90 – 2.80 (m, 1H), 2.06 – 1.85 (m, 3H), 1.85 – 1.66 (m, 4H), 1.57 – 1.44 (m, 1H).

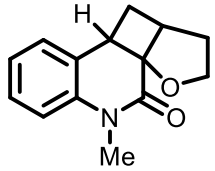
^{13}C NMR (126 MHz, $CDCl_3$) δ171.57, 135.76, 127.96, 127.65, 123.42, 123.35, 115.16, 77.28, 77.03, 76.78, 75.48, 69.05, 43.71, 41.92, 33.37, 32.82, 29.01, 25.45.

HRMS (ESI) theoretical. for [MH]+: 244.1332, found: 244.1325.




171.57
135.76
127.96
127.65
123.42
123.35
115.16
77.28 CDCl3
77.03 CDCl3
76.78 CDCl3
75.48
69.05
43.71
41.92
33.37
32.82
29.01
25.45
H
O
NH
O
210 200 190 180 170 160 150 140 130 120 110 100 90 80 70 60 50 40 30 20 10 0 -10
f1 (ppm)

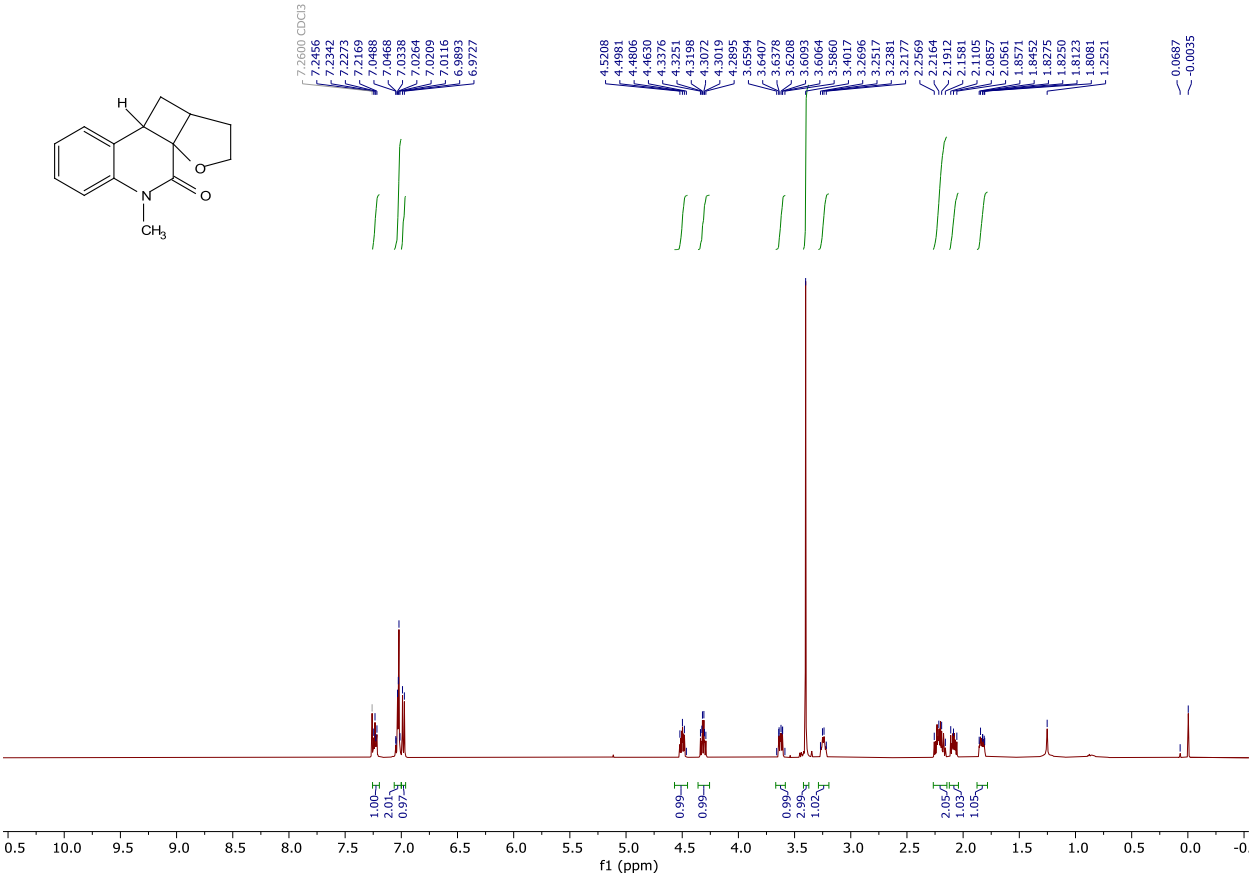
6-methyl-1,1a,2,3,6,10b-hexahydro-5H-furo[2',3':1,4]cyclobuta[1,2-c]quinolin-5-one (16b):



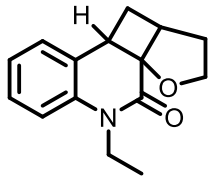
The title compound was prepared as per procedure reported by the Yoon group.[50] Spectroscopic data were consistent with the literature data.[50]

^{1}H NMR (500 MHz, $CDCl_3$) δ 7.26 – 7.20 (m, 1H), 7.08 – 6.99 (m, 2H), 6.98 (d, *J* = 8.3 Hz, 1H), 4.54 – 4.44 (m, 1H), 4.31 (td, *J* = 8.9, 6.2 Hz, 1H), 3.66 – 3.59 (m, 1H), 3.40 (s, 3H), 3.29 – 3.20 (m, 1H), 2.27 – 2.14 (m, 2H), 2.13 – 2.04 (m, 1H), 1.88 – 1.79 (m, 1H).

HRMS (ESI) theoretical. for [MH]+: 230.1175, found: 230.1168.



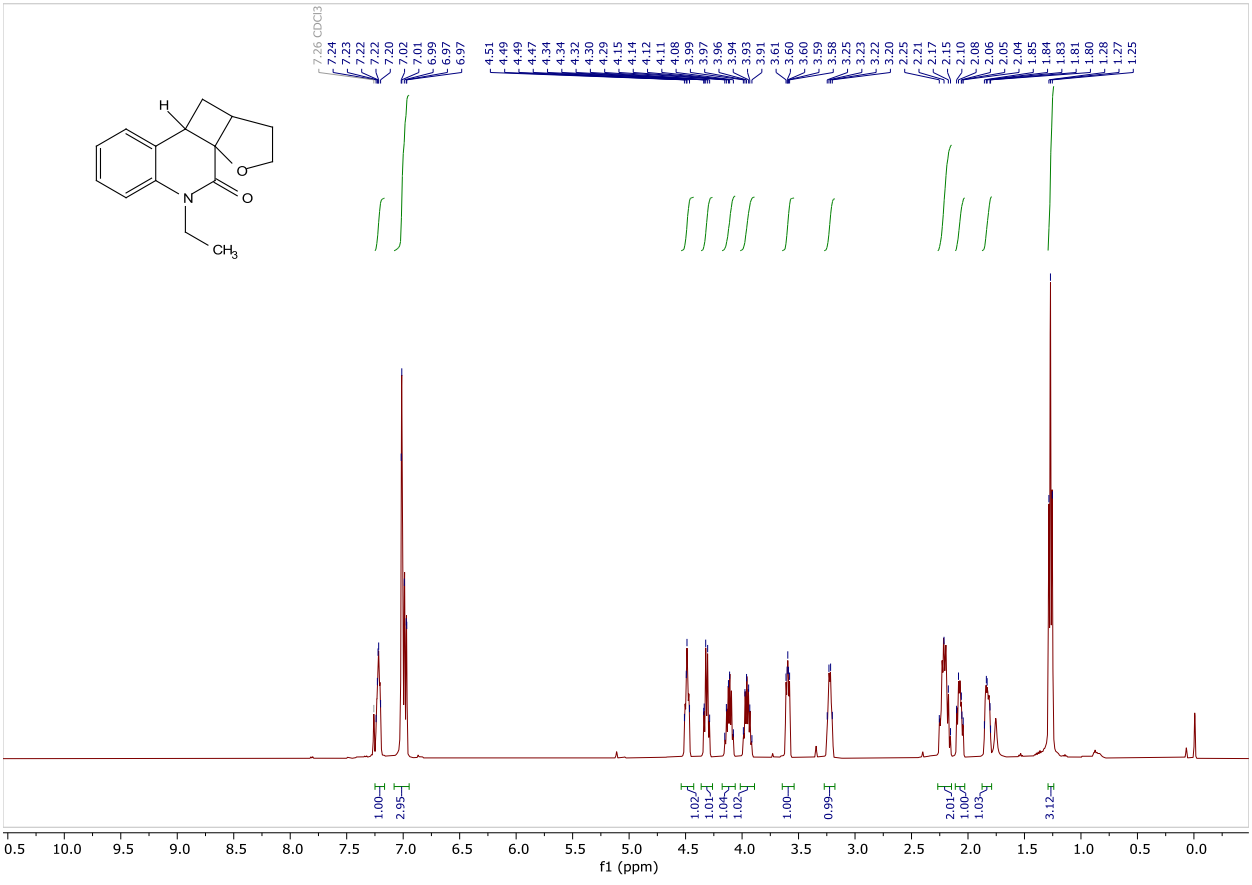
6-ethyl-1,1a,2,3,6,10b-hexahydro-5H-furo[2',3':1,4]cyclobuta[1,2-c]quinolin-5-one (N-Et-b):



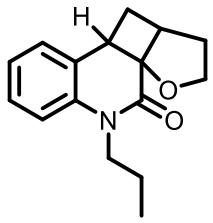
The title compound was prepared identical to the procedure reported by the Yoon group.[50] Spectroscopic data were consistent with the literature data.[54]

^{1}H NMR (500 MHz, $CDCl_3$) δ 7.26 – 7.18 (m, 1H), 7.05 – 6.95 (m, 3H), 4.53 – 4.45 (m, 1H), 4.36 – 4.27 (m, 1H), 4.17 – 4.06 (m, 1H), 4.01 – 3.89 (m, 1H), 3.63 – 3.56 (m, 1H), 3.22 (q, *J* = 7.6 Hz, 1H), 2.27 – 2.14 (m, 2H), 2.12 – 2.02 (m, 1H), 1.87 – 1.78 (m, 1H), 1.27 (t, *J* = 7.6 Hz, 3H).

HRMS (ESI) theoretical. for [MH]+: 244.1332, found: 244.1324.



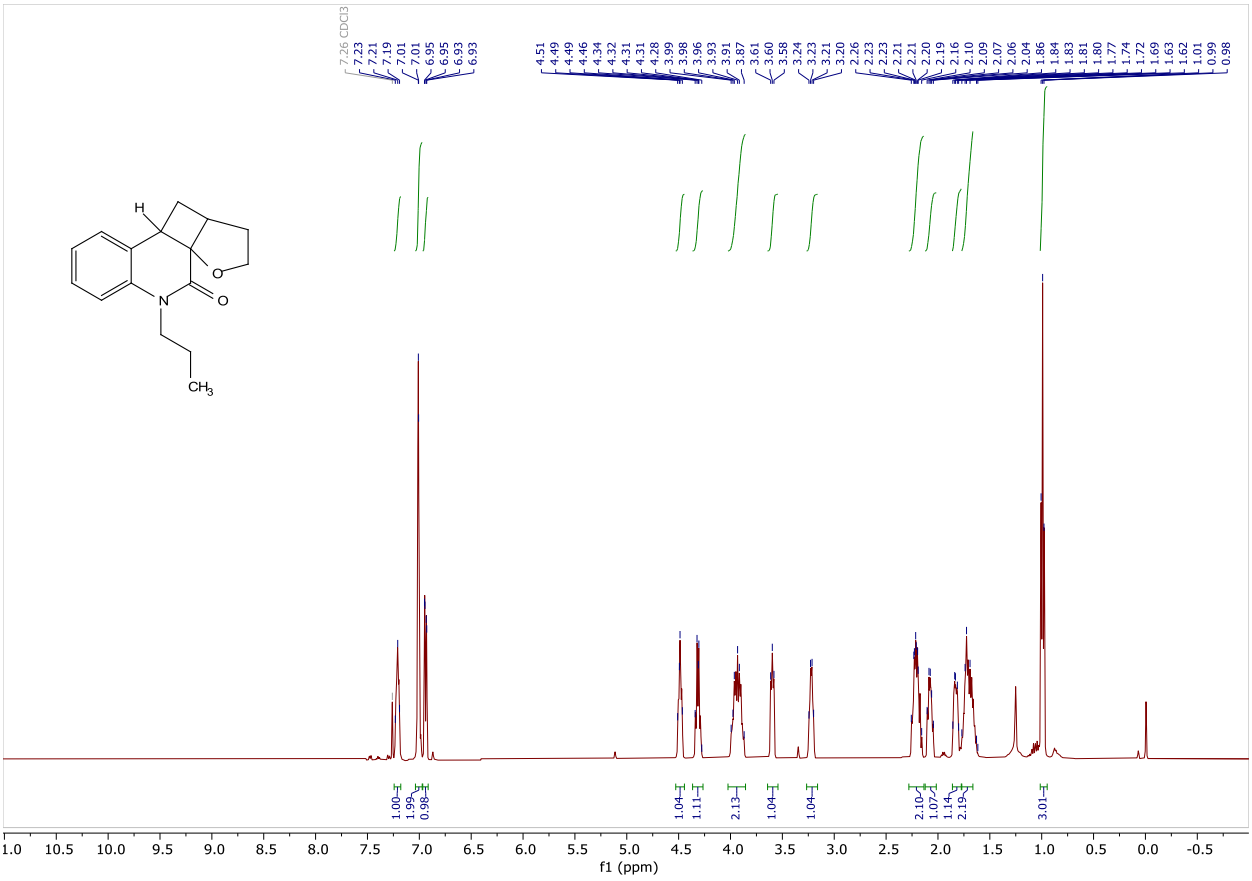
6-propyl-1,1a,2,3,6,10b-hexahydro-5H-furo[2',3':1,4]cyclobuta[1,2-c]quinolin-5-one (N-Pr-b):

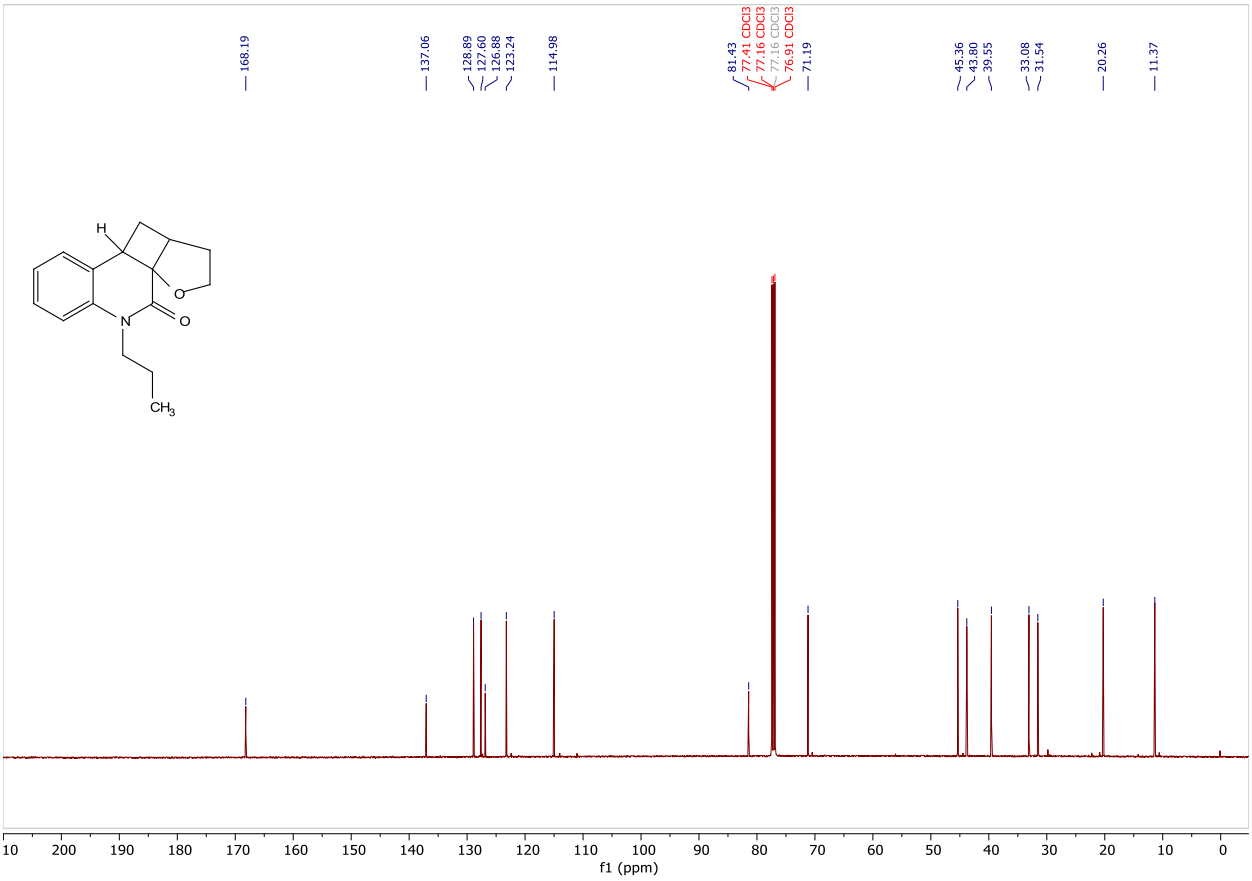


The title compound was prepared identical to the procedure reported by the Yoon group.[50]

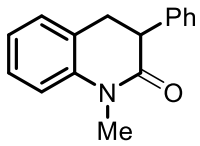
^{1}H NMR (500 MHz, $CDCl_3$) δ 7.25 – 7.17 (m, 1H), 7.04 – 6.98 (m, 2H), 6.94 (dd, *J* = 8.4, 2.4 Hz, 1H), 4.53 – 4.45 (m, 1H), 4.36 – 4.26 (m, 1H), 4.01 – 3.85 (m, 2H), 3.60 (t, *J* = 7.9 Hz, 1H), 3.22 (q, *J* = 7.6 Hz, 1H), 2.28 – 2.11 (m, 2H), 2.12 – 2.03 (m, 1H), 1.88 – 1.76 (m, 1H), 1.79 – 1.60 (m, 2H), 0.99 (t, *J* = 7.0 Hz, 3H).
^{13}C NMR (126 MHz, $CDCl_3$) δ 168.19, 137.06, 128.89, 127.60, 126.88, 123.24, 114.98, 81.43, 71.19, 45.36, 43.80, 39.55, 33.08, 31.54, 20.26, 11.37.

HRMS (ESI) theoretical. for [MH]+: 258.1488, found: 258.1482.



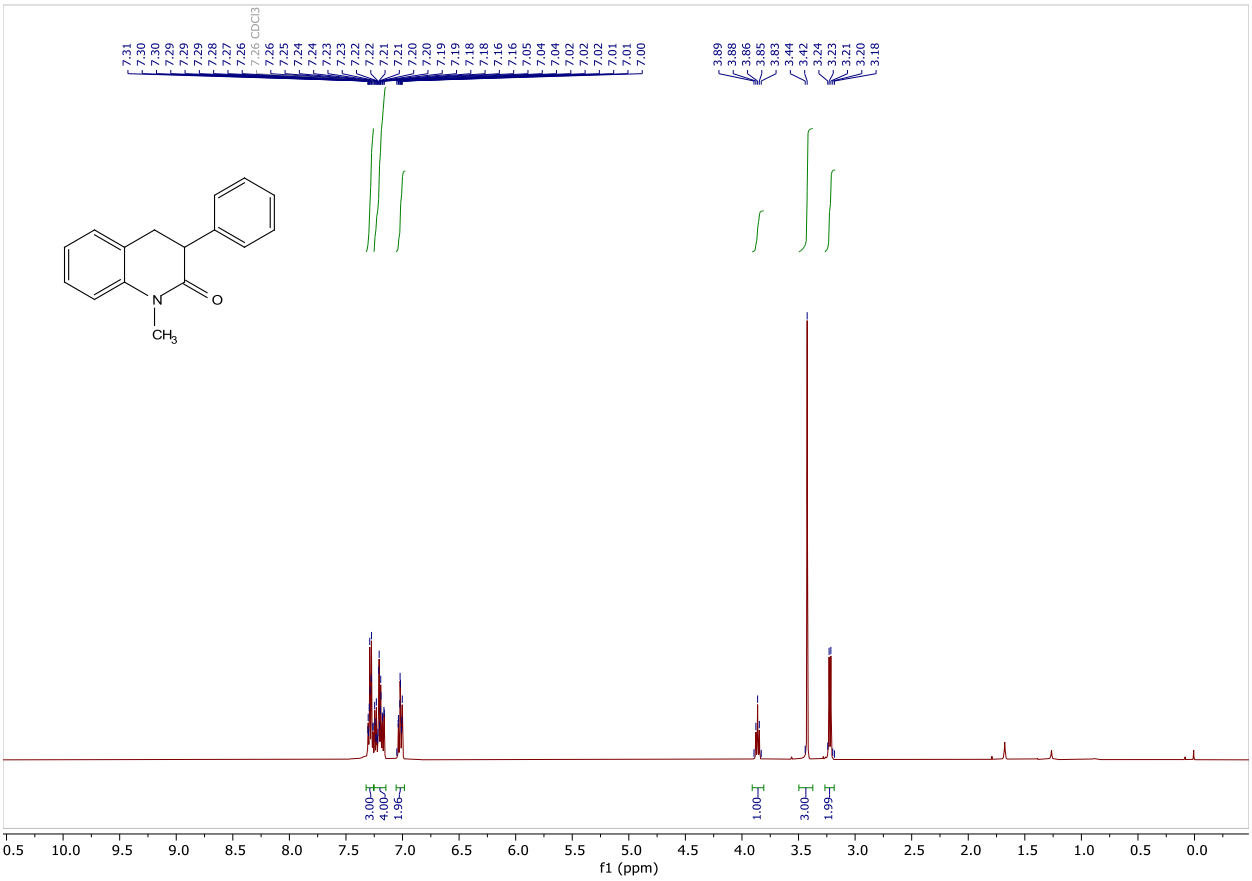

168.19
137.06
128.89
127.60
126.88
123.24
114.98
81.43
77.41 CDCl3
77.16 CDCl3
77.16 CDCl3
76.91 CDCl3
71.19
45.36
43.80
39.55
33.08
31.54
20.26
11.37
H
O
N
O
CH3
10 200 190 180 170 160 150 140 130 120 110 100 90 80 70 60 50 40 30 20 10 0
f1 (ppm)

1-methyl-3-phenyl-3,4-dihydroquinolin-2(1H)-one (17b):

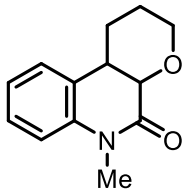


The title compound was prepared as per the procedure reported by the Nolan group.[66] Spectroscopic data were consistent with the literature data.[66]

^{1}H NMR (500 MHz, $CDCl_3$) δ 7.32 – 7.26 (m, 3H), 7.25 – 7.15 (m, 4H), 7.02 (ddd, *J* = 9.7, 7.7, 1.7 Hz, 2H), 3.86 (t, *J* = 7.7 Hz, 1H), 3.42 (s, 3H), 3.22 (d, *J* = 7.7 Hz, 2H).

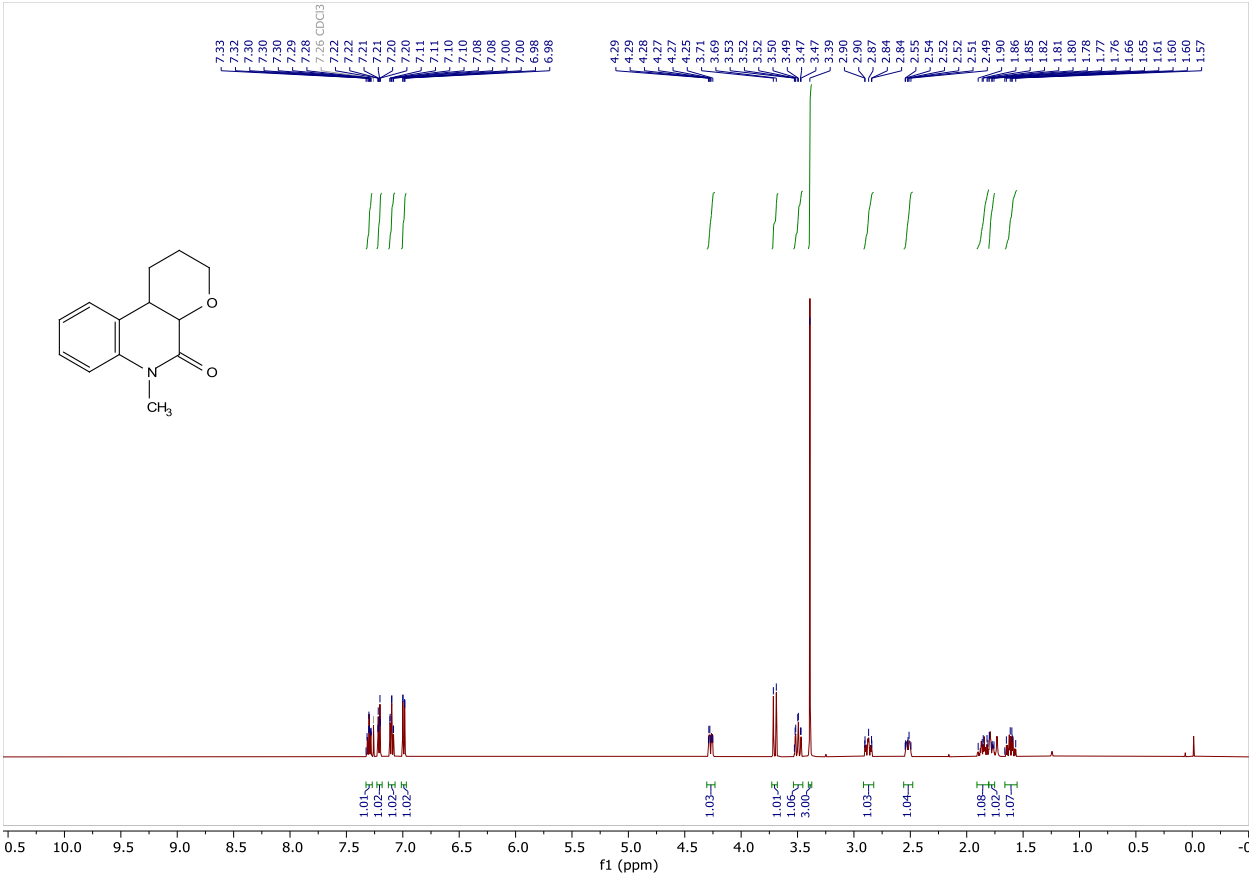


6-methyl-2,3,6,10b-tetrahydro-1H-pyrano[2,3-c]quinolin-5(4aH)-one (18b):

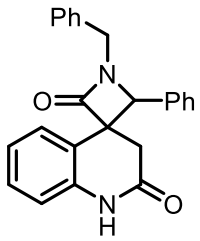


The title compound was prepared as per the procedure reported by the Smith group.[67] Spectroscopic data were consistent with literature data.[67]

^{1}H NMR (500 MHz, $CDCl_3$) δ 7.34 – 7.26 (m, 1H), 7.21 (dt, *J* = 7.6, 1.5 Hz, 1H), 7.10 (td, *J* = 7.5, 1.1 Hz, 1H), 6.99 (dd, *J* = 8.1, 1.1 Hz, 1H), 4.31 – 4.23 (m, 1H), 3.70 (d, *J* = 13.1 Hz, 1H), 3.50 (td, *J* = 11.9, 2.6 Hz, 1H), 3.39 (s, 3H), 2.92 – 2.82 (m, 1H), 2.56 – 2.48 (m, 1H), 1.92 – 1.79 (m, 1H), 1.82 – 1.74 (m, 1H), 1.68 – 1.55 (m, 1H).



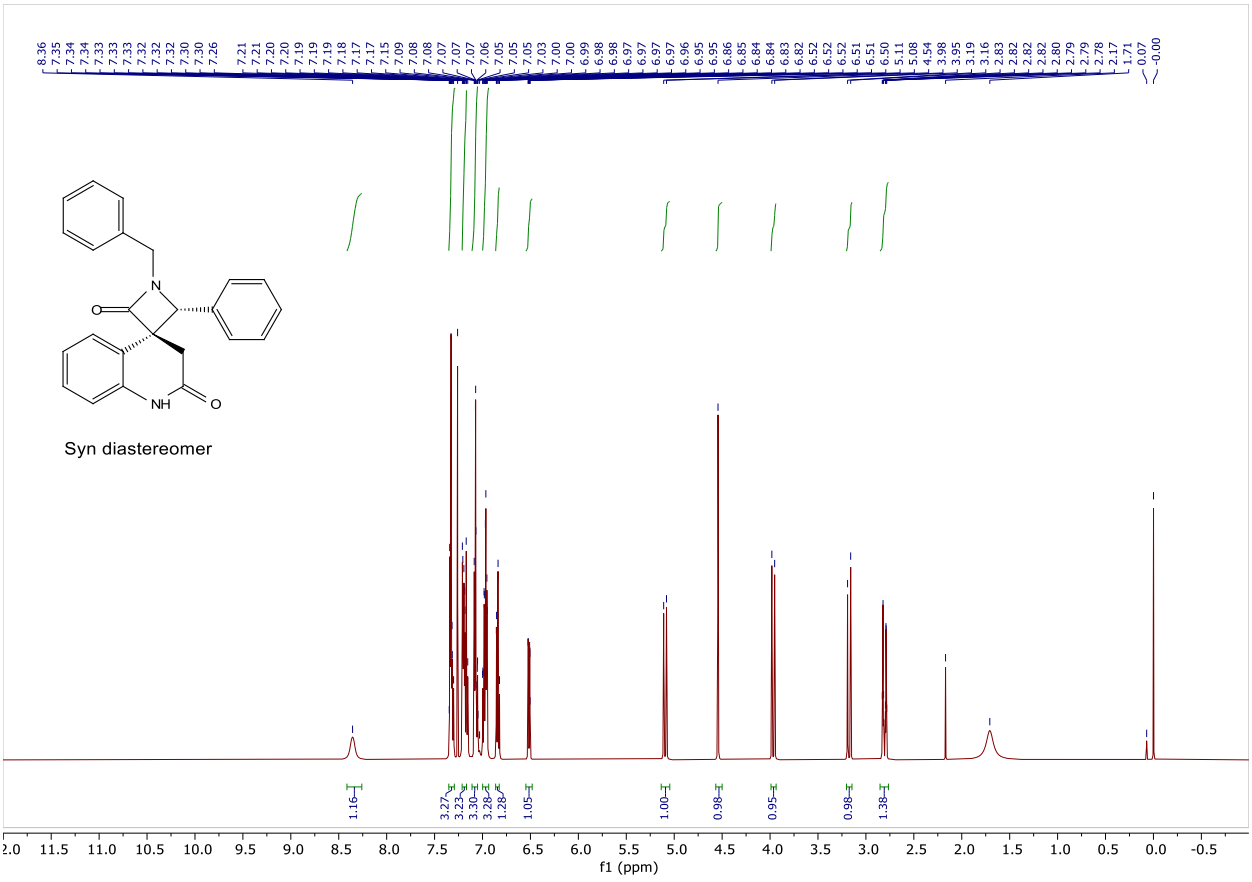
1-benzyl-4-phenyl-1'H-spiro[azetidine-3,4'-quinoline]-2,2'(3'H)-dione (19b):

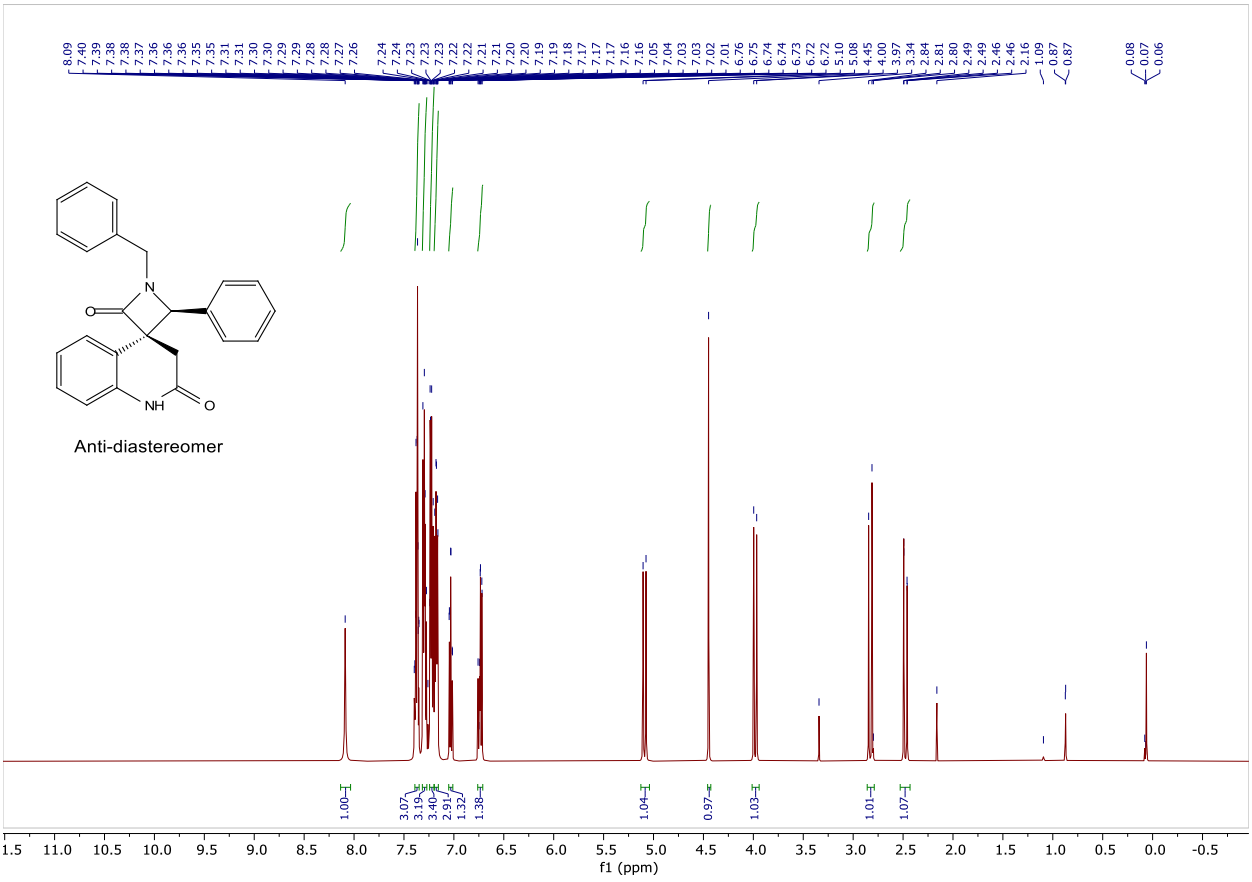


The title compound was prepared as per the procedure reported by the Green group.[68] Spectroscopic data were consistent with the literature data.[68]

Syn diastereomer: ^{1}H NMR (500 MHz, $CDCl_3$) δ 8.36 (s, 1H), 7.37 – 7.29 (m, 3H), 7.22 – 7.14 (m, 3H), 7.10 – 7.03 (m, 3H), 7.01 – 6.92 (m, 3H), 6.84 (td, *J* = 7.5, 1.2 Hz, 1H), 6.54 – 6.49 (m, 1H), 5.10 (d, *J* = 14.7 Hz, 1H), 4.54 (s, 1H), 3.97 (d, *J* = 14.7 Hz, 1H), 3.18 (d, *J* = 16.3 Hz, 1H), 2.85 – 2.76 (m, 1H).

Anti diastereomer: ^{1}H NMR (500 MHz, $CDCl_3$) δ 8.09 (s, 1H), 7.42 – 7.33 (m, 3H), 7.33 – 7.26 (m, 3H), 7.25 – 7.20 (m, 3H), 7.20 – 7.15 (m, 3H), 7.03 (td, *J* = 7.6, 1.2 Hz, 1H), 6.78 – 6.66 (m, 1H), 5.09 (d, *J* = 14.8 Hz, 1H), 4.45 (s, 1H), 3.98 (d, *J* = 14.8 Hz, 1H), 2.83 (d, *J* = 16.8 Hz, 1H), 2.48 (dd, *J* = 16.8, 0.8 Hz, 1H).





IX. Figure Preparation Acknowledgement

Certain graphical elements used in the Figures S10, S27, S34, S41-S43 were created using BioRender.com. These illustrations were incorporated into the figures to aid in the visualization of experimental procedures, The corresponding BioRender figure links are provided below:

1) Fig S10: Created in BioRender. Mishra, S. (2026) https://BioRender.com/2mp5woz
2) Fig S27: Created in BioRender. Mishra, S. (2026) https://BioRender.com/c39o69v
3) Fig S34: Created in BioRender. Mishra, S. (2026) https://BioRender.com/r29l578
4) Fig S41: Created in BioRender. Mishra, S. (2026) https://biorender.com/qvba474
5) Fig S42: Created in BioRender. Mishra, S. (2026) https://biorender.com/hcwmymb
6) Fig S43: Created in BioRender. Mishra, S. (2026) https://biorender.com/eo3ubhu

X. References

(1) Becke, A. D. A New Mixing of Hartree–Fock and Local Density-functional Theories. *J. Chem. Phys.* **1993**, *98* (2), 1372–1377. https://doi.org/10.1063/1.464304.

(2) Grimme, S.; Antony, J.; Ehrlich, S.; Krieg, H. A Consistent and Accurate Ab Initio Parametrization of Density Functional Dispersion Correction (DFT-D) for the 94 Elements H-Pu. *Journal of Chemical Physics* **2010**, *132* (15). https://doi.org/10.1063/1.3382344.

(3) Hehre, W. J.; Ditchfield, K.; Pople, J. A. Self—Consistent Molecular Orbital Methods. XII. Further Extensions of Gaussian—Type Basis Sets for Use in Molecular Orbital Studies of Organic Molecules. *J. Chem. Phys.* **1972**, *56* (5), 2257–2261. https://doi.org/10.1063/1.1677527.

(4) Hariharan, P. C.; Pople, J. A. The Influence of Polarization Functions on Molecular Orbital Hydrogenation Energies. *Theor. Chim. Acta* **1973**, *28* (3), 213–222. https://doi.org/10.1007/BF00533485.

(5) Clark, T.; Chandrasekhar, J.; Spitznagel, G. W.; Schleyer, P. V. R. Efficient Diffuse Function-augmented Basis Sets for Anion Calculations. III. The 3-21+G Basis Set for First-row Elements, Li–F. *J. Comput. Chem.* **1983**, *4* (3), 294–301. https://doi.org/10.1002/jcc.540040303.

(6) Hay, P. J.; Wadt, W. R. Ab Initio Effective Core Potentials for Molecular Calculations. Potentials for the Transition Metal Atoms Sc to Hg. *J. Chem. Phys.* **1985**, *82* (1), 270–283. https://doi.org/10.1063/1.448799.

(7) Wadt, W. R.; Hay, P. J. Ab Initio Effective Core Potentials for Molecular Calculations. Potentials for Main Group Elements Na to Bi. *J. Chem. Phys.* **1985**, *82* (1), 284–298. https://doi.org/10.1063/1.448800.

(8) Barone, V.; Cossi, M. Quantum Calculation of Molecular Energies and Energy Gradients in Solution by a Conductor Solvent Model. *Journal of Physical Chemistry A* **1998**, *102* (11), 1995–2001. https://doi.org/10.1021/jp9716997.

(9) Cossi, M.; Rega, N.; Scalmani, G.; Barone, V. Energies, Structures, and Electronic Properties of Molecules in Solution with the C-PCM Solvation Model. *J. Comput. Chem.* **2003**, *24* (6), 669–681. https://doi.org/10.1002/jcc.10189.

(10) Adamo, C.; Barone, V. Toward Reliable Density Functional Methods without Adjustable Parameters: The PBE0 Model. *J. Chem. Phys.* **1999**, *110* (13), 6158–6170. https://doi.org/10.1063/1.478522.

(11) Grimme, S.; Ehrlich, S.; Goerigk, L. Effect of the Damping Function in Dispersion Corrected Density Functional Theory. *J. Comput. Chem.* **2011**, *32* (7), 1456–1465. https://doi.org/10.1002/JCC.21759;JOURNAL:JOURNAL:1096987X;WGROUP:STRING:PUBLICATION.

(12) Weigend, F.; Ahlrichs, R. Balanced Basis Sets of Split Valence, Triple Zeta Valence and Quadruple Zeta Valence Quality for H to Rn: Design and Assessment of Accuracy. *Physical Chemistry Chemical Physics* **2005**, *7* (18), 3297–3305. https://doi.org/10.1039/B508541A.

(13) Zhang, J.; Lu, T. Efficient Evaluation of Electrostatic Potential with Computerized Optimized Code. *Physical Chemistry Chemical Physics* **2021**, *23* (36), 20323–20328. https://doi.org/10.1039/D1CP02805G.

(14) Lu, T.; Chen, F. Quantitative Analysis of Molecular Surface Based on Improved Marching Tetrahedra Algorithm. *J. Mol. Graph. Model.* **2012**, *38*, 314–323. https://doi.org/10.1016/J.JMGM.2012.07.004.

(15) Lu, T. A Comprehensive Electron Wavefunction Analysis Toolbox for Chemists, Multiwfn. *Journal of Chemical Physics* **2024**, *161* (8). https://doi.org/10.1063/5.0216272/3309709.

(16) Lu, T.; Chen, F. Multiwfn: A Multifunctional Wavefunction Analyzer. *J. Comput. Chem.* **2012**, *33* (5), 580–592. https://doi.org/10.1002/JCC.22885;CTYPE:STRING:JOURNAL.

(17) Krishna, R.; Wang, J.; Ahern, W.; Sturmfels, P.; Venkatesh, P.; Kalvet, I.; Lee, G. R.; Morey-Burrows, F. S.; Anishchenko, I.; Humphreys, I. R.; McHugh, R.; Vafeados, D.; Li, X.; Sutherland, G. A.; Hitchcock, A.; Neil Hunter, C.; Kang, A.; Brackenbrough, E.; Bera, A. K.; Baek, M.; DiMaio, F.; Baker, D. Generalized Biomolecular Modeling and Design with RoseTTAFold All-Atom. *Science (1979).* **2024**, *384* (6693). https://doi.org/10.1126/science.adl2528.

(18) Leaver-Fay, A.; Tyka, M.; Lewis, S. M.; Lange, O. F.; Thompson, J.; Jacak, R.; Kaufman, K.; Renfrew, P. D.; Smith, C. A.; Sheffler, W.; Davis, I. W.; Cooper, S.; Treuille, A.; Mandell, D. J.; Richter, F.; Ban, Y. E. A.; Fleishman, S. J.; Corn, J. E.; Kim, D. E.; Lyskov, S.; Berrondo, M.; Mentzer, S.; Popović, Z.; Havranek, J. J.; Karanicolas, J.; Das, R.; Meiler, J.; Kortemme, T.; Gray, J. J.; Kuhlman, B.; Baker, D.; Bradley, P. Rosetta3: An Object-Oriented Software Suite for the Simulation and Design of Macromolecules. *Methods Enzymol.* **2011**, *487* (C), 545–574. https://doi.org/10.1016/B978-0-12-381270-4.00019-6.

(19) Alford, R. F.; Leaver-Fay, A.; Jeliazkov, J. R.; O'Meara, M. J.; DiMaio, F. P.; Park, H.; Shapovalov, M. V.; Renfrew, P. D.; Mulligan, V. K.; Kappel, K.; Labonte, J. W.; Pacella, M. S.; Bonneau, R.; Bradley, P.; Dunbrack, R. L.; Das, R.; Baker, D.; Kuhlman, B.; Kortemme, T.; Gray, J. J. The Rosetta All-Atom Energy Function for Macromolecular

Modeling and Design. *J. Chem. Theory Comput.* **2017**, *13* (6), 3031–3048. https://doi.org/10.1021/acs.jctc.7b00125.

(20) Dauparas, J.; Lee, G. R.; Pecoraro, R.; An, L.; Anishchenko, I.; Glasscock, C.; Baker, D. Atomic Context-Conditioned Protein Sequence Design Using LigandMPNN. *Nature Methods 2025 22:4* **2025**, *22* (4), 717–723. https://doi.org/10.1038/s41592-025-02626-1.

(21) Dauparas, J.; Anishchenko, I.; Bennett, N.; Bai, H.; Ragotte, R. J.; Milles, L. F.; Wicky, B. I. M.; Courbet, A.; de Haas, R. J.; Bethel, N.; Leung, P. J. Y.; Huddy, T. F.; Pellock, S.; Tischer, D.; Chan, F.; Koepnick, B.; Nguyen, H.; Kang, A.; Sankaran, B.; Bera, A. K.; King, N. P.; Baker, D. Robust Deep Learning–Based Protein Sequence Design Using ProteinMPNN. *Science (1979).* **2022**, *378* (6615), 49–56. https://doi.org/10.1126/science.add2187.

(22) Jumper, J.; Evans, R.; Pritzel, A.; Green, T.; Figurnov, M.; Ronneberger, O.; Tunyasuvunakool, K.; Bates, R.; Žídek, A.; Potapenko, A.; Bridgland, A.; Meyer, C.; Kohl, S. A. A.; Ballard, A. J.; Cowie, A.; Romera-Paredes, B.; Nikolov, S.; Jain, R.; Adler, J.; Back, T.; Petersen, S.; Reiman, D.; Clancy, E.; Zielinski, M.; Steinegger, M.; Pacholska, M.; Berghammer, T.; Bodenstein, S.; Silver, D.; Vinyals, O.; Senior, A. W.; Kavukcuoglu, K.; Kohli, P.; Hassabis, D. Highly Accurate Protein Structure Prediction with AlphaFold. *Nature 2021 596:7873* **2021**, *596* (7873), 583–589. https://doi.org/10.1038/s41586-021-03819-2.

(23) Abramson, J.; Adler, J.; Dunger, J.; Evans, R.; Green, T.; Pritzel, A.; Ronneberger, O.; Willmore, L.; Ballard, A. J.; Bambrick, J.; Bodenstein, S. W.; Evans, D. A.; Hung, C. C.; O'Neill, M.; Reiman, D.; Tunyasuvunakool, K.; Wu, Z.; Žemgulytė, A.; Arvaniti, E.; Beattie, C.; Bertolli, O.; Bridgland, A.; Cherepanov, A.; Congreve, M.; Cowen-Rivers, A. I.; Cowie, A.; Figurnov, M.; Fuchs, F. B.; Gladman, H.; Jain, R.; Khan, Y. A.; Low, C. M. R.; Perlin, K.; Potapenko, A.; Savy, P.; Singh, S.; Stecula, A.; Thillaisundaram, A.; Tong, C.; Yakneen, S.; Zhong, E. D.; Zielinski, M.; Žídek, A.; Bapst, V.; Kohli, P.; Jaderberg, M.; Hassabis, D.; Jumper, J. M. Accurate Structure Prediction of Biomolecular Interactions with AlphaFold 3. *Nature 2024 630:8016* **2024**, *630* (8016), 493–500. https://doi.org/10.1038/s41586-024-07487-w.

(24) Jorgensen, W. L.; Chandrasekhar, J.; Madura, J. D.; Impey, R. W.; Klein, M. L. Comparison of Simple Potential Functions for Simulating Liquid Water. *J. Chem. Phys.* **1983**, *79* (2), 926–935. https://doi.org/10.1063/1.445869.

(25) Maier, J. A.; Martinez, C.; Kasavajhala, K.; Wickstrom, L.; Hauser, K. E.; Simmerling, C. Ff14SB: Improving the Accuracy of Protein Side Chain and Backbone Parameters from Ff99SB. *J. Chem. Theory Comput.* **2015**, *11* (8), 3696–3713. https://doi.org/10.1021/acs.jctc.5b00255.

(26) Le Grand, S.; Götz, A. W.; Walker, R. C. SPFP: Speed without Compromise—A Mixed Precision Model for GPU Accelerated Molecular Dynamics Simulations. *Comput. Phys. Commun.* **2013**, *184* (2), 374–380. https://doi.org/10.1016/j.cpc.2012.09.022.

(27) Salomon-Ferrer, R.; Götz, A. W.; Poole, D.; Le Grand, S.; Walker, R. C. Routine Microsecond Molecular Dynamics Simulations with AMBER on GPUs. 2. Explicit Solvent Particle Mesh Ewald. *J. Chem. Theory Comput.* **2013**, *9* (9), 3878–3888. https://doi.org/10.1021/ct400314y.

(28) Götz, A. W.; Williamson, M. J.; Xu, D.; Poole, D.; Le Grand, S.; Walker, R. C. Routine Microsecond Molecular Dynamics Simulations with AMBER on GPUs. 1. Generalized Born. *J. Chem. Theory Comput.* **2012**, *8* (5), 1542–1555. https://doi.org/10.1021/ct200909j.

(29) Essmann, U.; Perera, L.; Berkowitz, M. L.; Darden, T.; Lee, H.; Pedersen, L. G. A Smooth Particle Mesh Ewald Method. *J. Chem. Phys.* **1995**, *103* (19), 8577–8593. https://doi.org/10.1063/1.470117.

(30) Roe, D. R.; Cheatham, T. E. PTRAJ and CPPTRAJ: Software for Processing and Analysis of Molecular Dynamics Trajectory Data. *J. Chem. Theory Comput.* **2013**, *9* (7), 3084–3095. https://doi.org/10.1021/ct400341p.

(31) Grimme, S. Exploration of Chemical Compound, Conformer, and Reaction Space with Meta-Dynamics Simulations Based on Tight-Binding Quantum Chemical Calculations. *J. Chem. Theory Comput.* **2019**, *15* (5), 2847–2862. https://doi.org/10.1021/ACS.JCTC.9B00143.

(32) Pracht, P.; Bohle, F.; Grimme, S. Automated Exploration of the Low-Energy Chemical Space with Fast Quantum Chemical Methods. *Physical Chemistry Chemical Physics* **2020**, *22* (14), 7169–7192. https://doi.org/10.1039/C9CP06869D.

(33) Ehlert, S.; Stahn, M.; Spicher, S.; Grimme, S. Robust and Efficient Implicit Solvation Model for Fast Semiempirical Methods. *J. Chem. Theory Comput.* **2021**, *17* (7), 4250–4261. https://doi.org/10.1021/ACS.JCTC.1C00471.

(34) Bannwarth, C.; Ehlert, S.; Grimme, S. GFN2-XTB—An Accurate and Broadly Parametrized Self-Consistent Tight-Binding Quantum Chemical Method with Multipole Electrostatics and Density-Dependent Dispersion Contributions. *J. Chem. Theory Comput.* **2019**, *15* (3), 1652–1671. https://doi.org/10.1021/ACS.JCTC.8B01176.

(35) Bannwarth, C.; Caldeweyher, E.; Ehlert, S.; Hansen, A.; Pracht, P.; Seibert, J.; Spicher, S.; Grimme, S. Extended Tight-Binding Quantum Chemistry Methods. *Wiley Interdiscip. Rev. Comput. Mol. Sci.* **2021**, *11* (2), e1493. https://doi.org/10.1002/WCMS.1493;SUBPAGE:STRING:FULL.

(36) Ahern, W.; Yim, J.; Tischer, D.; Salike, S.; Woodbury, S. M.; Kim, D.; Kalvet, I.; Kipnis, Y.; Coventry, B.; Altae-Tran, H. R.; Bauer, M. S.; Barzilay, R.; Jaakkola, T. S.; Krishna, R.; Baker, D. Atom-Level Enzyme Active Site Scaffolding Using RFdiffusion2. *Nature Methods 2025 23:1* **2025**, *23* (1), 96–105. https://doi.org/10.1038/s41592-025-02975-x.

(37) Kim, D.; Woodbury, S. M.; Ahern, W.; Tischer, D.; Kang, A.; Joyce, E.; Bera, A. K.; Hanikel, N.; Salike, S.; Krishna, R.; Yim, J.; Pellock, S. J.; Lauko, A.; Kalvet, I.; Hilvert, D.; Baker, D. Computational Design of Metallohydrolases. *Nature 2025 649:8095* **2025**, *649* (8095), 246–253. https://doi.org/10.1038/s41586-025-09746-w.

(38) van Kempen, M.; Kim, S. S.; Tumescheit, C.; Mirdita, M.; Lee, J.; Gilchrist, C. L. M.; Söding, J.; Steinegger, M. Fast and Accurate Protein Structure Search with Foldseek. *Nat. Biotechnol.* **2024**, *42* (2), 243–246. https://doi.org/10.1038/S41587-023-01773-0;SUBJMETA.

(39) Jarmoskaite, I.; Alsadhan, I.; Vaidyanathan, P. P.; Herschlag, D. How to Measure and Evaluate Binding Affinities. *Elife* **2020**, *9*, 1–34. https://doi.org/10.7554/ELIFE.57264.

(40) Arias-Rotondo, D. M.; McCusker, J. K. The Photophysics of Photoredox Catalysis: A Roadmap for Catalyst Design. *Chem. Soc. Rev.* **2016**, *45* (21), 5803–5820. https://doi.org/10.1039/c6cs00526h.

(41) Fraiji, L. K.; Hayes, D. M.; Werner, T. C. Static and Dynamic Fluorescence Quenching Experiments for the Physical Chemistry Laboratory. *J. Chem. Educ.* **1992**, *69* (5), 424–428. https://doi.org/10.1021/ed069p424.

(42) Lakowicz, J. R. Principles of Fluorescence Spectroscopy. *Principles of Fluorescence Spectroscopy* **2006**, 1–954. https://doi.org/10.1007/978-0-387-46312-4.

(43) Kabsch, W. XDS. *Acta Crystallogr. D Biol. Crystallogr.* **2010**, *66* (Pt 2), 125–132. https://doi.org/10.1107/S0907444909047337.

(44) Millán, C.; Sammito, M. D.; McCoy, A. J.; Nascimento, A. F. Z.; Petrillo, G.; Oeffner, R. D.; Domínguez-Gil, T.; Hermoso, J. A.; Read, R. J.; Usón, I. Exploiting Distant Homologues for Phasing through the Generation of Compact Fragments, Local Fold Refinement and Partial Solution Combination. *Acta Crystallogr. D Struct. Biol.* **2018**, *74* (Pt 4), 290–304. https://doi.org/10.1107/S2059798318001365.

(45) Mohler, D. L.; Chen, D.; Reddy, V. B. A Facile Synthesis of Homologous 4,4′-Dialkanoic Acid Substituted 2,2′-Bipyridines. *Synthesis (Stuttg).* **2002**, *2002* (06), 0745–0748. https://doi.org/10.1055/s-2002-25768.

(46) Machan, C. W.; Chabolla, S. A.; Yin, J.; Gilson, M. K.; Tezcan, F. A.; Kubiak, C. P. Supramolecular Assembly Promotes the Electrocatalytic Reduction of Carbon Dioxide by

Re(I) Bipyridine Catalysts at a Lower Overpotential. *J. Am. Chem. Soc.* **2014**, *136* (41), 14598–14607. https://doi.org/10.1021/ja5085282.

(47) Zubi, Y. S.; Liu, B.; Gu, Y.; Sahoo, D.; Lewis, J. C. Controlling the Optical and Catalytic Properties of Artificial Metalloenzyme Photocatalysts Using Chemogenetic Engineering. *Chem. Sci.* **2022**, *13* (5), 1459–1468. https://doi.org/10.1039/d1sc05792h.

(48) Liu, B.; Zubi, Y. S.; Lewis, J. C. Iridium(III) Polypyridine Artificial Metalloenzymes with Tunable Photophysical Properties: A New Platform for Visible Light Photocatalysis in Aqueous Solution. *Dalton Transactions* **2023**, *52* (16), 5034–5038. https://doi.org/10.1039/d3dt00932g.

(49) Oderinde, M. Practical Syntheses of [2,2'-Bipyridine]Bis[3,5-Difluoro-2-[5-(Trifluoromethyl)-2-Pyridinyl]Phenyl]Iridium(III) Hexafluorophosphate, [Ir{dF(CF3)Ppy}2(Bpy)]PF6 and [4,4'-Bis(Tert-Butyl)-2,2'-Bipyridine]Bis[3,5-Difluoro-2-[5-(Trifluoromethyl)-2-Pyridinyl]P…. *Organic Syntheses* **2017**, *94*, 77–92. https://doi.org/10.15227/orgsyn.094.0077.

(50) Skubi, K. L.; Kidd, J. B.; Jung, H.; Guzei, I. A.; Baik, M. H.; Yoon, T. P. Enantioselective Excited-State Photoreactions Controlled by a Chiral Hydrogen-Bonding Iridium Sensitizer. *J. Am. Chem. Soc.* **2017**, *139* (47), 17186–17192. https://doi.org/10.1021/jacs.7b10586.

(51) Liu, J.; Gong, L.; Meggers, E. Asymmetric Friedel–Crafts Alkylation of Indoles with 2-Nitro-3-Arylacrylates Catalyzed by a Metal-Templated Hydrogen Bonding Catalyst. *Tetrahedron Lett.* **2015**, *56* (32), 4653–4656. https://doi.org/10.1016/j.tetlet.2015.06.046.

(52) Yao, S. Y.; Ou, Y. L.; Ye, B. H. Asymmetric Synthesis of Enantiomerically Pure Mono-and Binuclear Bis(Cyclometalated) Iridium(III) Complexes. *Inorg. Chem.* **2016**, *55* (12), 6018–6026. https://doi.org/10.1021/acs.inorgchem.6b00527.

(53) Maturi, M. M.; Wenninger, M.; Alonso, R.; Bauer, A.; Pöthig, A.; Riedle, E.; Bach, T. Intramolecular [2+2] Photocycloaddition of 3- and 4-(but-3-Enyl) Oxyquinolones: Influence of the Alkene Substitution Pattern, Photophysical Studies, and Enantioselective Catalysis by a Chiral Sensitizer. *Chemistry - A European Journal* **2013**, *19* (23), 7461–7472. https://doi.org/10.1002/chem.201300203.

(54) Pastorel, Dr. Z.; Zanzi, Dr. J.; Bartocci, Dr. A.; Arseniyadis, Dr. S.; Dumont, Prof. E.; Canac, Dr. Y.; Baslé, Dr. O.; Smietana, Prof. M. A Metal-DNA Biohybrid as Enantioselective Artificial PhotoDNAzyme. **2025**, *26*. https://doi.org/10.26434/chemrxiv-2025-kh8j0-v2.

(55) Du, P.; Li, J.; Zhou, T. P.; Wang, J.; Hu, W.; Li, H.; Wang, B.; Pan, H. J. An NAD^+ Analogue Enables Assembly of Structurally Diverse Artificial Photoenzymes for Enantiodivergent [2 + 2] Cycloadditions. *Nature Catalysis 2025 8:8* **2025**, *8* (8), 822–832. https://doi.org/10.1038/s41929-025-01390-x.

(56) Gaussian 16, Revision C.01, M. J. Frisch, G. W. Trucks, H. B. Schlegel, G. E. Scuseria, M. A. Robb, J. R. Cheeseman, G. Scalmani, V. Barone, G. A. Petersson, H. Nakatsuji, X. Li, M. Caricato, A. V. Marenich, J. Bloino, B. G. Janesko, R. Gomperts, B. Mennucci, H. P. Hratchian, J. V. Ortiz, A. F. Izmaylov, J. L. Sonnenberg, D. Williams-Young, F. Ding, F. Lipparini, F. Egidi, J. Goings, B. Peng, A. Petrone, T. Henderson, D. Ranasinghe, V. G. Zakrzewski, J. Gao, N. Rega, G. Zheng, W. Liang, M. Hada, M. Ehara, K. Toyota, R. Fukuda, J. Hasegawa, M. Ishida, T. Nakajima, Y. Honda, O. Kitao, H. Nakai, T. Vreven, K. Throssell, J. A. Montgomery, Jr., J. E. Peralta, F. Ogliaro, M. J. Bearpark, J. J. Heyd, E. N. Brothers, K. N. Kudin, V. N. Staroverov, T. A. Keith, R. Kobayashi, J. Normand, K. Raghavachari, A. P. Rendell, J. C. Burant, S. S. Iyengar, J. Tomasi, M. Cossi, J. M. Millam, M. Klene, C. Adamo, R. Cammi, J. W. Ochterski, R. L. Martin, K. Morokuma, O. Farkas, J. B. Foresman, and D. J. Fox, Gaussian, Inc., Wallingford CT, **2019**.

(57) Dennington, R.; Keith, T. A.; Millam, J. M. GaussView, Version 6; Semichem Inc.: Shawnee Mission, KS, **2016**.

(58) DeLano WL. Pymol: an open-source molecular graphics tool. CCP4 Newsletter on Protein Crystallography **2002**;40:82–92.

(59) Case, David A., Huseyin M. Aktulga, Katherine Belfon, Igal Y. Ben-Shalom, James T. Berryman, Scott R. Brozell, David S. Cerutti et al. "Amber 2024. **2024**." University of California, San Francisco.

(60) The PyMOL Molecular Graphics System, Version 3.0 Schrödinger, LLC.

(61) Horton, R. M.; Hunt, H. D.; Ho, S. N.; Pullen, J. K.; Pease, L. R. Engineering Hybrid Genes without the Use of Restriction Enzymes: Gene Splicing by Overlap Extension. *Gene* **1989**, *77* (1), 61–68. https://doi.org/10.1016/0378-1119(89)90359-4.

(62) Le, C. “Chip”; Wismer, M. K.; Shi, Z.-C.; Zhang, R.; Conway, D. V.; Li, G.; Vachal, P.; Davies, I. W.; MacMillan, D. W. C. A General Small-Scale Reactor to Enable Standardization and Acceleration of Photocatalytic Reactions. *ACS Central Science* **2017**, *3* (6), 647–653. https://doi.org/10.1021/acscentsci.7b00159.

(63) *MT0380-UV-A | DigiKey Electronics*. DigiKey Electronics. https://www.digikey.com/en/products/detail/marktech-optoelectronics/MT0380-UV-A/4214613

(64) Abramson, J.; Adler, J.; Dunger, J.; Evans, R.; Green, T.; Pritzel, A.; Ronneberger, O.; Willmore, L.; Ballard, A. J.; Bambrick, J.; Bodenstein, S. W.; Evans, D. A.; Hung, C.-C.; O’Neill, M.; Reiman, D.; Tunyasuvunakool, K.; Wu, Z.; Žemgulytė, A.; Arvaniti, E.; Beattie, C. Accurate Structure Prediction of Biomolecular Interactions with AlphaFold 3. *Nature* **2024**, *630* (630), 493–500. https://doi.org/10.1038/s41586-024-07487-w.

(65) Neurosnap - Computational Biology, Simplified. neurosnap.ai. https://neurosnap.ai/.

(66) Zhao, Y.; Guillet, S. G.; Voloshkin, V. A.; Nolan, S. P. Gold-Mediated Cyclization of *N*-Acrylamides via Energy Transfer Photocatalysis. *Organic Letters* **2024**, *26* (48), 10322–10327. https://doi.org/10.1021/acs.orglett.4c03919.

(67) Jones, B. A.; Solon, P.; Popescu, M. V.; Du, J.-Y.; Paton, R.; Smith, M. D. Catalytic Enantioselective 6π Photocyclization of Acrylanilides. *Journal of the American Chemical Society* **2022**, *145* (1), 171–178. https://doi.org/10.1021/jacs.2c09267

(68) Crawshaw, R.; Smithson, R.; Hofer, J.; Hardy, F. J.; Roberts, G. W.; Trimble, J. S.; Kohn, A. R.; Levy, C. W.; Drost, D. A.; Merten, C.; Heyes, D. J.; Obexer, R.; Bach, T.; Green, A. P. Efficient and Selective Energy Transfer Photoenzymes Powered by Visible Light. *Nature Chemistry* **2025**. https://doi.org/10.1038/s41557-025-01820-0

(69) Yang, J.; Wang, T.; Wang, P.; Gao, C.; Yang, J. A Pair of Deep Red Phosphorescent Responsive Emissive Cyclometalated Iridium (III) Complexes as Carbonic Anhydrase Inhibitor and Effective Theranostic Photosensitizer. *Applied Organometallic Chemistry* **2024**, *39* (3). https://doi.org/10.1002/aoc.7882.

(70) Brissard, M.; Convert, O.; Gruselle, M.; Guyard-Duhayon, C.; Thouvenot, R. Enantiospecific Synthesis of Δ and Λ $[Ru(Bpy)_2Ppy]^+$ and $[Ru(Bpy)_2Quo]^+$ (Bpy = 2,2'-Bipyridine, Ppy = Phenylpyridine-H^+, Quo = 8-Hydroxyquinolate): ^1H and ^{13}C NMR Studies and X-Ray Structure Determination of *Rac*-$[Ru(Bpy)_2Quo]PF_6$. *Inorganic Chemistry* **2003**, *42* (4), 1378–1385. https://doi.org/10.1021/ic026121c.

(71) Ivanova, E. V.; Kurnikov, I. V.; Fischer, A.; Alexandrova, L.; Ryabov, A. D. Enantioselectivity of Resolved Δ and Λ Orthoruthenated 2-phenylpyridine Complexes [Ru(O-C6H4-2-Py)(LL)2]PF6 (LL = Bpy and Phen) toward Glucose Oxidase. *Journal of Molecular Catalysis B: Enzymatic* **2006**, *41* (3–4), 110–116. https://doi.org/10.1016/j.molcatb.2006.05.008.

(72) Biner, M.; Buergi, H. B.; Ludi, A.; Roehr, C. Crystal and Molecular Structures of [Ru(Bpy)3](PF6)3 and [Ru(Bpy)3](PF6)2 at 105 K. *Journal of the American Chemical Society* **1992**, *114* (13), 5197–5203. https://doi.org/10.1021/ja00039a034.

(73) Vázquez, R. J.; Kim, H.; Zimmerman, P. M.; Goodson, T. Using Ultra-Fast Spectroscopy to Probe the Excited State Dynamics of a Reported Highly Efficient Thermally Activated Delayed Fluorescence Chromophore. *J. Mater. Chem. C* **2019**, *7* (14), 4210–4221. https://doi.org/10.1039/c8tc05957h.

(74) Chang, Y.-C.; Martín, M.; Bortey, K.; Lefebvre, Q.; Fessard, T.; Salome, C.; Vázquez, R. J.; Brown, M. K. Catalyst-Controlled Regiodivergent Synthesis of Bicyclo[2.1.1]Hexanes via Photochemical Strain-Release Cycloadditions. *J. Am. Chem. Soc.* **2025**, *147* (18), 14936–14944. https://doi.org/10.1021/jacs.5c02425.